Modification of electrostrictive polymers and their electromechanical applications

Xunqian Yin

To cite this version:

Xunqian Yin. Modification of electrostrictive polymers and their electromechanical applications. Materials. INSA de Lyon, 2015. English. NNT : 2015ISAL0041 . tel-01278439

HAL Id: tel-01278439
https://theses.hal.science/tel-01278439
Submitted on 19 Jul 2016

Numéo d'ordre : 2015ISAL0041 Année 2015

THÈSE

Déivrée par

Institut National des Sciences Appliquées de Lyon (INSA de Lyon)
Spécialité : Génie Électrique

DIPLÔME DE DOCTORAT

(Soutenue le 07 Mai 2015 devant la Commission d'examen)

ÉCOLE DOCTORALE : ÉLECTRONIQUE, ÉLECTROTECHNIQUE, AUTOMATIQUE

Modification of Electrostrictive Polymers and Their Electromechanical Applications

Xunqian YIN

Jury MM.

Dr. Gisèle BOITEUX	CNRS	Présidente & Examinatrice
Pr. Benoît GUIFFARD	Universitè de Nantes	Rapporteur
Dr. Eric DANTRAS	Universitè de Toulouse	Rapporteur
Pr. Colette LACABANNE	Universitè de Toulouse	Examinatrice
Pr. Denis REMIENS	Universitè de Valenciennes	Examinateur
Pr. Daniel GUYOMAR	INSA de Lyon	Directeur de Thèse
Dr. Jean-Fabien CAPSAL	INSA de Lyon	Co-Directeur de Thèse

Laboratoire de recherche : LGEF, INSA de Lyon

INSA Direction de la Recherche - Ecoles Doctorales – Quinquennal 2011-2015

SIGLE	ECOLE DOCTORALE	NOM ET COORDONNEES DU RESPONSABLE
CHIMIE	**CHIMIE DE LYON** **http://www.edchimie-lyon.fr** Sec : Renée EL MELHEM Bat Blaise Pascal 3e etage 04 72 43 80 46 Insa : R. GOURDON secretariat@edchimie-lyon.fr	M. Jean Marc LANCELIN Université de Lyon – Collège Doctoral Bât ESCPE 43 bd du 11 novembre 1918 69622 VILLEURBANNE Cedex Tél : 04.72.43 13 95 directeur@edchimie-lyon.fr
E.E.A.	**ELECTRONIQUE, ELECTROTECHNIQUE, AUTOMATIQUE** **http://edeea.ec-lyon.fr** Sec : M.C. HAVGOUDOUKIAN Ecole-doctorale.eea@ec-lyon.fr	M. Gérard SCORLETTI Ecole Centrale de Lyon 36 avenue Guy de Collongue 69134 ECULLY Tél : 04.72.18 60.97 Fax : 04 78 43 37 17 Gerard.scorletti@ec-lyon.fr
E2M2	**EVOLUTION, ECOSYSTEME, MICROBIOLOGIE, MODELISATION** **http://e2m2.universite-lyon.fr** Sec : Safia AIT CHALAL Bat Atrium- UCB Lyon 1 04.72.44.83.62 Insa : S. REVERCHON Safia.ait-chalal@univ-lyon1.fr	M. Fabrice CORDEY Laboratoire de Géologie de Lyon Université Claude Bernard Lyon 1 Bât Géode – Bureau 225 43 bd du 11 novembre 1918 69622 VILLEURBANNE Cédex Tél : 04.72.44.83.74 Sylvie.reverchon-pescheux@insa-lyon.fr fabrice.cordey@ univ-lyon1.fr
EDISS	**INTERDISCIPLINAIRE SCIENCES-SANTE** **http://www.ediss-lyon.fr** Sec : Safia AIT CHALAL Bat Atrium – UCB Lyon 1 04 72 44 83 62 Insa : Safia.ait-chalal@univ-lyon1.fr	Mme Emmanuelle CANET-SOULAS INSERM U1060, CarMeN lab, Univ. Lyon 1 Bâtiment IMBL 11 avenue Jean Capelle INSA de Lyon 696621 Villeurbanne Tél : 04.72.11.90.13 Emmanuelle.canet@univ-lyon1.fr
INFOMATHS	**INFORMATIQUE ET MATHEMATIQUES** **http://infomaths.univ-lyon1.fr** Sec :Renée EL MELHEM Bat Blaise Pascal 3e etage infomaths@univ-lyon1.fr	Mme Sylvie CALABRETTO LIRIS – INSA de Lyon Bat Blaise Pascal 7 avenue Jean Capelle 69622 VILLEURBANNE Cedex Tél : 04.72. 43. 80. 46 Fax 04 72 43 16 87 Sylvie.calabretto@insa-lyon.fr
Matériaux	**MATERIAUX DE LYON** **http://ed34.universite-lyon.fr** Sec : M. LABOUNE PM : 71.70 –Fax : 87.12 Bat. Saint Exupéry Ed.materiaux@insa-lyon.fr	M. Jean-Yves BUFFIERE INSA de Lyon MATEIS Bâtiment Saint Exupéry 7 avenue Jean Capelle 69621 VILLEURBANNE Cedex Tél : 04.72.43 71.70 Fax 04 72 43 85 28 Ed.materiaux@insa-lyon.fr
MEGA	**MECANIQUE, ENERGETIQUE, GENIE CIVIL, ACOUSTIQUE** **http://mega.universite-lyon.fr** Sec : M. LABOUNE PM : 71.70 –Fax : 87.12 Bat. Saint Exupéry mega@insa-lyon.fr	M. Philippe BOISSE INSA de Lyon Laboratoire LAMCOS Bâtiment Jacquard 25 bis avenue Jean Capelle 69621 VILLEURBANNE Cedex Tél : 04.72 .43.71.70 Fax : 04 72 43 72 37 Philippe.boisse@insa-lyon.fr
ScSo	**ScSo*** **http://recherche.univ-lyon2.fr/scso/** Sec : Viviane POLSINELLI Brigitte DUBOIS Insa : J.Y. TOUSSAINT viviane.polsinelli@univ-lyon2.fr	Mme Isabelle VON BUELTZINGLOEWEN Université Lyon 2 86 rue Pasteur 69365 LYON Cedex 07 Tél : 04.78.77.23.86 Fax : 04.37.28.04.48 isavonb@dbmail.com

*ScSo : Histoire, Géographie, Aménagement, Urbanisme, Archéologie, Science politique, Sociologie, Anthropologie

Acknowledgements

With the accomplishment of this thesis, I have finished my PhD study and also ended my career as a student. First and foremost, I would like to express my deeply gratitude to everyone who helped me during my PhD study and who was with me during the past more than three years. Also I also appreciate the China Scholarship Council (CSC) who provided me the chance and financial support for my PhD study in the lab Laboratoire de Génie Electrique et Ferroélectricité (LGEF) at the Institut National des Sciences Appliquées de Lyon (INSA de Lyon).

I would like to express my special appreciation and thanks to my advisors Prof. Daniel Guyomar and Dr. Jean-Fabien Capsal for their guidance and indefatigable support without which this PhD thesis would not have been achievable. Prof. Daniel Guyomar has been a great advisor who has always provided me profound idea and discussions. It was a very pleasant experience working with Dr. Jean-Fabien Capsal. I am very grateful for his guide during my whole PhD study, his careful revise of my publications and thesis, and most importantly his support and encouragement when I experienced the tough time during my PhD study. He was my adviser in work, also friend in life. It was a great honor for me to be his first advised PhD student. Thanks my advisors again and their work ethic, enthusiasm, sense of responsibly will influence me throughout my professional career. In addition, I would like to my appreciation to Dr. Gael Sebald for his help during the first year of my PhD study. He was a good scientific researcher and always had creative ideas which enlightened me deeply thinking about my work.

I also would like to express my gratitude to the committee members: Dr. Gisèle Boiteux, Pr. Benoît Guiffard, Dr. Eric Dantras, Pr. Colette Lacabanne and Pr. Denis Remiens for their evaluation of my work, and letting my defense be an enjoyable moment due to their brilliant comments and insightful suggestions.

I would like to thank all members in the lab LGFE. It was a great honor and opportunity to work with you in LGEF and to get professional skills in the interdisciplinary research field of materials science and electrical engineering. It was your company and help that made me have an agreeable study experience in France. I would like to give my thanks to Dr. Mickael Lallart, Dr. Pierre-Jean Cottinet, and Dr. Jeremy Galineau for their help and discussions in my PhD study. I would like to express my gratitude to

Dr. Laurence Seveyrat, Mrs. Véronique Perrin, and Mr. Frédéric Defromerie for their technical help. I would like to thank Prof. Laurent Lebrun, the director of LGEF, for his amazing leadership of the lab and also his encouragement and kindness. I am also very grateful for Mrs. Evelyne Dorieux, the secretary of the lab, for her administrative work and kindness. Thanks also to my colleagues in LGFE: Dr. Jiawei Zhang, Dr. Dan Wu, Dr. Qin Liu, Dr. Yi-Chieh Wu, Dr. Linjuan Yan, Dr. Bin Zhang, Dr. Yang Li, Dr. Liuqing Wang, Mr. Zhongjian Xie, Mr. Qing Liu, Mr. Bin Bao, Mr. Alexandru Cornogolub, Mr. Yukihiro Yoshida and all my friends in the lab, where I am not able to list all the names for whom I am grateful.

Also I would like to express appreciations to my friends who we met from the French training at Shanghai in 2011 and who we met in France. It was because of you that I passed a very colorful life during the past more than three years.

Lastly, I would like to express my great appreciation to my family, my parents and my brother, who are always there helping me with courage, patience and comprehension. And I would like to express my apology to them for not being so far with them. And I love my family and I will devote more time with you in the future.

Thank you very much and this work is dedicated to you.

– Xunqian YIN

Abstract

Electroactive polymers (EAPs), which can realize the conversion between electrical and mechanical energy, have been emerging as one of the most interesting smart materials in the past two decades due to their low density, excellent mechanical properties, ease of processing, low price and potential applications in the fields of sensors, actuators, generators, biomimetic robots and so on. Among all of EAPs, ferroelectric poly(vinylidene fluoride) [PVDF] based electrostrictive terpolymers have been greatly investigated due to their high electromechanical response. A longitudinal strain of 7 % and an elastic energy density as high as 1.1 J/cm^3 have been observed for PVDF based terpolymers. One major concern for PVDF based electrostrictive polymers is the requirement of high driven electric field, which is not convenient and safe for practical applications. In addition, the electromechanical performances of electrostrictive polymers are closely related to the material properties such as dielectric properties, mechanical properties and the dielectric breakdown strength. The object of this work is to modify electrostrictive terpolymers with different approaches to improve the electromechanical performances and to develop some applications based on modified terpolymers.

Firstly, an organic/inorganic (terpolymer/carbon black) nanocomposite was prepared to improve the dielectric permittivity based on the percolation theory. The dielectric properties, dielectric breakdown strength and the mechanical properties were carefully investigated for electrostrictive applications. Results indicate that the introduction of conductive carbon black brought about an enhanced dielectric permittivity, but more significantly reduced the dielectric breakdown strength, leading to a declined electrostrictive performance of terpolymer.

Secondly, based on the heterogeneous nature of semi-crystalline terpolymer and the important role that interface polarization plays for dielectric and electromechanical response, small molecular plasticizer bis(2-ethylhexyl) phalate (DEHP) was introduced into electrostrictive terpolymer to form an all-organic polymer composite with improved electromechanical performances. As expected, the introduction of DEHP contributes to greatly increased dielectric permittivity at low frequency, decreased Young's modulus and moderately reduced dielectric breakdown strength of terpolymers, which are closely related with the increased mobility of polymer chains caused by DEHP. As a result, DEHP modified terpolymers exhibit well improved electromechanical performances in contrast with pure terpolymer.

Finally, two applications including mechanical energy harvesting and microfluidic pump based on DEHP modified terpolymers were investigated.

Keywords: *Electrostrictive polymer; Carbon black; Plasticizer DEHP; Composite; Energy harvesting; Microfluidic pump*

Résumé

Les polymères électroactifs (PAE), sont des matériaux permettant de réaliser une conversion entre l'énergie électrique et mécanique. Ces polymères sont particulièrement intéressant en raison de leur faible densité, d'excellentes propriétés mécaniques, leur facilité de traitement, ainsi que leur faible coût. Ils ouvrent la voie vers des applications potentielles dans les domaines des capteurs, des actionneurs, des générateurs, des robots biomimétiques, etc. Parmi tous les PAE, les terpolymères fluorés électrostrictifs de type P(VDF-TrFE-CTFE/CFE) à base de poly(vinylidene fluoride) [PVDF] ont été considérablement étudiés en raison de leur réponse électromécanique élevée. En effet, cette famille de terpolymère présente une déformation longitudinale de l'ordre de 7 % et une densité d'énergie élastique élevée i.e. 1.1 J/cm^3. Cependant, ces polymères électrostrictifs nécessitent l'application de champs électriques élevés, ce qui représente un verrou technologique majeur en vue d'applications. En outre, les performances électromécaniques des polymères électrostrictifs sont étroitement liées aux propriétés intrinsèques du matériau polymère, telles que les propriétés diélectriques, les propriétés mécaniques et la résistance à la rupture diélectrique. L'objet de ce travail est de proposer des procédés de modifications des terpolymères électrostrictifs par voies composites basés sur différentes approches dans le but d'améliorer les performances électromécaniques et de développer des applications à partir de ces matériaux modifiés.

Dans un premier temps, un nano-composite à base de terpolymère et de noir de carbone a été préparé pour améliorer la permittivité diélectrique. Cette approche est basée sur la théorie de la percolation. Les propriétés diélectriques, la résistance à la rupture diélectrique et les propriétés mécaniques ont été soigneusement étudiées pour des applications électrostrictives. Les résultats indiquent que l'introduction de noir de carbone conducteur a permis d'améliorer de manière notable la permittivité diélectrique. Cependant cette approche réduit de manière significative la résistance à la rupture diélectrique, ce qui représente un effet néfaste sur le rendement électromécanique maximum du terpolymère.

Dans un deuxième temps, sur la base de la nature hétérogène de terpolymère semi-cristallin ainsi que du rôle important que la polarisation interfaciale joue sur la réponse diélectrique et électromécanique, une faible quantité d'agent plastifiant (bis (2-ethylhexyl) phalate (DEHP)) a été introduite dans le terpolymère électrostrictif afin de former un composite tout organique permettant l'amélioration des performances électromécaniques. L'introduction de DEHP contribue à considérablement augmenter la permittivité diélectrique à basse fréquence, diminue le module de Young et réduit modérément la résistance à la rupture diélectrique du terpolymère. Ces effets sont étroitement liés à la mobilité accrue des chaînes de polymère causée par le plastifiant. En conséquence, les terpolymères modifiés DEHP présentent bien une amélioration significative des performances électromécaniques en comparaison du terpolymère pur avec un gain de 500 % en déformation.

Enfin, l'utilisation de ces matériaux modifiés dans deux applications spécifiques a été étudiée: La récupération de l'énergie mécanique et une pompe microfluidique sans valve.

Mots-clés: *Polymères électrostrictifs; P(VDF-TrFE-CFE/CTFE), Noir de carbone; Plastifiant DEHP; Composite; Conversion énergétique; Diaphragme; Pompe microfluidique sans valve.*

Contents

List of Symbols and Abbreviations

Symbols

C	Capacitance
D	Electric displacement or area charge density
d	Piezoelectric coefficient
E	Electric field
E_b	Dielectric breakdown strength
E_c	Coercive electric field
f_c	Percolation threshold
I	Current
k_{31}	Transverse electromechanical coupling factor
k_{33}	Longitudinal electromechanical coupling factor
P_r	Remnant polarization
$\boldsymbol{p}$	Dipole moment
S	Strain
s	Elastic compliance
S_m	Maximum strain
T	Stress
T_c	Curie temperature
T_m	Melting temperature
Y	Young's modulus or elastic modulus
μ	Dipole moment
ε_0	Vacuum dielectric permittivity, $8.854 \times 10^{-12} (F/m)$
ε_r	Relative dielectric permittivity or dielectric constant
ε_r'	The real part of dielectric constant
ε_r''	The imaginary part of dielectric constant
$tan\delta$	Dielectric loss factor
υ	Poisson's ratio

Abbreviations

$BMIBF_4$	1-butyl-3-methylimidazolium tetrafluoroborate
CB	Carbon black
CNTs	Carbon nanotubes
CVD	Chemical vapor deposition
CuPc	Copper-phthalocyanine
DBS	Dielectric breakdown strength
DC	Direct current
DEs	Dielectric elastomers
DMA	Dynamic mechanical analysis
DVB	Divinylbenzene
ILs	Ionic liquids
IPCNCs	Ionic polymer-conductor network composites
IPMCs	Ionic polymer-metal composites
IPN	Inter-penetrating network
EAPs	Electroactive polymers
EMITFSI	1-ethyl-3-methylimidazolium bis(trifluoromethylsulfonyl)imide
FCCVD	Floating catalyst chemical vapor deposition
LCEs	Liquid crystal elastomers
LED	Light-emitting diode
LOC	Lab-on-chips
MEMS	Micro-electromechanical systems
MEK	Methyl ethyl ketone
MWNT	Multi-walled carbon nanotubes
OLEDs	Organic light-emitting diodes
PANI	Polyaniline
PDMS	Polydimethylsiloxane
PE	Polyethylene
PEEK	Poly(ether ether ketone)
PET	Polyethylene terephthalate
PMN-PT	Lead magnesium niobate-lead titanate
PolyCuPc	Copper phthalocyanine oligomer
PPS	Polysulfone
PPy	Polypyrrole
PT	Polythiophene
P3HT	Poly(3-hexylthiophene)

PU	Polyurethane
PVDF	Polyvinylidene fluoride
P(VDF-HFP)	Poly(vinylidene fluoride-hexafluoropropylene)
P(VDF-TrFE)	Poly(vinylidene fluoride-trifluoroethylene)
P(VDF-TrFE-CFE)	Poly(vinylidene fluoride-trifluoroethylene-chlorofluoroethylene)
P(VDF-TrFE-CTFE)	Poly(vinylidene fluoride-trifluoroethylene-chlorotrifluoroethylene)
SPIE	International Society for Optical Engineering
SPPSU	Sulfonated polyphenylsulfone
SSEBS	Sulfonated poly(styrene-b-ethylene-co-butylene-b-styrene)
SWNT	Single-walled carbon nanotubes
TiO_2	Titanium dioxide
μTAS	Micrometer-scale total analysis systems
VA-CNTs	Vertically aligned carbon nanotubes

Chapter 1

Literatures Review and General Conceptions

In this chapter, a brief introduction of biological muscle and development history of electroactive polymers (EAPs) were first presented. Subsequently, commonly investigated EAPs including ionic EAPs (conductive polymers, carbon nanotubes, ionic polymer-metal composites) and electronic EAPs (dielectric elastomer, liquid crystalline elastomers and fluoride polymers) were reviewed. With a comparison of actuation performances of EAPs, fluoride electrostrictive polymers (terpolymer) as a promising EAP material with excellent electromechanical performances were chosen as the material for our investigation. The work mechanism for electrostrictive polymers was given in the third part. Lastly, the proposed objective of this work is to enhance the electromechanical performances of fluoride terpolymer by physical modification with inorganic and organic materials, and to develop electromechanical applications based on modified terpolymers.

1.1 Introduction of electroactive polymers

Due to their versatilely functional properties and inherent properties of low price, robust behavior, mechanical flexibility and easy processing, organic polymers, which are widely used as passive materials for a very long time, have become the material of choice for an increasing number of mature and cutting-edge technologies such as actuators [1], sensors [2], generators [3], solar cells [4], light-emitting diodes (LED) [5] and memory devices [6]. Among these polymer materials, electroactive polymers (EAPs), which can respond to the external applied electric stimulation with large shape or size changes relative to their counterparts of traditional inorganic materials, have emerged as one of the most interesting smart materials in the past two decades. The significant electromechanical properties of EAPs materials, which can realize the conversion between electrical energy and mechanical energy, enable them serve as sensors and actuators. More specially, since their action mode is very similar to biological muscles, EAPs are well known as artificial muscle.

During the past decades, considerable progress have been made in developing soft biomimetic robots [7–9], since a animal or muscle like technology would be of enormous benefits for medical implants and human assist devices, as well as for minimally invasive surgical and diagnostic tools. One of the most important research emphases is to develop lightweight, high-performance motors for the robots. Currently, the most commonly used motor technologies include electromagnetic motors, combustion engines, shape memory alloy (SMA), and piezoelectrics [10]. Electromagnetic motors and combustion engines are generally the most powerful actuators, but they need heavy and large-volume power supply and complicated gearing systems, leading to a reduced energy density and mobility. Moreover, they generate much noises and heat, which is not favorable fro certain applications. Piezoceramics can achieve high power densities but suffer from small strains (0.1 %) and high stiffness. SMAs are capable of generating relatively large linear displacements, but their actuation requires relatively complicated heating and cooling process, which contributes to a slow response speed and limited lifetime. These smart materials are thus not suitable for lightweight and high-performance artificial muscle applications.

The emerging EAPs actuators possess excellent electromechanical performances exceeding biological muscles in many aspects [11], making them promising candidate materials to develop muscle-like actuators. EAPs can generate large strain and useful stress with a fast response time. Also, they are intrinsically flexible and can be processed to any desired size and shape, which enable them meet different environment requirements. The appearance of EAPs will open up a new era of development of soft biomimetic actuator based robots. In the following parts of this section, I will give a brief introduction of biological muscles and a general outlook of the development of EAPs materials.

1.1.1 Biological muscles

Even biological muscles are surpassed by artificial muscles in many aspects, biological muscles are considered as highly optimized systems, in which the mechanical force generation and transmission system, power supply system and control systems are well integrated, providing attractive features for artificial muscles technology to emulate.

As shown in Fig. 1.1, muscles consist of bundles of parallel muscle fibers (or muscle cells) held together by connective tissues such as fascia. Nerve fibers, blood and lymphatic vessels swing besides muscle fibers throughout the whole muscle. Muscles cells typically have a cylindrical shape with a diameters between 10 and 100 μm and a length up to several centimeters [1]. A muscle fiber is a bundle of even smaller fibbers named fibrils which are composed of sarcomere, the basic function union. Within sarcomere, the relative movement between two important protein, myosin and actin, contributes to the actuation of muscle, and this process is regulated and controlled by the diffusion of Ca^{2+} ions. The mechanical energy is provided by the chemical free energy of the hydrolysis of adenosine triphosphate (ATP), which is binded to the myosin head [12].

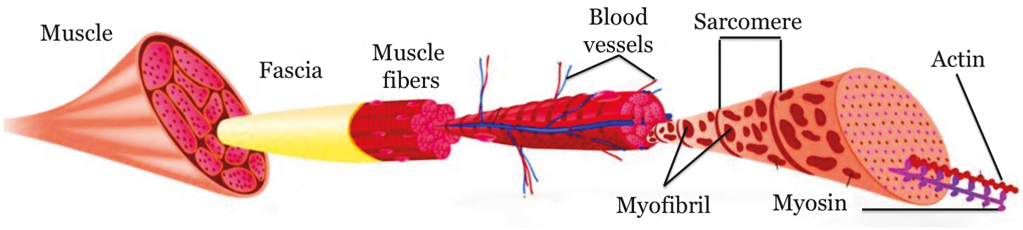

Figure 1.1: Diagram of skeletal muscle structure. (Reproduced from *www.wisegeek.org*)

The actuation properties of skeletal muscles are shown in Table 1.1. The maximum force generated by natural muscle is 0.35 MPa and the maximum sustainable static stress generated by muscle is 0.1 MPa, since the maximum sustainable force is usually 30 % of the peak value [12]. The typically specific power for human muscles is about 50 W/kg but can be as high as 284 W/kg.

Table 1.1: Properties of mammalian skeletal muscle [11, 12].

Properties	Typical Value	Maximum Value
Strain (%)	20	>40
Stress (MPa)	0.1 (sustainable)	0.35
Work Density (kJ/m^3)	8	40
Density (kg/m^3)	1037	
Strain Rate (%/s)		>50
Specific Power (W/kg)	50	284
Efficiency (%)		40
Cycle Life (Times)		>10^9
Modulus (MPa)	10-60	

1.1.2 History and recent developments of EAPs

The EAPs field can be dated back to an experiment conducted by Roentgen [13] in 1800. In his experiment, a 16×100 cm natural rubber strip with one end fixed and the other end attached to a mass was subjected to an electric field across the rubber band and an elongation was observed. Laterly in 1899, Sacerdote [14] followed this experiment by formulating a theory on the strain response to the electric field activation. These milestones were followed in 1925 with the discovery of a polymer with piezoelectric properties named electret, when the combined carnauba wax, rosin and beeswax were cooled with an applied dc bias electric field [15]. A electret is a dielectric material with a quasi-permanent electric charge or dipolar polarization. It is generally formed by freezing dipolars inside a melted dielectric material in a very strong electric field. Electrets can generate voltage when subjected to stress and deform in response to an applied electric field. However, the low deformation limits its applications as actuator and it is widely used as sensors or transducers such as an electret microphone [16].

It wasn't until 1969 that Kawai [17] first demonstrated the piezoelectricity in stretched and polarized polyvinylidene fluoride (PVDF) and subsequently in 1971 the pyroelectric and ferroelectric properties of PVDF were also reported by J. G. Bergman [18]. Since then, a new field of ferroelectric polymers opened up to the scientific and industry community and large amounts of research attention have been paid to the investigation on the ferroelectric properties of PVDF and some other polymers. They can be used as alternative materials to inorganic piezoelectric ceramics in a wide range of potential applications such as sensors, actuators, medical imaging, IR detectors, underwater acoustic transducers and the emerging organic electronics. The piezoelectric [19, 20], pyroelectric [21–24], ferroelectric [25, 26] electrostrictive [27–29] properties and transition behaviors [30, 31] of PVDF and its copolymer P(VDF-TrFE) were extensively investigated during 1970s and 1980s. Ferroelectric materials refer to the materials possessing a spontaneous polarization which can be switched by an applied external electric field. The traditional ferroelectric materials are inorganic ceramics, however, they are brittle and can not withstand the high electric field which limits their application. The discovery of organic ferroelectric materials made up some special application fields which can not be fulfilled by inorganic ferroelectric materials.

It has been known for decades that polymers can generate shape or size change in response to electric field caused by the electrostrictive effects but only with a very small strain. Since the beginning of 1990s, a serials of new polymers with large induced strain have been developed, leading to a flourishing research due to their muscle-like action mode which can be used to mimic the movement of animals and inspects. For example, an exceptionally high and fast electrostrictive strain about 4 % under an applied electric field of 150 MV/m in electron-irradiated poly(vinylidene fluoride-trifluoroethylene) [P(VDF-TrFE)] copolymer was demonstrated by Zhang *et al.* [32] in 1998. A strain up to 4 % was also achieved by ultrathin (less than 100 nm) ferroelectric liquid-crystalline elastomer but only at an electric field of 1.5 MV/m [33]. In this work, liquid-crystalline polymers with chiral mesogens were attached to a polysiloxane backbone, combining the ferroelectric properties of liquid-crystalline phase and the rubber-like elasticity of polymer networks. Moreover, Pelrine et al. [34] reported very high electric field induced area strains up to 117 % (54 % thickness strain) and 215 % (68 % thickness strain) [35] for prestrained silicon elastomers and acrylic elastomers, respectively. At the same time, some electronic devices based on these exciting EAPs were also developed. In 2002, an aquarium of swimming robotic fish, which is the first commercial EAPs product, was fabricated by Eamex Corporation[1] in Osaka, Japan, as is shown in Fig. 1.2. What makes it remarkable is that the brightly colored plastic fish propelling themselves through the water in a fair imitation of life do not contain mechanical parts: no motors, no drive shafts, no gears, not even a battery.

Figure 1.2: The first reported commercial EAPs robotic fish.

In order to enhance the international cooperation among scientific researchers, potential investors and users, Yoseph Bar-Cohen, one of the EAPs field's pioneers, organized the first EAPs conference through the International Society for Optical Engineering (SPIE) as a part of the Smart Structures and Materials Symposium in 1999. Since then, the EAP Actuators & Devices (EAPAD) conference is held annually and it has become the largest communicating platform for researchers and investors involved in the field of EAPs. Besides, a website named *Worldwide EAP (WW-EAP) Webhub*[2] was built to gather and archive related information about the development of EAPs. And a semi-annual WW-EAP newsletter has been published electronically with short summary from authors worldwide to provide a snapshot of the latest advances related any respect of this field, such as materials, processing approach, analytical modeling, applications, and so on.

---

[1] http://www.eamex.co.jp

[2] http://eap.jpl.nasa.gov

Now, with about two decades' development, the EAPs materials are becoming more and more ready for practical applications. Many high-tech companies have been established and more resources are being invested in this field to accelerate the transfer process of EAPs technology. In early 2004, Artificial Muscle Inc. (AMI)[3] was spun out of SRI International to commercialize EAPs technology. On June 23, 2014, Parker Hannifin Corporation[4], the global leader in motion and control technologies, announced that it purchased intellectual property and licenses from Bayer MaterialScience LLC and its AMI business unit. The acquired EAPs technology will be used in new and existing Parker products and services in medical devices, remote monitoring and industrial systems and it will strengthen Parker's smart material development capabilities. According to the IDTechEx Research report[5] "Electroactive Polymers and Devices 2013-2018: Forecasts, Technologies, Players", the EAPs potential market would be US$ 245 million in 2013 and this value will increase up to as high as US$ 2.25 billion by 2018. Actuators and sensors will remain prominent applications in the next five years. The highest potential lies in new application fields, such as consumer electronics. For instance, with touchscreens everywhere, haptics for consumer portable touch screen devices and peripherals is going to be the next big application and potentially the first large-scale implementation of EAP actuators in general with an expected penetration of 60 % for haptic feedback in mobile phones. The first prototypes and evaluation studies have been just recently demonstrated as is shown in Fig. 1.3. It is the world's next-generation ultrathin and flexible keyboard via EAPs by Novasentis, Inc.[6] (formerly Strategic Polymers, SPS). The Awake^{TM} keyboard features a super-slim profile and appealing design with haptic keys that are integrated with localized HD vibra-tactile and audio effects when pressed. It is designed to replace the bulk mechanical keyboards with increased efficiency and a revolutionary typing experience. The Electro-Mechanical Polymer (EMP) actuator technology of Novasentis, Inc. also won the 2014 CES (well-known as the Customer Electronics Show) Innovation Awards in the Embedded Technologies category. Recently, a new lens focusing system in which

Figure 1.3: Haptic keyboard via ultrathin and flexible EAPs technology by Novasentis, Inc.

---

[3] http://www.artificialmuscle.com

[4] http://www.parker.com

[5] http://www.idtechex.com/eap

[6] http://www.novasentis.com

EAPs were used as an actuator to aid the lens' focusing and image capture was unveiled in Apple's patent [36]. Apple's artificial muscle provides both lens displacement control and a variable aperture. According to Apple, this flexible camera tech could allow for slimmer mobile systems that can carry larger camera components.

In general, EAPs are very attractive materials and technology with a wide range of applications such as sensors, actuators, biometric devices and customer electronic devices. Although they have been well-investigated in the past two decades, they are still far from mature, there are still many challenges for practical applications. One of the key issue is to develop new EAPs materials with required performance to meet different application environment. Today, the EAPs encompass a wide variety of materials ranging from soft dielectric elastomers (DEs) to the rigid carbon nanotubes (CNTs). There are existing a number of reviews about these EAPs materials [35, 37–40]. In the next section, I will provide a short survey of the common EAPs materials and their recent developments.

1.2 Survey of electroactive polymers

In this section, I will review the currently documented electroactive polymers of each type. EAPs can be routinely divided into two general categories on the basis of their physical state or actuation mechanism: ionic (or wet), wherein the actuation of EAPs are based on the diffusion or transport of ions with the presence of a liquid medium, and electronic (or dry), wherein the EAPs intrinsically driven by electric field or Coulomb forces.

1.2.1 Ionic EAPs

A. Conductive polymers

It wasn't until Alan J. Heeger, Alan MacDiarmid and Hideki Shirakawa reported high conductivity in oxidized iodine-doped polyacetylene in 1977 [41] that the concept which polymer materials were well-known as electrical insulators changed. For this research, they were awarded the 2000 Nobel Prize in Chemistry "for the discovery and development of conductive polymers". Since the late 1980s, conductive polymers have emerged as organic electronic materials in a wide range of applications such as batteries, supercapacitors, electrochromic devices, solar cells and organic light-emitting diodes (OLEDs).

Conductive polymers are conjugated polymers which have backbones of contiguous sp^2 hybridized carbon centers. A molecule wide delocalized set of orbitals provides the possibility of the long-range mobility of electrons. However, the energy gap of conjugated polymers can be larger than 2 eV, which is too large for thermally activated conduction. Therefore, conjugated polymers are typically semiconductors or insulators. In order to greatly enhance conductivity, conjugated polymers require doping with donors or acceptors in solid state to form a charge-transfer complexes. This is a redox process, in which polymers will be oxidated or reduced. Consequently, the electrochemical or chemical doping of conductive polymers results in dramatic property changes including electrical, optical and mechanical properties, and it provides potential applications of conductive polymers in intelligent systems.

The first conceptional application of conducting polymers for direct conversion of electrical energy into mechanical energy was proposed by Baughman *et al.* in 1990 [42, 43]. It featured large dimension changes (over 10 %), stress and work density which are all of an order of magnitude higher than those of piezoelectric PVDF but achieved at a low voltage about an order of magnitude lower than piezoelectric materials. Subsequent work was followed by Pei and Inganäs [44–46]. They reported a successful bending cantilever actuator prepared by bipolymer strips of polypyrrole (PPy) and polyethylene (PE), which can response to various stimuli. The actuation mechanism of conductive polymers is on the basis of simple physical separations of polymer chains due to the uptake and expulsion of counter-ions which occurs during the electrochemical or chemical redox cycling, possibly along with associated solvating spices. The most widely used conductive polymers for actuators are PPy, polyaniline (PANI) and polythiophene (PT) [47]. As is shown in Fig. 1.4a, conductive polymers possess conjugated backbone. When oxidative state of conductive polymers is electrochemically changed, a charge flux along the conjugated polymer backbone will be induced and counter-ions from the electrolyte migrate to balance the charge. Due to the counter-ions incorporation between the polymer chains, the major expansion appears to be perpendicular to the polymer chain direction, as depicted in Fig. 1.4b. As mentioned above, the volume change is dominated by ion insertion and deinsertion. For conductive polymers doped with bulky immobile anions in contact with electrolyte, cations are inserted and deinserted and polymer will expand in reduced state. While for polymers doped with small size anions, anions are inserted and deinserted,and therefore polymer will expand in oxidized state [48].

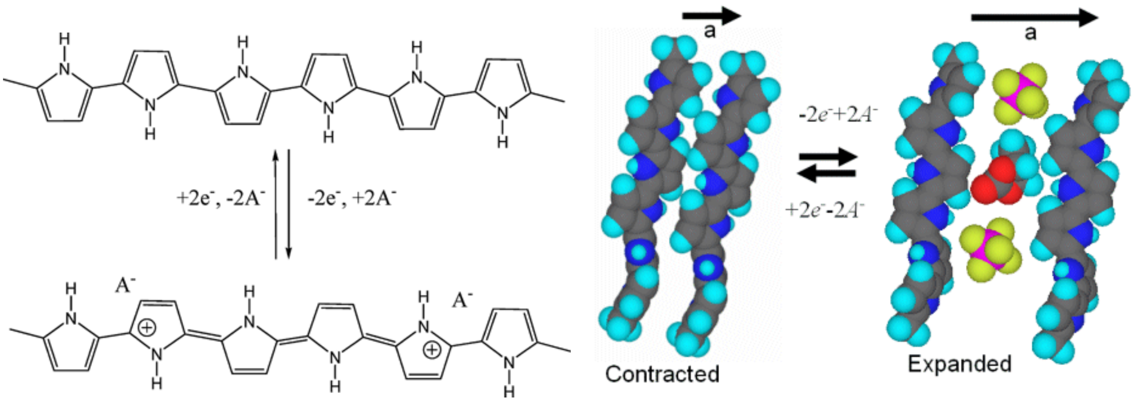

(a) (b)

Figure 1.4: Schematic representation of actuation mechanism for PPy: (a) The oxidized and reduced states of a PPy chain [35]; (b) The uptake and expulsion of ions PF_6^- (yellow/purple) and concomitant solvent (red/blue/grey) between PPy chains [37].

Conductive polymers have been one of the most promising materials as artificial muscles because of their electromechanical performances and biological compatibility. Two important figure of merits are the displacements and force generated from conductive polymer actuators which can be characterized by strains and stress (force generated per cross-sectional area), respectively. Actuation strains are large, ranging from a few percent to about 40 % [49], so the strain can be exploited in either bending geometries, which work well at the micro-scale, or directly through linear expansion/contraction, which is important on the macro-scale, at which greater forces are typically required. It has been demonstrated that the generated force is limited by the break strength of the actuator material. Baughman [50] theoretically predicted that the maximum generated stress can be estimated as 50 % of the breaking strength and a high maximum stress about 450 MPa will be achievable. In practice, the stress is about 3-5 MPa [49], 10 times larger than that (0.35 MPa) of mammalian skeletal muscles. This value can be improved by properly material modification or actuator structure design. For instance, Spinks *et al.* [51] incorporated carbon nanotube into the PANI fibers. The prepared fibers have a high break strength of 255 MPa and results in a maximum stress about 125 MPa, which means that useful strains can be achieved at a substantial stress in excess of 100 MPa, 300 times higher than skeletal muscles. A high work density per cycle of 325 kJ/m^3, which is 8-40 times higher than that of skeletal muscles (see Table 1.1), was also observed. The other important advantage of conductive polymer actuator is the low operate voltage (1-2 V). The obained maximum power density is 150 W/kg [11]. Nevertheless, several drawbacks remain for wide application of conductive polymers actuators, including the low efficiency (on the order of 1 %), low electromechanical coupling (< 1 %), as well as the low strain rate ($\ll 1$ %/s and maximum rate up to 12 %/s was observed) due to the relative low ion transport [11, 42] and the internal resistance between the electrolyte and polymers [52]. To drive the conductive polymer actuators electrochemically, an ion source is required. Typically, aqueous electrolyte is used as a part of the actuator cell, in which the conductive polymer strip is immersed into the liquid electrolyte [44]. In macro-actuators, polymer electrolyte which is sandwiched between two conjugated polymers enables conductive polymer actuators can work in the air environment instead of in an aqueous electrolyte. For example, Sansiñena *et al.* [53] developed a solid state actuator based on two PPy films and a sandwiched polymeric electrolyte, poly(epichlorohydrin-co-ethylene oxide) [P(ECH-co-EO)]/$LiClO_4$. Another way to operate conductive polymer actuator out of aqueous environment is to encapsulate the complete device: the electroactive polymer layer, a hydrogel electrolyte, and the counter electrode into an actuator cell [54].

Even though the fundamental investigation of conductive polymer as artificial muscles materials is still on the way, there are already some practical applications especially in the biomedical field due to its low operate voltage, high generated force, high work density as well as biological compatibility. Blood vessel connectors, braille displays, and cochlear implants based on conductive polymers have already been successfully commercialized [55]. Possible applications of interest can be found in many literatures including: propulsion or locomotion systems for swimming devices, micro pump, automotive and prosthetic devices [56].

B. Carbon nanotubes (CNTs)

Since the discovery of multi-walled carbon nanotubes (MWNT) in 1991 by Ijima of NEC cooperation [57] and single-walled carbon nanotubes (SWNT) two years later [58,59], carbon nanotubes (CNTs) have emerged as materials of considerable interest for various high-tech applications due to their excellent mechanical and electrical properties. SWNT can be viewed as a sheet of graphite rolling into a cylinder and MWNT is composed of concentric SWNT of different diameters with an interlayer spacing of 0.34 nm. Nanotube properties are highly dependent on its nano-scale atom arrangement, tube diameter and length, and macro-scale material structure. For instance, despite graphite is semiconductor with zero band gap, SWNT may be either semiconductive or metallic depending on the sheet direction about which the graphite sheet is rolled into a cylinder (as shown in Fig. 1.6a). CNTs are very strong and stiff. Based on experimental and theoretical results, the Young's modulus of a individual SWNT should be as high as 640 GPa, approaching that of diamond, and the corresponding tensile strength is predicted to 37 GPa with a strain-to-failure about 5.8 %, which is about 10 times higher than any other type of continuous fiber [60,61]. However, the observed mechanical properties for nanotube assemblies, such as sheets, fibers and yarns, are much lower that the above mentioned values of individual SWNT.

The conception and theoretical analyses of non-faradaic (in contrast with faradic process, i.e., the electrochemical reaction of conductive polymer actuators) actuators via high surface-area materials such us CNTs were initially proposed in 1996 [50] and experimentally demonstrated 3 years later [62] by Baughman, and since then Baughman's group in NanoTech Institue of the University of Texas at Dallas has done a series of leading work in the CNTs actuator field. The actuation of CNTs results from the charge injection based quantum chemical effects and double-layer electrostatic effect. As is depicted in Fig. 1.5a and 1.5b, charges are injected into SWNT electrodes by an applied potential, and balanced by the ions from electrolyte, forming a so-called double layer. The injected charges cause dimension changes in covalent C-C bond, leading to the actuation behavior of CNTs. For low charge density, quantum mechanical effect is dominant to the strain, while both quantum chemical effect and electrostatic double layer charging contribute to the strain for high charge density. The electrochemical charge injection process can be characterized by gravimetric capacity of CNTs in different electrolyte. The typical value of gravimetric capacity for SWNT is 15 F/g. Fig. 1.5c shows the first reported biomorph cantilever based CNT actuator operated in aqueous NaCl electrolyte. It consists of two strips of MWNT bulky paper adhered to two opposite sides of a scotch. Electron injection induced expansion and hole injection induced contraction result into the bending behavior of CNT actuator. A maximum strain of 0.2 % and a stress of 0.75 MPa were observed. The electromechanical properties of CNTs sheets made from SWNT and/or MWNT were first investigated in detail by Vohrer *et al.* [63] with a self-developed experimental setup. Results indicate that actuator performances of CNTs are not only dependent on the material itself but also affected by used electrolyte, applied voltage and so on.

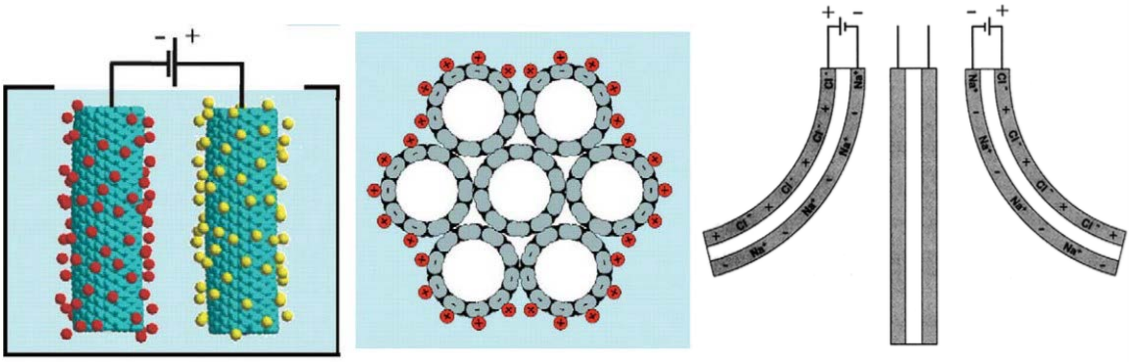

(a) (b) (c)

Figure 1.5: Schematic illustration of actuation mechanism of CNTs artificial muscles: (a) An applied potential injects charge into two SWNT electrodes which are immersed in electrolyte, and the injected charges are compensated by ions from the electrolyte [64]; (b) Charge injection at the surface of a nanotube bundle; (c) Biomorph cantilever based CNTs actuator operated in aqueous NaCl electrolyte [62].

The performances of CNTs actuators are highly dependent on the mechanical properties of the used CNTs assemblies. The inherent extremely high Young's modulus, combined with the predicted strain (1 % for SWNT in aqueous electrolyte) contributes to high stress generation and unexpected work density per cycle. However, the actual performances of CNTs actuators are much lower than the predicted ones. For example, the typically strain for SWNT actuators is between 0.06∼0.2 % [65] and maximum observed isometric SWNT actuator stress is 26 MPa [61]. One major cause for this discrepancy is the poor stress transfer [66] between nanotube bundles since the nanotubes are jointed by mechanical entanglement and val de Waals force within CNTs assemblies, which also result into the common creep behavior of CNTs actuators. Therefore, one challenge for improving actuation performances of CNTs actuator is to convert available nanotube powders into useful assemblies with high mechanical property, creep resistance as well as conductivity. Fig. 1.6 shows the development of CNTs materials for actuator applications. Given the difficulty to control the purity and high cost during the synthesis process of SWNT, most CNTs actuators are made of MWNT. Hughes *et al.* [65] demonstrated the first CNTs actuator using free-standing MWNT mats, exhibiting a maximum strain about 0.2 % and a high gravimetric capacity as high as 113 F/g. MWNT forest, which comprises approximately parallel nanotubes resembling trees in bamboo forest (as shown in Fig.1.6b), is synthesized by chemical vapor deposition on an iron catalyst-coated substrate using acetylene gas as the carbon source. Zhang *et al.* [67, 68] reported the mechanically drawn high oriented, strong, transparent, and conductive ultrathin CNTs sheet and spun-twisted multi-functional CNTs yarns from MWNT forest. The fabrication process of CNTs sheet and yarns are shown in Fig. 1.6c and 1.6d, respectively. The diameter of CNTs yarns is typically 1∼60 μm, depending upon the width of the forest sidewall used for spinning. Two-ply and four-ply yarns are obtained by over twisting a single yarn and the two-ply yarn with opposite twist direction, respectively (as is shown in Fig. 1.6 e-g). The as-prepared CNTs yarns exhibit high creep resistance, high electrical conductivity, increased strain-to-failure (as high as 13 %) and enhanced tensile strength (up to 460 MPa) [67]. The actuation performance of CNTs yarns was investigated by Mirfakhral *et al.* [64] via a 12 mm length single yarn with a diameter of 18 μm submerged in 0.2 M tetrabutylammonium hexafluorophosphate (TBAP)/acetonitrile (AN) electrolyte. Strains up to 0.5 % in response to an applied voltage of 2.5 V and a gravimetric capacity of 26 F/g were observed.

In addition to the cantilever-based CNTs actuators, rotational actuation for CNTs was first reported by Fennimore *et al.* [69]. Recently, Foroughi *et al.* [70] developed an electrolyte-filled CNTs yarn based tensile and rotational actuator, and the basic configuration is shown in Fig. 1.7a, in which three electrodes (reference electrode, actuating CNT yarn electrode and counter-electrode from left to right) were used and half length of the MWNT yarn was immersed into the electrolyte with a paddle in the middle of the yarn. The tensile and torsion actuation of the MWNT yarn originate from the volume expansion caused by charge injection. As is depicted in Fig. 1.7b and 1.7c, the untwist behavior of the yarn resembles a helically wound finger cuff toy, where simultaneous yarn contraction and torsional rotation occur to increase the volume. The actuator provides a reversible 15,000°rotation and a fast actuation of 590 revolutions per minute. A large torsional stork of 250°/mm of the actuator length, a peak work density per cycle of 61 W/kg and strains up to 1 % were observed.

Another issue is to develop CNTs actuators without aqueous electrolyte. As is known, the use of aqueous electrolyte will lead to low work density and difficulty to realize the miniaturization of the actuation system. A hybrid CNTs actuator with an introduce guest (paraffin waxes) which can be electrically, chemically and photonically driven in air was demonstrated by Lima *et al.* in 2012 [71]. Torsional and tensile actuation of these hybrid muscles result from dimensional changes of a yarn guest caused by different external stimuli. This artificial muscle provides fast (11,500 revolutions per minute), and large-stroke tensile (strain 3 %) and torsional actuation with a high work density of 27.9 kW/kg. Lee *et al.* [72] reported an all-solid tensile and torsional CNTs actuator, in which the liquid electrolyte was replaced by poly(vinylidene fluoride-hexafluoropropylene) [P(VDF-HFP)] based $TEABF_4$ solid gel electrolyte. A large torsion stroke of 53°/mm at a low applied voltage of 5 V and useful tensile stroke (1.3 % at 2.5 V and 0.52 % at 1 V) were obtained.

Unlike conductive polymer actuators, there is no ion intercalation included in the actuation process of CNTs actuators, resulting a relatively high strain rate. Madden *et al.*

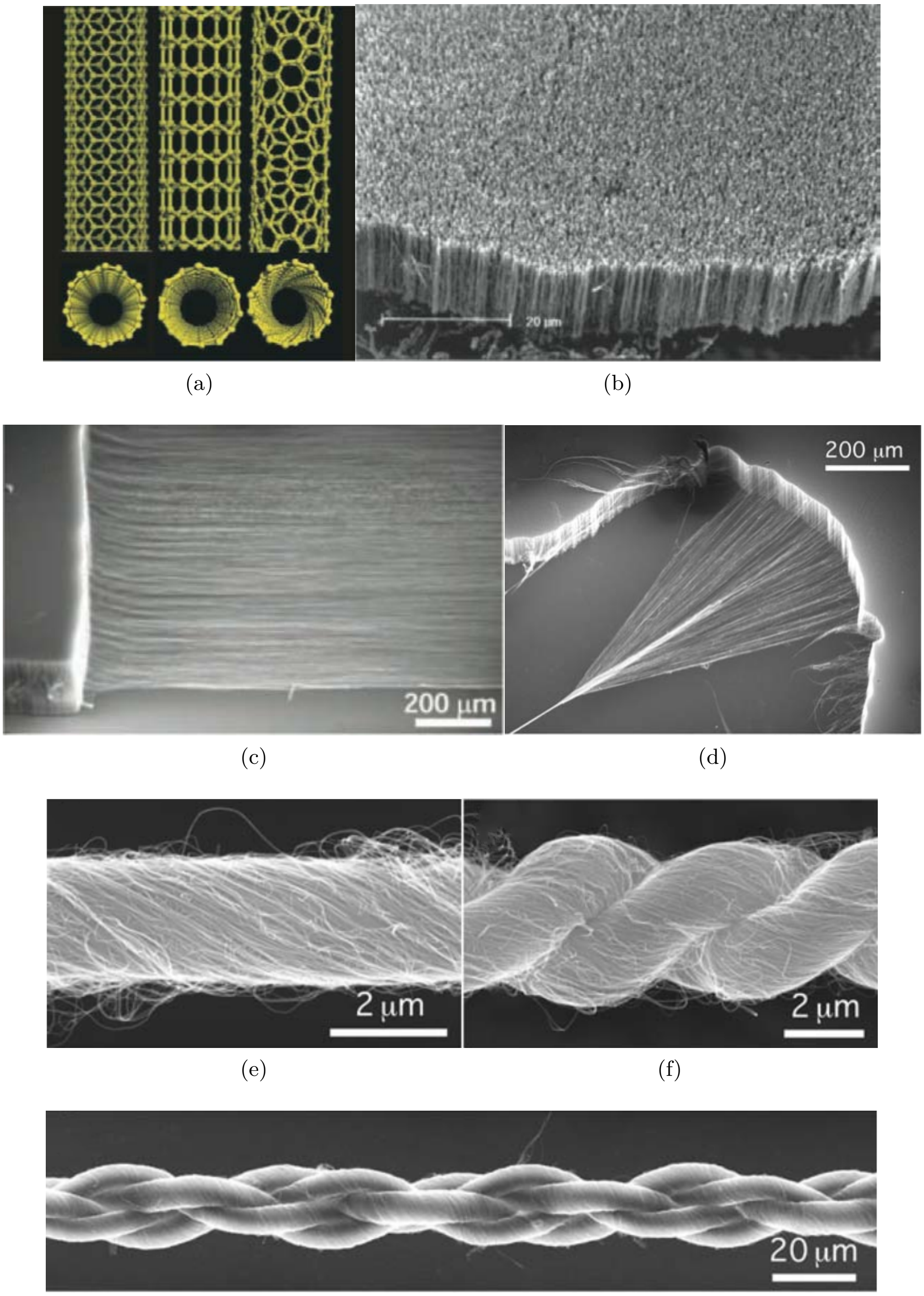

(a) (b) (c) (d) (e) (f) (g)

Figure 1.6: Schematic illustration of development of CNTs materials: (a) Structures of SWNT: armchair (left), zigzag (middle), and chiral (right) [61]; (b) Scanning electron microscope image of MWNT forest [61]; (c) Mechanically drawn ultrathin CNTs sheet [68]; CNTs yarns: (d) the preparation process of CNTs yarns, (e) single, (f) two-ply and (g) four-ply yarns [67].

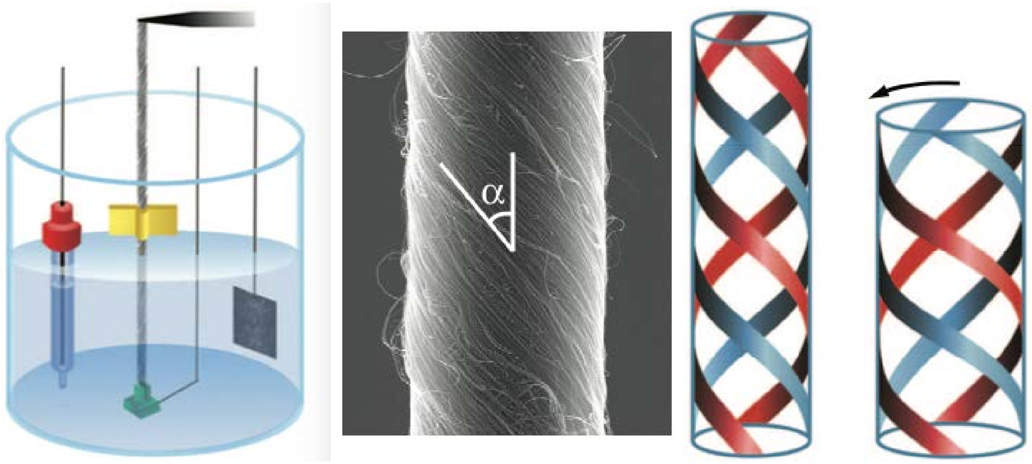

(a) (b) (c)

Figure 1.7: Schematic illustration of rotational actuation of CNTs artificial muscles [70]: (a) A simple three-electrode configuration of torsional CNTs actuator; (b) Scanning electron micrograph of a carbon nanotube yarn (d = 3.8 mm, $\alpha = 37°$) that was symmetrically twist-spun from a MWCNT forest; (c) Effect of yarn volume expansion during charge injection, behaving like a helically wound finger cuff toy. The amount of yarn untwist during yarn volume expansion is indicated by the arrow.

[73] demonstrated a stroke rate of 19 %/s and an instantaneous power density of 270 W/kg for a carefully designed carbon nanotube muscle. The typical value of gravimetric capacity of CNTs actuator is in the range of 15~200 F/g [66], depending the CNTs materials and electrolyte, meaning that application of a few volts can produce a large amount of charge injection and corresponding mechanical deformation of nanotubes, therefore, CNTs actuators can be operated at a low voltage of few volts. Due to its thermal and chemical stability, CNTs actuator can work at a wide temperature range (liquid nitrogen to 1000 °C) [61,67], and harsh chemical environment [69]. Possible eventual applications for CNTs muscles are in micro electromechanical systems (MEMS) devices, such as for controlling valves and stirring liquids in micro-fluidic circuits, and in medical catheters.

C. Ionic polymer-metal composites (IPMCs)

Ionic polymer-metal composites (IPMCs) as one of the most promising smart materials has been intensively investigated since a decade ago for their impressive large deformation in response to low voltage stimulation and air-working capability. IPMCs can act as soft biomimetic sensors and actuators [74]. A general overview about IPMCs can be referred to a series of four journal articles written by Shahinpoor and his co-worker Kim [75–78], in which fundamental concepts, fabrication method, modeling and applications of IPMCs were reviewed.

Typically, IPMCs have a sandwiched structure where an ion-exchange membrane is laminated between two noble metal electrodes (Pt, Au). There are two main material used as ion-exchange membrane: perfluorinated alkenes with short side-chains terminated by hydrophilic ionic groups and styrene/divinylbenzene-based polymer with ionic groups substituted from the phenyl rings [75]. Since styrene-based polymers are highly cross-linked and very rigid, perfluorinated alkenes are generally chosen as the ion-exchange membrane. The chemical structure of perfluorinated polymers combines a hydrophobic Teflon-like backbone with short side-chains terminated by hydrophilic sulfonic acid (Nafion) or carboxylated groups (Flemion). Hydrated Nafion has a phase-separated structure, *i.e.*, the hydrophobic polymer network which provides the main mechanical and chemical stability and the covalently fixed hydrophilic ionic groups which form a cluster and offer the nanochannel for the mobile cations. It has been demonstrated that the water channels within Nafion membrane have a diameter between 1.8 and 3.5 nm [79, 80]. Therefore, Nafion is capable to absorb large amount of polar solvent (i.e. water) and good ionic conductivity (in the order of mS cm^{-1} [81, 82]).

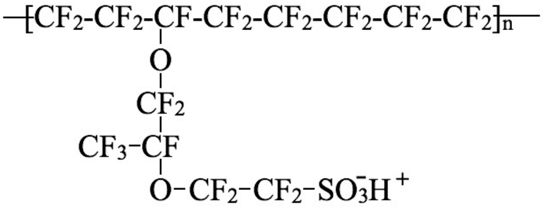

Figure 1.8: Chemical structure of Nafion

IPMCs were initially developed as a solid polymer electrolyte for water electrolysis by Takenaka and Millet [83, 84]. The state-of-art fabrication method of IPMCs involves a two-step processes: the first in-depth composite process and the secondary surface electroding process. In the first step, the Nafion membrane is immersed into a precursor salt solution containing the noble metal cations (such as $Pt(NH_3)_4Cl_2$) for the permeation of metal cations and exchange with H^+ and then a reduce agent ($NaBH_4$ or $LiBH_4$) is introduced into the solution to reduce the metal cations into atoms, leading to a Nafion/metal composite. In order to improve the electrical conductivity, a layer of metal is deposited on the initial metallic surface with the same chemical reduction reaction in the second stage. The metal particles distribute homogeneously within the polymer membrane and predominate near the two surfaces with a typical depth of 1-10 μm [76]. Pretreatment including roughening the surfaces with sandpaper and cleaning the Nafion membrane are required to improve the adhesive strength and to reduce the resistance of the deposited electrode. An extra ion-exchange of H^+ in the IPMCs membrane with the other desired counter ions such as Li^+ or Na^+ is applied to fabricate different type actuators.

With an applied voltage on two sides of IPMCs, the mobile cations with associated water migrate along the water-channels from the anode to cathode, resulting in a volume expansion in the cathode side and contraction in the anode side and finally a bending of the IPMCs to the anode side (as shown in Fig. 1.9). As the pressure from strained polymer membrane usually causes water to diffuse out of the cation-gathered areas, the displacement can not be kept and slow relaxation toward the cathode layer happens. The

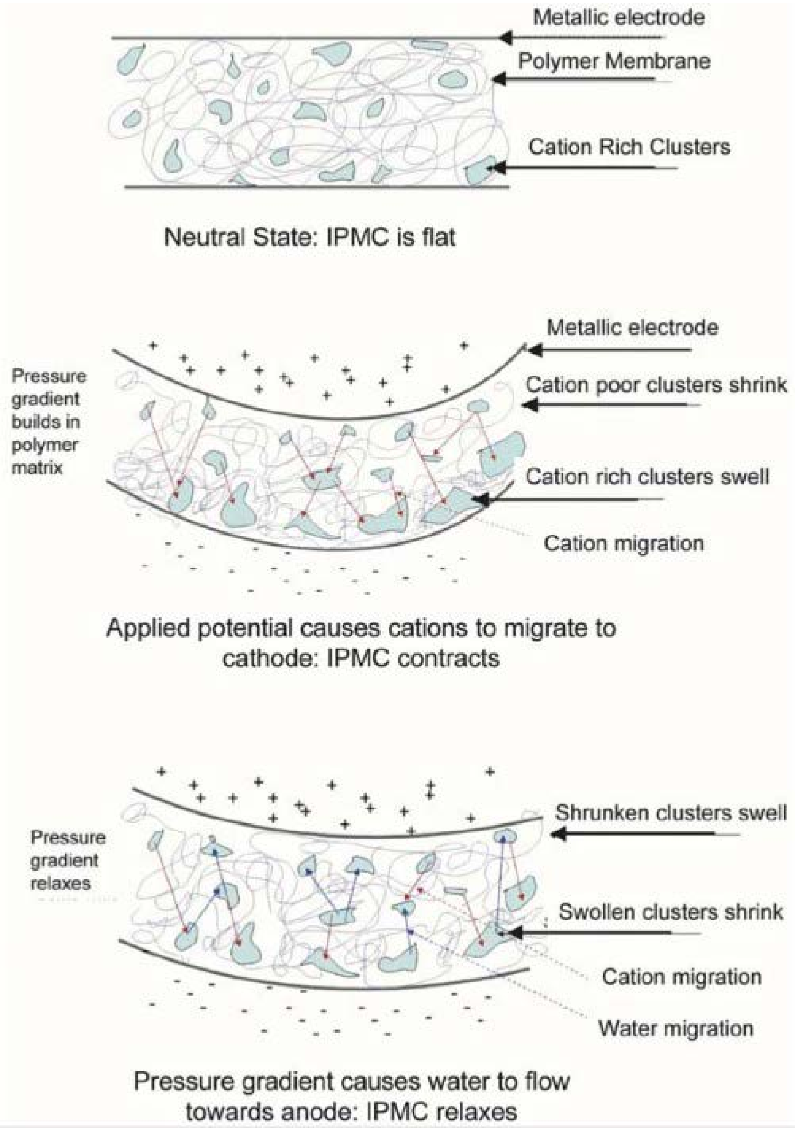

Figure 1.9: Schematic illustration of the actuation mechanism of IPMCs [11].

performance of the IPMCs actuator is obviously determined by the nature of the ion-exchange membrane and mobile cations, the electrode materials and structures, and the level of hydration solvent saturation. The relationship between the performance of IPMCs and aforementioned factors was qualitatively and quantitatively investigated by Nemat-Nasser*et al.* [85, 86] via a proposed physic based model of Nafion-based IPMCs actuator.

However, the traditional Nafion-based IPMCs actuators have some disadvantages which hinder their wide practical applications with high performance. For instance, the use of water as electrolyte solvent leads to a quick performance decline of IPMCs actuators operating in air due to the water losing caused by evaporating, electrolysis (> 1.23 V, the potential window of water) and leakage during actuation due to the porous metallic electrode [76]. The Nafion membrane has good chemical and mechanical stability but expensive, low blocking force, environmental-unfriendliness and back relaxation under direct current (DC) voltage, and it is difficult to tune the properties of the membrane such as the proton conductivity and ion-exchange capacity. In addition to the electrolyte layer, the low flexibility, strain resistance, high cost of noble metal electrode layer also restrict the practical application of IPMCs actuators. Therefore, recent development of the new generation of IPMCs actuators focus on new ion-exchange membrane materials, solvent and electrode materials with high performance.

For the development of ion-exchange membrane based electrolyte layers, nonfluorinated hydrocarbon polymers instead of Nafion have been used to develop the novel IPMCs actuators. Sulfonation and carboxylic acidification are two major methods of chemical modification in order to transform ordinary polymers into polyelectrolytes. A lot of sulfonated and a few of carboxylated polymers with good ion-exchange capacity, proton conductivity, low cost and environmental-friendly have been synthesized for IPMCs actuators including sulfonated poly(ether ether Ketone) (PEEK), sulfonated poly(styrene-b-ethylene-co-butylene-b-styrene) (SSEBS), acrylic acid copolymers, etc. Various types of novel hydrocarbon-backbone ionic polymer membranes used in the IPMCs application have been reported in a review paper by Jo *et al.* [87] and the corresponding IPMCs actuator exhibit improved response time, displacement and no observed back-relaxation. Very recently, Tang *et al.* [88, 89] first developed sulfonated polysulfone (PPS) and sulfonated polyphenylsulfone (SPPSU) membranes based IPMCs actuators which show enhanced ionic exchange capacity and water uptake capacity. The electromechanical properties were also improved including fast response which is several times higher than the Nafion based IPMCs actuator and excellent fatigue resistance under sustaining sinusoidal electric stimulation. Another group of used electrolyte layers is the polymer supported ionic liquids (ILs) in which no ion-exchange membrane is used. As organic salts consisting of only ions, ILs have attracted much attention for applications in many fields of chemistry and industry due to their chemical stability (non-flammability), thermal stability, negligible vapour pressure combined with high ionic conductivity (10^{-4} - $8{\times}10^{-2}$ S cm^{-1}) and wide electrochemical stability window (as high as 5.7 V) [90, 91]. Fig. 1.10 shows the chemical structure of commonly used imidazolium-ion-based ILs. The combination of no-volatile

ILs with supported polymers converts liquid electrolyte into a promising solid electrolyte membrane, and the performance decline of traditional IPMCs caused by losing of water due to evaporation and electrolysis no longer exists. Meanwhile, it has been demonstrated [93] that the electrode materials with complicated structures play much more important role in influencing the final performance of IPMCs actuators than the electrolyte layers since the actuation of IPMCs arises from the volume change of the electrodes due to the accumulation and depletion of the ions. Electrodes with proper flexibility, high conductivity and well arranged ion-migration path will greatly enhance the electromechanical performance of IPMCs actuators. The unique structure of CNTs and graphene allow them possessing excellent mechanical and electrical properties which make them the ideal flexible electrode materials as a promising alternative of the conventional noble metal materials.

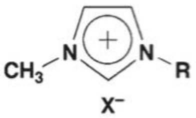

[emim][BF$_4$] : R = C_2H_5, X = BF_4
[emim][Tf$_2$N]: R = C_2H_5, X = $(CF_3SO_2)_2N$
[bmim][BF$_4$] : R = C_4H_9, X = BF_4
[bmim][PF$_6$] : R = C_4H_9, X = PF_6
[bmim][Tf$_2$N]: R = C_4H_9, X = $(CF_3SO_2)_2N$
[omim][PF$_6$] : R = C_8H_{17}, X = PF_6

Figure 1.10: Molecular formulas and schematic structures of typical imidazolium-ion-based ionic liquids [92].

By taking advantage of polymer supported non-volatile ILs electrolyte layer and carbon-based electrode materials, the new generation IPMCs actuators with greatly improved performance have been reported in the past several years. For instance, Asaka's group conducted a lot of remarkable investigation of SWNT and ILs based IPMCs actuator. In 2005, Fukushima *et al.* [94] reported the first dry actuator in which bucky-gel electrode layer containing well dispersed SWNT, ILs 1-butyl-3-methylimidazolium tetrafluoroborate (BMIBF$_4$) and supporting polymer poly(vinylidene fluoride-hexafluoropropylene) [P(VDF-HFP)] and electrolyte layer including BMIBF$_4$ and supporting polymer P(VDF-HFP) were fabricated via a simple layer-by-layer casting of SWNT and BMIBF$_4$ in the gelatinous P(VDF-HFP). The as-prepared actuator can response fast and operate in air for a long time with only 20 % decrease of the initial displacement after being actuated for 8000 cycles. And generated strain of 0.9 % (comparable to the SWNT sheet based actuator [62]) and stress of 0.1 MPa were observed at an applied voltage of ± 3.5 V (0.01 Hz). Whereafter, ball-mill method was used to create electrode with high content well dispersed CNTs, contributing to a bucky-gel IPMCs with a maximum stress and strain of 4.7 MPa and 1.9 % (± 2.5 V), respectively [95]. And it also features a maximum strain rate of 0.29 %/s, response frequency more than 30 Hz and a lift-time more than 9000 cycles. Detailed electromechanical behavior of this kind of IPMCs was investigated by Takeuchi *et al.* [96] concluding that both the steric repulsion effect due to the transfer of ions to the electrode and 'the charge injection' give the bending motion of the bucky-gel actuator. However, the robust supporting polymer lowers the ionic conductivity and capacitance of the electrode layers. The second generation SWNT actuator with of polymer-free electrode was developed by Mukai *et al.* [97] in 2009. The resulting electrode sheet via casting the solution of millimeter-long 'super-growth' carbon nanotubes (SG-SWNTs) and ILs 1-ethyl-3-methylimidazolium bis(trifluoromethylsulfonyl)imide (EMITFSI) exhibited very good mechanical properties (Young's modulus of 156 ± 59 MPa, breaking strength of 17 ± 4 MPa), high conductivity (169 S/cm) and capacitance (45 F/g at a sweep rate of 1 mV/s). The corresponding actuator underwent a fast response (4 mm per 0.05 s), with observed strain rate of 2.28 %/s, and related stress rate of 3.26 MPa/s and a durability upon 10 000 times continuous operations(± 1 V, 1 Hz) in air without any notable deterioration.

Continuous efforts have been put on careful design of hierarchal structure of electrodes in order to facilitate the transport of ions which determines the final performance of the IPMCs actuators. Li *et al.* [98] reported a novel SWNT based IPMCs actuator, in which chitosan electrolyte layer consisting of an ionic liquid is sandwiched by two as-grown SWNT electrodes. Since the hierarchal SWNT electrode synthesized by floating catalyst chemical vapor deposition (FCCVD) has a high electrical conductivity (2000 S/cm), Young's modulus (5 GPa) and stregth (360 MPa), the actuator shows enhanced mechanical properties (Young's modulus of 1-2 GPa and an average strength of 50 MPa), leading to high mechanical output work and power densities (244 W/kg). More importantly, it has a super-fast response of 19 ms, quite wide available frequency range (dozens to hundreds of hertz) and incredible large stress generating rate (1080 MPa/s). The excellent performance arises from the hierarchal structure of SWNT electrode and the compatibility of SWNT with chitosan and ionic liquid. Recently, vertically-aligned nanomaterials have been introduced into the electrode layer to provide the continuous path for the ion transport. For example, vertically aligned carbon nanotubes (VA-CNTs) based Nafion-IPMCs actuator shows fast actuation speed (> 10 %/s) due to the fast ion migration within the interface of electrolyte and electrode and also within the electrode. A remarkable large strain more than 8 % is also achieved [99]. Wu *et al.* [100] also demonstrated a hierarchically structured electrode with vertically aligned NiO nanowall arrays *in situ* grown on a free-standing graphene-carbon nanotube hybrid film. The large specific surface area and fast ion transmission channels of this kind of electrode realize large deformation in short time (18.4 mm per 0.05 s), high strain and stress rates (8.31 %/s and 12.16 MPa/s) and excellent durability upon 500 000 times continuous operations in air.

As discussed above, the development of IPMCs actuators went through a evolution from the traditional Nafion-based IPMCs to the new generation ILs and carbon-based ionic-polymer-conductor network composites (IPCNCs). Various material choice of the electrolyte system and multi-level electrode design form one-dimensional CNTs to three dimensional hierarchal and hybrid material system provide great potential for the development of next generation of IPMCs actuators. Even great advances have been achieved for IPMCs actuators, there are still some drawbacks which restrict their wide applications, such as long response time, low and narrow available frequency range and low output power. Potential applications such as biomimetic robot fish [101,102], biomedical devices and human friendly applications [87] have been under investigation. Medical and industrial products based on IPMCs or IPCNCs as biomimetic nanosensors, nanoactuators, nanotransducers and artificial muscles are extensively being developed by Environmental Robots Inc.[7], the current world's leader company of IPMCs products.

1.2.2 Electronic EAPs

1.2.2.1 Dielectric elastomers

Development history and actuation principle

The actuation behavior of dielectric elastomers (DEs) was first observed in a natural rubber strip that was charged and discharged by Roentgen [13] in 1880. However, Roentgen contributed the observed volume changes to the thermal effect of electric field. In fact, A DEs actuator device has a capacitor structure, in which a dielectric elastomer film is sandwiched by tow compliant electrodes. As shown in Fig. 1.11, when an electric field is applied to the DEs film, charges on opposite electrodes will attract one another, resulting in a reduction in thickness as well as a concomitant increase in area since the material is incompressible. Likewise, charges on each electrode with same sign will also repel each other causing an increase in area and a concomitant reduction in thickness. The stress generated by electrostatic force form charges on opposite electrodes is well known as Maxwell stress, the magnitude of which is determined by the dielectric permittivity of the elastomers and the applied electric field. In order to realize a high Maxwell stress, DEs should have a high dielectric permittivity and operate at a relatively high electric field. The corresponding actuation strain is dependent on the Young's modulus of the elastomer. To ensure a high performance actuation with high elastic energy density, the DEs have to meet the requirements such as high dielectric permittivity, high breakdown strength and a moderate Young's modulus.

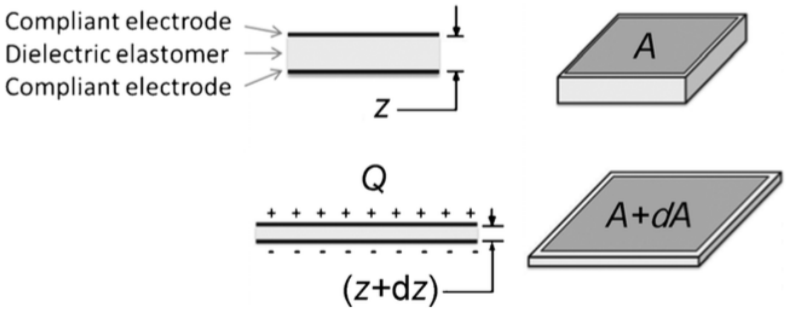

Figure 1.11: The actuation principle of dielectric elastomers [40].

The investigation of DEs actuators began in 1990s [103, 104], and the generated strain is up to 30 to 40 %. The performance is mainly limited by three failure: Pull-in, dielectric breakdown and mechanical break [105]. The pull-in failure is a fundamental limit to

---

[7] http://www.environmental-robots.com

materials with a pure linear elasticity which behave as the material's mechanical instability and collapse due to the electromechanical instability when the thickness strain is over 33 %. In 2000, a great breakthrough of DEs actuators with significantly enhanced actuation performance was made by Pelrine *et al.* [34]. In their work, biaxial or uniaxial stretch was used to prestrain the DEs films, resulting actuated area strains up to 117 % for silicone elastomers and up to 215 % for acrylic elastomers, respectively. It has been demonstrated that prestrain can provide an increase of dielectric breakdown strength (DBS) which can be explained by thermodynamic stability criterion [106] and it likely prevents pull-in failure [35]. Since then, prestrain as an efficient approach to achieve high performance DEs actuators with area strain level exceeding 100 % has been widely used.

DE materials

The commonly investigated DEs mainly include three different materials: acrylates, silicons and polyurethanes (PUs).

DEs based commercially available 3M VHB acrylics have shown the most promising strains up to 380 % in area for highly prestrained films. Furthermore, the elastic energy density (work density, 3.4 J/cm^3, which is about 400 times higher than that of nature muscles), stress (up to 8 MPa) and electromechanical conversion efficiency (60-90 %) are all extraordinarily high [107]. The acrylates has a low modulus (1-2 MPa) enable that they can be prestrained on the order of 200-300 %, much higher than the other elastomers for which prestrain is limited to less than 50 %. However, there are some drawbacks for acrylate elastomers which imped their commercial applications such as their sensitivity to temperature and humanity as well as slow response time owing to the viscoelasticity of the polymer network [40].

Silicone elastomers are the basis of the commercials products from Bayer MaterialScience under intense investigation. Silicone elastomers consist of a silicon-oxygen backbone with two side groups covalently attached to Si atoms. Compared to acrylate elastomers, silicon elastomers shows a moderate actuation performance due to its low dielectric permittivity ($\varepsilon_r \sim 3$), which results from its non-polar nature and low modulus (0.1-1 MPa). The maximum electromechanical coupling efficiency, which is in the range of 63-79 % is a little lower than that of acrylate [38]. Moreover, the self-reinforcing behavior decrease the application of prestrain as a efficient way to improve the actuation performance of DEs. In spite of these, silicon elastomers feature higher resistance than acrylates leading to a lower leakage current, low viscoelasticity contributing to a fast response and stable actuation performance owning to less sensitivity to the environment conditions. More importantly, they are bio-compatible. And therefore, silicon elastomers have great potential for practical actuation applications.

PU is another group of elastomers used as actuators. Unlike the strictly chemically crosslinked acrylate and silicon elastomers, PU can be chemically as well as physically crosslinked since the significant hydrogen-bonding and/or crystalline of polyurethane can act as crosslink point. The thermoplastic nature of physically crosslinked PU makes it can be processed very easily to the desired configuration. Another advantage for PU is the relative high dielectric constant (∼ 7) originating from its polar nature of the polyurethane fragments which allows that PU can be operated at a relatively low electric field. Like acrylate elastomers, the high polarity of PU also lead to a sightly sensitivity to humidity compared to silicons. Also PU is kind of limited to its ability to generate large strain [35]. The properties of representative DEs materials are shown in Table 1.2.

Table 1.2: Properties of several DE films [40].

Elastomer materials	Film thickness (μm)	Strain at break (%)	Young's modulus at 50 % (MPa)	Relative dielectric constant at 1/8 Hz	Breakdown strength (MV/m)
Polyurethane TPU LPT 4210 UT 50	50	421	3.36	6.0	218
Polyurethane Bayfol EA102	50	300	1.44	7.1	130
Silicon proprietary	45	422	0.25	2.4	80
Acrylate VBH 4905	498	879	0.04	4.5	31

Performance enhancement of DE actuators

Much efforts have been made to improve the performances of DEs actuation devices. Acrylate elastomer films possess excellent actuation strain, energy density and electromechanical efficiency but suffer from temperature sensitivity and viscoelasticity, which limits their overall efficiency, the maximum response frequency and response speed. The addition of low molecular weight plasticizers can widen the temperature range, increase the response frequency of acrylate elastomer and decrease the modulus without sacrificing the elasticity [108, 109]. The volatilization or migration nature of plasticizers which will limit the lifetime of DEs devices can be solved by reactive plasticizers or monomers, which can be grafted to the existing elastomer network or react together to form an inter-penetrating network (IPN). The formed IPN can reduce the viscoelasticity limitations of acrylate elastomers [110]. An IPN within acrylate elastomer was synthesized by Ma *et al.* [111] and interestingly, such an IPN can efficiently acts as the frame support of prestrain instead of the additional bulky frame support, leading to a high power-to-mass ratio. Without externally applied prestrain, the IPN containing 3M VBH films underwent a thickness strain up to 75 %, with a stress of 5.1 MPa, an energy denstiy of 3.5 MJ/m^3, coupling efficiency of 94 % and a DBS of 420 MV/m [112].

For DEs, one key issue is to reduce the high operating voltage to remove the danger associated with the high voltage and consequently increase their commercial viability. There are two major ways to reduce the operating voltage: increasing the dielectric constant and reducing the thickness of the elastomer films. The reduction of thickness can benefit of keeping the dielectric breakdown and dielectric loss but suffers from increased inhomogeneities and reduced output force. Much works have been done on the enhancement of the dielectric constant via physical approach such us incorporation of particles with high dielectric constant or conductive materials into polymer matrix or by chemical modification such as introduction of polar groups into polymer network. For the physically modified elastomers, various kinds of fillers including organic/inorganic, metallic/ceramic materials have been investigated as a filler introduced into elastomer matrix to improve the dielectric constant of the DEs composite. For instance, an all-organic dielectric-percolative three-component composite composed of high-dielectric copper phthalocyanine oligomer (PolyCuPc) and conductive polyanline (PANI) within PU matrix showed enhanced dielectric properties and improved electromechanical response with an strain of 9.3 % and elastic energy density of 0.4 J/cm^3 under an electric field of 20 MV/m [113]. Recently, Carpi *et al.* [114] reported an silicon elastomer blends with very low content of highly polarizable conjugated poly(3-hexylthiophene)(P3HT) exhibited an increased dielectric constant with a relatively small increase in dielectric loss and a reduction of tensile modulus. The best electromechanical response was obtained for a blend with 1 wt.% P3HT, providing a transverse strain of 7.6 % at a very low electric field of 8 MV/m.

Inorganic ceramic materials such as titanium dioxide (TiO_2) [115] and lead magnesium niobate-lead titanate (PMN-PT) [116] were also introduced into DEs, achieving elevated dielectric constant. However, such an composite approach even improved the dielectric constant but also met with the concomitant increase of dielectric loss and reduction of DBS as well as influences on the elastic modulus due to the addition of high modulus fillers. One possible way to solve this problem is the filler-polymer matrix interface modification. For example, Molberg *et al.* [117] reported a reliable elastomer composites with increased dielectric constant and high dielectric strength. In their work, conductive PANI particles were encapsulated into an insulating polymer divinylbenzene (DVB) shell via miniemulsion polymerization and then dispersed into polydimethylsiloxane (PDMS) elastomers. The composite showed a more than threefold increase in dielectric constant, breakdown field strengths above 50 MV/m (a high value for conductive polymer/polymer composites), and increased strain at break. Besides composite approach, chemical graft of polar groups offers another method to improve the DEs performances. As shown in Fig. 1.12, push-pull dipoles (N-allyl-N-methyl-p-nitroaniline) are chemically grafted to PDMS networks through silicone crosslinking chemistry. The resulting elastomer possess un homogeneous structure at molecular scale, yielding an increased dielectric constant (from 3.0 to 5.9) and decreased elastic modulus (from 1900 to 550 kPa) and contributing to an improvement of the actuation response of more than six times [118].

Compliant electrodes

In addition to DEs materials, compliant electrodes also play a very important role in the actuation performance of DEs actuator devices. A good electrode must closely adhere to the elastomer films and follow the deformation without constraining it either mechanically or electrically [40]. That is to say, the electrodes should maintain high

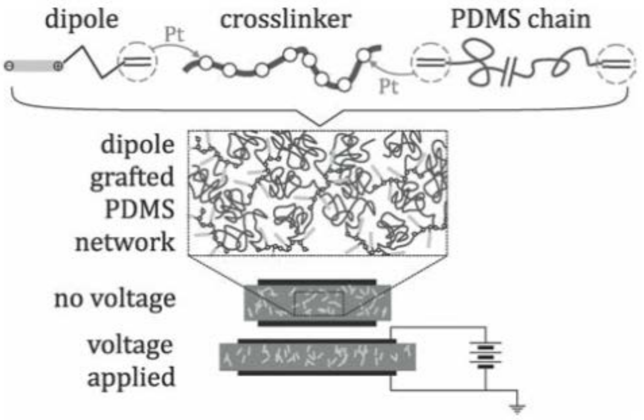

Figure 1.12: Schematic illustration fo dipole functionalization of the PDMS elastomer network and actuation mechanism [118].

conductivity at large strain, have negligible stiffness (softer than elastomers), good stability and fault tolerance. Therefore, the electrodes are defined as compliant. Common solutions of compliant electrodes include metallic paint (silver grease or paint) and carbon based electrodes (carbon black powder, carbon grease, graphite and CNTs). Detailed information can be refereed to a review written by Rosset *et al.* in 2013 [119]. Some representative advances of compliant electrodes will be presented here.

For thin metal film electrode, the Young's modulus is several orders of magnitude higher than that of dielectric elastomers (50-100 GPa compared to 0.2-1 MPa), which will have a significant stiffening impact on the elastomer, leading to a negligible actuation strain. And also, the limit of elasticity for metals is very low, typically 2-3 % and if a metal electrode is strained above this limit, it will crack and form islands separated by non-conductive polymer. Solutions such as patterned electrodes [120], of out-of-plane buckled electrodes [121], and of corrugated membranes [122] have been investigated as compliant metallic electrodes. Recently, a metal ion implantation technology was first demonstrated by Rosset *et al.* [123]. Nanometer-size metal clusters 50 nm below the surface of PDMS elastomer films were created by filtered cathodic vacuum arc. When the elastomer is stretched, these small clusters can move relative to one another, maintaining electrical conduction at strains of up to 175 %. Among three tested metals (gold, palladium, and titanium), gold has the best performance, combining low and stable surface resistance, very high strain capabilities before loss of electrical conduction, and low impact on the Young's modulus of the PDMS membrane. These electrodes are cyclically strained to 30 % for more than 10^5 cycles and remain conductive. Since they remain conductive at high strain and can sustain large numbers of cycles without electrical or mechanical failure, metal-ion-implanted electrodes represent a promising technology to make easily patternable electrodes for EAPs devices.

It has been demonstrated that [124], conductive PANI nanofibers, P3DOT, and CNT thin films are capable of forming highly compliant electrodes with fault-tolerant behavior. Prestrained VHB 4905 films with PANI nanofiber electrode provided a maximum area strain of 97 % at 3 kV, fault tolerance, and had a negligible influence on the mechanical properties of the film [125]. Compared with carbon grease, graphite, and carbon powder electrodes, ultrathin CNTs electrodes show very impressive "self-clearing" capability, which means when a local breakdown happens, the actuators can well recover from the local failures and retain the high actuation strains [126]. The introduction of a thin layer of dielectric oil on the CNTs electrodes effectively reduces the corona discharging in air due to the high voltage, further improved the lifetime of the DEs actuators [127]. The improvement of electrodes materials will promote the commercial application of DEs actuators.

Configurations and applications of DE actuators

The applications of DEs actuators are designed based on both area expansion and thickness reduction of DE film with various configurations such as rolled (spring and core free), tube, unimorph, bimorph, stretched- frame, diaphragm, bowtie, spider, and extender [35]. Among them, two most interesting device designs are the spring roll and stacked actuator, since both of them are able to effectively couple the deformations of

(a)

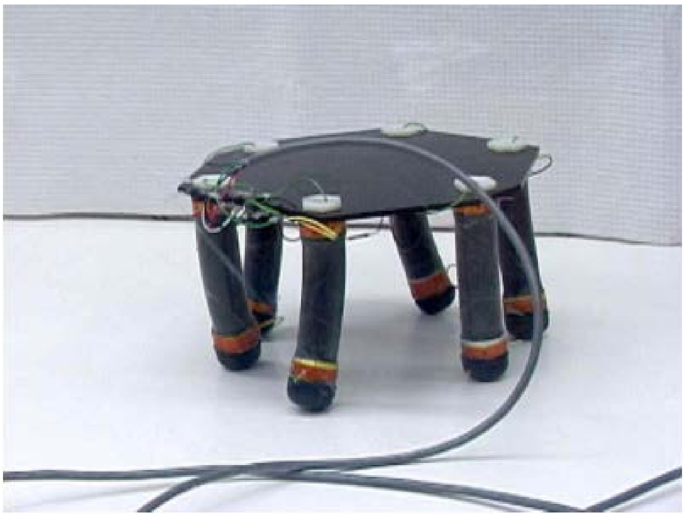

(b)

Figure 1.13: DE actuators with spring roll configuration. (a) Fabrication of spring roll actuator; (b)Robot: a six-legged robot with 2-degree-of-freedom spring rolls as legs [35, 128].

DEs to provide linear actuation. Fig. 1.13a shows the fabrication of a spring roll actuator by compressing a spring between two endcaps and rolling a DE/electrode/DE/electrode layered strip around it, and a robot with six legs consist the 2-degree-of-freedom spring rolls is shown in Fig. 1.13b [128]. For stacked and folded configurations consisting of tens to thousands of DE films stacked together, thickness reduction is used as their actuation way [129]. Due to its excellent electromechanical response, DEs have variety of applications, such as micro-electromechanical systems (MEMS), robot, force and strain sensors. And there are already some commercial products. For example, Bayer MaterialScience have developed EAP actuator which can enhance the sound dimensions of headphones[8].

1.2.2.2 Liquid crystal elastomers (LCEs)

Liquid crystals are unique molecular materials because of the large anisotropies in many of their properties, such as the dielectric, optical and mechanical anisotropies. As early as 1975, de Gennes and his co-worker Chung [130] predicted that the reorientation of liquid crystal molecular (known as mesogens) during a phase transition could lead to a mechanical strain and stress. However, the liquid crystal has a crystalline ordering only in one dimension, perpendicular to the layer planes. In the other two dimensions, they have a liquid-like structure. Therefore, static forces is impossible to built inside liquid crystal and they can neither sustain nor exert mechanical stress. Liquid crystal elastomers (LCEs), just as the name implies, they combine the orientational ordering properties of liquid crystal and the elastic properties of elastomers. By incorporating mesogens into a flexible polymer backbone or as a side chains, the reorientation capacity of mesogens is sufficiently kept, and meanwhile, the free flow of mesogens is prevented by their bonds to the polymer network. The stress or strain originating from mesogens changes upon external thermal or electrical stimuli can be transfered to the bulk LCEs via the bond and backbone to perform mechanical work. As a result, LCEs can be used to produce the electric field-induced actuation.

The basic actuation principle of LCE is shown in Fig. 1.14. In LCEs, the polymer chains experience an anisotropic environment due to the introduction of the anisotropic mesogens of liquid crystal. When such an elastomer loss its anisotropy upon the external stimuli, an isotropic chain conformation will be adopted again and the sample as a whole will have to change its shape [131]. There are two different categories of liquid crystal depending on the phase present: nematic and smectic (see Fig. 1.15). This principle is true for all LC phases, but the details of this process and the physical properties of networks for nematic and smectic phases are different. LCEs can be chemically synthesized with three distinguished structures: the mesogens are introduced into the main chain of polymer, or can be attached as side-chains via flexible spacer at the ends (end-on) or in the middle (side-on) of mesogens.

LCEs can be activated thermally, optically and electrically [132–136]. Thermally acti-

---

[8] http://www.sri.com/engage/products-solutions

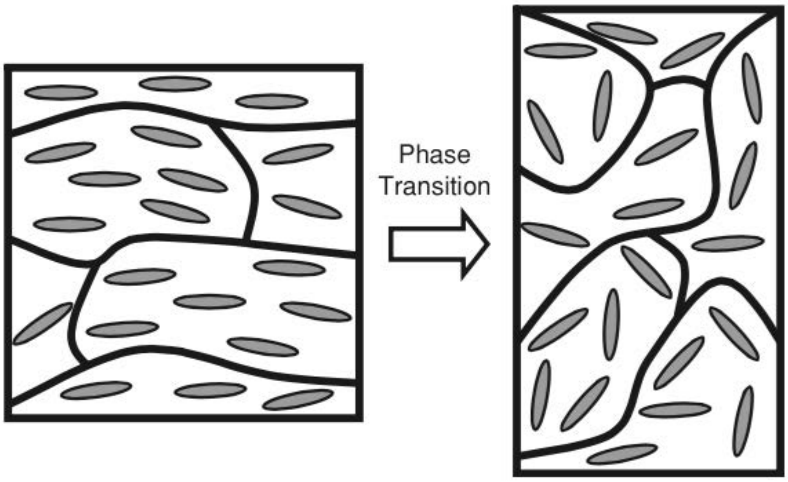

Figure 1.14: Schematic illustration of actuation principle of LCEs [131].

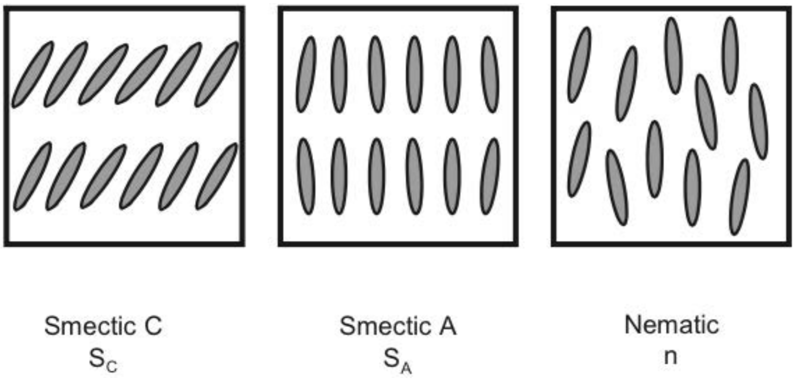

Figure 1.15: Different types of liquid crystal: In smectic C phases, the mesogens are additionally tilted towards the layer normal; Smectic A phases exhibit a layered structure with the mesogens parallel to the layer normal; In the nematic phase, the mesogens posses a short-range order and are aligned parallel in a uniform direction [131].

vated LCEs display length changes up to 400 % [137,138], but their response rate is limited to the heat diffusion process and also there is the thermal relaxation problem [35]. Here, I will put the focus on the electrically activated LCEs. Given the dielectric anisotropy properties, the intrinsically polarized mesogens can reorientation in the presence of electric field, generating the bulk LCEs stress and strain [139]. Unlike thermal energy, electric field can be applied on LCEs very quickly, contributing to a very fast electromechanical response. The response speed of LCEs is greatly dependent on the used mesogens, the polymer backbone structure and the degree of cross-linking. In 2001, Lehmann *et al.* [33] reported an ultrathin (less than 100 nm) ferroelectric LCEs film which exhibited a strain of 4 % at a very low electric field of 1.5 MV/m at 133 Hz.

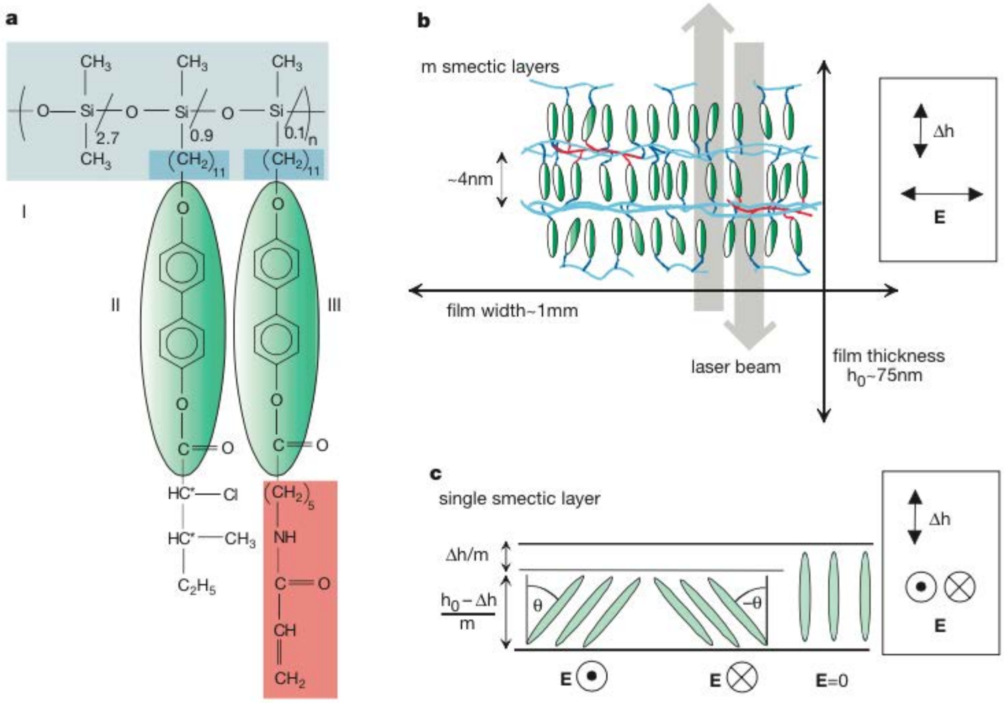

Figure 1.16: The electroclinic effect in ferroelectric liquid crystalline elastomers. (a) The chemical structure of ferroelectric LCEs. I (blue), the polysiloxane backbone; II (green), the core of the chiral mesogen; III (green), the core of the crosslinkable mesogen; Red part,the crosslinkable end group of the mesogen. (b) Scheme of the measurement geometry. (c) The electroclinic effect [33].

The chemical structure and actuation mechanism of ferroelectric LCEs are shown in Fig. 1.16. The large electrostricitive strain originates from the combination of electroclinic effect (see Fig. 1.16c) of the ferroelectric liquid crystal and polysiloxane network. And the ferroelectricity and piezoelectricity properties of ferroelectric LCEs mainly arise from the uniqueness of the chiral smectic mesogens since the tilt of the mesogens causes a permanent dipole moment perpendicular to the tilt direction [131,140]. The reported Young's modulus of ferroelectric LCEs is below 3 MPa and hence, the corresponding elastic energy density is below 0.002 J/cm^3. In order to improve the elastic energy density, an nematic anisotropic

LCE was investigated by Huang *et al.* [139]. A high electromechanical response (thickness strain > 2 %) with a high electromechanical conversion efficiency (~75 %) were observed under an electric field of 25 MV/m for a homeotropically aligned nematic LCE, which also possesses a relatively high elastic modulus (100 MPa) along the actuation direction, leading to an elastic energy density of 0.02 J/cm^3. However, the use of rigid LCEs results to a low response frequency of 1 Hz.

In general, actuators based electrically activated LCEs feature fast response speed (10 ms) [33] at a relative low electric field, strain less than 10 % and a low elastic energy density due to the low Young's modulus. The possibilities of applications are wide and range from micromechanical systems (e.g., in atomic force microscopes, as valves in microfluidic systems, as artificial muscles in robots) to propulsion systems and active smart surfaces, which can change their properties according to the environment [131, 141].

1.2.2.3 Fluoride-based electrostrictive polymers

From a structure-property point of view, a piezoelectric material should be a crystalline material lacking a symmetric center. The highly electro-negative fluoride atom with a very small van der Waals radius (1.35 Å), which is only slightly larger than that of hydrogen (1.2 Å), can form a highly polar fluoride-carbon bond with a dipole moment of $\mu = 6.4 \times 10^{-30}$ C·m, and consequently, the fluoride polymers can form multiple crystalline structures through molecular design and material process conditions. The ferroelectricity origin of PVDF was explained in detail by Lovinger [142] in terms of structures at different levels from the molecular chains, and chains conformations to crystalline phases. As depicted in Fig. 1.17, there are two most common chains conformations in PVDF: the alternative *trans-gauche-trans-gauche'* [$TGTG'$ or tg^+tg^-] conformations and *all-trans* conformations. For *all-trans* conformation, all the dipoles align in the same direction essentially perpendicular to the molecular axis, contributing to the most highly polar conformation in PVDF ($\mu = 7.0 \times 10^{-30}$ C·m per repeat). While for the tg^+tg^- conformation, due to the inclination of dipoles to the chain axis, it has dipole moment both parallel ($\mu = 3.4 \times 10^{-30}$ C·m) and normal ($\mu = 4.0 \times 10^{-30}$ C·m) to the chain axis. PVDF is a polycrystalline polymer and has four major crystalline phases. Among them, β-phase and α-phase are the most common phases for practical ferroelectric and piezoelectric applications, and the other two phases (γ-phase and δ-phase) only exist at some special conditions. In β-phase, two *all-trans* chains are packed with their dipole pointing to the same direction into individual orthorhombic unit cells, having lattice dimensions of a = 8.58 Å, b = 4.90 Å and chain direction c = 2.56 Å. Such a crystalline structure without a symmetric center and the existing polarization are responsible for the piezoelectric and ferroelectric properties of PVDF. α-phase has two tg^+tg^- chains packed in orthorhombic unit cell, whose dipole component perpendicular to the chain axis are anti-parallel, canceling each other. The dipole direction along the chain axis consist of a statistical average of up-up and up-down orientation. The resulting orthorhombic α-phase has a lattice dimensions of a = 4.96

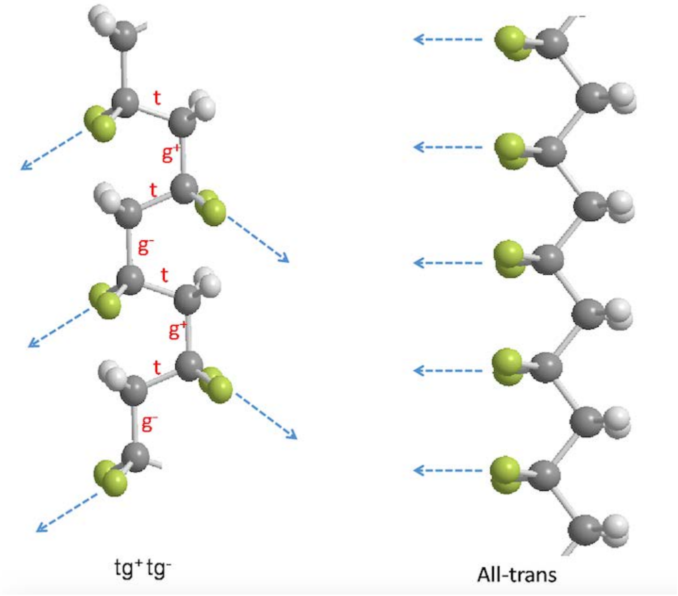

Figure 1.17: Schematic description of two most common conformations of PVDF. The left one is $tg^{+}tg^{-}$ and the right one is *all-trans*, the yellow sphere represents fluorine atom, the white sphere represents hydrogen atom and the grey sphere represents the carbon atom. The arrows show the projections of -CF_2 dipole direction on planes defined by the carbon backbone.

Å, b = 9.64 Å and chain direction c = 4.62 Å. And α-phase is a non-polar phase without piezoelectric and ferroelectric properties. Unfortunately, PVDF crystallizes directly into a non-polar α-phase rather than ferroelectric β-phase from the melt crystallization or solution cast. Even there are ferroelectric β-phase domains in stretched PVDF, these crystallites are randomly oriented within bulky PVDF, displaying the absence of overall piezoelectricity for the bulky PVDF. In order to obtain the piezoelectricity, PVDF thick films have to be mechanically stretched several times of its original length and poled under an electric field more than 100 MV/m at an elevated temperature. Such a complicated fabrication process has kind of limited the development of PVDF-based electroactive devices. Moreover, the electromechanical applications of PVDF are mostly based on the piezoelectricity, exhibiting very small strain which is far insufficient for high performance actuators' application.

Unlike PVDF, copolymer P(VDF-TrFE) exhibits a directly formed ferroelectric β-phase from melt crystallization and solution cast. It has been demonstrated that [143], P(VDF-TrFE) copolymer with a VDF content from 12.5 to 85 % always shows the ferroelectric β-phase and can not be transformed into α-phase by any thermal treatment. Moreover, a high room temperature dielectric constant (15 at 1 kHz) which is about 2 times higher than that of both PVDF and PTrFE is observed for 55 %VDF copolymer due to its high content of head-to-tail sequences (-CF_2-CH_2-CF_2-CHF-). One important issue for P(VDF-TrFE) copolymer is its ferroelectric-to-paraelectric (F-P) transition which involves a phase transition from polar *all-trans* chains to a non-polar mixture of *trans* and *gauche* chains. The TrFE molecules in copolymers acting as defects in PVDF polymer chains contribute to a deceased Curie temperature (T_c) with the increased TrFE content and the Curie temperature is below melting temperature (T_m) which is different with the pure PVDF (as shown in Fig. 1.18). And also, the F-P transition appears most clearly for copolymers containing 50-80 %VDF at temperatures from 70 to 140 °C [144]. As mentioned above, ferroelectric phases which consist of *all-trans* conformation have a unit cell with a large lattice constant along the polymer chain direction and a small unit cell dimension perpendicular to the chain, while paraelectric phases which adopt a mixture of *trans* and *gauche* conformations have a significantly shortened unit cell dimension along the chain direction and an expanded cell dimension perpendicular to the chain direction. As a result, such a lattice difference will lead to a lattice strain and a dimensional change for ferroelectric polymers during its F-P transition. In fact, large lattice strains and sample dimensional changes about 10 % have been observed in x-ray diffraction and thermal expansion experiments [25, 145–147]. However, the large strain induced by such a transition is always accompanied with a relative large hysteresis due to the large energy barrier when orienting the large polarization domains and it is unexpected to develop the high-performance electromechanical devices.

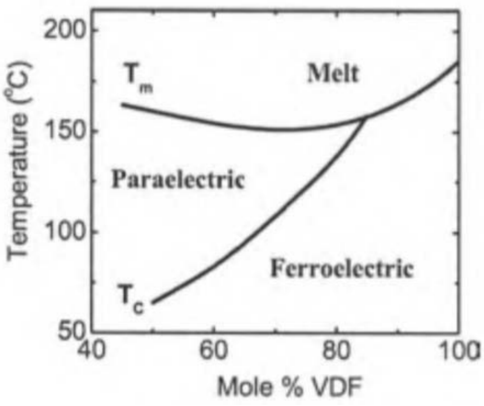

Figure 1.18: Phase diagram of PVDF and P(VDF-TrFE) polymers [144].

A possible approach to solve the large hysteresis problem of ferroelectric materials is to reduce or eliminate the energy barrier by reducing the size of large polarization domains to a nanometer scale. In 1998, Zhang *et al.* [148] reported a high energy electron-irradiated P(VDF-TrFE) 50/50 (50 mol% VDF) with a large longitudinal (or thickness) strain more than 4 % and very little strain hysteresis in response to an applied electric field of 150 MV/m at room temperature. It has been demonstrated that, the electron irradiation breaks up the long-range polar regions into micro non-polar domains (nanometer-size all-trans chains interrupted by trans and gauche bonds) and transforms the normal ferroelectric material into a relaxor ferroelectrics (as shown in Fig. 1.19). Due to the reduction of polar regions, the hysteresis features a slim loop with smaller remnant polarization (P_r) and coercive electric field (E_c) than ferroelectric P(VDF-TrFE) copolymer. As a result, this polymer can response at a wide temperature and frequency range. The electrostrictive properties of irradiated P(VDF-TrFE) were further investigated by Zhang's group [149–151]. Owning to the large anisotropy in the response along and perpendicular to the polymer chain, the transverse strain can be tuned by film stretching. The transverse strain of the stretched film along the stretch direction can reach a comparable with the longitudinal strain. In addition to high strain response, irradiated copolymers also have high elastic energy density ($Y{S_m}^2/2 = 0.5$ J/cm^3) and mechanical load capability (20 MPa) because of the high elastic modulus ($Y = 0.4$ GPa) and high strain level (maximum strain, $S_m = 5$ %). In comparison, the corresponding strain and the elastic energy density for copolymer are 0.15 % and 0.0045 J/cm^3, respectively. A relatively high longitudinal electromechanical coupling factor k_{33} of 0.33 [149] and a high transverse coupling factor k_{33} of 0.45 [151] was also observed for irradiated copolymer. Since the energy conversion efficiency is proportional to the square of the coupling factor, such an improvement is significant.

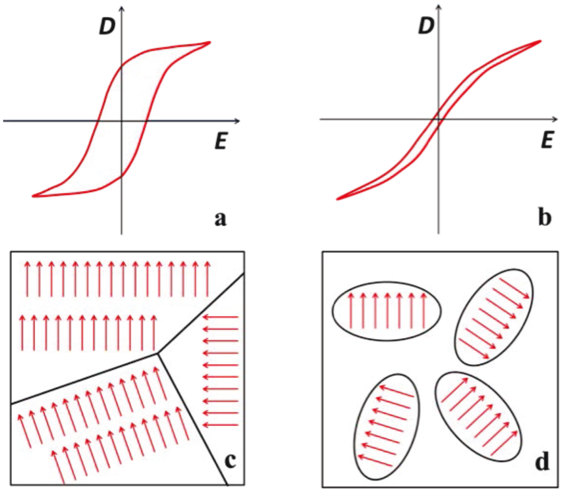

Figure 1.19: Schematic comparison of hysteresis loops (up) and microscopic crystalline structures (down) for ferroelectric (a and c) and relaxor ferroelectric polymers (b and d).

However, high energy irradiation is not a commercially available approach to produce fluoride based EAPs due to its high cost and undesirable side effects to the polymer. Thanks to the richness of fluorinated polymer chemistry, a relatively simple and low-cost alternative method by introducing a bulky monomer such as chlorotrifluoroethylene (CTFE) or chlorofluoroethylene (CFE) into the P(VDF-TrFE) chain to transform a normal ferroelectric copolymer into a relaxor ferroelectric terpolymer has been developed by PiezoTech S.A. France [152, 153] and it is now commercially available [154]. The electromechanical properties of poly(vinylidene fluoride-trifluoroethylene-chlorotrifluorothylene) [P(VDF-TrFE-CTFE)] and poly(vinylidene fluoride-trifluoroethylene-chlorofluorothylene) [P(VDF-TrFE-CFE)] terpolymers were investigated. A thickness strain of 4 % under an electric field of 150 MV/m at room temperature was observed for terpolymer P(VDF-TrFE-CTFE) 65/35/10 [155], and a thickness strain of 4.5 % was achieved for terpolymer P(VDF-TrFE-

CFE) 62/38/4 at a relative low electric field of 130 MV/m [156]. The enhanced electromechanical response compared to P(VDF-TrFE) results from the defects modification effects of the third monomer. The introduction of CFE or CTFE reduced the polar *all-trans* conformation into room temperature stable non-polar phases, in which random oriented nano-polar regions (with *all-trans* conformation) were surrounded by a mixture of *trans* and *gauche* bonds. The large lattice strain associated with the reversible molecular conformation change from $TGTG'$ and T_3GT_3G' to *all-trans* induced by applied electric field, coupled with expansion and contraction of the crystalline domains, generate the large electromechanical strain response [156, 157]. Although both CFE and CTFE can transform the ferroelectric P(VDF-TrFE) into ferroelectric relaxor terpolymer, CFE monomers are more efficient than CTFE monomers in reduction the *all-trans* conformation. It has been demonstrated that, 4 mol% of CFE is adequate to eliminate the large hysteresis of P(VDF-TrFE), but a higher fraction of 10 mol% for CTFE is required to achieve the same reduction of hysteresis [156]. It is worthy to note that the introduction of the third monomer will also lead to a decreased crystallinity and corresponding decreased elastic modulus which is not favorable to achieve a high elastic energy density. Therefore, P(VDF-TrFE-CFE) terpolymer possess a higher elastic energy density and electromechanical coupling factor than P(VDF-TrFE-CTFE) terpolymer (see Table 1.3). Moreover, the introduction of CFE or CTFE also give rise to enhanced dielectric properties with a dielectric constant larger than 45, which is more than 3 times higher than that of P(VDF-TrFE).

Table 1.3: Comparison of electromechanical properties [148, 155, 156].

Materials	Y (GPa)	S_m (%)	$YS_m^2/2$ (J/cm^3)	k_{33}
Piezoceramic	64	0.2	0.13	-
Piezo P(VDF-TrFE)	4	0.15	0.0045	0.27
Irradiated P(VDF-TrFE)	0.4	5	0.5	0.30
P(VDF-TrFE-CTFE)	0.4	4	0.32	0.28
P(VDF-TrFE-CFE)	1.1	4.5	1.1	0.55

Like DEs, the electromechanical performance of fluoride polymers can also be enhanced by improving the dielectric properties via composites means. In 2002, Zhang *et al.* [158] reported an all-organic composite materials based on electrostrictive copolymer P(VDF-TrFE), in which an organic filler copper-phthalocyanine (CuPc) oligomers with very high dielectric constant ($> 10^4$) were dispersed into P(VDF-TrFE) matrix by solution casting method. The as-prepared all-organic composites exhibited a significantly enhanced dielectric properties (dielectric constant of 225 and loss factor of 0.4) and elastic modulus almost the same as the polymer matrix. For 40 wt.% CuPc containing composite with a elastic modulus of 0.75 GPa, a strain about 2 % and a elastic energy density of 0.13 J/cm^3 were observed at a very low electric field of 13 MV/m, which corresponds to the breakdown strength. Conductive fillers such as conductive polymer or carbon materials were also incorporated into polymer matrix to improve the electromechanical properties of fluoride based polymers. For instance, with a PANI volume fraction of 0.251, a very flexible P(VDF-TrFE-CTFE)/PANI all-organic composite with a very high dielectric constant up to 7000 was achieved, and consequently, a strain of 2.65 % with an elastic energy density of 0.18 J/cm^3 were observed under a field of 16 MV/m, which is nearly one order of magnitude reduction in the applied field level compared with that of the polymer matrix [159]. P(VDF-TrFE-CFE)/ CNTs composite with 0.5 wt.% CNTs, showing a strain of nearly 2 % and an elastic energy density of 0.028 J/cm^3 under a field of 54 MV/m was reported by Zhang *et al.* [160]. One problem for these composites is the decreased breakdown strength which limits the capability to get a much better electromechanical response of fluoride polymers.

In general, electrostrictive fluoride polymers feather high room temperature relative dielectric constant (~ 50), which is the highest among all the known polymers, high induced polarization (~ 0.05 C/m) and high electric breakdown field (> 400 MV/m) [161]. Therefore, electroactive fluoride polymers can generate a high electrostrictive strain (> 7 %) and high stress (~ 45 MPa) [11] with relatively high modulus (> 0.4 GPa), and a high elastic energy density up to 1.1 J/cm^3. Moreover, it has been also observed that the large electrostrictive strain is nearly constant in the temperature range from 20 °C to 80 °C and the fluoride polymer can response very fast with a wide operating frequency range from low frequency to 100 KHz [11].

Based on the excellent properties such as high dielectric constant, ferroelectric, piezoelectric, pyroelectric properties and impressive electromechanical response, fluoride polymers have a wide range of potential applications. Organic electronics such as organic solar cells [4], memory devices [6], generators [3] and printed sensors [2, 162] with fluoride polymers have been under investigation. Due to the high electromechanical response capabilities, electroactive fluoride polymers are more attractive than other electroactive polymers for actuator-based applications. A microfluidic pump based on high-energy irradiated P(VDF-TrFE) unimorph actuators was realized by integrating a nozzle/diffuser type fluidic mechanical-diode structure with the polymer microactuator [164]. The actuator was observed to pump methanol at a rate of 25 μL/min at 63 Hz with a back pressure of 350 Pa and the flow rate can be easily controlled by external electrical field. An efficiency

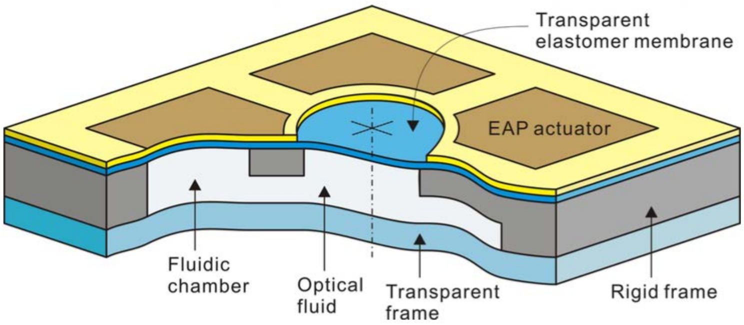

Figure 1.20: Scheme of the liquid-filled varifocal lens [163].

of 11.7 % was deduced for the fabricated nozzle/diffuser pump. Choi *et al.* [163] developed a liquid-filled varifocal lens on a chip operated by electroactive polymer actuators. When an electric field is applied, the multilayered P(VDF-TrFE-CFE) polymer actuators push the optical fluid so that the elastomer membrane together with the internal fluid changes their shape, which alters the light path of the varifocal lens (see Fig. 1.20). Optical analysis showed that the deformation shape of the optical membrane could be successfully used to design phone camera modules with auto-focus function.

1.2.3 Comparison of different EAPs

1.2.3.1 Figures of merit for EAPs actuators

Before comparison of different EAPs, some important figures of merit used to evaluate the performances of EAPs actuators are described in this part [11].

Strain (S) is the size deformation normalized by the original size in the direction of actuation. The most reported strain in the literature are the thickness strain or longitudinal strain (S_3), the transverse strain (S_1) and sometimes the area strain. The maximum strain (Sm) is used to describe the deformation capability of an EAP actuator. It is worthy to note that, the maximum strain generally obtained at free load, not at the peak stress.

Stress (T) gives the typical force per cross-sectional area. The peak stress is the maximum force generated by EAPs actuators, and it is achieved when the displacement of the actuator is completely blocked. Blocking force is measured as follows: The actuator length before operation is recorded. The actuator is displaced without a load to the nominal displacement and then pushed back to the initial position with an increasing external force. The minimum force required for pushing back which is equal to the force generated by actuator, is the blocking force. That is to say, the maximum block stress is the stress under which EAPs can maintain position.

Work density or ***elastic energy density*** is the amount of mechanical work generated in a one actuation cycle normalized by the volume or mass of actuator, in which the power supply, packing electrolyte, counter electrodes are not included. Te volumetric and gravimetric energy density can be described as $YS_m^2/2$, $YS_m^2/2\rho$, respectively, where ρ is density of actuator materials [148].

Specific power or ***power to mass ratio*** is the output power per unit mass of actuator material.

Efficiency or ***electromechanical coupling*** refers to the ratio of converted mechanical work (energy) to the input electric energy [165].

Response time or ***strain rate*** is a parameter to describe the response speed of EAP actuators. It is the average change in strain per unit time during an actuator stroke. The maximum strain rate is usually achieved at high frequency at which the strain is very small. *Bandwidth*, the frequency at which the strain drops to half of its value at low frequency, is also used to describe an actuator.

Operation voltage is the voltage required to actuation of EAPs.

Cycle life is the number of useful strokes that EAP materials are able to undergo.

1.2.3.2 Actuation performance comparison of EAPs

The emerging EAPs represent a promising class of actuator materials which exhibit tunable muscle-like mechanical response in response to applied electrical stimuli. Unlike traditional electromagnetic motors and combustion motors, EAPs do not require large power supply and complicated gear system. In contrast to the other electroactive materials, EAPs can generate strains two orders of magnitude higher than piezoceramics, exhibiting more reliable, faster electromechanical response and longer lifetime than shape memory alloys. As mentioned in previous section, EAPs can be generally divided into two categories - ionic and electronic - based on their actuation mechanism. The electromechanical performance of different EAPs are very different, and a general comparison is shown in Table 1.4.

Ionic EAPs exhibit low strain and low stress. The most important advantage is their low operation voltage (usually 1-2 V). However, the involvement of ion transport process for actuation on the one hand leads to a low response speed and also contributes to a very low energy efficiency on the other hand, since the applied electrical energy is not only stored and converted to mechanical energy, but also used to driven the ion transport. Moreover, the requirement of wet environment (electrolyte) for ion transport and possible encapsulation usually brings about a low specific power and difficulty of miniaturization of systems. For water-contained ionic EAPs, the applied voltage is typically limited to 1.23 V due to water hydrolysis.

The actuation of electronic EAPs originate from the electrostatic force or the dipolar reorientation in response to the applied electric field without ion migration. Therefore, electronic EAPs can exhibit faster response (in the order of ms) and higher efficiency (one order of magnitude higher) than ionic EAPs. DEs always show strains tens to more than hundred percent, but they have small elastic modulus (1-2 MPa), which results into a relatively low stress. A very high electric field is required for DEs to actuate due to their low dielectric permittivity. Also, for most DEs materials, they are sensitive to the environment conditions and hence their electromechanical performance is not reliable. LCEs are electronic EAPs at their new development stage, which feature low operating electric field (< 25 MV/m) and high efficiency (75 %). However, they have small strain and stress level, and hence an associated low work density. Fluoride polymers, especially the ferroelectric relaxor terpolymers show promising electromechanical performances. Their high dielectric permittivity enable them response at an electric field smaller than 150 MV/m with a moderate strain of 7 %. Combined with the higher elastic modulus than DEs, a higher load capability and work density (elastic energy density) can be achieved. As shown in Table 1.4, fluoride polymers exhibit more reliable actuation performances than DEs, and their performance is comparable or better than natural muscle.

Table 1.4: Comparison of properties of different EAP materials.

EAPs	Strain (%)	Stress (MPa)	Work density (kJ/m^3)	Efficiency (%)	Strain rate (%/s)	Voltage (V)	Refs.
Conductive polymer	2	3~5 Max > 100	100	1	$\ll 1$	1-2	[11, 49] [42, 51]
CNTs	0.2	1 Max 26	2 Max 40	0.1	0.6 Max 19	1-2	[11, 61] [63, 65, 73]
IPMCs	0.5 Max 8	3	5.5	3	3.3 Max 10	1-2	[11, 99]
DEs	20-380	0.3-1.6 Max 8	10-150 Max 3400	> 15 Max 94	> 450 Max 34000	> 1000 E > 150 MV/m	[11, 107, 112]
LCEs	2-4	Low	2-20	75	1000	< 1000 E < 25 MV/m	[11, 139]
Fluoride polymer	7	20-45	320 Max > 1000	30 Max 55	> 2000	> 1000 E < 150 MV/m	[11, 148, 150] [151, 155, 156]
Biological muscle	20 Max > 40	0.1 Max 0.35	Max > 40	Max 40	Max > 50	–	[11, 12]

1.3 Work mechanism of electronic EAPs

As reviewed in previous section, EAPs are promising materials which can realize energy conversion between electrical energy and mechanical energy. As a result, EAPs have a various potential applications in fields of actuators, sensors, artificial muscles, robots and energy generators. For electrical EAPs, the electromechanical response of these polymer can be linear such as the typical piezoelectric polymers or nonlinear such as Maxwell stress effect induced response and electrostrictive response. From the basic material consideration, the electromechanical strain response can be contributed to reorientation of dipole moment within material in response to externally applied electric field such as piezoelectric effects and electrostrictive effect, or the electrostatic attraction of charges with opposite signal of two sides electrode of polymer film such as Maxwell effect stress. In this section, a brief introduction of work mechanism of these polymers will be given.

1.3.1 Piezoelectric effect

The piezoelectric effect is the basic electromechanical effect for crystalline materials without symmetric center. There are 32 point groups for crystallines and 20 of them are non-symmetric. Dimension changes of these crystalline materials in response the external stimuli such as electric field will result in a change in electric polarization and hence give rise to occurrence of piezoelectric effect or even pyroelectric (with spontaneous polarization) and ferroelectric effects (with electrically reversible spontaneous polarization).

Piezoelectric effect is a linear electromechanical effect where the mechanical strain (S) and stress (T) are coupled with electric field (E) and displacement (or area charge density, D), expressed as following:

$$S = d\ E, \tag{1.1a}$$

$$D = d\ T, \tag{1.1b}$$

where d is the piezoelectric coefficient. The effect in Eq. 1.1a and 1.1b are known as the converse piezoelectric effect and direct piezoelectric effect, respectively. Adding the linear elastic (Hook's law) and dielectric relations into Eq. 1.1, we can have the constitutive piezoelectric equations [166]:

$$S_{ij} = d_{kij} E_k + s^E_{ijkl} T_{kl}, \tag{1.2a}$$

$$D_i = \varepsilon^T_{ik} E_k + d_{ikl} T_{kl}, \tag{1.2b}$$

where s^E_{ijkl} is the elastic compliance, ε^T_{ik} is the dielectric permittivity and $i, j, k, l = 1 - 3$. Depending on the different boundary conditions, the compete constitutive piezoelectric equations have three other forms, which can be referred to the "*IEEE standard on Piezoelectricity*" [166] for detailed investigation.

1.3.2 Electrostrictive effect

Unlike piezoelectric effect, electrostrictive effect is a quadratic dependence of strain or stress on polarization (P), which exists in all dielectric materials,

$$S_{ij} = Q_{ijkl} P_k P_l, \tag{1.3}$$

where Q_{ijkl} is the charge-related electrostrictive coefficient. For an isotropic polymer,

$$S_3 = Q_{33} P^2, \tag{1.4a}$$

$$S_1 = Q_{13} P^2, \tag{1.4b}$$

where S_3 and S_1 are the strains along and perpendicular to the polarization direction, also known as the longitudinal and transverse strain, respectively. For an isotropic incompressible polymer, experiment and theoretical investigations demonstrate that $S_3 < 0$ and $S_1 > 0$. Hence, the electric field induced polarization will lead to a contraction along polarization direction and an expansion in the direction perpendicular to polarization direction.

For linear dielectrics, the polarization density can be expressed as a function of the dielectric permittivity and electric field,

$$P = (\varepsilon - \varepsilon_0)E = (\varepsilon_r - 1)\varepsilon_0 E, \tag{1.5}$$

where ε_0 is the vacuum dielectric permittivity ($= 8.85 \times 10^{-12}$ F$\cdot$ m^{-1}), and ε_r is the relative dielectric permittivity. Therefore, Eq. 1.4 can be converted into

$$S_E = Q(\varepsilon_r - 1)^2 \varepsilon_0^2 E^2 = M' E^2, \tag{1.6}$$

where M' is the electric-field-related electrostrictive coefficient.

It should be noted that, most polymers exhibit nonlinear dielectric properties, and as a result, the induced strain especially at high electric field exhibits saturation rather than a quadratic relationship as described in Eq. 1.6.

1.3.3 Maxwell effect

When an electric field is applied to a thin dielectric film, charges with different signals on two electrode sides will attract each other, resulting into a electrostatic force which is know as the Maxwell stress. It has been demonstrated that [35, 104], the Maxwell stress across the thickness is proportional to the product of the dielectric permittivity and square of the applied electric field. And the Maxwell strain in the thickness direction can be expressed as [167],

$$S_M = \frac{1}{2}\frac{\varepsilon_r \varepsilon_0}{Y} E^2 (1 + 2\upsilon) = M'' E^2, \tag{1.7}$$

where Y is the Young's modulus of the dielectric materials, υ is the Poisson's ratio, and M'' is the as-defined Maxwell coefficient.

1.3.4 Work principle of electrostrictive polymers

As described above, there are three main effects accounting for the electromechanical response of electronic EAPs: piezoelectric effect, electrostrictive effect and Maxwell effect. The piezoelectric effect is most studied for piezoelectric PVDF and its copolymer P(VDF-TrFE) and the corresponding strain is very small due to they low piezoelectric constant. Electrostrictive effect is associated with the reorientation of dipoles, and it exists in all dielectrics, especially for ferroelectric relaxor polymers due to the large lattice strain during phase transition between polar phases and non-polar phases. Maxwell effect is related with electrostatic force, which exists for dielectrics with collective charges on its two sides. Since DEs are very soft and generally having low dielectric permittivity, Maxwell effect is prominent for their actuation. For electrostrictive polymers with higher dielectric permittivity and elastic modulus, the overall electrostrictive strain originates from both electrostrictive effect and Maxwell effect,

$$S = S_E + S_M = Q(\varepsilon_r - 1)^2 \varepsilon_0^2 E^2 + \frac{1}{2} \frac{\varepsilon_r \varepsilon_0}{Y} E^2 (1 + 2\upsilon) = ME^2, \tag{1.8}$$

where M is the globe electric-field-related electrostrictive coefficient.

1.4 Objective of this work

In this chapter, a brief introduction of development history of EAPs was first presented. And then different EAPs including ionic EAPs and electronic EAPs are reviewed. EAPs are promising actuator materials which exhibit tunable muscle-like mechanical response in response to applied electrical stimuli. With a comparison of actuation performances of EAPs, fluoride polymers are excellent candidate materials for electromechanical applications with moderate strain, high load capacity, high energy density, high efficiency and fast response.

As we can see from Eq. 1.8, the electric field induced strain for electrostrictive fluoride polymers is determined by the dielectric permittivity, dielectric breakdown strength and Young's modulus. In this work, fluoride electrostrictive polymers will be modified with inorganic filler and organic filler to improve their electromechanical performances. The influence of modification on dielectric properties, dielectric breakdown strength, mechanical properties and electromechanical performances of electrostrictive polymers will be carefully investigated. Two electromechanical applications including energy harvesting and micropump based on modified polymers with improved electromechanical performances will be developed and investigated.

Chapter 2

Organic/Inorganic Composites: Terpolymer/Carbon Black Nanocomposites

It has been demonstrated that, a high dielectric permittivity is desirable for electrostrictive terpolymers to reduce the required high actuation electric field and improve the electrostrictive performances at low electric field. In this chapter, an organic/inorganic composite, terpolymer/carbon black nanocomposite, was prepared to improve the dielectric permittivity based on percolation theory. The dielectric properties, dielectric breakdown strength and the mechanical properties were carefully investigated for electrostrictive applications. Results indicated that the introduction of conductive carbon black brought about an enhanced dielectric permittivity, but more significantly reduced dielectric breakdown strength, leading to declined electrostrictive performances of terpolymer.

2.1 Introduction

Electroactive polymers that can convert electric energy to mechanical energy by generating high mechanical in response to external electric field have a variety of attractive applications, such as actuators, sensors, artificial muscles and energy harvesting. Among all of electroactive polymers, ferroelectric PVDF, its copolymers P(VDF-TrFE), and terpolymers P(VDF-TrFE-CFE) or P(VDF-TrFE-CTFE) have been greatly investigated due to their low density, flexibility, processing capability and importantly, the excellent electromechanical response. For instance, a defect-modified P(VDF-TrFE)] exhibited a electrostrictive strain of about 4 % at an electric field of 150 MV/m [148] and a thickness strain of 4.5 % was observed for terpolymer P(VDF-TrFE-CFE) at an electric field of 130 MV/m [156].

As described in Section 1.3.4, strain induced by external electric field for electrostrictive polymers originates from two main effects: electrostrictive strain S_E associated with the interaction of dipoles inside dielectrics and the well-known Maxwell strain S_M resulting from the interaction of free charges on the opposite electrodes (Coulomb interaction). According to Eq. 1.8, the electromechanical strain of electrostrictive polymers is determined by dielectric permittivity, Young's modulus and dielectric breakdown strength (DBS). In order to improve the electromechanical performance of electrostrictive polymers, various fillers including inorganic ceramics with high dielectric constant and conductive fillers have been introduced to electrostrictive polymers matrix to improve the aforementioned properties. For instance, by introducing conductive polymer PANI into P(VDF-TrFE-CTFE) matrix, a very flexible composite with an significantly improved dielectric permittivity as high as 7000 was achieved, and consequently, a strain of 2.65 % with an elastic energy density of 0.18 J/cm^3 were observed under a field of 16 MV/m [159]. P(VDF-TrFE-CFE)/ CNTs composite with 0.5 wt.% CNTs loading, showing a strain of nearly 2 % induced under a field of 54 MV/m was reported by Zhang *et al.* [160].

However, most investigations have been carried out from the aspect of developing materials with high dielectric permittivity by introducing fillers. Even though the electromechanical performances have been enhanced to some extent, it is difficult to further improve the electromechanical performances which are limited by the actually decreased DBS, leading to the useless of composites for practical applications even with a very high dielectric permittivity.

In this chapter, we prepared an organic/inorganic nanocomposite via a simple solution blending and hot-pressing methods. Inorganic conductive carbon black (CB), a widely used conductive filler but barely introduced into electrostrictive polymers, was incorporated into P(VDF-TrFE-CFE) terpolymer matrix to improve the electromechanical performance of terpolymer. The major objective of this chapter is to comprehensively investigate the dielectric properties, mechanical properties and breakdown strength of the as-prepared P(VDF-TrFE-CTFE)/CB nanocomposites for electrostrictive applications.

2.2 Percolation theory

Percolation theory is a very powerful tool for investigations on physical properties of heterogeneous materials. For all heterogeneous materials, there are at least two components or phases within the bulky materials. A geometric transition, also called geometric phase transition or continuum percolation (to be distinguished from classic lattice percolation) occurs when particles of a minor phase (i.e., fillers) come into contact with each other, and a continuous network cluster extends throughout the system, as the volume fraction f of this minor phase approaches a critical value f_c, i.e., the percolation threshold.

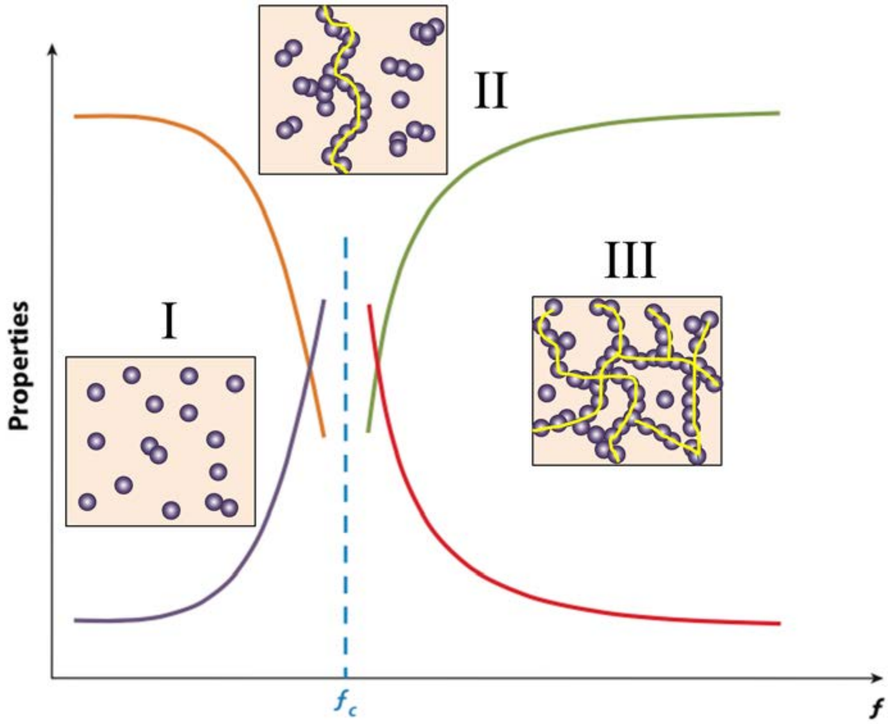

Figure 2.1: Schematic illustration of percolation theory: the nonlinear properties changes (the four colored curves denote different property parameters) near the percolation threshold f_c (dashed blue line). The insets show the geometric phase transition of fillers (denoted by dark spots) in the composites' microstructure near percolation: (I), without percolation; (II), critical fraction percolative network (yellow line indicates the network); (III), percolative network cluster. (reproduced from [168])

As indicated in Fig. 2.1, the significance of percolation transition is not only the structural evolution but also the dramatic changes of physical properties of the composites near percolation threshold. For composites with low loading of fillers, minor fillers particles are separated by continuous matrix, forming a *sea-island* structure (state I in Fig. 2.1), and physical properties of composite materials is mainly determined by matrix. With increasing loading of fillers, the physical properties change. Essentially, fillers start to connect to each other when the filler loading approaches the critical fraction, i.e., the percolation threshold, and finally a percolation network (indicated by yellow line in state II of Fig.

2.1) is formed. For state III with more filler concentration, 3-dimensional percolation networks are built throughout the overall composite material system. Due to the connection of minor fillers, physical properties (the four colored curves in Fig. 2.1) undergo significant transitions originating from the big property deferences of the components or phases within the heterogeneous materials. For example, a nonlinear evolution of transport properties such as electrical or thermal conductivity and diffusion associated with the direct global connection of fillers will be observed near percolation. In the vicinity of percolation, the dramatic changes of physical properties of heterogeneous materials can be described by a simple explicit law [168],

$$Properties \propto |f - f_c|^{\pm e} \tag{2.1}$$

where e is a well-known universal critical exponent that is different for various properties, which depends only on the spatial dimension of the composites. The percolation threshold f_c and the percolation transition behavior strongly depends on the micro-structure of the composite materials as well as the interactions of components.

The most importance of percolation theory lies in that it provides a theoretical guideline to investigate and develop composite materials with desired physical properties. For instance, polymer material has good mechanical properties and easy processability, but also has very high electrical resistance and low dielectric permittivity, which limit their potential applications in high-tech electronic fields. A very efficient way to get flexible polymer-based composites with high conductivity or dielectric permittivity is to introduce conductive fillers into insulate polymer matrix. When fillers with high electrical conductivity are continuously added to a matrix with low electrical conductivity, an abrupt increase of electrical conductivity and dielectric constant of the composites can be simultaneously observed, especially as the volume fraction f of the fillers approaches f_c. The electrical conductivity of composite during insulator-to-conductor transition with increased loading of conductive fillers can be given by

$$\sigma_c \propto \sigma_m (f_c - f)^{-s'}, for\, f < f_c \tag{2.2}$$

where σ_c and σ_m are the conductivity of composite and polymer matrix,respectively, s' is the critical exponent for electrical conductivity and it depends on the dimensionality of fillers, i.e., $s' = 1.1$~1.3 for d = 2, and $s' = 0.7$~1.0 for d = 3 [168]. The abrupt increase of conductivity of composite near percolation can be explained by the conducting network established through the intimate connection of adjacent conductive fillers and the tunneling of electrons between two adjacent conductive particles. The simultaneously significant increase of dielectric permittivity also can be described by percolation theory as following,

$$\varepsilon_c \propto \varepsilon_m (f_c - f)^{-s}, for\, f < f_c \tag{2.3}$$

where s is the critical exponent for dielectric permittivity, ε_c and ε_m are the dielectric permittivity of composite and polymer matrix, respectively. The universality of percolation theory suggests that the dielectric constant should follow the same power law dependence on the fraction as the conductivity below f_c, i.e., $s = s' \approx 1$ [168, 169]. The physical reason for the critical behavior of dielectric constant near percolation is the existence of micro-capacitor networks which are composed of adjacent conductive filler particles and a very thin layer of dielectrics in between.

Eq. 2.3 illustrates that a large dielectric constant can be achieved in composites as $f \to f_c$. As a result, different conductive fillers including metal particles, carbon-based materials have been widely investigated to improve the dielectric permittivity of polymer materials. For instance, Dang *et al.* [169] reported Ni-PVDF polymer composites with a high dielectric constant (400, about 50 times higher than PVDF) using a very simple blending and hot-pressing technique. PVDF/MWNTs composite with a low percolation threshold of 0.16 vol.% also shows a dielectric permittivity as high as 300 as well as a low dielectric loss less than 0.4 [170].

Based on the great entrancement of dielectric permittivity of polymer/conductive filler polymer composite, we prepared a terpolymer/carbon black nanocomposite to comprehensively investigate the dielectric properties, mechanical properties and breakdown strength of the as-prepared nanocomposites for electrostrictive applications.

2.3 Experiment

2.3.1 Materials

A. Terpolymer P(VDF-TrFE-CFE)

Large electromechanical response of fluoride polymers was first reported for irradiated copolymer P(VDF-TrFE) [148], in which a room temperature large electrostrictive strain more than 4 % was observed at an electric field of 150 MV/m and the electromechanical response can be operated at a broadband frequency (0.01 Hz to 10 KHz) [153] and temperature range. It was demonstrated that, the long-range polar region within copolymer was broken into micro-domains by the defect structure induced by irradiation, and therefore the energy barrier of transformation between polar and non-polar phases was eliminated, resulting into the large electromechanical strain with very little hysteresis. However, the high energy irradiation is not a commercially available approach to produce high electromechanical fluoride polymer due to its high energy cost and incontrollable side effects on the macromolecular structure.

Inspired by the idea of defect modification, semi-crystalline terpolymers consisting vinylidene fluoride (VDF, $-CH_2-CF_2-$), trifluoroethylene (TrFE, $-CHF-CF_2-$) and chlorofluoroethylene (CFE, $-CH_2-CFCl-$) or chlorotrifluoroethylene (CTFE, $-CF_2-CFCl-$) were synthesized by a combination of suspension polymerization process and an oxygen-activated initiator at a temperature of 40 °C [152]. The introduction of the third monomer CFE or CTFE causes changes of crystalline structure and phases composition. Large polar β-phase regions are transformed into nanopolar regions surrounded by nonpolar α-phase, and normal ferroelectric copolymer P(VDF-TrFE) is transformed into ferroelectric relaxor terpolymer.

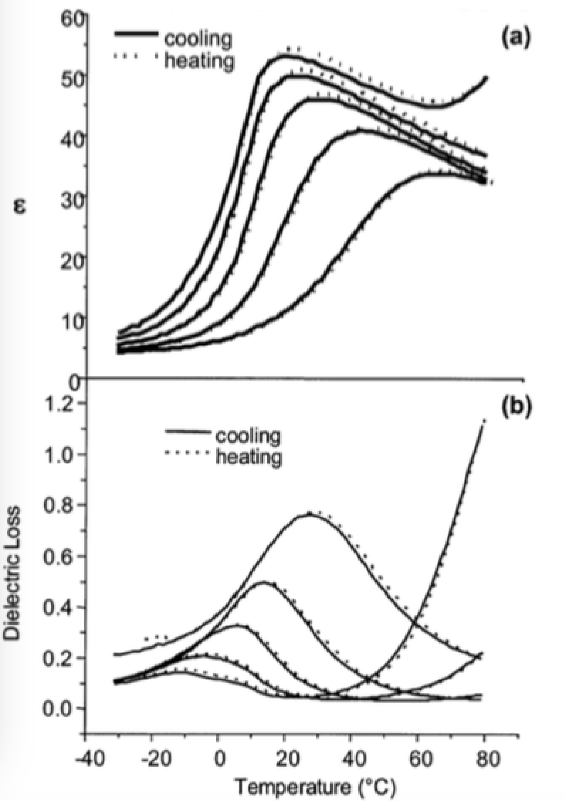

Figure 2.2: Temperature dependence of (a) dielectric constant and (b) dielectric loss for the 61/29/10 mol% P(VDF-TrFE-CFE) terpolymer. The measuring frequencies are: (from the top to bottom for the dielectric constant and from the bottom to top for the dielectric loss) 0.1, 1, 10, 100, and 1000 kHz. Both data acquired during the heating and cooling runs are presented [153].

Terpolymers have many promising properties for electromechanical applications. Firstly, terpolymers are ferroelectric relaxor with a very slim hysteresis (Fig. 2.3a) which is contributed to the reduced transition energy barrier between polar and nonpolar phases since the large polar regions are transformed into nonpolar regions by the defect effects of CFE or CTFE. Moreover, the introduction of the third monomer moves the phase transition peak to room temperature and with a wide temperature range (Fig. 2.2). As a result, large electromechanical strain can be realized at a wide temperature range around room temperature (2.3b). As depicted in Fig. 2.3 c and d, a longitudinal strain about 7 % and a transverse strain of 1.3 % are observed for a P(VDF-TrFE-CFE) 68/32/9 mol% terpolymer. Secondly, terpolymers possess a large dielectric permittivity which can achieve a value of 60, the highest value for polymer materials. Such a high dielectric permittivity contributes to not only a high electric energy density but also the high electromechanical strain. Thirdly, the dielectric breakdown strength is as high as 300 MV/m. and finally, the elastic modulus is > 0.3 GPa, two order of magnitude higher than that of dielectric elastomers, leading to a high load capacity.

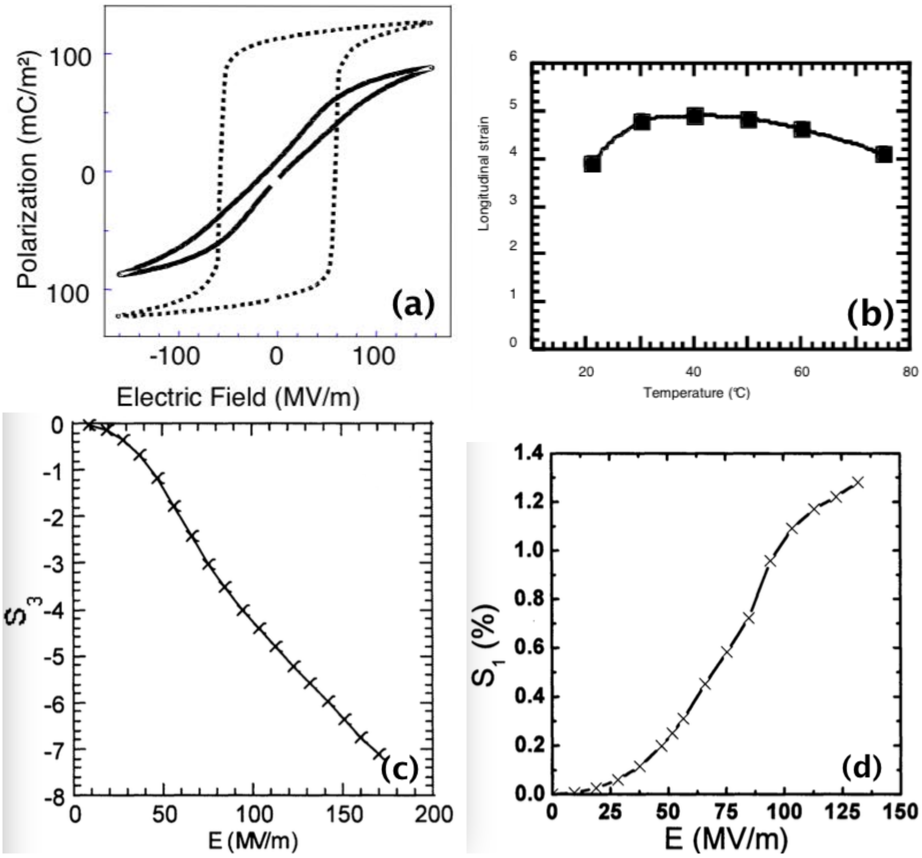

Figure 2.3: (a) Comparison of the polarization hysteresis of the normal ferroelectric polymer (dashed curve, large hysteresis) and relaxor ferroelectric polymer (black curve) at room temperature; (b) The electrostrictive strain as a function of temperature under 150 MV/m field; (c) Electric field induced longitudinal and (d) transverse strain P(VDF-TrFE-CFE) 68/32/9 mol%. [161, 171]

Due to the excellent properties for electromechanical response, terpolymer P(VDF-TrFE-CFE) was chosen as the polymer matrix for our composite. And it is supplied from PiezoTech (Arkema Group)[1], France.

B. Carbon black

Carbon black (CB) is a carbon material produced by incomplete combustion of heavy petroleum product. It consists of spheric particles being fused together (Fig. 2.4) and has a paracrystalline structure with a high surface-area-to-volume ratio. CB is widely used as a conductive filler, reinforcement filler and black paint filler for polymer materials. The electrical conduction properties was well investigated by Medalia [172].

In this chapter, CB nanoparticles (Vulcan XC72R) with an average diameter of 30 nm were obtained from the Cabot Corporation[2].

---

[1] www.piezotech.fr

[2] www.cabotcorp.com

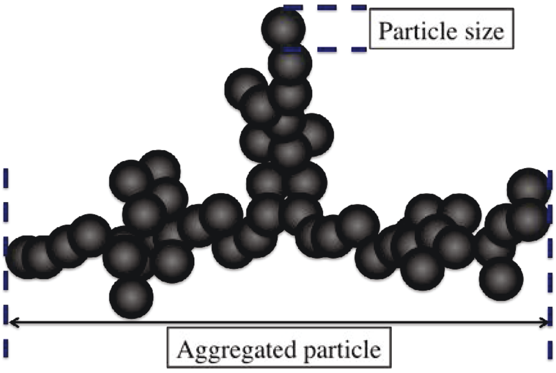

Figure 2.4: Schematic illustration of CB.

2.3.2 Composite fabrication

The P(VDF-TrFE-CFE)/CB nanocomposite was fabricated via a simple solution blending method (see Fig. 2.5).

1. Prepare the solution of P(VDF-TrFE-CFE) and methyl ethyl ketone (MEK).
   Terpolymer was dissolved in MEK with help of the electromagnetic stirrer at a temperature of 70 °C for 4h. The mass fraction of P(VDF-TrFE-CFE)/MEK solution is 4 wt.%.

2. Mix the as-prepared solution with CB nanoparticles.
   Required quantity of CB nanoparticles was introduced into the solution and dispersed to form a uniform mixture by ultrasonication for 5 min. The mass fraction of CB nanocomposite in polymer matrix ranges from 1.5 wt.% to 5 wt.%.

3. Get solid composite.
   After ultrasonication, the well dispersed solution was immediately poured into a beaker filled with water. A glass stick was used to stir the solution quickly. Since MEK and water is soluble to each other and terpolymer/CB is not soluble in water, the solid mixture terpolymer/CB will come out from the liquid and adhered to the glass stick due to the centrifugal force.

4. Dry the composite.
   The obtained mixture was washed with deionized water and then moved to a petri dish and was put into an oven at 110 °C over night to remove the residual solvent.

5. Hot press the composite.
   The resulting composites were finally hot-pressed at a temperature of 150 °C, above the melting temperature of P(VDF-TrFE-CFE). Films with a thickness typically about 100-200 μm were obtained for the next-step properties characterization.

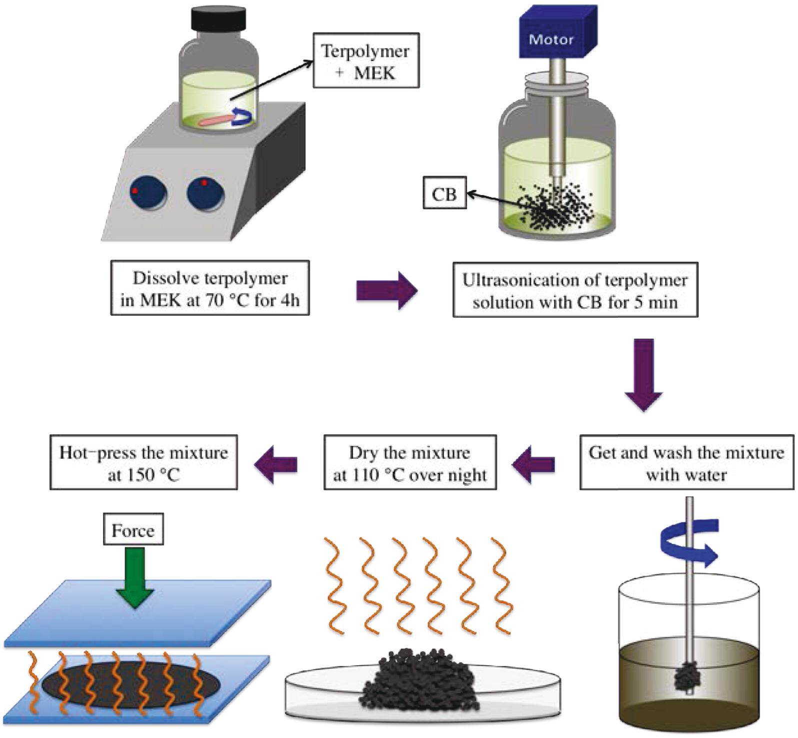

Figure 2.5: Schematic illustration of the fabrication process for P(VDF-TrFE-CFE)/CB nanocomposites.

2.3.3 Composite characterization

In this part, the dielectric properties, mechanical properties and dielectric breakdown strength were carefully characterized for the as-prepared P(VDF-TrFE-CFE)/CB nanocomposite films.

2.3.3.1 Characterization of dielectric properties

A. Basic concepts of dielectric phenomenon

The most common parallel plate capacitor equation with free space as an insulator is given by

$$C = \frac{\varepsilon_0 A}{d}, \tag{2.4}$$

where C is the capacitance of the capacitor, ε_0 is the vacuum dielectric permittivity, A is the plate area and d is the separated distance of the two plates. When a material medium is inserted between two plates, the capacitance, the charge storage ability per unit voltage, increases by a factor of ε_r, where ε_r is called dielectric constant or relative dielectric permittivity of the medium (or dielectrics). The increase of capacitance is ascribed to the polarization of dielectric materials under an electric field, which refers to the displacement of positive and negative charges with respect to their equilibrium positions. The acquired opposite surface charge density (also known as the polarization density, P) on the two opposite surface of dielectric medium is related to the amount of polarization within dielectrics. The basic conception to describe the relative displacement of a pair of negative and positive charges is electric dipole moment $\boldsymbol{p}$, which is defined by

$$\boldsymbol{p} = Q\boldsymbol{a}, \tag{2.5}$$

which means a pair of opposite charges $+Q$ and -Q separated by a finite distance $\boldsymbol{a}$, a vector from negative to positive charge.

When an electric field applied on a dielectrics, polarization with different levels occurs, including electronic polarization, ionic polarization, orientational polarization of dipolar and interfacial polarization of space charge. The macro polarization density is the sum of all the contributions of different polarization. The different response time of different polarization mechanism results into a complicated dielectric phenomenon, which can be given by the *complex dielectric constant*,

$$\varepsilon_r = \varepsilon_r' - j\varepsilon_r'', \tag{2.6}$$

where ε_r' and ε_r'' are the real part and imaginary part of the complex dielectric constant, respectively, and both are frequency dependent. The real part ε_r' represents the relative permittivity that is used to calculate the capacitance and energy stored within dielectrics, while ε_r'' stands for the energy lost within dielectrics to overcome the polarization barrier. The ratio of the magnitude of imaginary and real part is defined as the *loss tangent* or *loss factor*,

$$tan\delta = \frac{\varepsilon_r''}{\varepsilon_r'}. \tag{2.7}$$

The peak in loss tangent is called relaxation peak, which is at a frequency when the dipole relaxations are at the right rate for maximum power dissipation. This process is known as *dielectric resonance.*

The research object in dielectrics is the limited or confined charge, i.e,. the dipole moment, which can not perform a long-range movement in response to an applied electric field. Since it is closely related to the orientation of dipole moment which is dependent on frequency, temperature and material structures, dielectric resonance can be used a useful tool for materials investigation.

B. Dielectric measurement of P(VDF-TrFE-CFE)/CB nanocomposite

The measurement of dielectric permittivity is basically relied on Eq. 2.4, form which the relative dielectric permittivity can be easily calculated from the measured capacitance of the film,

$$\varepsilon_r = \frac{Cd}{\varepsilon_0 A}. \tag{2.8}$$

In our experiment, the dielectric properties were measured with a SI1260 (Solartron) impedance analyzer system in a frequency range of 0.1 to 1 MHz. Moreover, in order to investigate influence of introduced CB on phase transition behavior of terpolymer, a dielectric spectroscopy was performed from -100 °C to 95 °C using a broadband dielectric spectrometer BDS400.

Before dielectric measurement, P(VDF-TrFE-CFE)/CB nanocomposite film samples were sputtered circular golden electrodes on both sides of the films with a diameter of 20 mm. As indicated in Eq. 2.8, the diameter as well as the thickness of samples are the two key parameters for dielectric measurement.

2.3.3.2 Characterization of mechanical properties

Dynamic mechanical analysis (DMA) was used to investigate the influence of introduced CB on the mechanical properties of terpolymer in a wide temperature range. DMA works by applying a sinusoidal stress or deformation to a sample of known geometry. For an applied sinusoid stress, a viscoelastic material will respond with a sinusoidal strain for low amplitudes of stress. Due to the molecular movement and relaxation dependency of temperature, the shear modulus (G) can be written in a complex form,

$$G = G' + iG'', \tag{2.9}$$

where G' is the storage modulus and G'' is the loss modulus. And the phase angle (mechanical loss factor) is given by

$$tan\delta = \frac{G''}{G'}. \tag{2.10}$$

The dynamic loss modulus is often associated with “internal friction” and sensitive to different kinds of molecular motions, relaxation processes, transitions, morphology and other structural heterogeneities. Thus, the dynamic properties provide information at the molecular level for understanding the polymer mechanical behavior.

In our work, DMA was performed using an inverse torsion pendulum at 1 Hz [173], and the temperature range of 150-375 K was scanned at a heating rate of 1 K/min. The rectangular specimens with a size of 10 mm × 3.5 mm were cut from the stainless steel plates.

2.3.3.3 Characterization of dielectric breakdown strength

In addition to increasing the capacitance of a capacitor, another important property for dielectrics is their insulation and low electric conductivity so that the charge carrier are not simply conducted throughout the bulky dielectrics. The voltage across dielectrics and the resulting electric field within dielectrics, however, can not be increased without a limit. When voltage reaches the limitation, giant short-circuit current occurs between electrodes and leads to the dielectric breakdown, a permanent damage of dielectrics. The maximum electric field that can be applied to a dielectric materials without causing dielectric breakdown is the *dielectric breakdown strength* (E_b).

The mechanism of dielectric breakdown for solid dielectrics is very complicated, and it depends on a number of factors including molecular structure, impurity in the materials, sample geometry, nature of electrodes, temperature, and the ambient conditions as well the frequency and duration of the applied electric field. The most common breakdown mechanism are intrinsic breakdown, thermal breakdown, electromechanical breakdown and internal discharges.

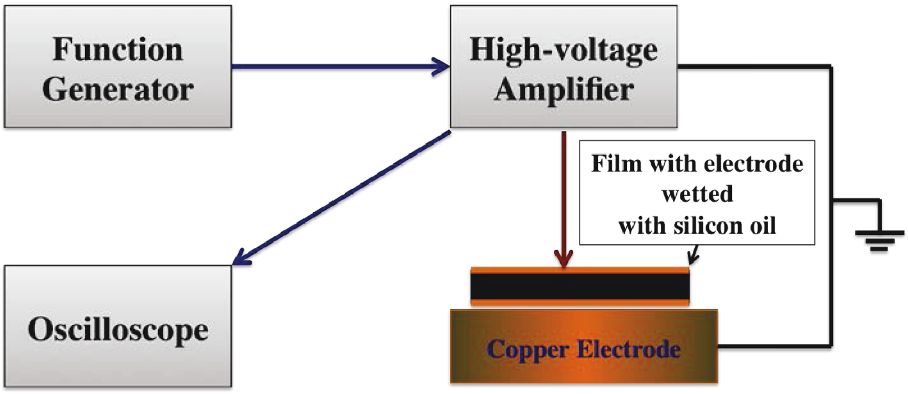

Figure 2.6: Schematic illustration of the dielectric breakdown strength measurement.

In our experiment, circle golden electrodes with a diameter of 8 mm were first sputtered on both sides of the film. E_b is measured with a self-made equipment. As shown in Fig. 2.6, a DC voltage with a ramp rate of 2 KV/3s was generated by a function generator and amplified by a high-voltage amplifier. Such a voltage was applied to the nanocomposite films until failure. In order to avoiding the air discharging and ionization, films were wetted with silicon oil during the measurement. The voltage at which breakdown took place was recorded by an oscilloscope. E_b was calculated from the recorded voltage divided by the thickness of the film. At least 13 breakdown tests were performed on each type of sample.

2.4 Results and discussion

2.4.1 Dielectric properties of P(VDF-TrFE-CFE)/CB nanocomposites

Fig. 2.7 shows the dielectric properties of nanocomposites as a function of frequency with a variation of CB mass fractions. As expected, an increased dielectric permittivity with increasing CB loading was observed. Compared to pure terpolymer P(VDF-TrFE-CFE) with a dielectric permittivity of 50 at 100 Hz, the nanocomposites with a CB loading of 4.5 wt.% has an increased dielectric permittivity of 140 at 100 Hz which is almost 3 times higher. This value is better than previous reported carbon black/ P(VDF-TrFE-CFE) composites with a dielectric permittivity of 102 ($tan\delta = 0.36$) at 100 Hz by inclusion of 2 % CB carbon nanotubes [160].

As we can see from Fig. 2.7a and 2.8a, the dielectric permittivity as a function of CB loading shows a first-step increase and second-step decrease. A sharp increase and then decrease of dielectric permittivity was found at the fraction range from 4.25 wt.% to 5

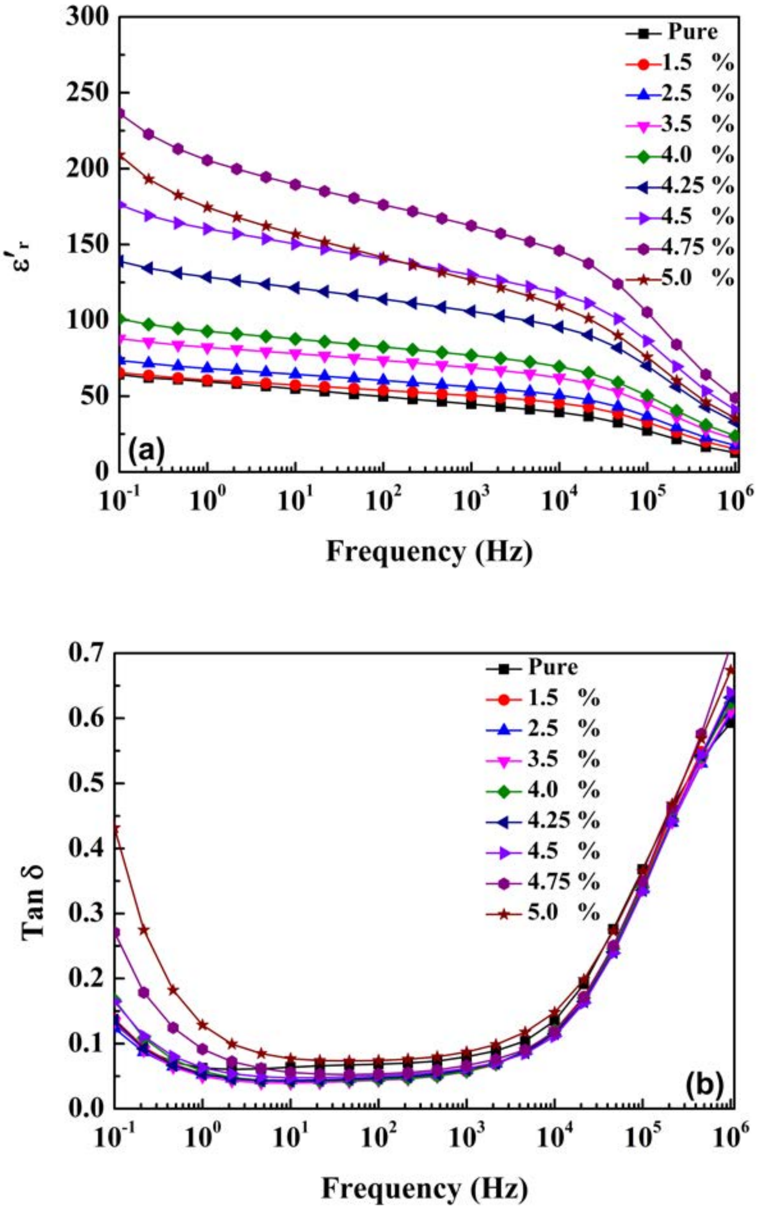

Figure 2.7: Dielectric properties of P[VDF-TrFE-CFE]/CB nanocomposites. Frequency dependency of (a) dielectric permittivity (ε_r') and (b) dielectric loss ($tan\delta$) of nanocomposites with different CB loadings (wt.%).

wt.%. This typical phenomenon can be explained by percolation theory [168], which is used to describe dramatic change of materials' properties for a mixture when the minor phase come into contact with each other forming a continuous network throughout the mixture system. As we can see from Eq. 2.3, giant enhancement of dielectric permittivity can be achieved in conductive particle filled composites when the conductive filler loading is very close to the percolation threshold in a very narrow fraction range. As is shown in Fig. 2.8b, a curve fitting to the measured dielectric values of nanocomposites is in good

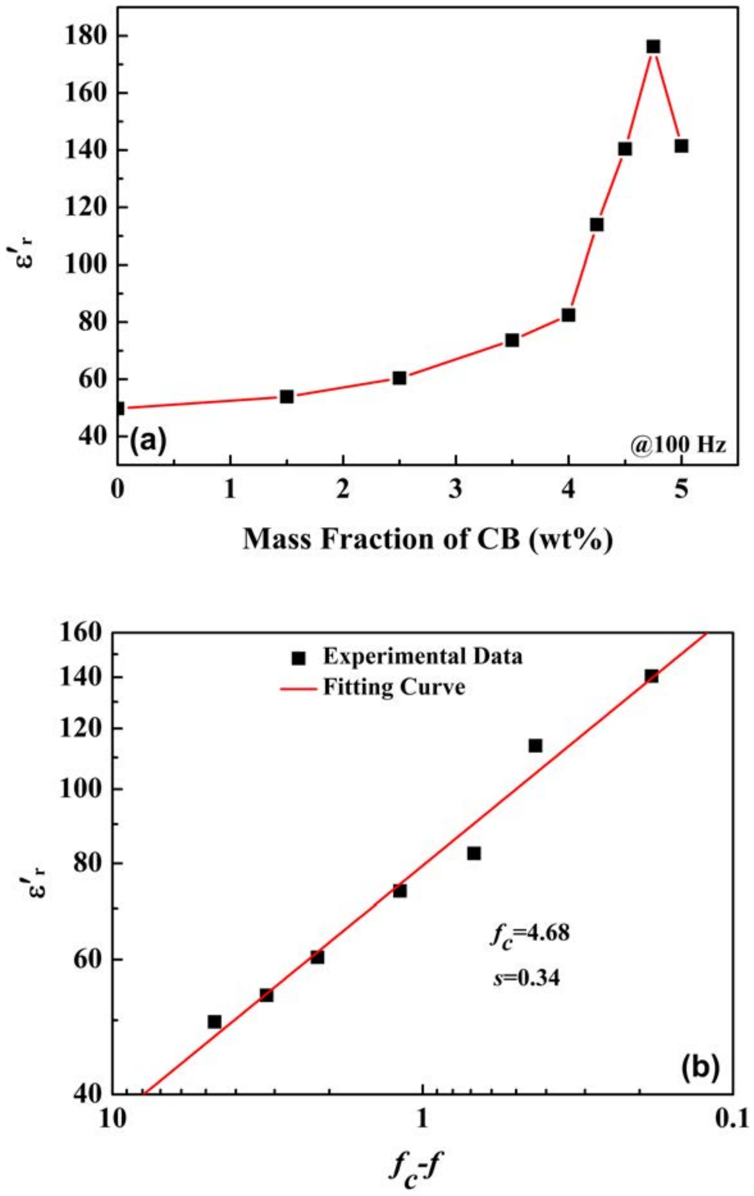

Figure 2.8: (a) CB loading dependency of dielectric permittivity of nanocomposite at 100 Hz and (b) its fitting curve using percolation theory.

agreement with Eq. 2.3, with $f_c = 4.68$ wt.% and $s = 0.34$. The percolation threshold is closely associated with the dispersion of filled particles. For same particles, a higher value of f_c will be obtained for a better dispersion of conductive fillers. According to the universality of percolation theory, the dielectric critical exponent should have a same value as the conductive critical exponent of approximate 1 (see Section 2.2). However, this is not always observed in practical continuum system [174], i.e., the fitted $s = 0.34$ here is not close to 1. The same results also can be found in other literatures [170, 175]. The discrepancy of the practical dielectric critical exponent with the universality of percolation theory is related to the distribution and the inter-particle contacts of the filled conductive fillers.

The existence of micro-capacitors [176] which are composed of conductive CB nanoparticles and thin layer of insulating polymer matrix are responsible for the increased dielectric permittivity. More micro-capacitors are formed with the increasing loading of CB nanoparticles, which leads to the mild increment of dielectric permittivity. Up to percolation threshold $f_c = 4.68$ wt.%, CB nanoparticles are isolated by very thin insulating polymers and a significant increase of micro-capacitance results in dramatic enhancement of dielectric permittivity. As CB loading exceeds percolation threshold, the dielectric permittivity decreases due to the formation of the conductive network throughout nanocomposites system.

At low frequency, a stronger frequency dependency of dielectric properties with increasing CB loading was observed, which can be explained with interfacial polarization, i.e. the well-known Maxwell-Wagner-Sillars polarization [177]. Due to the different dielectric properties of the CB particles and polymer, more and more charges were accumulated on the interface region between the conductive CB nanoparticles and insulating polymer matrix with increasing CB loadings. Since a longer time is required in contrast with other polarizations, interfacial polarization contributes to the general dielectric properties only at low frequency.

Fig. 2.7b shows the frequency dependency of dielectric loss with different loading of CB nanoparticles. For all nanocomposites without reaching the percolation threshold, nanocomposites exhibit nearly a same dielectric loss with the polymer matrix at a wide frequency range from 0.1 Hz to 1 MHz, which is different from the other percolative systems. The high dielectric loss at low frequency is caused by aforementioned interfacial polarization, and the increase of dielectric loss at high frequency above 10^5 Hz is ascribed to the orientation of the dipole of semi-crystalline P(VDF-TrFE-CFE) matrix. At a frequency from 10 Hz to 1000 Hz, the nanocomposites have a low dielectric loss of 0.05 which is comparable to pure P(VDF-TrFE-CFE) matrix.

It has been known that the large strain and dimensional change of ferroelectric polymers correspond to the transition between polar ferroelectric phases and non-polar paraelectric phases (F-P transition). Based on this fact, a comparison of the temperature dependent dielectric properties between pure P(VDF-TrFE-CFE) and nanocomposites with a CB loading of 4.0 wt.% was carried out to further understand the influence of the introduction of CB fillers on the dielectric properties of nanocomposites. Fig. 2.9 shows the nanocomposites exhibit the same relaxor behavior as the pure terpolymer with a broad dielectric peak at around room temperature, which is below the F-P transition temperature (about 70 °C). It illustrates that the introduction of CB fillers did not influence the relaxor ferroelectric nature of P(VDF-TrFE-CFE) terpolymer, which plays a very important role in the achievable large electrostrictive strain.

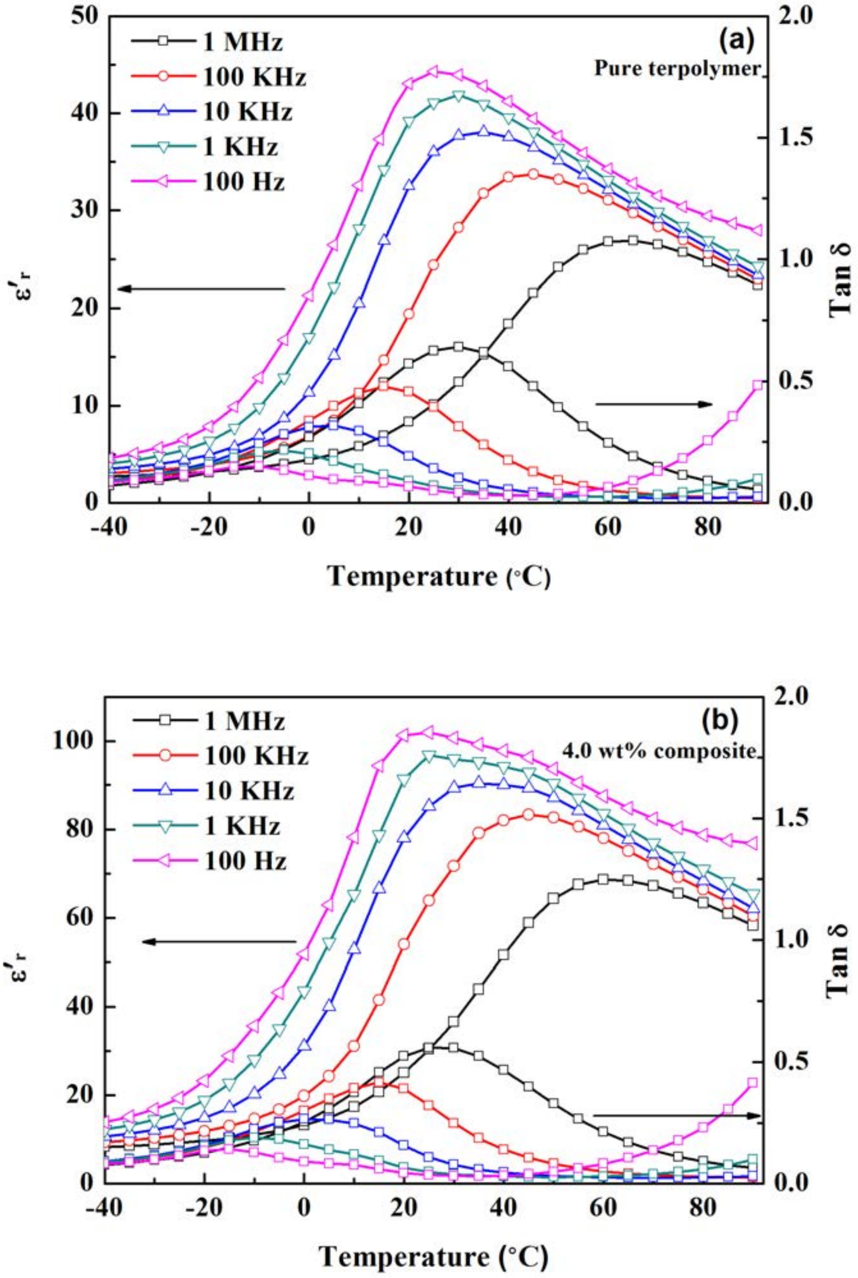

Figure 2.9: Temperature dependence of dielectric properties of (a) P(VDF-TrFE-CFE) and (b) its nanocomposite with a CB loading of 4.0 wt.% measured at different frequencies.

2.4.2 Mechanical properties of P(VDF-TrFE-CFE)/CB nanocomposites

As we can see from Eq. 1.8, the final electrostrictive property of nanocomposites is not only determined by dielectric properties, but also the mechanical properties. Young's modulus is a key parameter which directly controls the achievable strain. Dielectrics with low Young's modulus will provide a high electrostrictive strain at the same applied electric field. Although ceramic-based composites exhibit very high dielectric permittivity, high loading of ceramics results in a loss of flexibility, which limits their final electromechanical properties.

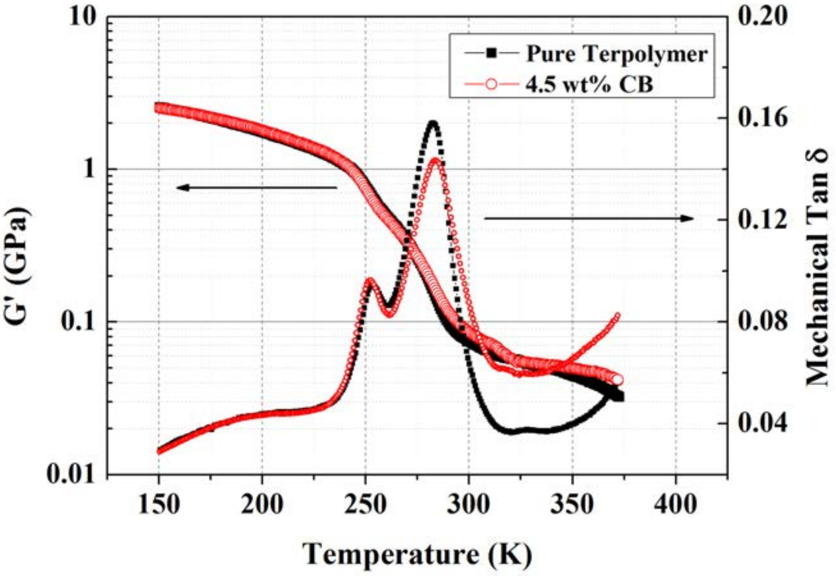

Figure 2.10: DMA curves of P(VDF-TrFE-CFE) and its nanocomposite with a CB loading of 4.5 wt.%.

Here, the mechanical properties of pure terpolymer and nanocomposite with a CB loading of 4.5 wt.% were investigated by DMA from 150 K to 375 K at 1 Hz. As is shown in Fig. 2.10, the nanocomposite exhibits almost the same mechanical behavior at the full temperature range. When the samples were heated from 150 K, a significant decrease of storage shear modulus was observed and it can be interpreted by two transitions of terpolymer matrix which is in correspondence with two relaxation peaks showing in the mechanical loss curves. The first relaxation is the glass transition originating from the micro-Brownian motion of main chains in the amorphous region, which displays a peak at 252 K. The second relaxation referring to the peak at 283 K is the structure transition aroused by the unstable crystal defects in which all-trans sequence randomly disturbed by gauche configuration [178].

It illustrates that the addition of CB nanoparticles into polymer matrix does not have a negative effect on the mechanical property of polymer matrix and the nanocomposites retain the flexibility of terpolymer. The calculated Young's modulus at room temperature with a Poisson's ratio of 0.33 is about 0.4 GPa. Thus P(VDF-TrFE-CFE)/CB nanocomposite can meet the mechanical requirement for electrostrictive applications.

2.4.3 Dielectric breakdown strength of P(VDF-TrFE-CFE)/CB nanocomposites

The DC breakdown strength results of the P(VDF-TrFE-CFE)/CB nanocomposites were investigated by a two-parameter Weibull analysis [179, 180],

$$P(E) = 1 - exp[-(E/\lambda)^k], \tag{2.11}$$

where $P(E)$ is the breakdown probability of the nanocomposites film at a certain electric field E, λ is the scale parameter reflecting the breakdown strength at which 63.2 % of the breakdown happened and the shape parameter k is the spread of the distribution. Fig. 2.11 presents the Weibull probability analysis results of breakdown strength for nanocomposites. For the dielectric films studied, a decrease of breakdown strength from 80.2 MV/m for pure terpolymer to 9.6 MV/m for a nanocomposite containing 4.5 wt.% CB fillers was observed.

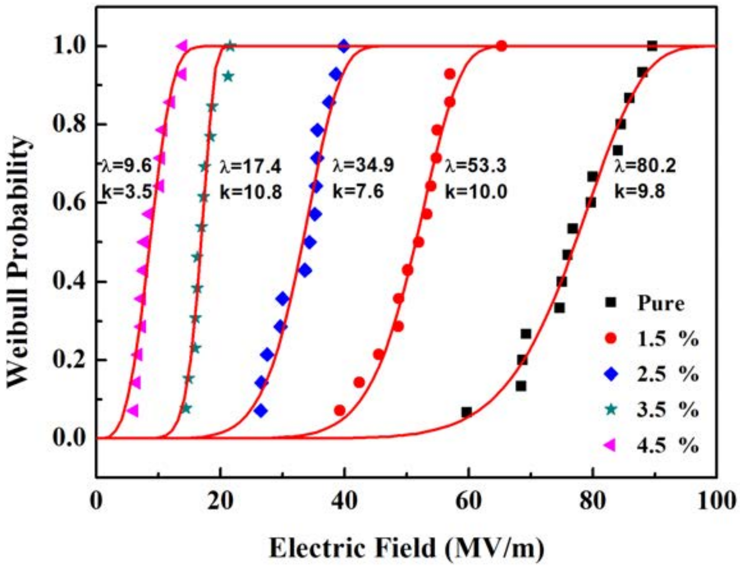

Figure 2.11: Weibull probability analysis for measured DC dielectric breakdown strength for P(VDF-TrFE-CFE)/CB nanocomposites.

The decreased insulating layer thickness between conductive fillers with CB loadings not only contributes a great enhancement of dielectric permittivity of the whole nanocomposites, but also causes an increased local electric field. Such an inhomogeneous local electric field which is closely related to the inter-particle insulating layers is responsible for the reduction of the breakdown strength. For composites under percolation threshold, tunneling is the dominant conductive mechanism in which conductive particles are not geometrically connected but electrically via electron tunneling [168, 181, 182]. The increased local electric field concentration facilitates tunneling connectivity at a lower electric field, resulting in reduced breakdown strength.

2.4.4 Theoretical estimation of electromechanical performances for P(VDF-TrFE-CFE)/CB nanocomposites

It has been demonstrated that [183], the electrostrictive response of terpolymers at electrical field below 100 MV/s is mainly ascribed to Maxwell force induced by the opposite charges on the surface generated by dipole orientation of within the crystalline phase of the polymer, i.e.,

$$S_M = \frac{1}{2}\frac{\varepsilon_r\varepsilon_0}{Y}E^2(1+2\upsilon). \tag{2.12}$$

Table 2.1: Estimation of electrostrictive performances for P(VDF-TrFE-CFE)/CB nanocomposites at 1 Hz and room temperature.

CB Loading (wt.%)	ε_r	Y (MPa)	E_b (MV/m)	$\varepsilon_r\varepsilon_0/Y$ (F/(m Pa))	S_m (%)	$YS_m^2/2$ (J/cm^3)
0	59.2	400	80.2	1.31×10^{-18}	0.70	9.79×10^{-3}
1.5	60.7	400	53.3	1.34×10^{-18}	0.32	2.01×10^{-3}
2.5	68.2	400	34.9	1.51×10^{-18}	0.15	4.66×10^{-4}
3.5	82.1	400	17.4	1.82×10^{-18}	0.046	4.17×10^{-5}
4.5	160.4	400	9.6	3.55×10^{-18}	0.027	1.48×10^{-5}

Here, the electromechanical performances of P(VDF-TrFE-CFE)/CB nanocomposites, including the electrostrictive coefficient, the maximum field induced strain and elastic energy density, were estimated with via Eq. 2.12. As shown in Table 2.1, the dielectric permittivity is improved with introduced CB nanoparticles, resulting into an increased electromechanical coefficient ($\propto \varepsilon_r\varepsilon_0/Y$). However, the corresponding maximum electric field induced strain (S_m) and elastic energy density ($YS_m^2/2$) were significantly reduced owning to the decreased dielectric breakdown strength. One order of magnitude drop for electrostrictive strain (form 0.7 % for pure terpolymer to 0.027 % for 4.5 wt.% CB composite) and two orders of magnitude drop for elastic energy density (form 9.79×10^{-3} J/cm^3 for pure terpolymer to 1.48×10^{-5} J/cm^3 for 4.5 wt.% CB composite) were observed (see Fig. 2.12).

As we can see from the estimated electromechanical performances of P(VDF-TrFE-CFE)/CB nanocomposites, the enhancement of electromechanical performance brought about by the improvement of dielectric permittivity can not compensate the decline of electromechanical performance associated with the significantly reduced dielectric breakdown strength, since the electric field induced strain for electrostrictive dielectrics has a quadratic relationship with applied electric field. Thus the reduced breakdown strength will limit the operation electric field and consequently the achievable strain.

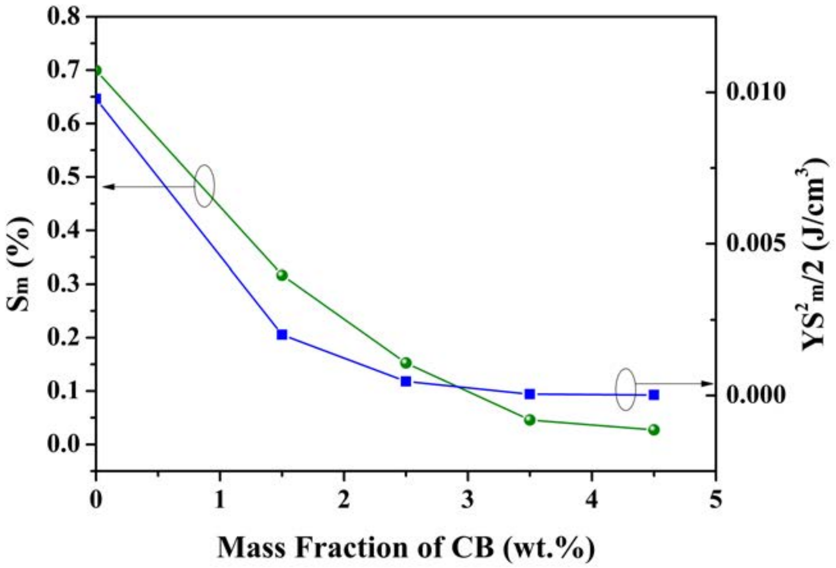

Figure 2.12: Estimation of the maximum longitudinal strain and elastic energy density of P(VDF-TrFE-CFE)/CB nanocomposite as a function of CB loading.

2.5 Conclusion

In this chapter, we demonstrated an organic/inorganic P(VDF-TrFE-CFE)/CB nanocomposites. The mechanical properties, dielectric properties and breakdown strength were carefully investigated for electrostrictive applications. Compared with ceramic or metal based composites in which a high dielectric permittivity was achieved at expense of flexibility due to high filler loading, the as-prepared P(VDF-TrFE-CFE)/CB nanocomposites exhibits an enhanced dielectric permittivity and almost the same flexibility as pure terpolymer. The dielectric results show that P(VDF-TrFE-CFE)/CB nanocomposites possess an elevated dielectric of 140 and low dielectric loss of 0.05 (comparable to polymer matrix) at 100 Hz. The percolation theory was used to explain the improvement of dielectric properties and a percolation threshold of 4.68 wt.% was observed. The low Young's modulus, improved dielectric permittivity and low dielectric loss of P(VDF-TrFE-CFE)/CB nanocomposites enable it more useful in actuator applications.

However, the thin insulating layer between CB fillers which contributes the great enhancement of dielectric permittivity also leads to enhanced local electric field and finally results in decreased breakdown strength which limits the practical applications of as-prepared composites as an electrostrictive material. The theoretically estimated electromechanical performance of P(VDF-TrFE-CFE)/CB nanocomposites shows that the introduction of conductive carbon black brought about an enhanced dielectric permittivity, but more importantly, a significantly reduced dielectric breakdown strength, leading to a declined electrostrictive performance of terpolymer.

Fortunately, it has been demonstrated that [184], insulating charge barrier introduced by surface modification of the inorganic filler can be used to improve the breakdown strength via preventing leakage current. It will be a promising way to develop new conductive material filled electrostrictive polymers based composite with improved overall properties by interfacial modification. For instance, TiO_2 inorganic particles, the surface of which is modified by organic Nitrophenyl phosphate (NPP) via a self-assembled monolayer (SAM) technology, were employed to improve the dielectric properties of epoxy by Siddabattuni *et al.* [185]. The modified interface between inorganic filler and organic polymer efficiently decreased the leakage current and dielectric loss, and significantly improved the breakdown strength. A high breakdown strength of 368 MV/s was achieved for NPP modified 5 vol.% TiO_2 composites, which is higher than that of non-modified 5 vol.% TiO_2 composite (247 MV/s) and pure epoxy (288 MV/m).

Chapter 3

All-organic Composites: Terpolymer Modified with Plasticizer DEHP

Based on the heterogeneous nature of semi-crystalline terpolymer and the important role that interface polarization plays for dielectric and electromechanical response, small molecular plasticizer bis(2-ethylhexyl) phalate (DEHP) was introduced into electrostrictive terpolymer to form an all-organic polymer composite with improved electromechanical performances.

As expected, the introduction of DEHP contributes to greatly increased dielectric permittivity at low frequency, decreased Young's modulus and moderately reduced dielectric breakdown strength of terpolymers, which are closely related with the increased mobility of polymer chains caused by DEHP. As a result, DEHP modified terpolymers exhibit well improved electromechanical performance in contrast with pure terpolymer.

3.1 Introduction

Fluoride based terpolymers, such as P(VDF-TrFE-CFE) or P(VDF-TrFE-CTFE), are promising candidate materials for electromechanical actuator applications due to their large electrostrictive strain (~ 7 %) and mechanical load capacity (> 20 MPa). The large electrostrictive strain arises from large lattice strain during the transition between polar phase and nonpolar phase within the ferroelectric relaxor terpolymers. Given the high elastic modulus (> 0.3 GPa), electrostrictive terpolymers exhibit higher stress and elastic energy density than dielectric elastomers (DEs).

Nevertheless, like DEs materials, the main drawback for fluoride based electrostrictive polymers is also the high electric field (> 100 MV/m) required to actuation. Low applied electric field can be achieved at low voltage with very thin films. The problem lies in the fact that it is difficult to produce large area thin films with uniform thickness and structure. Hence, films used for actuation devices are usually with a thickness of tens of micrometers, requiring driving voltages at least 1 kV. According to Eq. 1.8, the electrostrictive strain is dominated by the dielectric permittivity, the dielectric breakdown strength and the elastic modulus. By increasing the dielectric permittivity, large strain can be realized at a relatively low electric field. Also, the increase of dielectric permittivity will contribute to a high input electrical energy density, which is defined as $\varepsilon_r'\varepsilon_0 E^2/2$ for linear dielectrics.

An efficient approach to increase dielectric permittivity is on the basis of introducing particles with high dielectric permittivity or high conductivity into polymer matrix. However, a very common phenomenon is that the improvement of dielectric permittivity is always accompanied with a reduction of dielectric breakdown strength. Therefore, the enhancement of dielectric permittivity is compromised by significantly decreased breakdown strength. For instance, an all-organic composite materials [158], in which an organic filler copper-phthalocyanine (CuPc) oligomers with very high dielectric constant (> 10^4) was dispersed into P(VDF-TrFE) matrix, shows a high dielectric permittivity of 225, but a significantly decreased dielectric breakdown strength from 200 MV/m to 13 MV/m, yielding a strain of 2 % which can not be enhanced due to limitation of very small dielectric breakdown strength. This problem is also proved by our results presented in the previous chapter. So it is important to keep the dielectric breakdown strength as high as possible for the useful strain level. And in fact, $E_b/2$ is chosen as the maximum applied electric field for typical actuator designs for safe reason [186].

The relationship between macroscopic polarization or actuation abilities of electrostrictive polymers and the microscopic orientation of dipole moments within the dipolar electrostrictive polymers was evaluated by Capsal *et al.* via the Debye/Langevin formalism [183]. It is demonstrated that, for semi-crystalline polymers, they are heterogeneous by nature, and therefore, the macroscopic polarization or actuation behavior of these polymers can be expressed the summation of the dipolar orientation within the crystalline regions and the amorphous regions, also as well as in the interfacial regions. For semi-crystalline polymers above the glass transition temperature, the interfacial polarization of the trapped charges in the interfacial regions between the crystalline and amorphous region will contribute a lot to the macroscopic polarization and actuation performance. Another investigation on the actuation abilities of multiphase electroactive polymer systems made by Lallart *et al.* [187] reveals that, the interfacial polarization is preferable in response to the low frequency electric field, while at high frequency the orientation response is mainly given by the dipolar phases. Early research also indicates the interfaces within multiphase polymers have important electromechanical characters [188].

On the basis of the above-mentioned theoretical and experimental investigation results, here, we proposed a solution to improve the electromechanical performance of electrostrictive polymers by interfacial modification within polymers. In this chapter, a plasticizer was introduced into electrostrictive polymer matrix to form an all-organic composite. Plasticizers are typically small moleculars, which are usually added into polymer matrix to tune the intermolecular interaction of the macromolecular chains. The main subject of this chapter is to investigate the influences of the introduced plasticizer on dielectric properties, mechanical properties, breakdown strength, and of most importance, the electromechanical response.

3.2 Experiment

3.2.1 Materials

A. Terpolymer P(VDF-TrFE-CTFE)

P(VDF-TrFE-CTFE) is another commonly used P(VDF-TrFE) based terpolymers, in which the third monomer CTFE (-CF_2-CFCl-) is introduced into P(VDF-TrFE) copolymer chains as a defect to transform the normal ferroelectric copolymer into a ferroelectric relaxor terpolymer.

The electromechanical response performance of P(VDF-TrFE-CTFE) was carried out by Xu *et al.* [155] in 2001. The relaxor behavior of P(VDF-TrFE-CTFE) terpolymer is shown in Fig. 3.1: The original ferroelectric-to-paraelectric (F-P) transition peak of copolymer is moved from about 70 °C to room temperature; the transition peak becomes much more broader and its position progressively shifts to higher temperature with increased frequency; Compared with copolymer P(VDF-TrFE), there is almost no thermal hysteresis in dielectric data during heating and cooling cycles for terpolymers, that is to say, the broad dielectric peak associated with the F-P transition stays at the same position in heating and cooling cycles. In addition, as shown in the insert of Fig. 3.1a, the dispersion of T_m with frequency f can be modeled quite well with the Vogel-Folcher (V-F) law,

$$f = f_0 exp[\frac{-U}{k(T_m - T_f)}], \tag{3.1}$$

a relation observed in many relaxor ferroelectric systems and spin glass systems, where U is a constant related to the activation energy, k is the Boltzmann constant (1.38 ×

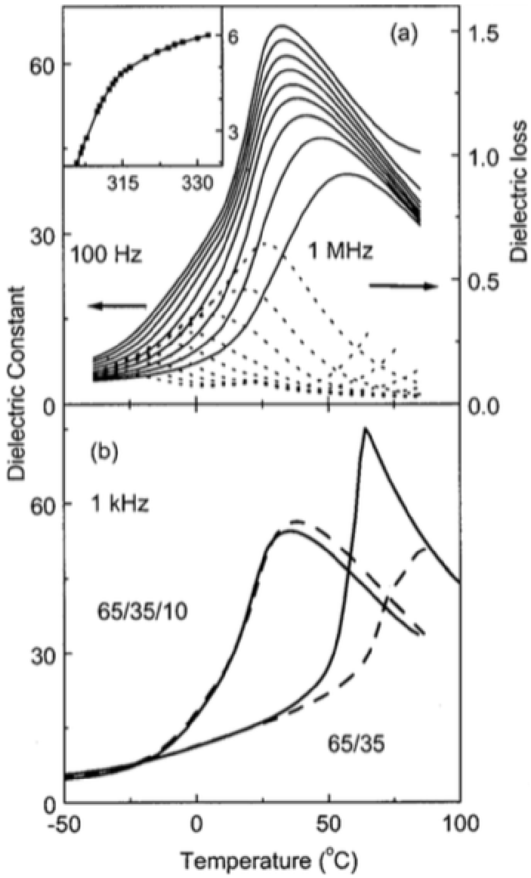

Figure 3.1: The relaxor ferroelectric behavior of P(VDF-TrFE-CTFE) 65/35/10 mol.%. (a) Dielectric constant (solid curves) and dielectric loss (dashed curves) as a function of temperature at frequencies (from top to bottom for the dielectric constant and for the dielectric loss from bottom to top): 100, 300 Hz, 1, 3, 10, 30 kHz, 0.1, 0.3, and 1 MHz. (b) Dielectric constant at 1 kHz of the 65/35/10 terpolymer and 65/35 copolymer for both heating (dashed curves) and cooling (solid curves) cycles measured at room temperature. [155]

10^{-23} J/K), T_f can be interpreted as the freezing temperature, corresponding to the peak temperature of the static dielectric constant (~ 0 Hz frequency) and the prefactor f_0 is the upper-frequency limit of the system, corresponding to the dipolar response when there is no coupling between the dipolar units in the system. P(VDF-TrFE-CTFE) also has a very slim hysteresis loop and a high dielectric permittivity as high as 60.

A electric field induced longitudinal strain about 4 % in response to an electric field of 150 MV/m was observed for P(VDF-TrFE-CTFE) terpolymer, which was measured at 10 Hz and room temperature. Given the elastic modulus of 0.4 GPa, P(VDF-TrFE-CTFE) terpolymer offers a relative high elastic energy density of 0.32 J/cm^3.

In this chapter, P(VDF-TrFE-CTFE) terpolymer purchased from PiezoTech (Arkema Group), France, was chosen as our polymer matrix for the electrostrictive performance investigation.

B. Plasticizer bis(2-ethylhexyl) phalate (DEHP)

Plasticizers are the additives mixed into polymer matrix to increase the flexibility and durability of polymer materials. Since plasticizers are small molecular by nature, the added plasticizer will embed themselves between polymer chains with non-covalent interactions. These interactions lower the free energy of the polymer-plasticizer system, increase the free volume of the polymer system and the mobility of polymer chains, and finally lower the glass transition temperature (T_g) of polymers, making polymers more soft for practical applications. Due to their efficient plasticizing effect and low cost to synthesize, phthalates are the most widely used plasticizers for polymers, especially for poly(vinyl chloride) (PVC).

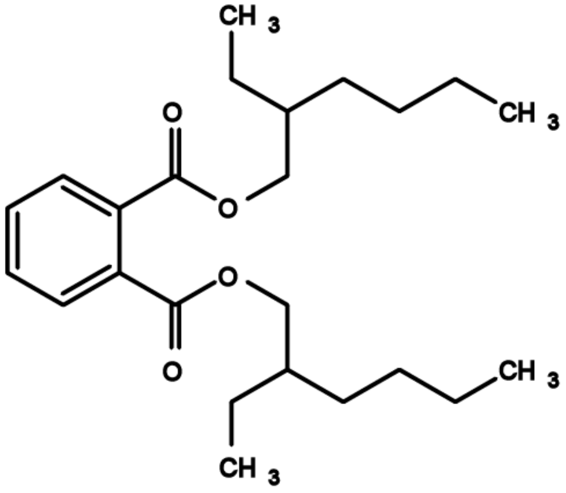

Figure 3.2: Molecular structure of DEHP.

In our experiment, phalate plasticizer bis(2-ethylhexyl) phalate (DEHP) was used to modify the electrostrictive terpolymer P(VDF-TrFE-CTFE). The molecular structure of

DEHP ($C_{24}H_{38}O_4$) is shown in Fig. 3.2. DEHP is colorless viscous liquid and not soluble in water. Its boiling point is 385 °C.

3.2.2 All-organic composite fabrication

The all-organic composite of P(VDF-TrFE-CTFE) terpolymer modified with plasticizer DEHP was prepared by a simple solution-casting method (see Fig. 3.3).

1. Prepare the solution of P(VDF-TrFE-CTFE)/DEHP/MEK.
   Terpolymer was first dissolved in MEK with help of the electromagnetic stirrer at a temperature of 70 °C for 4 h. The mass fraction of P(VDF-TrFE-CTFE)/MEK solution is 10 wt.%.
   DEHP was secondly added into the solution and stirred for another 4 h. The mass fraction of DEHP in the all-organic composite is 5, 10, 15 wt.%.
2. The as-prepared solution was cooled to room temperature and put into a refrigerator for 48 h to stabilize the solution and to move the air within the solution.
3. Solution with desired mass was poured into a petri dish with a diameter of 10 mm. A Teflon cover was used to cover the petri dish 3h to get a well distributed liquid within the petri dish.
4. The Teflon cover was taken off and the solvent MEK evaporated and finally we get the P(VDF-TrFE-CTFE)/DEHP composite film.
5. The solution-casted film was taken from the petri dish and put into an oven to remove the residual solvent at 70 °C for 2 h. And continuously, the film was annealed at 110 °C for 2 h to improve its crystallinity.

Table 3.1: Thickness control of P(VDF-TrFE-CTFE)/DEHP composite.

DEHP content (wt.%)	Terpolymer +DEHP (g)	Terpolymer (g)	MEK (g)	DEHP (g)	Required solution (g)
0	0.9	0,9	8,1	0	9
2.5	0.9	0.8775	7.8975	0.0225	8.7975
5	0.9	0.855	7.695	0.045	8.595
10	0.9	0.81	7.29	0.09	8.19
15	0.9	0.765	6.885	0.135	7.785

Since MEK will evaporate from the solution, the final thickness of film can be roughly determined by the mass of terpolymer and DEHP left in the petri dish. As shown in Table 3.1, assuming 0.9 g terpolymer/DEHP left in the petri dish, combined the mass faction of terpolymer/MEK of 10 wt.% and mass fraction of DEHP in terpolymer/DEHP, the mass of terpolymer, MEK and DEHP can be calculated, from which we can get the required solution. The thickness of prepared film was in the range of 70-80 μm.

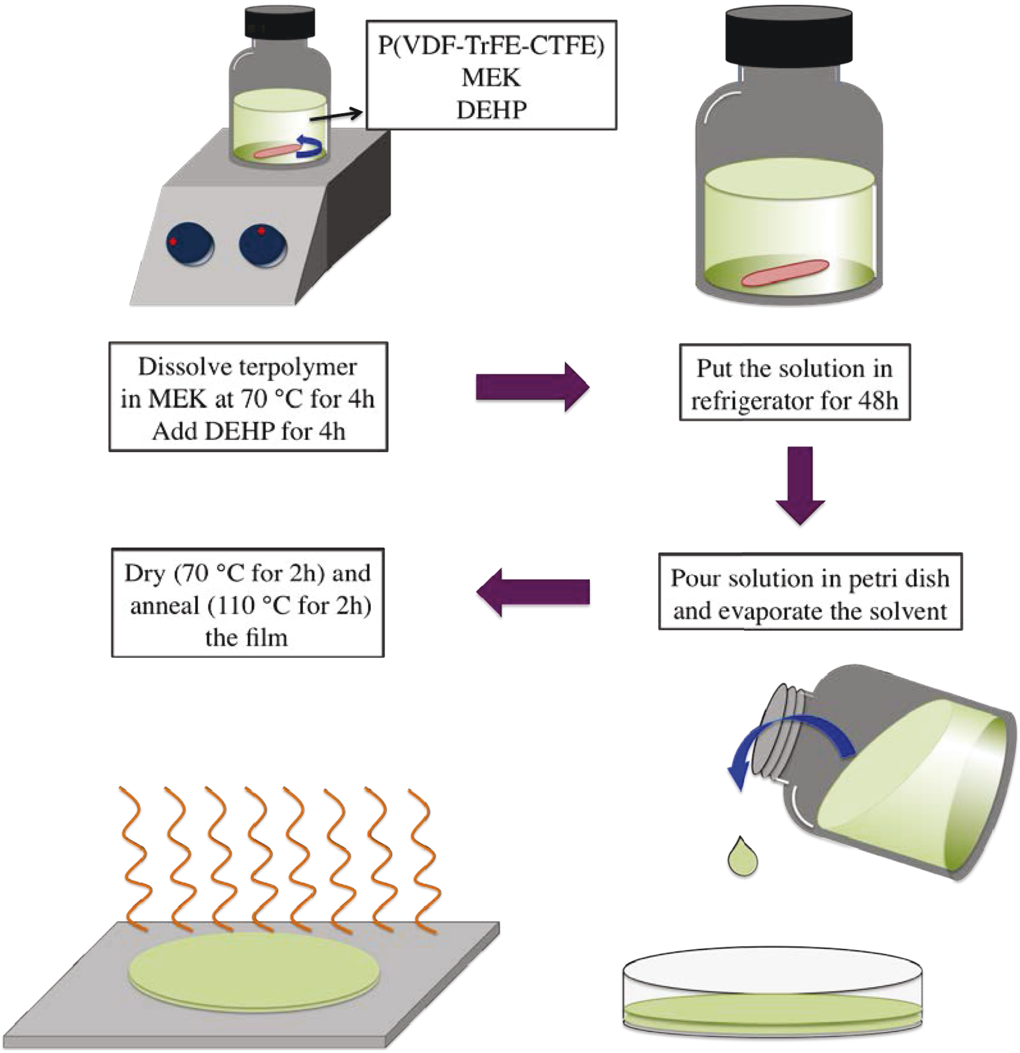

Figure 3.3: Schematic illustration of the fabrication process for P(VDF-TrFE-CTFE)/DEHP composite.

3.2.3 Properties characterization of the DEHP modified terpolymers

In this part, the dielectric properties, dielectric breakdown strength and mechanical properties of P(VDF-TrFE-CTFE)/DEHP composite were carefully characterized. Based on these properties, the electrostrictive response of P(VDF-TrFE-CTFE)/DEHP composite was also investigated.

A. Characterization of dielectric properties

For dielectric measurement, circular gold electrodes with a diameter of 8 mm were first sputtered on both sides of the P(VDF-TrFE-CTFE)/DEHP composite film samples using a Cressington Sputter Coater (208 HR). The dielectric properties was measured with a SI1260 (Solartron) impedance analyzer system in a frequency range 0.1 to 1 MHz.

B. Characterization of dielectric breakdown strength

The sample used for the characterization measurement is as same as those used for dielectric measurement. The measurement was carried out using a self-made equipments as shown in Fig. 2.6 in the previous chapter.

A DC voltage with a ramp rate of 500 V/s was generated by a function generator and amplified by a high-voltage amplifier. Such a voltage was applied to the nanocomposite films until failure. In order to avoid the air discharging and ionization, films were wetted with silicon oil during the measurement. The voltage at which the breakdown took place was recorded by an oscilloscope. E_b was calculated from the recorded voltage divided by the thickness of the film. 16 breakdown tests were performed on each type of sample.

C. Characterization of mechanical properties

The uniaxial tensile measurement were performed using a load (force) sensor cell and a Newport table micro-controller system. As shown in Fig. 3.4, a Microfused^{TM} load cell/force sensor and a ultra-precision linear motor stage (XM550) were mounted on a solid aluminum breadboard. A 4 cm length, 1 cm width film sample was clamped on one side to a fixed clamp and the other side to a mobile clamp. The maximum strain of the film during measurement was set to 1 %, which is realized by precisely controlled motor (1 mm/100 mV). The motor was driven by the voltage signal produced by a function generator. The force generated during stretching the film process was measured by the load cell (250 N/12 V). The strain and stress of the film were finally calculated with the voltage signals from both load cell and motor, which were recorded by the oscilloscope.

Young's modulus of the samples was determined from the slope of the linear dependence of stress versus strain and it was measured at 0.1 Hz, 1 Hz and 10 Hz.

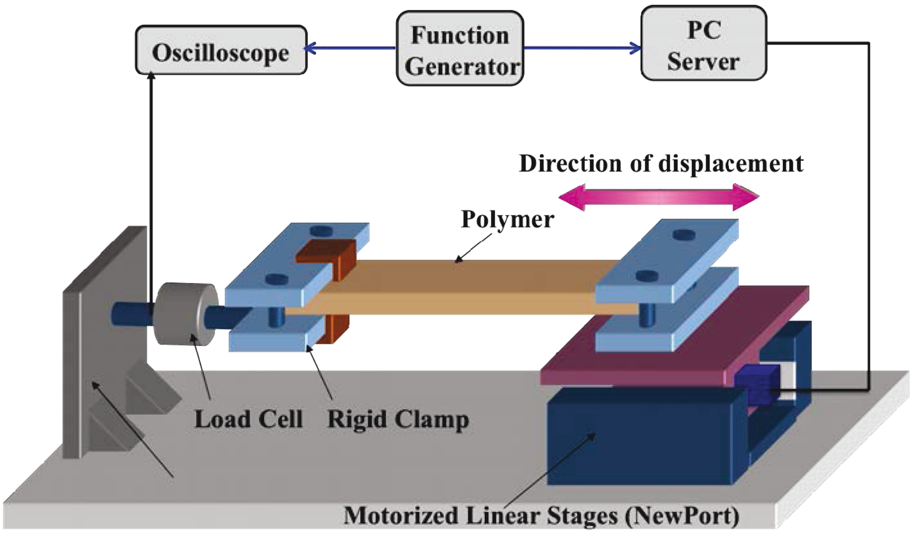

Figure 3.4: Schematic illustration of the equipment for the measurement of mechanical properties for P(VDF-TrFE-CTFE)/DEHP composite.

D. Characterization of electrostrictive strain

The electromechanical properties of DEHP modified terpolymers films were evaluated via a dedicated test bench based on a cantilever theory. After deposition of gold electrode by sputtering (Cressington 208 HR) through a designed mask (Fig. 3.5a), the electroactive film was bonded to a 100 μm-thick PET film using a pressure sensitive adhesive (25 μm-thick Scotch 3M ATG 924). The samples were then laminated at room temperature for 15 minutes using a D&K 4468H laminator machine in order to optimize the bonding of the polymer on the substrate. As shown in Fig 3.5b, the as-prepared cantilever was assembled by three layers, i.e., electroded electroactive films, adhesive and polyethylene terephthalate (PET) substrate.

To perform the electromechanical measurement, the cantilever was hold on a test bench (see Fig. 3.6), in which aluminum profiles were used to fabricate the test bench scaffold on a breadboard. The cantilever was attached to a home-made sample holder comprising a pocket to hold the cantilever and a spring contact to apply the electric field. After being clamped, the effective length of the cantilever for electromechanical measurement was 41 mm (as shown in Fig 3.5c). A laser (BAUMER CH8501) was mounted on the scaffold to record the deflection at the end of the cantilever. And a Labview program was developed to generate and control the applied electric field signal which was amplified by a TREK 609D-6 high-voltage amplifier, and to collect and process the data of the deflection which was measured by the laser and recorded by a National Instrument NIDAQ-9174 test system. Subsequently, the deflection and transverse strain could be directly exported from this program.

The strain can be deduced from the deflection measurements of a unimorph under

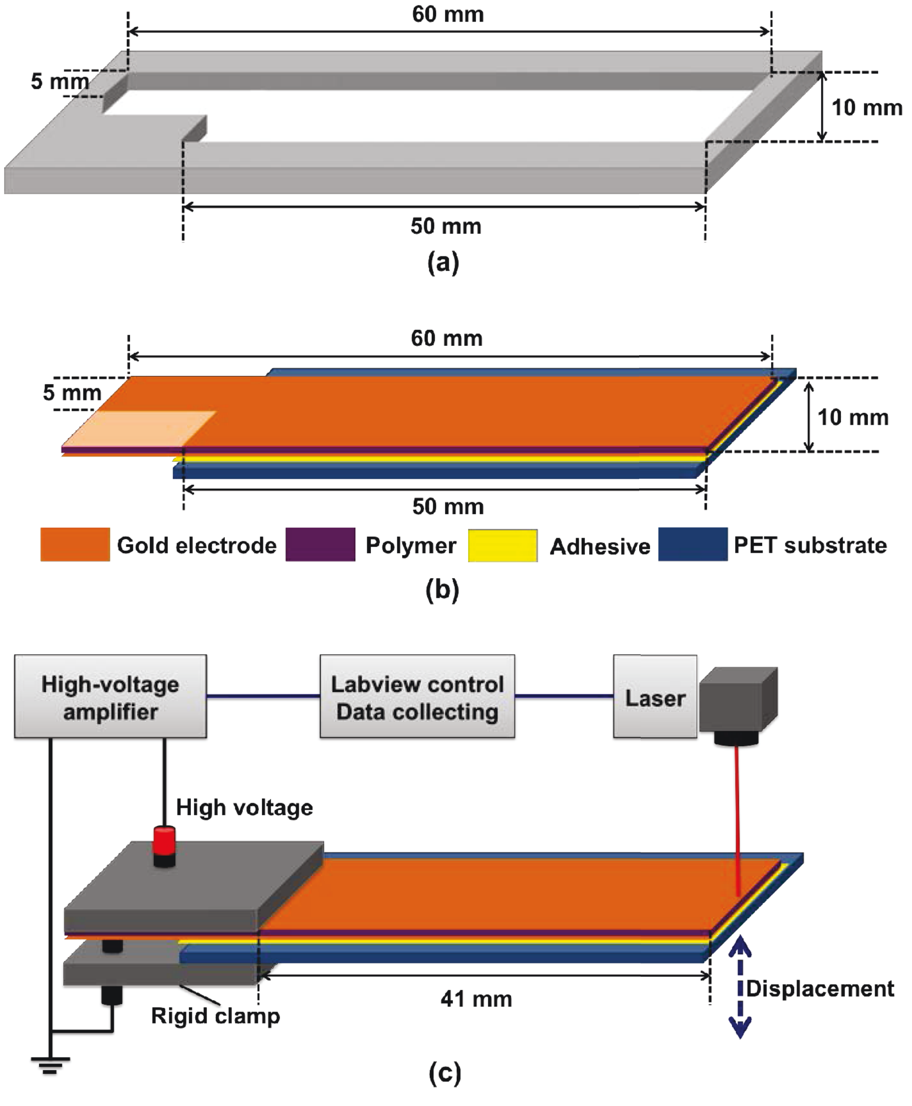

Figure 3.5: Schematic illustration of (a) the mask used for gold electrode sputtering on the polymers, (b) the assembled cantilever polymer bender and (c) the measurement system for electromechanical characterization.

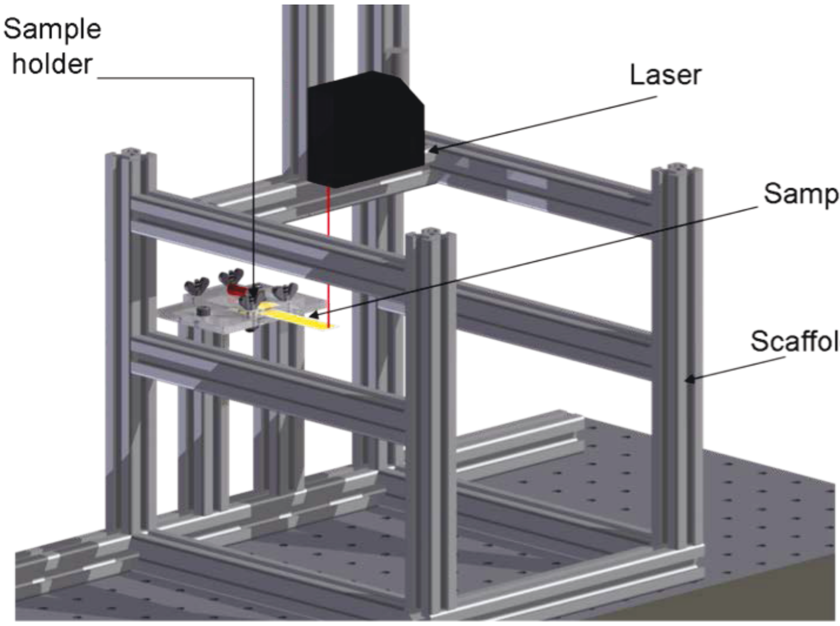

Figure 3.6: Schematic illustration of the test bench developed for the electromechanical characterization.

quasi-static condition using the following expression [151]:

$$\delta_0 = \frac{3L^2}{2e} \frac{2AB(1+B)^2}{A^2B^4 + 2AB(2+3B+2B^2)+1} S_{31}, \tag{3.2}$$

where δ_0 is the cantilever tip deflection, L and e are respectively the effective length and thickness of the electrostrictive polymer samples, $A = Y_{substrate}/Y_{polymer}$ and $B = e_{substrate}/e_{polymer}$ with $Y_{substrate}$, $Y_{polymer}$, $e_{substrate}$, $e_{polymer}$ giving the Young's modulus of electrostrictive polymer, Young's modulus of substrate, thickness of electrostrictive polymer and thickness of substrate, respectively.

The Young's modulus of PET used as the substrate in our experiment is 4.5 GPa, and the electromechanical measurements were carried out at 0.1 Hz and 1 Hz.

3.3 Results and discussions

3.3.1 Dielectric properties of P(VDF-TrFE-CTFE)/DEHP composites

Fig. 3.7a presents the dielectric permittivity of pure terpolymer and DEHP modified terpolymer composites as a function of frequency from 0.1 Hz to 1 MHz at room temperature. At low frequency (lower than 10 Hz), the dielectric permittivity of terpolymer was greatly enhanced with increased DEHP loading. With increased frequency, the dielectric permittivity dramatically decreased and no obvious difference of dielectric permittivity between pure terpolymer and DEHP modified terpolymer was observed when frequency went larger than 100 Hz. Compared with pure terpolymer, which has a dielectric permittivity of

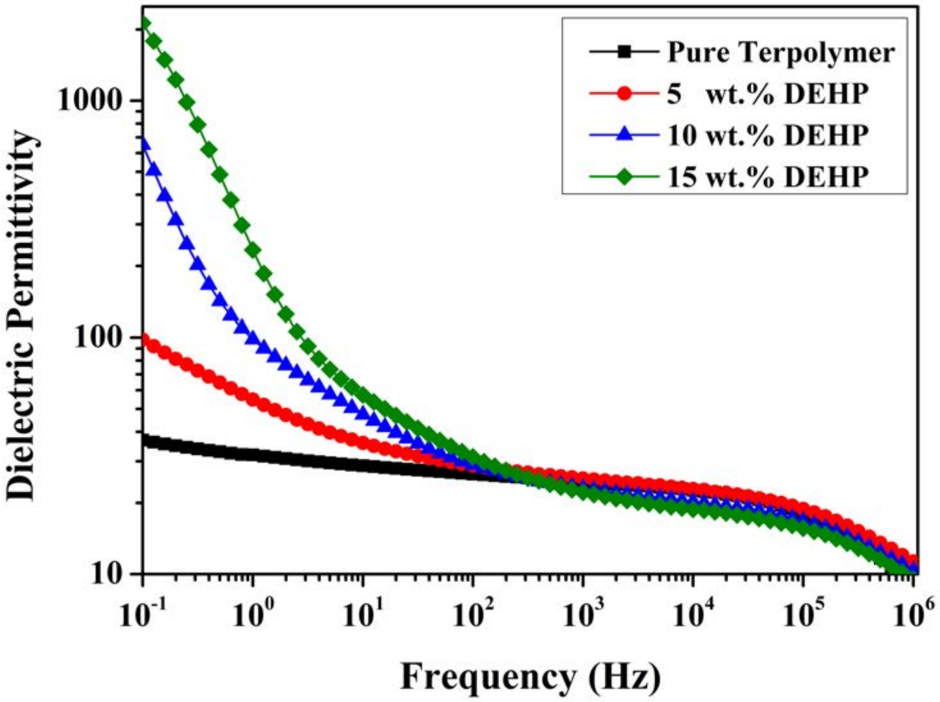

(a)

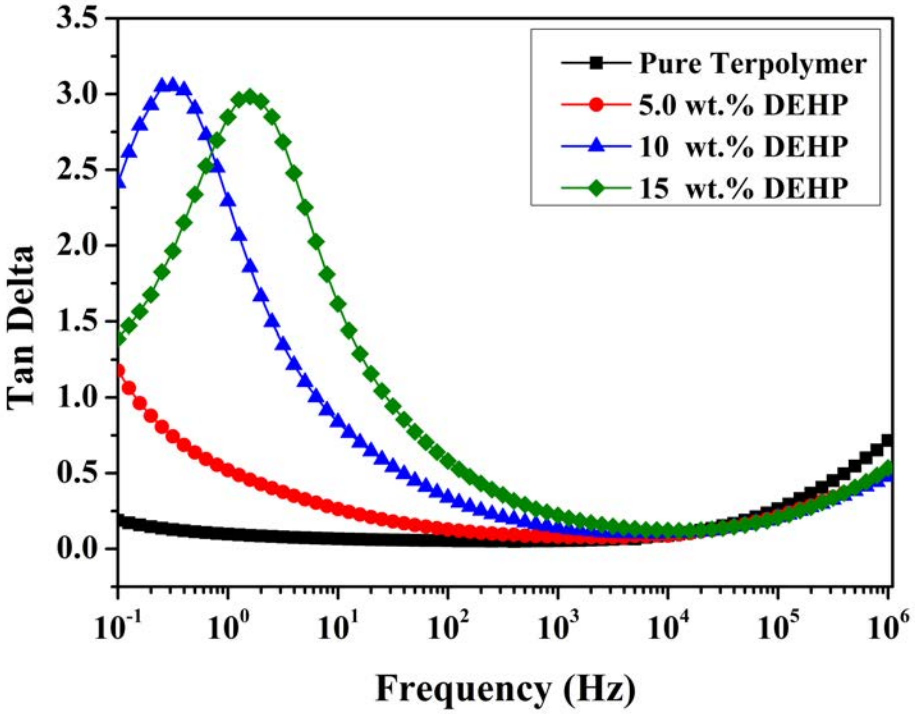

(b)

Figure 3.7: Dielectric properties of P(VDF-TrFE-CTFE)/DEHP composite. Frequency dependency of (a) dielectric permittivity (ε_r') and (b) dielectric loss ($tan\delta$) of composite with different fraction of DEHP (wt.%).

36.8 at 0.1 Hz, the dielectric permittivity was raised to 98.2, 651.2 and 2127.3 at 0.1 Hz for P(VDF-TrFE-CTFE)/DEHP composites with 5, 10, 15 wt.% DEHP loading, respectively. Dielectric permittivity about 60 times higher than pure terpolymer was obtained for 15 wt.% DEHP modified terpolymer. Such a great enhancement of dielectric permittivity with small molecule plasticizer has rarely reported in literatures. The frequency dependence of the dielectric loss ($tan\delta$) for pure terpolymer and DEHP modified terpolymer composites at room temperature is shown in Fig. 3.7b. Correspondingly, increased dielectric loss with DEHP loading was also observed at low frequency. The dielectric loss was increased from 0.19 for pure terpolymer to 2.4 for 10 wt.% DEHP containing terpolymers at 0.1 Hz. A relaxation peak with a dielectric loss about 3 appeared for terpolymers with high loading DEHP and this peak moved to high frequency with increased DEHP loading. According to the typical dielectric spectroscopy, the observed enhancement of dielectric permittivity and the relaxation behavior at low frequency (0.1 to 10 Hz) can be explained by interfacial polarization.

Interfacial polarization, also well-known as Maxwell-Wagner-Sillars (MWS) effect, is a very important polarization mechanism for heterogeneous systems composed of at least two phases [189]. Due to the difference in conductivity and permittivity of different continuous phases within the heterogeneous material system, charge carriers can be blocked and accumulate at the macroscopic inner dielectric boundary layers (interface regions among phases). The blocked charges will be separated by an applied electric field, leading to an additional contribution to the polarization. Unlike other types of polarization (atomic, electronic, dipolar) induced by the displacement or orientation of bonded charge carriers, the charge carriers can be separated over a considerable distance. Therefore the contribution to the dielectric loss can be by orders of magnitude larger than the dielectric response due to the molecular fluctuations. In addition, such a polarization requires more time than the other polarization and it usually occurs in the frequency range from 0.01 to 100 Hz around room temperature, which is the typical work frequency range for soft actuators.

As a result of the kinetic difficulty to form large extended crystals due to the high molecular weight, polymers are typically semi-crystalline by nature. Therefore, semi-crystalline polymers are at least biphasic material consisting of amorphous and crystalline regions. The dielectric permittivity and conductivity of amorphous and crystalline phases are different. Even the crystallites are not electrically conducting, the conductivity of amorphous domains increases with the increasing temperature, especially passing glass-rubber transition temperature (T_g). Charge carriers can move through the amorphous region, but are hindered by the crystalline domains and then pile up near the interface between amorphous and crystalline phases. Hence, a strong interfacial polarization effect is always observed for semi-crystalline polymers at the temperature above T_g of the amorphous domains.

It has been demonstrated that [190], the influence of increased plasticizer loading on the dielectric properties can be equivalent to the influence of elevated temperature on the dielectric properties. The introduced plasticizer DEHP with small molecules acts as a lubricating agent. They insert themselves among polymer chains, expand the free volume and interface region within polymer system and increase the mobility of polymer chains with an decreased T_g. Additionally, plasticizers typically have a higher conductivity (in the order of 10^{-12} - 10^{-9} S·cm) than polymers (in the order of 10^{-16} - 10^{-15} S·cm) [191], and consequently, the conductivity of terpolymer will be definitely increased with the introduction of plasticizer DEHP. Given the two behavior of plasticizer DEHP within terpolymer matrix, more charges can be injected into polymer matrix and larger volume of interface regions with more charges will be formed in the dielectric boundary layers between amorphous phase and crystalline phase, giving rise to the enhanced interface polarization at low frequency. As a result, greatly improved dielectric permittivity and increased dielectric loss were observed at low frequency with increased DEHP loading.

The plasticizing effect of DEHP is also responsible for the evolution of relaxation peak to high frequency. The results depicted in Fig. 3.7b reveal that the accumulated charge carriers at the interface of amorphous region and crystalline region within 15 wt.% DEHP modified terpolymer exhibit a shorter relaxation time than that within 10 wt.% DEHP modified terpolymer. It has been proved that [192], the movement of charge carriers within polymers depends on the motion of polymer chains. With increased DEHP loading, the motion of polymer chains increases in amorphous region and interface region, and as a result, the movement of charge carriers increases. The relaxation time of interface polarization decrease with increasing DEHP loading associated with the increased mobility of charge carriers.

3.3.2 Mechanical properties of P(VDF-TrFE-CTFE)/DEHP composites

The influence of introduced DEHP on the mechanical properties of terpolymer was characterized by a tensile stress verse strain measurement. As we can see from Fig. 3.8a, the measured strain-stress curves exhibit a slight mechanical hysteresis loop for both pure terpolymer and DEHP modified terpolymer. The mechanical loss is associated with the viscoelasticity nature of polymer materials. Since stress has a linear relationship with strain before the yielding point, the Young's modulus was given by the slope of the linearly fitted strain-stress curve from the experimental data.

The Young's modulus of modified terpolymer as a function of DEHP loading measured at different frequency and room temperature is shown in Fig. 3.8b. As depicted, the Young's modulus of terpolymer decreased with increased DEHP loading. For pure terpolymers, the Young's modulus is 163 MPa (at 0.1 Hz). As the DEHP loading was increased, the Young's modulus was reduced to 95.7 MPa for 10 wt.% DEHP modified terpolymer and 87.8 MPa for 15 wt.% DEHP modified terpolymer. The results observed here is in good agreement with plasticizing effect of DEHP. The incorporated DEHP small molecules are distributed among the polymer chains and the free volume which is required for the movement of polymer chains is expanded, leading to an increased mobility of polymer chains and reduced glass-rubber transition temperature. Terpolymer becomes more flexible with more introduced DEHP and exhibits reduced Young's modulus. The increase

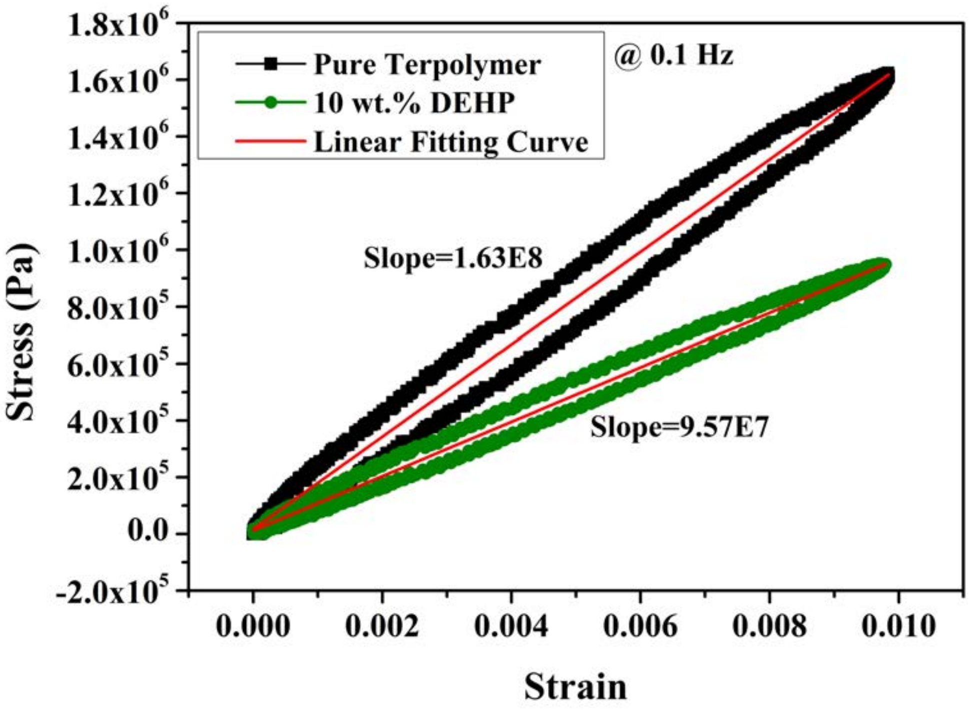

(a)

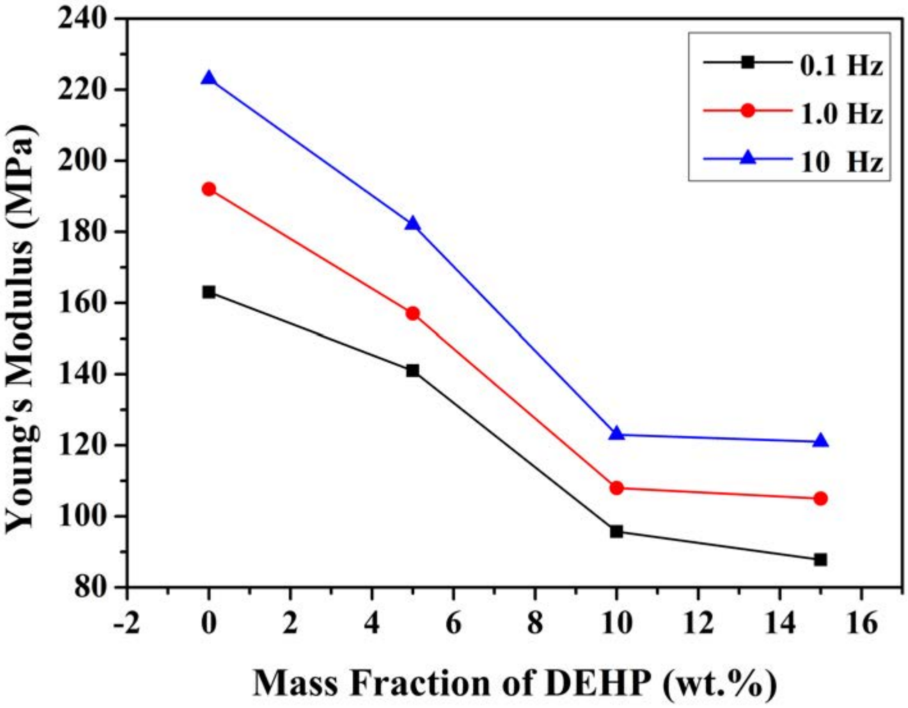

(b)

Figure 3.8: The mechanical properties of P(VDF-TrFE-CTFE)/DEHP composites. (a) The strain-stress curve for pure and 10 wt.% modified terpolymers at 0.1 Hz; (b) The Young's modulus of P(VDF-TrFE-CTFE)/DEHP composites as a function of DEHP loading at 0.1, 1 and 10 Hz.

of Young's modulus with frequency is also contributed to viscoelasticity nature of polymer materials. At high frequency, polymer chains do not have enough time to move and response to the applied external mechanical force, yielding a decreased deformation and increased elastic modulus.

3.3.3 Dielectric breakdown strength of P(VDF-TrFE-CTFE)/DEHP composites

The dielectric breakdown strength was measured with 16 samples for each type of DEHP modified P(VDF-TrFE-CTFE) terpolymer. The Weibull probability analysis (see Section 2.4.3) results of measured dielectric breakdown strength for pure terpolymer and DEHP modified P(VDF-TrFE-CTFE) terpolymer are presented in Fig. 3.9. As depicted, a decrease of dielectric breakdown strength was observed with increased DEHP loading. For pure terpolymer, the dielectric breakdown strength has a value as high as 269 MV/m and decreases to 207 MV/m for terpolymer with a DEHP loading of 10 wt.%. Dramatically decrease of dielectric breakdown strength is found for 15 wt.% DEHP containing terpolymers with a value of 79 MV/m. Such a decrease of breakdown strength always accompany with the increase of dielectric permittivity for composite materials.

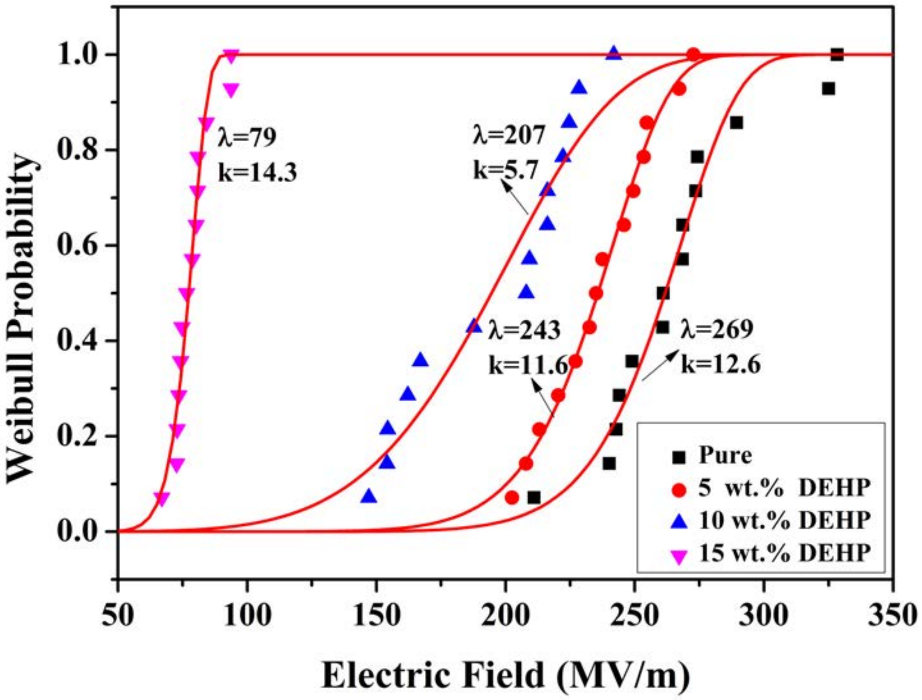

Figure 3.9: Weibull probability analysis of measured DC dielectric breakdown strength for P(VDF-TrFE-CTFE)/DEHP composites.

The decreased dielectric breakdown strength maybe contributed to three aspects:

Firstly, as we discussed in previous section, the introduced plasticizer DEHP improves the mobility of polymer chains and correspondingly enhances the mobility of charge carriers; Secondly, the higher conductivity of plasticizer compared with terpolymer increased the overall conductivity of DEHP modified terpolymer; Thirdly, semi-crystalline terpolymer is biphasic material by nature and the expanded interfacial region due to the plasticizing effect of DEHP further enhances the heterogeneousness of the polymer system, resulting into increased non-uniformity of the distribution of electric field within terpolymer. All of these lead to the reduction of dielectric breakdown strength with increased DEHP loading. Fortunately, unlike polymer composite mixed with inorganic fillers, the breakdown strength for DEHP modified terpolymer even with a very high DEHP loading is not reduced to a very low level. The introduction of plasticizer DEHP greatly increased the low frequency dielectric permittivity, and more importantly in the meanwhile, a breakdown strength as high as possible was achieved, which is favorable for the electromechanical application of electrostrictive polymers.

3.3.4 Electromechanical performances of P(VDF-TrFE-CTFE)/DEHP composites

The electromechanical performance of DEHP modified terpolymer was carried out by applying a sinuous electric field with different frequency to an electrostrictive polymer cantilever bender as described in section 3.2.3. Deflexion and corresponding transverse strain calculated from the Eq. 3.2 during one cycle of an applied electric field were directly exported from the Labview program. The electric field induced transverse strain for pure terpolymer and 10 wt.% DEHP modified terpolymer as a function of applied sinuous electric field with a maximum value of 20 MV/m at 0.1 Hz is presented in Fig. 3.10a. The observed hysteresis loops for both pure and modified polymers represent the mechanical loss during electromechanical cycles due to the viscoelasticity of polymer as we discussed in elastic modulus part. As we can see, the electromechanical response of terpolymer was improved by introduced plasticizer DEHP. The maximum transverse strain measured at 20 MV/m and 0.1 Hz was increased from 0.094 % for pure terpolymer to 0.63 % for 10 wt.% DEHP modified terpolymer, which is about 6.6 times higher.

In order to further investigate the relationship between electrostrictive strain and applied electric field for pure and modifier terpolymers, transverse strain as a function of increased electric field during one cycle is depicted in Fig. 3.10b, which was taken from the downside curve of the loop shown in Fig. 3.10a. It is worthy to note that, for pure terpolymer and 5 wt.% DEHP modified terpolymer, field induced strains exhibit an quadric relationship with applied electric field, whereas non-quadric behavior between field induced strain and applied electric field was observed for 10 wt.% and 15 wt.% DEHP modified terpolymers. Since the field induced strain as a function of electric field can be given by

$$S_{31} = M_{31}E^2, \tag{3.3}$$

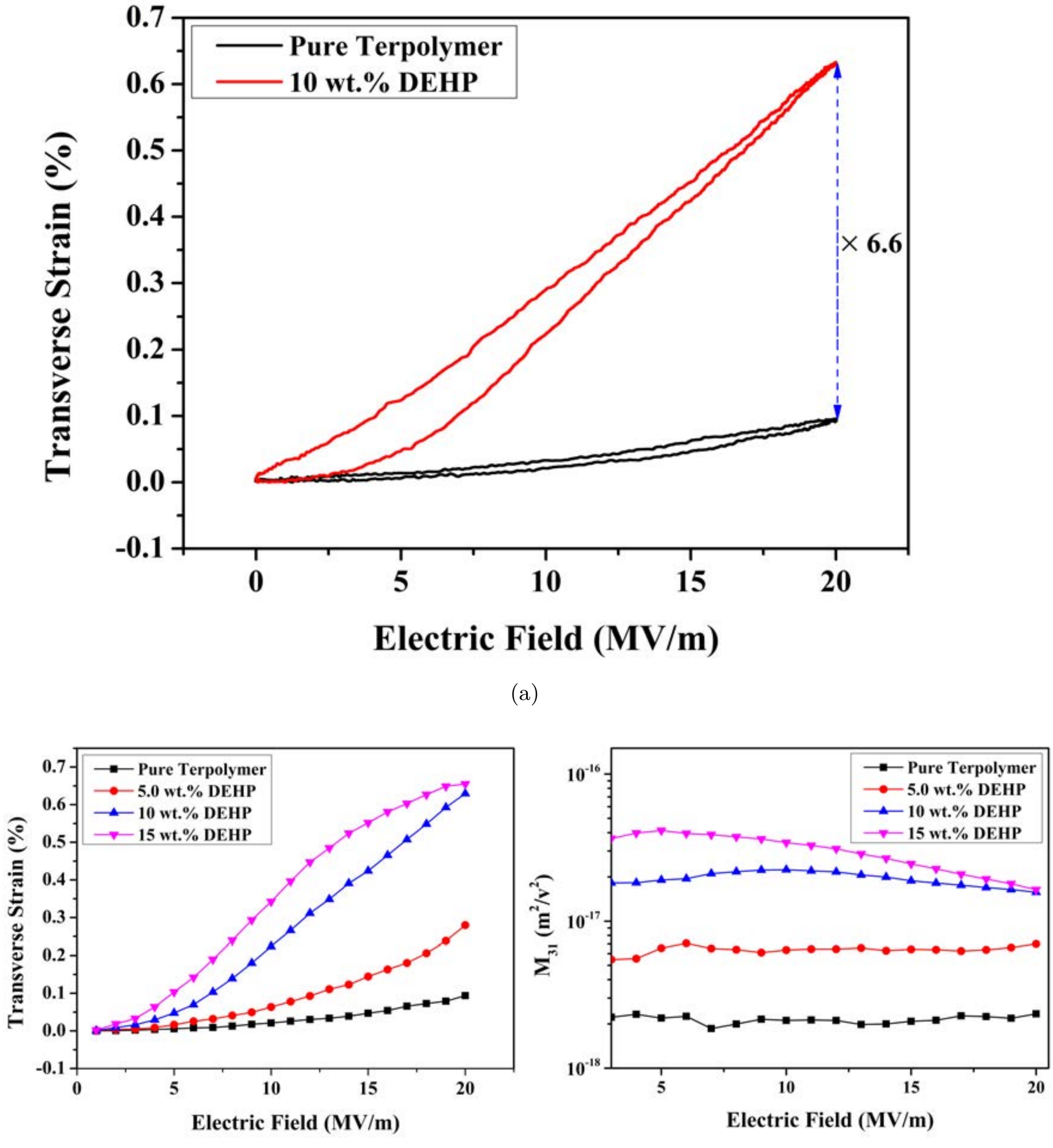

(a)

(b)

(c)

Figure 3.10: Electrostrictive performance measured at electric field with an amplitude of 20 MV/m at 0.1 Hz and room temperature: (a) The transverse strain-electric field loop during one applied electric field cycle for pure and 10 wt.% DEHP modified terpolymer; (b) The transverse strain as a function of increased electric field during one cycle for pure and modified terpolymer; and (c) The evolution of electrostrictive coefficient (M_{31}) derived from (b) with electric field.

where S_{31} is the transverse strain and M_{31} is the electrostrictive coefficient, the evolution of electrostrictive coefficient M_{31} for pure terpolymer and modified terpolymer derived from Fig. 3.10b was presented in Fig. 3.10c. As depicted, 5 wt.% DEHP modified terpolymer and pure terpolymers show a generally constant electrostrictive coefficient M_{31} at the measured electric field range. The average value of M_{31} for 5 wt.% DEHP modified terpolymer is about 6.75×10^{-18} m^2/V^2, which is more than 3 times higher than that for pure terpolymer ($M_{31} = 2.01 \times 10^{-18}$ m^2/V^2). However, a decrease of M_{31} with increased electric field was observed for 10 wt.% and 15 wt.% DEHP modified terpolymers. The difference is that the electric field (E_s) at which the decrease of M_{31} occurs for 15 wt.% DEHP modified terpolymer is lower than that for 10 wt.% DEHP modified terpolymer. The values of E_s are about 10 MV/m and 5 MV/m for 10 wt.% and 15 wt.% DEHP modified terpolymers, respectively. Consequently, M_{31} for 15 wt.% DEHP modified terpolymer is about 20 times higher than that for pure terpolymer at $E = 5$ MV/m, while it is about 7 times higher at $E = 20$ MV/m.

Fig. 3.11 presents the maximum field induced deflexion of the end of electroactive polymer cantilever bender and calculated transverse strain as a function of the electric field amplitude at 0.1 Hz. It is clear that the DEHP modified terpolymers exhibit higher field induced deflexion and strain than pure terpolymer at the same electric field. At $E =$ 25 MV/m, modified terpolymer with 5 wt.% and 10 wt.% DEHP exhibit a cantilever end deflexion of 6.88 mm and 13.22 mm, respectively, in comparison with 2.78 mm for pure terpolymer (see Fig. 3.11a). At $E = 30$ MV/m, the modified terpolymer with 10 wt.% DEHP demonstrates a transverse strain of 1 %, whereas the transverse strain for pure terpolymer shows a more than 5 times lower value of 0.17 % (see Fig. 3.11b).

The maximum field induced transverse strain of DEHP modified terpolymer as a function of DEHP loading measured at 0.1 Hz is shown in Fig. 3.12. At low electric field, the transverse strain increases with increasing DEHP loading. For instance, At $E = 15$ MV/m, modified terpolymers with 5 wt.%, 10 wt.% and 15 wt.% DEHP exhibit transverse strains of 0.19 %, 0.45 % and 0.60 %, respectively, while the transverse strain for pure terpolymer is only 0.06 %. However, at electric field larger than 15 MV/m, modified terpolymer with 10 wt.% DEHP loading exhibits an even stronger strain response than 15 wt.% DEHP containing terpolymer. As we can see from Fig. 3.11b, for both 10 wt.% and 15 wt.% DEHP loading terpolymers, field induced strains increase with increased electric field, but increment of strain for 15 wt.% DEHP containing terpolymer with increased electric field is smaller than that for 10 wt.% DEHP containing terpolymer. As discussed in previous section, the modification of terpolymer with plasticizer DEHP gives rise to the greatly improved dielectric permittivity and slightly reduced elastic modulus, both of which lead to observed enhanced field induced strain. The observed non-quartic relationship between field induced strain and applied electric field for high DEHP loaded terpolymer and obvious saturation behavior of electrostrictive strain for 15 wt.% DEHP modified terpolymer are associated with the dielectric saturation phenomenon of terpolymer [183]. For dielectrics, the overall polarization is contributed to all the polarization

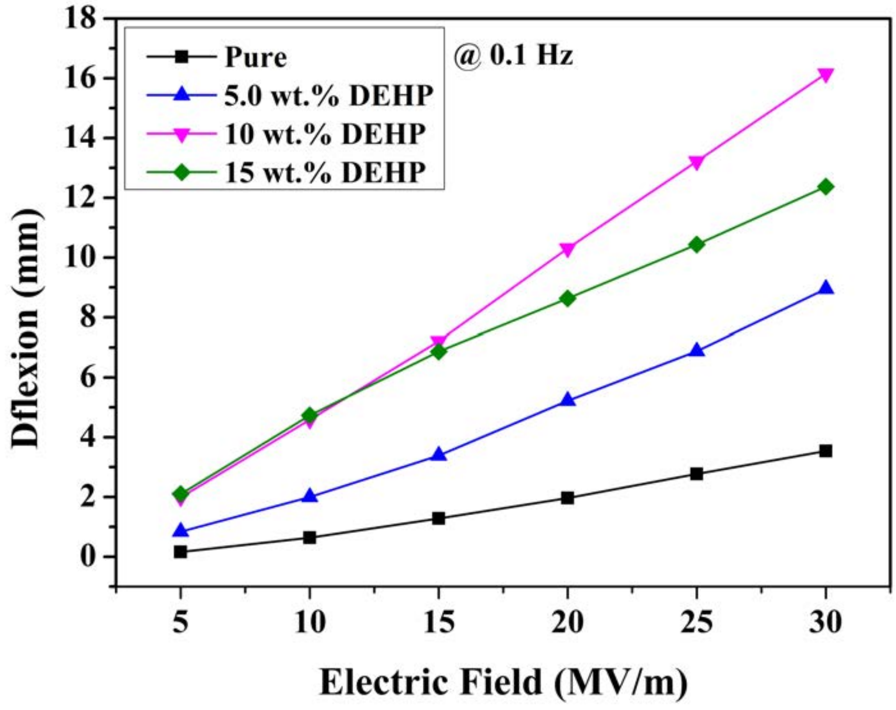

(a)

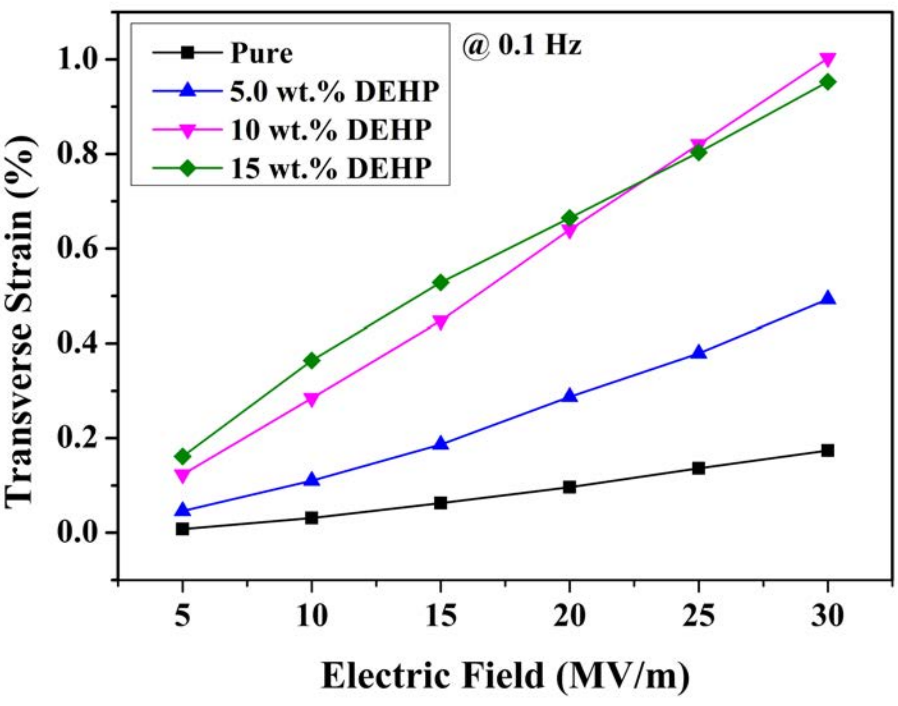

(b)

Figure 3.11: Electrostrictive performance: (a) Deflexion of the end of electroactive polymer cantilever and (b) transverse strain as a function of applied electric field amplitude for pure and DEHP modified terpolymers measured at 0.1 Hz and room temperature.

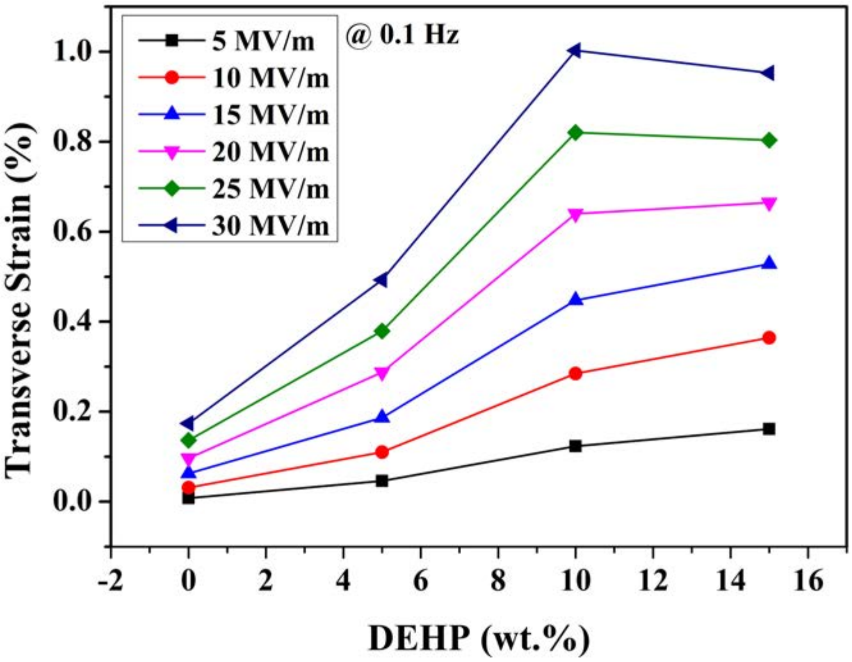

Figure 3.12: Transverse strain as a function of different DEHP loading measured at different electric field at 0.1 Hz.

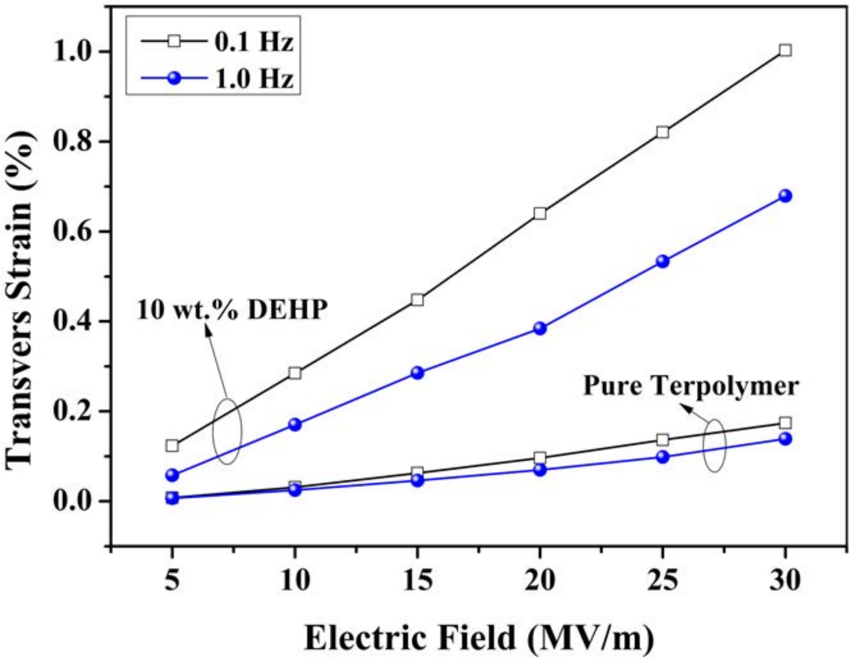

Figure 3.13: Frequency dispersion of field induced transverse strain for pure and 10 wt.% modified terpolymer.

mechanism, including atomic polarization, electronic polarization, orientation polarization and interfacial polarization. For atomic polarization and electronic polarization, the polarization-field relationship should keep linear even at high electric field. However, the linear polarization-field relationship for orientation polarization of dipolar and interfacial polarization of separation of trapped charge carrier is only valid at low electric field and becomes nonlinear at high fields. For orientation polarization, all individual molecules will be largely oriented at high electric field, and meanwhile, for interfacial polarization, charge carriers will be separated to the maximum distance at high electric field since they are tapped in the confined interface region. As a result, there can be little extra polarization from the further orientation of dipolar or separation of charge carriers when the field is further increased. Under this situation, the polarization becomes saturated. Hence, the dielectric permittivity will decrease with increased electric field and reaches a stable value at saturation state. Since electrostrictive effect arises from polarization effect in response to the applied electric field, the saturation of polarization leads to a decrease of electrostrictive coefficient (M_{31}) and finally the saturation behavior of the field induced strain. For DEHP modified terpolymers, the increased mobility of polymer chains facilitates the orientation of dipolar of terpolymer and the mobility of charge carriers. As a result, terpolymers with more plasticizer DEHP exhibit dielectric saturation and corresponding electrostrictive saturation at lower electric field.

Fig. 3.13 presents the frequency dispersion of field induced strain for pure terpolymer and 10 wt.% DEHP modified terpolymer. A typical decrease of field induced strain with increased frequency of applied electric field was observed, since the electrostrictive response is related with the microscopic dipolar orientation and involved motion of polymer chains, both of which require certain time to response. 10 wt.% DEHP modified terpolymer shows much stronger frequency dependence than pure terpolymer. For 10 wt.% DEHP modified terpolymer, 32 % decrease of field induced strain measured at $E = 30$ MV/m was observed from 1 % at 0.1 Hz to 0.68 % at 1 Hz, whereas smaller strain decrease of 20 % was found for pure terpolymer from 0.174 % at 0.1 Hz to 0.139 % at 1 Hz. The increased nonuniform of charge carrier distribution due to introduced DEHP is responsible for the strong frequency dependence of DEHP modified terpolymer [193].

Table 3.2: Comparison of electromechanical performances of DEHP modified terpolymer at 20 MV/m and 0.1 Hz.

DEHP Loading (wt.%)	Y (MPa)	ε_r at 0.1 Hz	E_b (MV/m)	S_{31} (%)	M_{31} (m^2/V^2)	$YS_{31}^2/2$ (J/cm^3)
0	163	36.8	269	0.094	2.34×10^{-18}	7.16×10^{-5}
5	141	98.2	243	0.28	7.00×10^{-18}	5.52×10^{-4}
10	95.7	651.2	207	0.63	1.57×10^{-17}	1.90×10^{-3}
15	87.8	2127.3	79	0.66	1.63×10^{-17}	1.88×10^{-3}

In addition to improved field induced strain of electroactive polymer, an enhanced

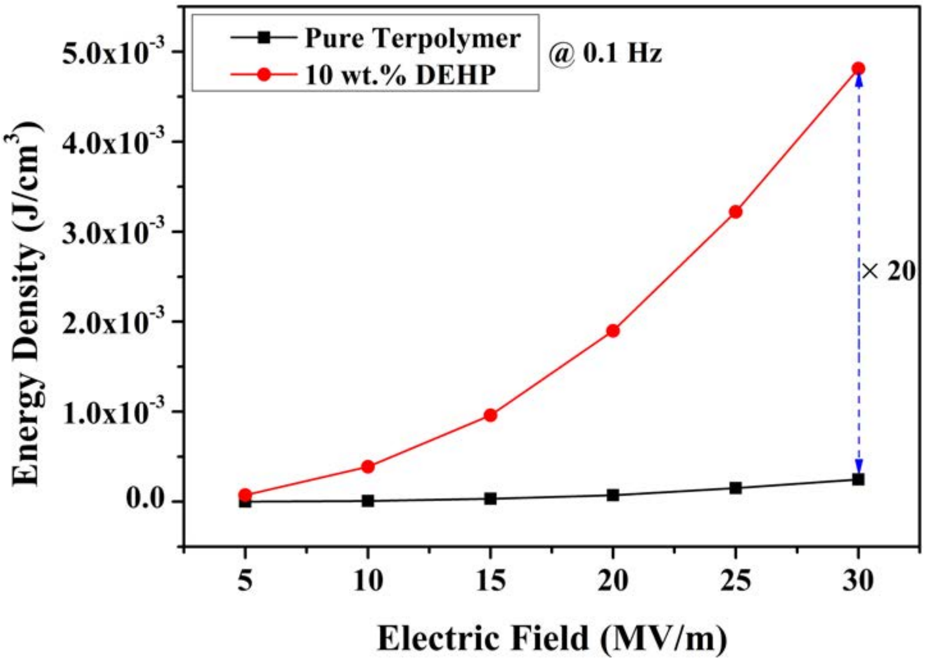

Figure 3.14: Evolution of elastic energy density of pure and 10 wt.% DEHP modified terpolymer measured at 0.1 Hz.

elastic energy density is also required for a high performance electroactive polymer. Here, the elastic energy density is evaluated by $YS_m^2/2$ at 0.1 Hz and the comparison of elastic energy density of pure terpolymer and 10 wt.% modified terpolymer at different electric field is shown in Fig. 3.14. It is obvious that DEHP modified terpolymer demonstrates higher elastic energy density than pure terpolymer. At $E = 30$ MV/m, the elastic energy density for 10 wt.% modified terpolymer is 4.81×10^{-3} J/cm^3, which is about 20 times higher than that of pure terpolymer of 2.47×10^{-4} J/cm^3. The properties and comparison of electromechanical performance of pure and modified terpolymer at $E = 20$ MV/m and 0.1 Hz are summarized in Table 4.1. The introduction of DEHP into terpolymer matrix improved the field induced strain, electrostrictive coefficient and elastic energy density. Due to the saturation of dielectric permittivity and low elastic modulus, 15 wt.% DEHP modified terpolymer exhibit lower elastic energy density than 10 wt.% DEHP modified terpolymer.

3.4 Conclusion

Based on the heterogeneous nature of semi-crystalline terpolymer and the important role that interface polarization plays for dielectric and electromechanical response, small molecular plasticizer DEHP was introduced into electrostrictive terpolymer to form an all-organic polymer composite with improved electromechanical performances.

The experimental results indicate that, the introduced plasticizer DEHP expands the free volume of the terpolymer and increased the mobility of polymer chains. As a result, more charge carriers are trapped in the expanded interface region between amorphous region and crystalline region, leading to a dramatically increased dielectric permittivity at low frequency due to the enforced interfacial polarization and moderately decreased dielectric breakdown strength. In addition, terpolymer becomes softer (lower Young's modulus) with increased DEHP loading than pure terpolymer.

On the basis of the modification of terpolymer's properties with plasticizer DEHP, terpolymers with improved electromechanical performance were achieved. DEHP modified terpolymers exhibit much higher field induced strain and elastic energy density than pure terpolymer. For instance, terpolymer with 10 wt.% DEHP loading has a field induced transverse strain of 1 % and elastic energy density of 4.81×10^{-3} J/cm^3 at an electric field of 30 MV/m and 0.1 Hz, which are about 5 times and 20 times higher than those of pure terpolymer, respectively. It is worthy to note that, terpolymers with 10 wt.% DEHP loading shows better electrostrictive performance than terpolymers with 15 wt.% DEHP loading. Saturation of field induced strain occurs for 15 wt.% DEHP modified terpolymer at high electric field, which is associated with the early appearance of dielectric saturation behavior at lower electric field due to the accelerated orientation of dipolar by DEHP.

In summary, the modification of electrostrictive terpolymer with plasticizer DEHP provide a promising way to achieve an all-organic electroactive polymer with improved electromechanical properties. Potential applications based on such an electroactive polymers addressed here can be developed.

Chapter 4

Energy Harvesting via DEHP Modified Terpolymer

Energy harvesting is a very attractive technology which can convert ambient energy available in the environment into electrical energy. Electrostrictive polymers with high electromechanical performances have great potential for mechanical energy harvesting due to their low cost, good mechanical property and ease of processability.

In this chapter, terpolymer modified with 2.5 wt.% DEHP was investigated for energy harvesting applications. Due to the improved electromechanical properties by DEHP, modified terpolymer exhibits an enhanced energy harvesting performance in contrast of pure terpolymer. The generated maximum short-circuit current and power density are 3.635 μA and 607 μW/cm^3 for modified terpolymer, respectively. Based on the quadric relationship between the energy conversion efficiency and DC bias electric field, an estimated energy conversion efficiency as high as 34 % and a corresponding electrical power density of 4.31 mW/cm^3 can be achievable for modified terpolymer working at a DC bias electric field of 30 MV/m.

4.1 Introduction of energy harvesting technologies

Energy harvesting, also referred to energy scavenge, is without any doubt an emerging and very attractive technology which is used to convert ambient energy available in the environment into electrical energy. The development of state-of-the-art energy harvesting technology is driven mainly by two aspects as follows: The first motivation is energy crisis which is caused by the contradiction between the ever-increasing energy demands for industrial and civil applications and limited reserves of non-renewable energy sources such as petroleum, coal and natural gas. A pressing matter of the moment is to search and develop new renewable energy sources and technology to solve the energy crisis and corresponding environmental problems such as globe warming caused by the consumption of traditional energy. The second motivation is the requirement for reliable energy sources for nowadays ubiquitously deployed mobile and autonomous wireless electronic devices. A typical example of such electronic devices is wireless sensor network nods [194], each of which compromises a sensor, process electronics, wireless communication components and power supply. In general, these electronic devices features small size, little power consumption and are usually integrated or implanted in a complicated system. As a result, the widely used batteries, which have been the power supply of choice for traditional mobile electronic devices, are not practicable for the emerging electronic devices with scaled-down size, since batteries typically have a limited capacity of electrical energy and a periodic change or charging is needed. In addition, there are environmental concerns about disposing of batteries. Energy harvesting technology, therefore, has been developed under this background to provide a renewable energy sources and an alternative power supply for mobile and wireless electronic devices. By converting ambient energy in the environment, electronic devices with energy harvesters can be uninterruptedly self-powered during their lifetime, which is preferable for minimized implantable and wearable electronic systems.

4.1.1 Potential energy resources and energy harvesting technologies

Various types of energy resources existing in the ambient environment can be exploited for energy harvesting, including electromagnetic wave radiation (Radio-Frequency radiation and light), thermal gradient (thermal fluctuation), kinetic energy (vibration/motion, air flow, human activity). Although several authors have already literatured the energy harvesting technologies [195–198], a brief review of the state-of-the-art development of energy harvesting with different ambient energy sources will be presented here for a clear understanding and comparison.

A. Radio frequency energy harvesting

With proliferation of wireless and mobile electronic devices, the ubiquitous ambient radio frequency (RF) radiation in the air have attracted much of interest as an energy reservoir for self-powered devices. A typical RF energy harvesting system is composed of an antenna which is used to receive radio waves, a RF-to-DC converting component, a power conditioning component and a working load [199]. It works on the same principles as the widely used passive radio frequency identification (RFID) systems for data collection, which are driven by the RF waves emitted from the tag reader. In 2009, Nokia [200] proposed a project aiming at charging batteries of cell phone with ambient electromagnetic radiations emitted from Wi-Fi transmitters, cell-phone antennas, TV masts. In recent years, an new concept "internet of things (IoT)" based on the cluster of miniatured logistic electronic devices is emerging and in the word of IoT, each object has its unique identity and the ability to communicate with each other. The IoT units can be powered by RF energy harvesting from ambient RF signals including TV, cellular and Wi-Fi transmissions but the traditional Wi-Fi technology is not practical for transferring data among IoT units since the power used to send data via Wi-Fi is in the level of hundreds of milliwatts, which is tens of thousands of times higher than the harvested energy from RF radiations. Very recently, Kellogg *et al.* [201] reported a new communication system named Wi-Fi backscatter. With incorporation of ambient backscatter technology, Wi-Fi backscatter devices can be driven by harvested energy from ambien RF signals, and can communicate with Wi-Fi-enabled devices with negligible power consumption. Such a system pave the way for the development of IoT. However, the RF energy harvesting is very limited in power, generally in the range of few μW. In addition, RF energy harvesting requires a very large area for collecting radiation energy and should be very close to the radiation source to get useful energy level [195].

B. Light and solar energy harvesting

Another form of available radiation energy is light radiation, especially the solar energy. The investigation of solar cell which can be used to convert solar energy into electrical energy by photovoltaic effect have always been one of the most intensively researched field. When photons are absorbed by materials like semi-conductive silicon, the energy of photons is transfered to the electrons within materials and as a result electrons can flow through materials to produce electricity. There are many members of solar cell family, including mono-crystalline/multi-crystalline silicon cell, cadmium telluride thin film cell, multi-junction cell, dye-sensitized cell, organic cell, the emerging perovskite cell and so on. The main problems for solar cells are the low power conversion efficiency (PCE) and high cost. For commercially applied solar sell, PCE typically has a value of 15 % - 20 %, while, according to the latest research cell efficiency records (up to January 2015) of National Center for Photovoltaic[1], a new record of PCE has reached to 46 % in the laboratory (Fig. 4.1).

The typical generated power are 15 mW/cm^2 and 10 μW/cm^2 for solar cells outdoor and indoor, respectively [202]. Moreover, the power generation capacity is closely depen-

---

[1] www.nrel.gov/ncpv/

dent on the light vibration, and sufficient light energy is required to produce large power. Therefore, solar cells are clearly not unsuitable for embedded applications where no light may be present.

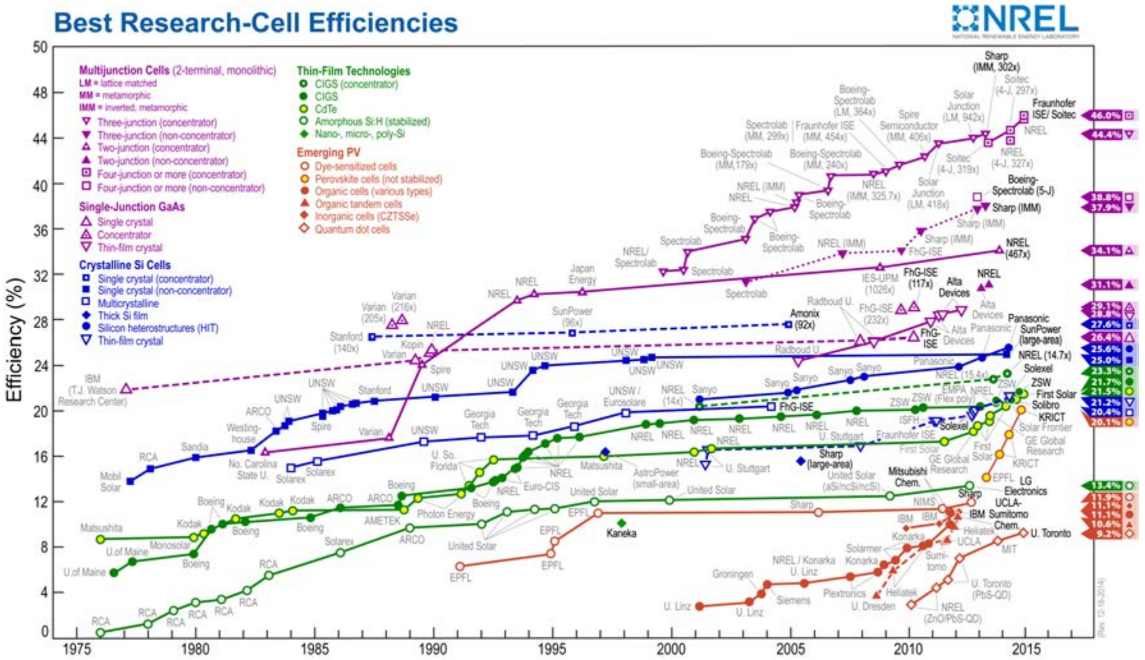

Figure 4.1: Research cell efficiency records of photovoltaic by NREL.

C. Thermal energy harvesting

Thermal energy can be converted into electric energy by thermoelectric or pyroelectric effect. When a thermal gradient is applied on a thermoelectric material, charge carriers within materials will diffuse from the hot side to the cold side, resulting the flow of charge carriers and a voltage, while for pyroelectric effect, the generated voltage arises from the change of spontaneous polarization of certain crystals due to the temperature change of the environment. Thermoelectric effect includes three identified effects: seebeck effect, peltier effect, and thomson effect [203]. Since a thermal gradient is required and the generated power depends on the thermal conductivity of materials, thermoelectric energy harvesting shows a low energy converting efficiency. In contrast, a temporal temperature change (fluctuation) in the environment is necessary without imposing an thermal gradient. It has been demonstrated by Sebald *et al.* that [204], pyroelectric device shows a efficiency of 50 % and a generated power of 1 μW/cm^3, while thermoelectric device shows a efficiency of 1.7 % with a same level of generated power. Ferroelectric materials like PZT and P(VDF-TrFE) can be used as pyroelectric energy harvesting materials [205]. Like solar cells, sufficient temperature changes are required for thermal energy harvesting, which limits its application field.

D. Kinetic energy harvesting

Kinetic energy harvesting refers to the conversion of ambient energy in the form of mechanical movement into electrical energy. Kinetic energy is very common in the environment in the form of mechanical vibration or motions. They range from the subtle vibrations of the floors and walls, the flow of air or liquid and rotating machinery to the very high loads of mechanical vibration of an automobile or aircraft engine. They exist ubiquitously even inside human bodies such as heart beats, muscle stretching. It varies widely in frequency and amplitude with different energy level. Unlike the aforementioned ambient energy sources, kinetic energy features less application restriction from exterior environmental factors. Regardless of the input energy and energy conversion efficiency, the achievable generated power from different power sources is shown in Fig. 4.2 [202,206]. It can be found that energy harvesting based on vibration energy resources perform much better than other potential ambient energy sources in terms of generated power, including solar and thermal energy sources. In addition, the power density of vibration-based energy harvesting devices can be comparable to some lithium-ion batteries with a value up to 100 mW/cm^3 [207].

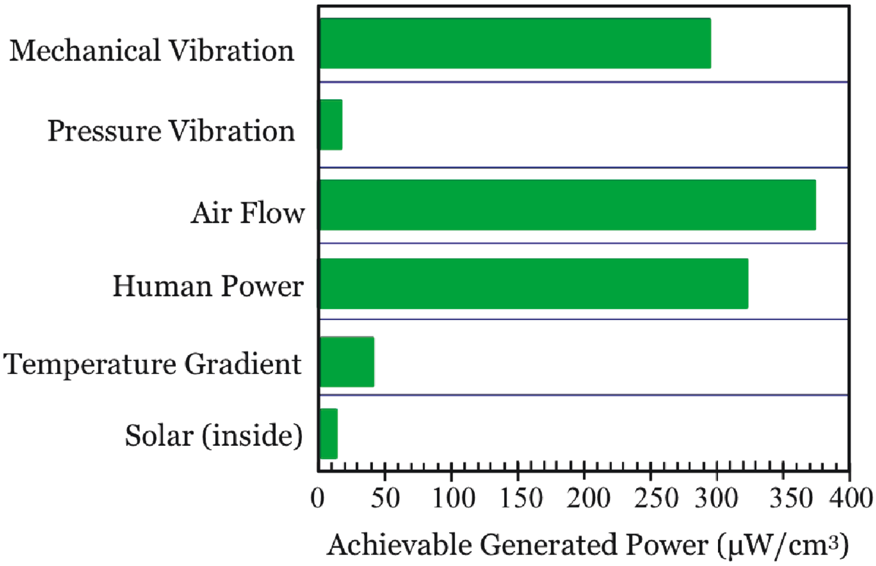

Figure 4.2: Comparison of achievable generated power from different power sources. (Reproduced from [206])

The kinetic energy can be converted into electrical energy by three different transduction methods: electromagnetic, electrostatic and piezoelectric transduction [208, 209]. Due to the ability of directly converting mechanical energy into usable electrical energy and the ease to be integrated into a system, piezoelectric materials have attracted most investigation in the past decade. A typical energy harvesting system is composed of an energy harvester which can extract and convert ambient energy into electric energy, an power processing interface which can optimize the energy conversion efficiency, an electrical energy storage or voltage regulation component and a load. Much attention have been paid to improve the energy conversion efficiency and power generation by design of the piezoelectric configuration, interface circuitry and power storage methods. Detailed discussion can be referred to the review paper of Anton *et al.* [210]. Here, we focus on the piezoelectric materials which plays a prerequisite role in energy conversion process.

The most widely used piezoelectric materials for energy harvesting are piezoelectric ceramics such as lead zirconate titanate (PZT) [211] and lead-free piezoelectric ceramics [212] due to their high electromechanical coupling coefficient ($k_{33} > 0.5$). However, piezoelectric ceramics typically have a very high modulus, and therefore they can sustain very small strain up to 0.1 % especially in response to the ambient vibration with small energy level, yielding a small elastic energy density available for energy conversion. In addition, they are very brittle in nature and susceptible to fatigue crack growth when subjected to high frequency cyclic loading [210]. The disadvantages of piezoelectric ceramics limited its practical applications.

4.1.2 Mechanical energy harvesting via piezoelectric/electrostrictive polymers

Piezoelectric polymers such as PVDF and its copolymer P(VDF-TrFE) have attracted considerable research interest for mechanical energy harvesting due to their low price, flexibility, ease of processability, low density and biocompatibility. For instance, Sun *et al.* [3] reported energy harvesting from human respiration via PVDF microbelts with a thickness smaller than 26 μm, and the output power is in the range of nW-μW. Very recently, electrospun was used to produce high performance piezoelectric polymer nanofiber mats/sheets for energy harvesting and sensor applications [213, 214]. The resulting P(VDF-TrFE) or PVDF nanofibers have good alignment at both the level of the fibers and the polymers, and therefore exhibit excellent piezoelectric response and high β-phase fraction without further processing. And the generated power can be used to drive a thermoelectric cooler.

Another group of electroactive polymers which can be used for mechanical energy harvesting is electrostrictive polymers, such as P(VDF-TrFE-CFE) and P(VDF-TrFE-CTFE). As we discussed in Section 1.2.2.3, PVDF-based electrostrictive terpolymers exhibit excellent electromechanical properties with higher strain (7 %), higher elastic energy density than piezoelectric polymers and ceramics, and comparable electromechanical coupling coefficient with piezoelectric ceramics. The flexible electrostrictive polymers show advantages for mechanical energy harvesting [215]: (i) High strain energy density which is required for high mechanical energy and for an reduced volume of the device; (ii) Smaller Young's modulus than piezoelectric ceramic which is preferred since force or stress level is typically not very high in most of energy harvesting cases; (iii) Light density which significantly reduces the weight of the energy harvesting device. Liu *et al.* [216] investigated electrostrictive polymers for energy harvesting via established models for different electrical and mechanical boundaries and it is suggested that electrostrictive energy harvesting systems are preferable for 'small' energy harvesting applications with low-frequency excitation. Whereafter, Ren *et al.* [217] demonstrated an electrostrictive energy harvester yielding a harvested electric energy density of 40 mJ/cm^3 with an efficiency of 10 %.

Recently, the group LGEF, INSA de Lyon, France, carried out a series works on electrostrictive polymer based energy harvesting devices. Cottinet *et al.* [218] proposed new means for electrostrictive energy harvesting, and a model based on the electrostrictive constitute equations was developed to predict the energy harvesting capability of electrostrictive polymers. Experiment results based on P(VDF-TrFE-CFE) composite with 1 % carbon black shows a good agreement with the modeling results, and enhanced energy harvesting property due to the improved dielectric properties caused by introduced carbon black was observed. In addition to material issues, electronic circuit is another concern for energy harvesting efficiency. With an investigation on the analysis of AC-DC for energy harvesting using P(VDF-TrFE-CFE) [219], a nonlinear technique synchronized switch harvesting on inductor (SSHI) [220,221] was applied to increase the energy conversion abilities and an enhanced harvesting efficiency of 1200 % was observed.

As discussed in previous Chapter, the introduction of plasticizer DHEP can improve the electromechanical properties of electrostrictive terpolymers. In this chapter, terpolymer modified with DEHP was investigated for mechanical energy harvesting applications. The generated short-circuit current and power via pure and modified terpolymer will be characterized.

4.2 Materials used for energy harvesting

The introduction of plasticizer DEHP greatly enhanced the dielectric permittivity of terpolymers at low frequency, and as a result, an improved electromechanical performance was observed for DEHP modified terpolymers. However, the improvement of dielectric permittivity is accompanied with a largely increased dielectric loss, especially for terpolymers with high DEHP loading, which will reduced the energy conversion efficiency and it is not favorable for energy harvesting applications.

Hence, terpolymers modified with low DEHP loading of 2.5 wt.% was used for energy harvesting applications in this chapter. Pure and 2.5 wt.% DEHP modified terpolymer films were prepared via a solution-casting method as described in the previous chapter (see Fig. 3.3). The dielectric properties, mechanical properties and the electromechanical properties were characterized also with the method described in the previous chapter.

Fig. 4.3 presents the dielectric properties of pure and 2.5 wt.% DEHP modified terpolymers as a function of frequency from 0.1 Hz to 1 MHz measured at room temperature. At low frequency region, an enhanced dielectric permittivity was observed for terpolymers modified with plasticizer DEHP. For instance, pure terpolymer has a dielectric permittivity of 36.8 at 0.1 Hz, while for DEHP modified terpolymer, the dielectric permittivity at 0.1 Hz is 57.8. However, the dielectric permittivity of DEHP modified terpolymer decreased quickly with increased frequency. At frequency larger than 100 Hz, DEHP modified terpolymers exhibit almost the same dielectric permittivity as pure terpolymer. Meanwhile, an increase of dielectric loss from 0.18 for pure terpolymer to 0.55 for DEHP modified terpolymer was also observed at low frequency region. The increase of dielectric permittivity and dielectric loss at low frequency region can be explained by interfacial polarization (MWS effect) caused by plasticizer DEHP. Since terpolymers are semi-crystalline, they are heterogeneous composite in nature. Charge carriers will be trapped in the interface region between amorphous region and crystalline region. The separation of charge carriers in response to applied electric field will contribute to dielectric response. The introduction of plasticizer with small molecular will expand the free volume and increase the interface region, improve the mobility of polymer and therefore more charger carriers will be trapped in the interface region. As a result, interfacial polarization at low frequency region is enhanced, contributing to the observed improved dielectric permittivity and increased dielectric loss at low frequency region for 2.5 wt.% DEHP modified terpolymer.

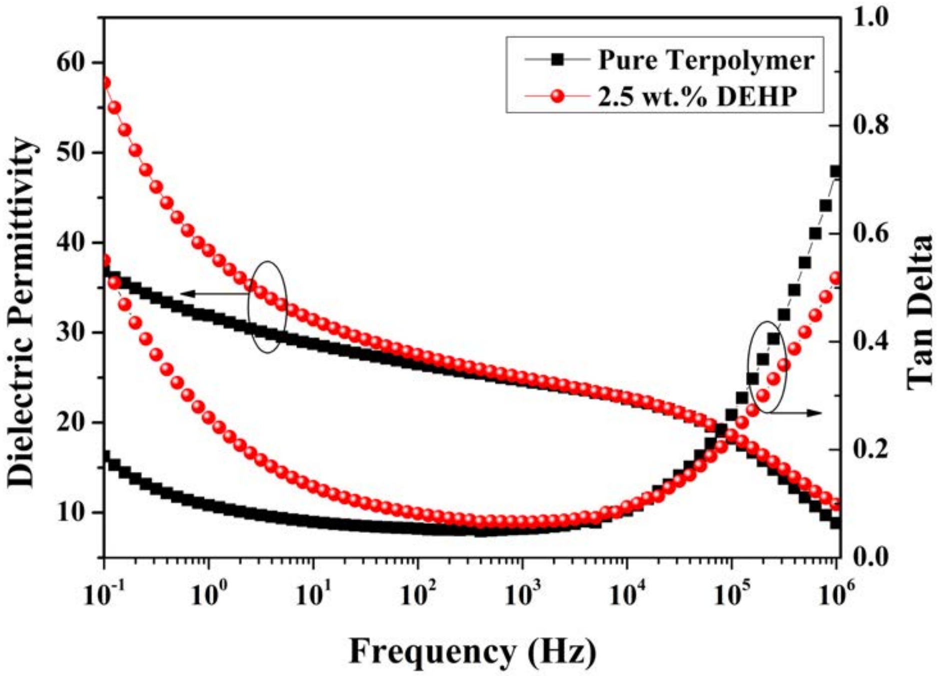

Figure 4.3: Dielectric properties of pure and 2.5 wt.% DEHP modified terpolymers as a function of frequency measured at room temperature.

The electric field induced transverse strains as a function of applied electric field amplitude for pure and 2.5 wt.% DEHP modified terpolymers measured at 0.1 Hz and room temperature are shown in Fig. 4.4. As we can see, the electromechanical performances were improved by introduction of plasticizer DEHP due to the enhanced dielectric properties. At $E = 30$ MV/m, 2.5 wt.% DEHP modified terpolymer exhibits a transverse strain of 0.308 %, which is about 1.8 times higher than that of pure terpolymer with a value of 0.174 %. Correspondingly, 2.5 wt.% DEHP modified terpolymer demonstrates a higher electric-field-related electrostrictive coefficient ($M_{31}= S_{31}/E^2$) of 3.42×10^{-18} $\mathrm{m}^2/\mathrm{V}^2$ and a higher elastic energy density ($YS_{31}^2/2$) of 5.98 × 10^{-4} J/cm^3 at $E = 30$ MV/m and 0.1 Hz than those of pure terpolymer, as shown in Table 4.1.

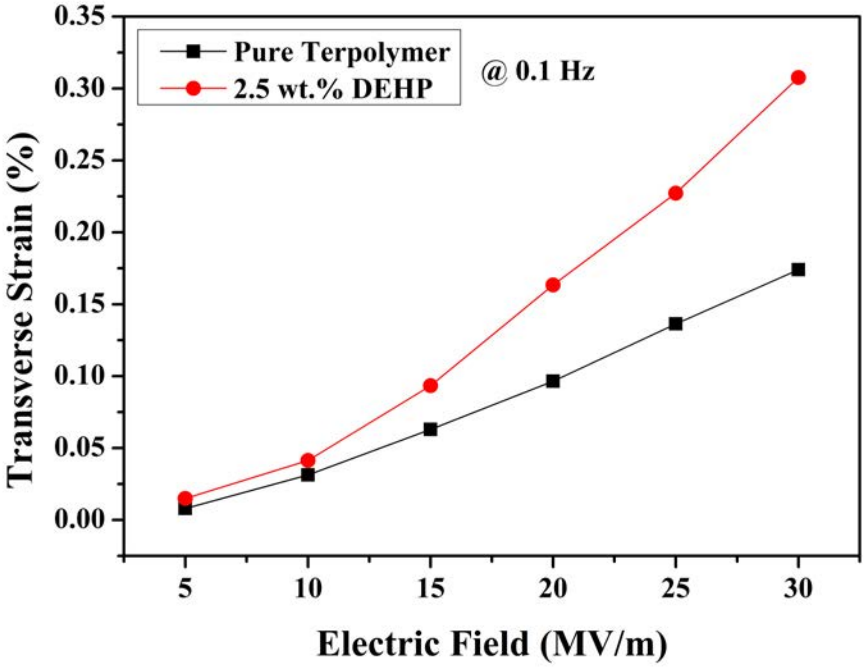

Figure 4.4: Transverse strain as a function of applied electric field amplitude for pure and 2.5 wt.% DEHP modified terpolymers measured at 0.1 Hz and room temperature.

Table 4.1: Comparison of material properties and electromechanical properties at 30 MV/m and 0.1 Hz for pure and 2.5 wt.% DEHP modified terpolymers.

DEHP Loading (wt.%)	ε_r 0.1 Hz	Y (MPa) 0.1 Hz	S_{31} (%)	M_{31} (m^2/V^2)	$YS_{31}^2/2$ (J/cm^3)
0	36.8	163	0.174	1.93×10^{-18}	2.47×10^{-4}
2.5	57.8	126	0.308	3.42×10^{-18}	5.98×10^{-4}

As discussed above, terpolymer modified with 2.5 wt.% DEHP demonstrates improved dielectric permittivity and electromechanical properties. It shows a higher elastic energy density at a lower Young's modulus than pure terpolymer. Furthermore, the dielectric loss (tan $\delta = 0.55$ at 0.1 Hz) is much smaller than that of 5 wt.% DEHP modified terpolymer with a value of 1.18 at 0.1 Hz. Therefore, terpolymer modified with 2.5 wt.% DEHP and pure terpolymer were chosen for the investigation of energy harvesting applications.

4.3 Work principle and validation of energy harvesting via electrostrictive polymers

In this section, the theoretical fundament of energy harvesting operation via electrostrictive polymers will be first demonstrated. Subsequently, a dedicated experimental setup based on the theoretical fundament will be presented to validate the energy harvesting via electrostrictive polymers.

4.3.1 The theoretical fundament of energy harvesting via electrostrictive polymers

In general, the field induced thickness strain for dielectric materials as a function of applied electric field can be expressed as a series of expansions [103, 222]:

$$S = dE + ME^2 + \gamma E^3 + \ldots, \tag{4.1}$$

where the first item is the linear piezoelectric effect, which only exists in crystalline dielectrics without a symmetric center, the following items contribute the nonlinear relationship between strain and applied electric field and the second item is the electrostrictive effect which exists in all dielectric materials and M is the electrostrictive coefficient. The thickness electromechanical coefficient d_T can be defined as:

$$d_T = \frac{\partial S}{\partial E} = d + 2ME + 3\gamma E^2 + \ldots \tag{4.2}$$

If the first item piezoelectric effect is zero and omit the higher items, the coefficient is given by

$$d_T = 2ME. \tag{4.3}$$

For electrostrictive materials without piezoelectric properties, piezoelectric effect can be induced by an applied large bias DC electric field (E_{DC}) and a small driven AC electric field (E_{AC}), and the resulting strain generated by E_{AC} can be given by

$$S = d_T E_{AC} = 2ME_{DC} \cdot E_{AC}, \tag{4.4}$$

where the item $2ME_{DC}$ can be taken as the piezoelectric coefficient. As a result, a pseudo-piezoelectric effect is induced by an applied large DC electric field for electrostrictive polymers and it can be used to harvest electrical energy from mechanical vibration as a generator or *vice versa*.

4.3.2 Experimental setup for energy harvesting via electrostrictive polymers

In order to valid energy harvesting via electrostrictive polymers, a DC bias electric field is necessary to be applied on the polymers to obtain a pseudo-piezoelectric behavior due to the non-piezoelectric nature of the electrostrictive polymers.

The experimental setup for energy harvesting using electrostrictive terpolymer is shown in Fig. 4.5. The solution-casting polymer film with gold electrodes sputtered at two sides was mounted in a sample holder composed of two parts: One is fixed and the other one can be moved in 1-direction with the help of an ironless linear motor XM550, which is driven by the signal produced by a function generator. Thus the film was driven with a given strain at desired frequency along 1-direction. A bias DC electric field provided by a function generator and voltage amplifier was applied to the polymer film along 3-direction to obtain a pseudo-piezoelectric behavior electrostrictive polymer film.

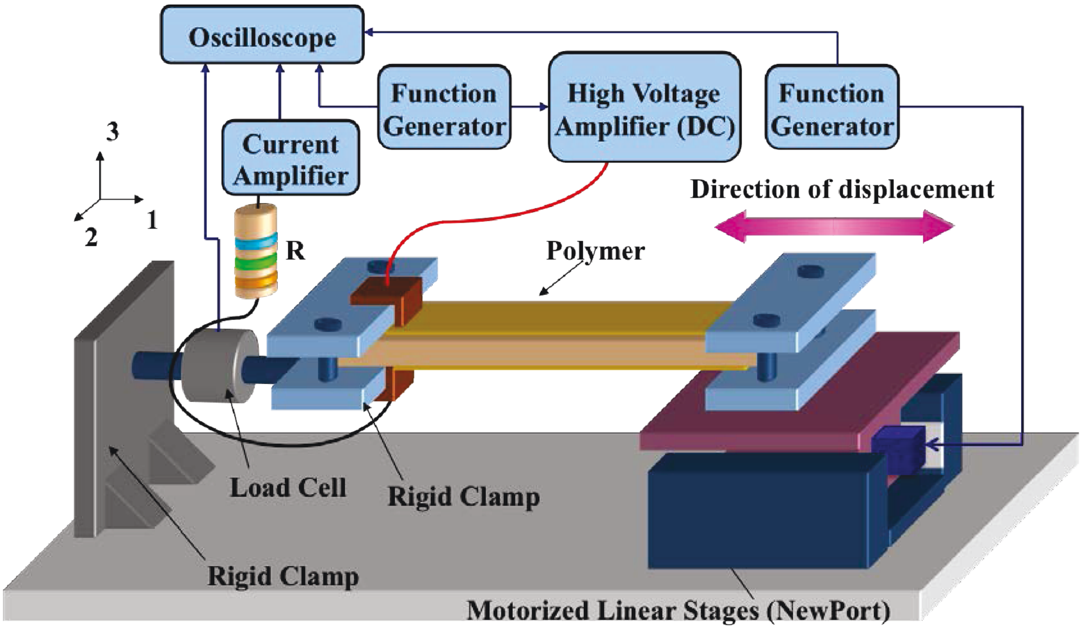

Figure 4.5: Schematic illustration of the experimental setup for energy harvesting via electrostrictive polymers.

The displacement of films precisely controlled by motor XM550 and the generated current from electrostrictive polymer film, which was monitored by a current amplifier, was recorded with an oscilloscope. For each sample, the short-circuit current was measured at different electric field (2, 4, 6, 8, 10 MV/m), different strain level (0.5, 1, 1.5, . . . , 5 %) and different frequency (0.1, 1, 10 Hz). For generated power characterization, an electrical load R was connected to the sample in series. The generated power on the load was subsequently derived by $P = I_{RMS}^2 \cdot R$, where the I_{RMS} is the root mean square of the current measured by the current amplifier. For each sample, the current was measured at different electric field (2, 4, 6, 8, 10 MV/m), different strain level (0.5, 1, 1.5, . . . , 5 %), different resistance load at 10 Hz.

The size of electrostrictive films for short-current measurement are 5 cm × 1 cm × 76.6 μm and 5 cm × 1 cm × 65 μm for pure and 2.5 wt.% DEHP modified terpolymer, respectively. The size of electrostrictive films for power characterization are 5 cm × 1 cm × 75.6 μm and 5 cm × 1 cm × 60.1 μm for pure and 2.5 wt.% DEHP modified terpolymer, respectively. For all of the samples, 1 cm is clamped for the electrical contact, and thus the effective length of polymer films used for energy harvesting is 4 cm.

4.4 Modeling of generated current

Electrostrictive effect is generally defined as a quadratic coupling between induced strain and applied electric field. For isotropic dielectrics, the strain S_{ij} and the electric flux density D_m can be expressed as independent variables of the electric field intensity E_m, E_n and the stress T_{ij} by the constitutive relation as [216]:

$$S_{ij} = s^E_{ijkl} T_{ij} + M_{mnij} E_n E_m \tag{4.5a}$$

$$D_m = \varepsilon^T_{mn} E_n + 2M_{mnij} E_n T_{ij} \tag{4.5b}$$

where s^E_{ijkl} is the elastic compliance under constant electric field, M_{mnij} is the electric-field-related electrostriction coefficient, and ε^T_{mn} is the linear dielectric permittivity under constant stress.

For isotropic linear dielectrics, it contracts along the thickness direction and expends along the film direction when an electric field applied across the thickness. The constitutive relation of electrostrictive polymer Eq. 4.5 can be simplified as

$$S_1 = s^E_{11} T_1 + M_{31} E_3^2 \tag{4.6a}$$

$$D_3 = \varepsilon^T_{33} E_n + 2M_{31} E_3 T_1, \tag{4.6b}$$

The current generated by the transverse vibration can be derived by [218]:

$$I = A \cdot \frac{\partial D_3}{\partial t}, \tag{4.7}$$

where A is the area of electrostrictive polymer with electrode and t is time. Combined Eq. 4.7 with Eq. 4.6, the current induced by electrostrictive polymer can thus be related to the strain and applied DC bias electric field by

$$I = A \left[\frac{\partial E_3}{\partial t} \left(\varepsilon^T_{33} + \frac{2M_{31} S_1 - 6M_{31}^2 E_3^2}{s^E_{11}} \right) + \frac{2M_{31} \frac{\partial S_1}{\partial t} E_3}{s^E_{11}} \right]. \tag{4.8}$$

As the strains applied on electrostrictive polymers are not larger than 5 %, the thickness change of the film during vibration can be neglected. Hence, the applied electric field across the thickness can be taken as a constant, thus $\partial E_3/\partial t = 0$, and therefore the short-circuit current can be given by

$$I_0 = 2 \cdot A \cdot M_{31} \cdot Y \cdot E_{DC} \cdot \frac{\partial S_1}{\partial t}, \tag{4.9}$$

where the Young's modulus $Y = 1/s_{11}^E$. The Eq. 4.9 indicates that the generated short-circuit current has a linear relationship with the applied DC electric field or the changing rate of the transverse displacement of the film. The energy harvesting performances of pure and 2.5 wt.% DEHP modified terpolymer can be estimated by $\alpha = 2 \cdot A \cdot M_{31} \cdot Y$.

4.5 Investigation of energy harvesting performances of modified terpolymers

4.5.1 Short-circuit current

The equivalent electrical circuit for short-circuit current measurement is illustrated in Fig. 4.6. Since the electrostrictive polymer was subjected to an applied DC bias electric field and a sinuous transverse vibration driven by the motor, the observed short-circuit is composed by two parts: a constant current (I_{DC}) due to the applied electric field and the alternative current component (I_h) generated by vibration of the electrostrictive film.

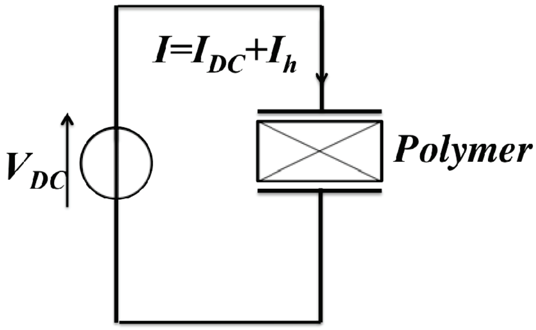

Figure 4.6: Schematic illustration of equivalent electrical circuit for short-circuit current measurement.

A. Real-time short-circuit current

Fig. 4.6 presents the real-time transverse strain and current as a function of time for 2.5 wt.% DEHP modified terpolymer measured at $E_{DC} = 10$ MV/m, a maximum strain of 5 % and 10 Hz. As expected, an sinuous current signal in response to the applied sinuous transverse displacement of the electrostrictive film was observed. A phase angle about 90°between the peaks of current and strain was observed. It is in good agreement with Eq. 4.9, which indicates that the generated current is proportional to the change rate of the transverse displacement of the film. The alternative current stands for the generated current from mechanical vibration of the film, and it can be given by the peak-peak value

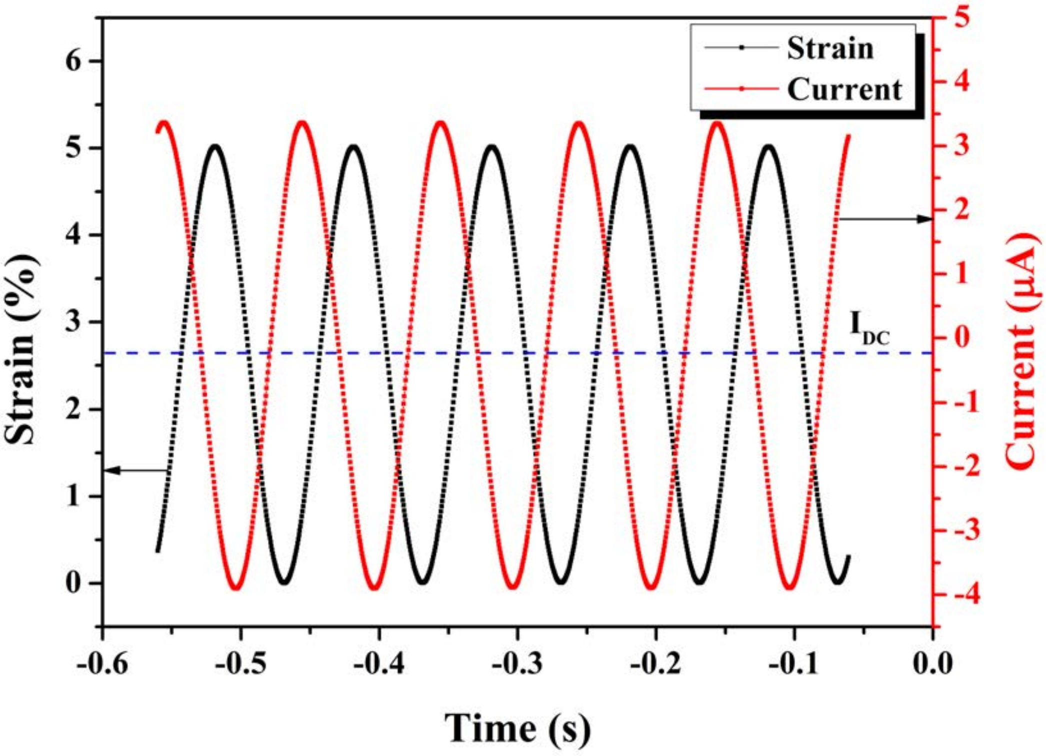

Figure 4.7: The real-time transverse strain and current for 2.5 wt.% DEHP modified terpolymer at E_{DC} = 10 MV/m, a maximum strain of 5 % and 10 Hz.

(I_{pp}) of the alternative current signal, and the maximum generated current is $I_{pp}/2$. While the average value of the alternative current signal presents the DC current (I_{DC}) due to the conductivity of electrostrictive polymers.

The peak-peak current (I_{pp}) and DC current (I_{DC}) as a function of DC bias electric field for 2.5 wt.% DEHP modified terpolymer at a maximum strain of 5 % and 10 Hz is illustrated in Fig. 4.8. As is demonstrated, both I_{pp} and I_{DC} increase with increased applied DC bias electric field. However, it is worthy to note that the I_{pp} is always higher than I_{DC}. For instance, at E = 10 MV/m, the I_{pp} is 7.27 μA, yielding a maximum generated current about 15 times higher than the I_{DC} with a value of 0.246 μA. It illustrates that the current generated by electrostrictive polymer is much larger than that caused by the conductivity of the polymer under the applied DC bias electric field.

B. Short-circuit current versus strain and DC bias electric field

The modeling results of the current generated by electrostrictive polymer Eq. 4.9 demonstrates that the current has a linear relationship with the applied DC electric field and change rate of the strain ($\partial S_1/\partial t$) which is determined by the strain amplitude and frequency of the applied mechanical excitation. In order to verify the modeling result, the current is measured at various DC electric field, strain amplitude and frequency, and the related results are shown in Fig. 4.9.

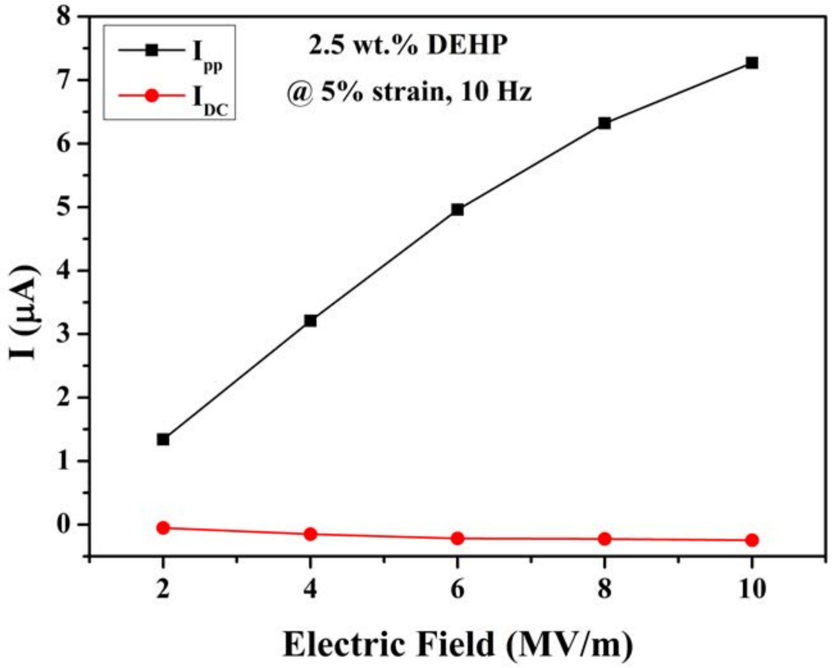

Figure 4.8: The peak-peak current (I_{pp}) and DC current (I_{DC}) as a function of DC bias electric field for 2.5 wt.% DEHP modified terpolymer at a maximum strain of 5 % and 10 Hz.

Current versus strain. As depicted in Fig. 4.9a-e, the induced current shows an expected linear relationship with strain at a constant DC electric field and frequency. When the strain increased from 0.5 % to 5 %, an approximate 10 times higher current was observed for all the experimental conditions. For instance, at $E = 10$ MV/m and 10 Hz, the I_{pp} for modified terpolymer with a strain of 0.5 % is 0.683 μA, and it is increased to 7.27 μA as the strain is increased to 5 % (see Fig. 4.9e).

Current versus frequency. It is clear to note that the increase of frequency greatly increased the generated current from Fig. 4.9. However, the observed current does not show an linear relationship with the frequency of the mechanical excitation. A typical observed fact for both pure and modified polymers is that, when the frequency is increased from 0.1 Hz to 1 Hz and from 1 Hz to 10 Hz, the I_{pp} is increased about 8.5 times and 5.3 times, respectively, rather than 10 times. The discrepancy between the experimental results and modeling results is caused by the viscoelasticity nature of the electrostrictive polymers. The modeling of the current is based on assumption that electrostrictive polymers are lossless materials. However, electrostrictive polymers have lossy and dispersive dielectric properties as well as high mechanical viscoelastic losses and they are frequency-dependent. Energy harvester based on electrostrictive polymers working at a higher frequency of mechanical excitation will have a higher mechanical energy losses due to the viscoelasticity of polymers, which will comprised the improvement of the current by increased change rate

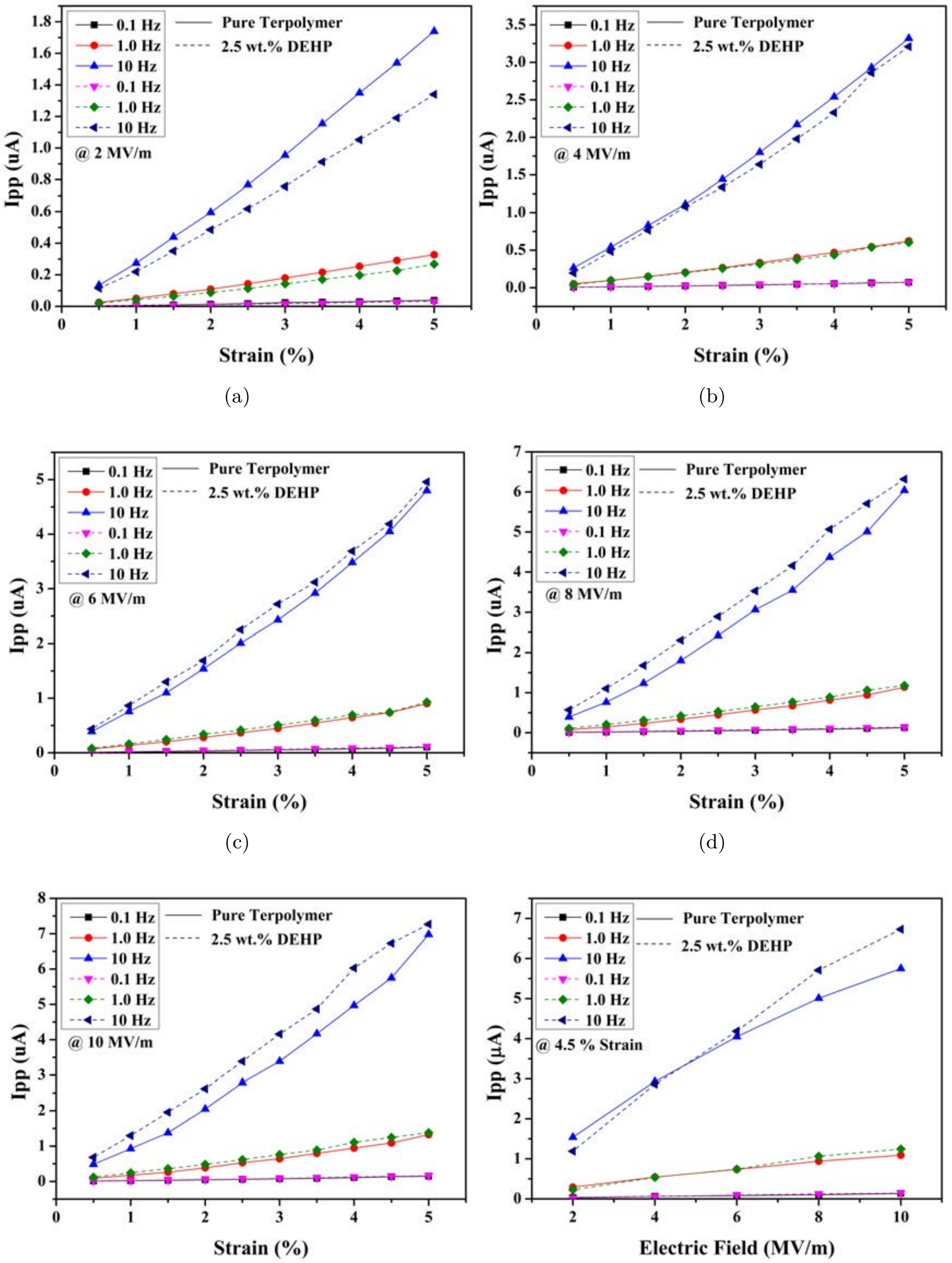

(a) (b) (c) (d) (e) (f)

Figure 4.9: The peak-peak current (I_{pp}) at different frequency as a function of maximum strain (a, b, c , d, and e) at different applied DC bias electric field and as a function of applied DC bias electric field (f) at maximum strain of 4.5 % for pure and 2.5 wt.% DEHP modified terpolymer .

of strain.

Current versus DC electric field. As expected, a general linear relationship between current and electric field was observed. As we can see from Eq. 4.9, for polymers with same area at the same frequency and strain amplitude, the current generation capacity can be estimated by the item of $M_{31} \cdot Y$. By taking advantage of the value listed in Table 4.1, DEHP modified terpolymer exhibits a 1.37 times higher value of $M_{31} \cdot Y$ than pure terpolymer, resulting a higher slope of the I-E curve as shown in Fig. 4.9f. However, it is interesting to find that pure terpolymer exhibits a higher current than DEHP modified terpolymer at lower electric field (see Fig. 4.9). This maybe associated with the higher dielectric lossy nature of electrostrictive terpolymers. As is known, the realization of energy conversion is based on the reorientation of dipolar within the polymers and it will consume certain energy, leading to the dielectric loss. At low electric field, the converted energy from mechanical vibration is very small for both pure and modified terpolymers and they are comparable to the energy losses due to the dielectric loss, resulting the nonlinear relationship between the current and DC bias electric field at low electric field. However, DEHP modified terpolymer has a higher dielectric loss than pure terpolymer, resulting a lower generated current than pure terpolymer. As electric field increases, more mechanical energy is converted and it becomes much larger than the energy consumed by the dielectric loss, and DEHP modified terpolymer can convert much more energy than pure terpolymer due to the higher current generation capacity. As a result, modified terpolymer has a higher current than pure terpolymer at high electric field, as is shown in Fig. 4.9f.

In summary, according to the modeling results of the current based on the constitutive relation of electrostrictive polymer, generated current from mechanical vibration can be enhanced by increasing the strain amplitude and frequency of the applied displacement of polymer and the DC bias electric field. However in the practical operation, these three parameters should be carefully optimized. The increase of strain can linearly increase the current, but it can not be increased without limitation due to the yielding behavior of polymer materials. The practical applied strain should be lower than the yielding point. In addition, the application of energy harvester is also confined to the vibration in the ambient environment. Another approach to improve current generation is to increase the frequency of the applied mechanical vibration. Due to the viscoelasticity nature of polymers, mechanical losses will play a much more important role at higher frequency, which will bring about more compromise of positive enhancement effect on the current generation of the increased frequency. Compared the aforementioned approach, increasing the applied DC bias electric field below the breakdown strength is an efficient way to improve the current generation since the pseudo-piezoelectric constant is proportional to the DC bias electric field (see Eq. 4.4). Furthermore, the energy consumption caused by dielectric loss is not neglectable at low electric field, and as a result, a high electric field is necessary to improve the energy conversion efficiency.

4.5.2 Generated power

The equivalent electrical circuit for short-circuit current measurement is illustrated in Fig. 4.10. In order the measure the power generation performances of electrostrictive polymer based energy harvester, a resistance R as a load is directly connected to the polymer film in series. Since polymer have a much larger resistance than R, the influence of load on the actual DC electric field applied on the polymer film can be neglectable which was verified by our experiment. Load with different values of resistance was used and the current I_{pp} was recorded. The generated power is calculated by

$$P = I_{RMS}^2 \cdot R = \left(\frac{I_{pp}/2}{\sqrt{2}}\right)^2 \cdot R = \frac{1}{8} I_{pp}^2 \cdot R, \tag{4.10}$$

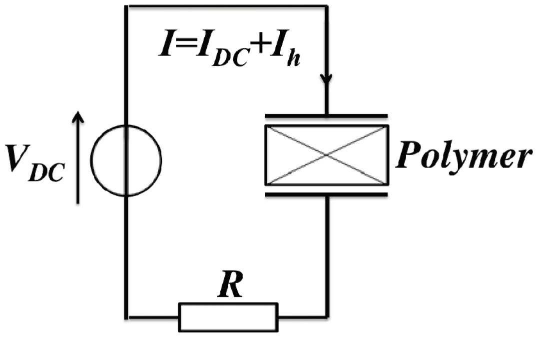

Figure 4.10: Schematic illustration of equivalent electrical circuit for current measurement with resistance load.

A. Generated power versus resistance R

Table 4.2: The calculation of optimal load resistance for pure and 2.5 wt.% DEHP modified terpolymers working at 10 Hz.

DEHP Loading (wt.%)	Length (cm)	Width (cm)	Thickness (μm)	Frequency (Hz)	ε_r	R_{opt} (MΩ)
0	5	1	75.6	10	35	8
2.5	5	1	60.1	10	36	6

The increase of resistance will result into a decreased current, and therefore, the generated power will reach a maximum value with an optimal load R_{opt}, and the optimal load resistance can be estimated by [218],

$$R_{opt} = \frac{1}{C_p \cdot w} = \frac{1}{\frac{\varepsilon_0 \varepsilon_r A}{d} \cdot 2\pi f}, \tag{4.11}$$

where w is the angle frequency, A and d are the area and thickness of the electrostrictive

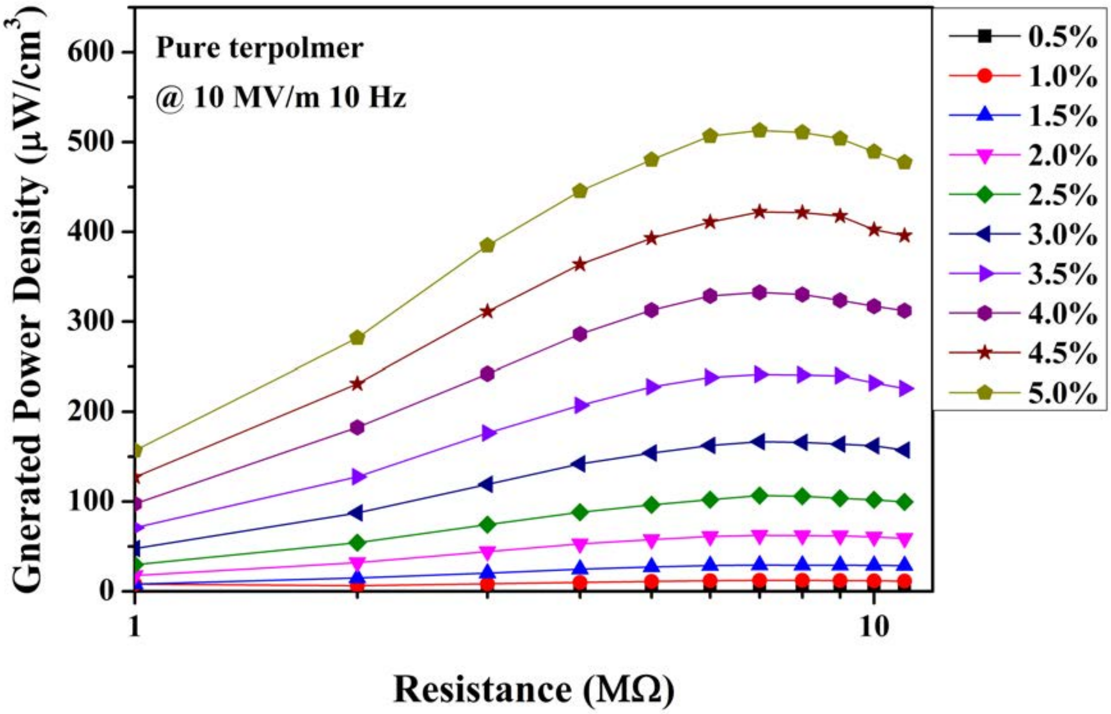

(a)

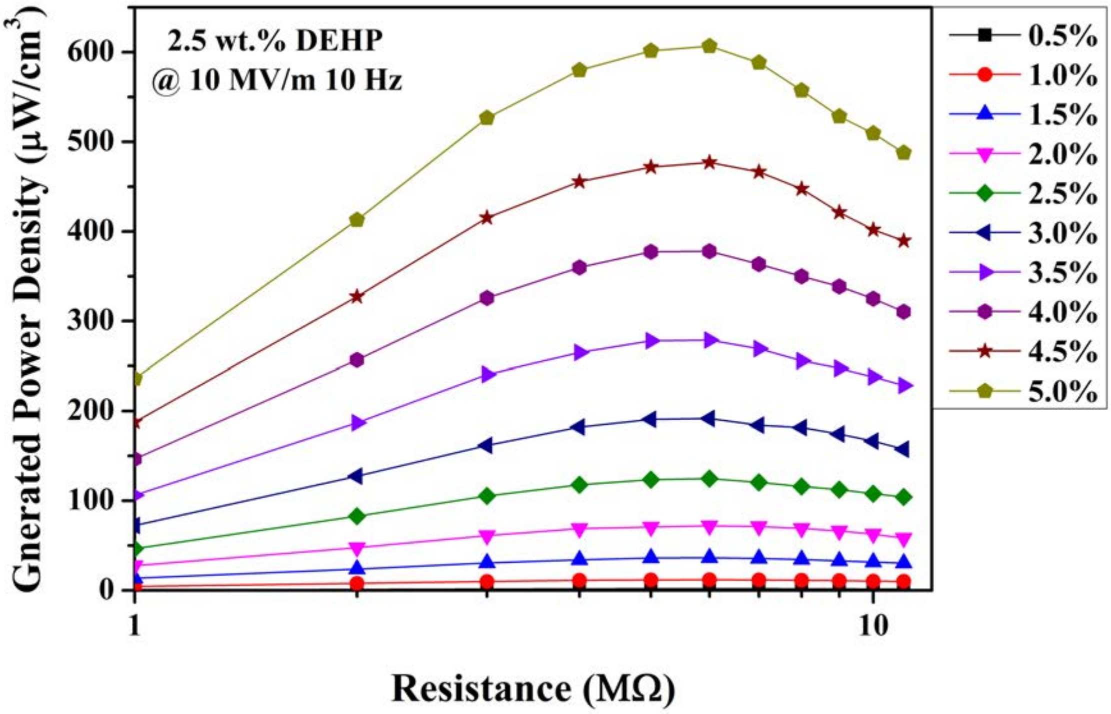

(b)

Figure 4.11: The generated power density as a function of load resistance for (a) pure and (b) 2.5 wt.% DEHP modified terpolymer working at $E = 10$ MV/m, 10 Hz and different transverse strain.

films, respectively, C_p and ε_r are the capacitance and dielectric permittivity of electrostrictive films at frequency f, respectively. Table 4.2 gives the calculated optimal load resistance for pure and 2.5 wt.% DEHP modified terpolymers working at 10 Hz. The resulting R_{opt} is 8 MΩ and 6 MΩ for pure and 2.5 wt.% DEHP modified terpolymers, respectively.

Fig. 4.11 gives the generated power density as a function of load resistance for (a) pure and (b) 2.5 wt.% DEHP modified terpolymer working at $E = 10$ MV/m, 10 Hz and different transverse strain. As expected, the generated power is first increased with the increase of load resistance until a maximum power and then decreased with continuously increase of load resistance. The optimal resistance R_{opt} at different strain level remains the same. The maximum generated power appears at a optimal resistance of 8 MΩ for pure terpolymer and 6 MΩ for DEHP modified terpolymers, which is in good agreement with the estimated optimal resistance listed in Table 4.2. And modified terpolymer shows higher power density than pure terpolymer. For instance, at a strain of 5 %, the power density for modified terpolymer is 607 μW/cm^3, which is about 1.2 times higher than that of pure terpolymer with a value of 513 μW/cm^3.

B. Generated power versus resistance strain and stress

In this section, the maximum power density at the optimal load resistance as a function of strain is investigated. As illustrated in Fig. 4.12a, the power density exhibit a quadric relationship with strain, which can be resulted from the linear relationship between the generated current and strain. DEHP modified terpolymer demonstrates a higher power density than pure terpolymer at the whole different strain range.

Fig. 4.12b presents the power density as a function of stress for both pure and DEHP modified terpolymers. Since DEHP modified terpolymer has a lower Yong's modulus, modified terpolymer shows a much higher energy density at the same level of stress. That is to say, when the energy harvester device is driven by an external force, modified terpolymer will be more efficient than pure terpolymer in energy conversion.

According to the previous investigation [218], the electrostrictive coefficient (M_{31}) is proportional to $\varepsilon_0(\varepsilon_r - 1)^2/(Y \cdot \varepsilon_r)$. The modification of terpolymer with DEHP improves the dielectric permittivity (ε_r) and Young's modulus (Y) and thus contribute to an enhanced electrostrictive coefficient. Even the dielectric permittivity is almost the same for pure and modified terpolymer at 10 Hz, the reduced Young's modulus contributes to the larger M_{31} of modified terpolymer than that of pure terpolymer. Compared to pure terpolymer, modified terpolymer exhibit a higher pseudo-piezoelectric constant ($2M_{31}E_{DC}$) and a resulted higher mechanical-to-electrical energy conversion performances.

C. Energy conversion efficiency

In this section, the mechanical-to-electrical energy conversion efficiency will be evaluated. For a given strain, the input mechanical power density during one cycle can be given

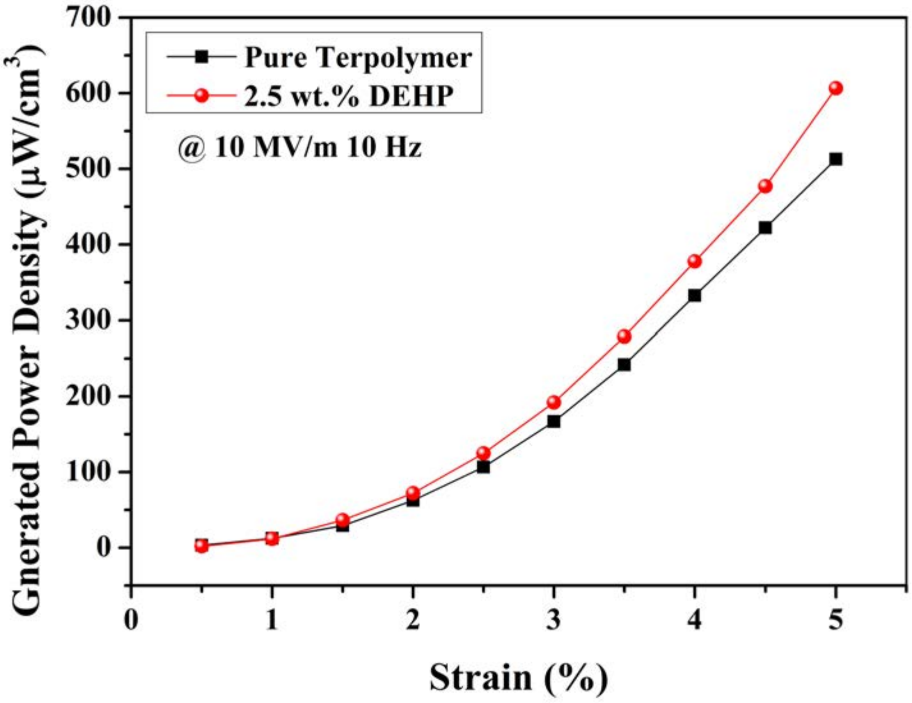

(a)

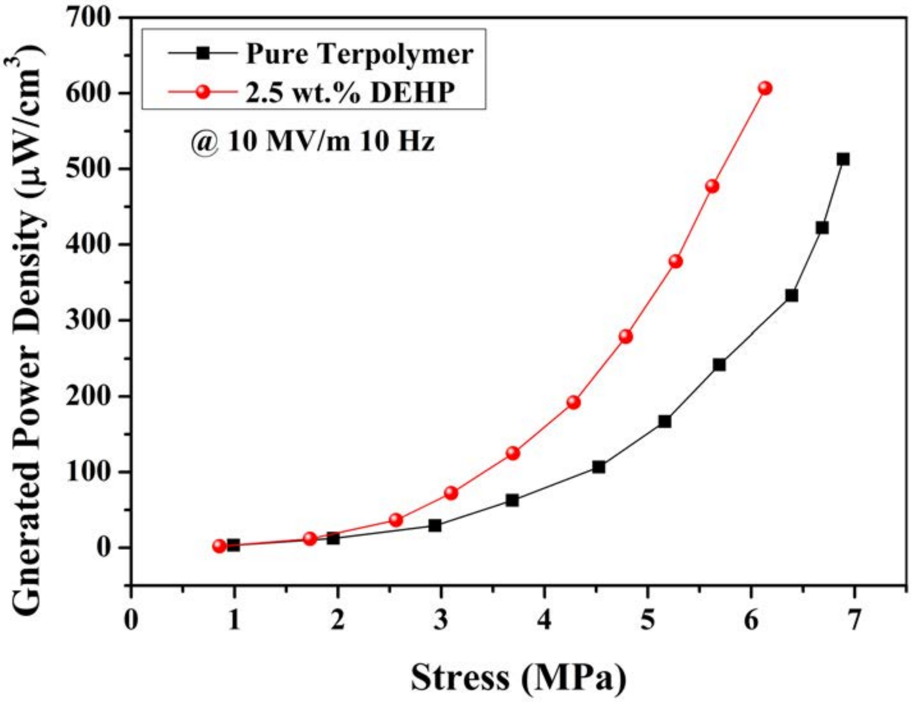

(b)

Figure 4.12: The generated power density as a function of (a) strain and (b) stress for pure and 2.5 wt.% DEHP modified terpolymer working at $E = 10$ MV/m, 10 Hz and the optimal load resistance.

by

$$P_{mechanical} = \frac{1}{2} Y S^2 \cdot f, \tag{4.12}$$

where f is the frequency of the mechanical vibration. And the mechanical-to-electrical energy conversion efficiency (η) be estimated by

$$\eta = \frac{P_{eletrical}}{P_{mechanical}} \tag{4.13}$$

where $P_{eletrical}$ is the maximum power destiny at the optimal resistance load.

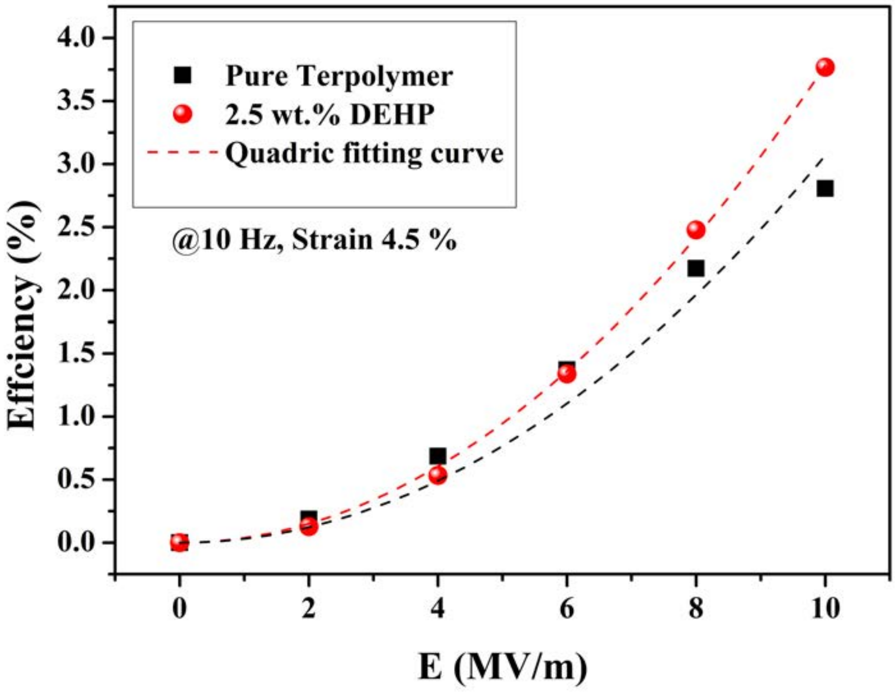

Figure 4.13: The energy conversion efficiency as a function of electric field for pure and modified terpolymers working at 10 Hz and strain of 4.5 %.

Fig. 4.13 presents the energy conversion efficiency as a function of electric field for pure and modified terpolymers working at 10 Hz and strain of 4.5 %. It is found that the energy conversion exhibits the same results as the short-circuit current for pure and modified terpolymers. At low electric field, pure terpolymer shows a higher efficiency, while at high electric field, modified terpolymer shows a higher efficiency. The results presented in Fig. 4.13 demonstrate again that the dielectric loss is not neglectable at low electric field, and a high electric field is necessary to improve the energy conversion efficiency for lossy materials. The energy conversion efficiency is 2.8 % and 3.8 % for pure and modified terpolymer, respectively. At constant strain and frequency, the input mechanical power density (Eq. 4.12) is a constant, and therefore the energy conversion efficiency is determined by the electrical power density. Since the generated current is proportional to the DC bias electric field, energy conversion efficiency should have a quadric relationship with DC bias electric field. As is shown in Fig. 4.13, a good agreement between the experimental results and the quadric fitting curve of energy conversion efficient versus electric field is observed. Thus increasing the applied DC bias electric field will be an efficient way to increase the energy conversion efficiency for electrostrictive polymers.

Table 4.3: The estimation of energy conversion performances for pure and 2.5 wt.% DEHP modified terpolymer working at E = 30 MV/m, 10 Hz and strain of 4.5 %.

DEHP Loading (wt.%)	Y (MPa)	$P_{mechanical}$ (mW/cm^3)	η (%)	$P_{electrical}$ (mW/cm^3)
0	149	15.0	27.6	4.14
2.5	125	12.7	34	4.31

It has been demonstrated that [183], the dielectric saturation will occur at an electric field larger than 50 MV/m, which is far below the dielectric breakdown strength of terpolymer. By taking advantage of the quadric relationship between the energy conversion efficiency and DC bias electric field, the efficient for pure and modified terpolymers perform at E = 30 MV/m can be estimated. Table 4.13 presents the estimation results of energy conversion performances for pure and 2.5 wt.% DEHP modified terpolymer working at E = 30 MV/m, 10 Hz and strain of 4.5 %. As illustrated, an energy conversion efficiency as high as 34 % for modified terpolymer can be achieved, a value that is much greater than typical piezoelectric PVDF based power generators (0.5 - 4 %) [223], and it is about 1.2 times higher than that of pure terpolymer. The resulting electrical power density is as high as 4.31 mW/cm^3.

4.6 Conclusion

In this chapter, terpolymer modified with 2.5 wt.% DEHP with smaller loss than higher content DEHP loading was used for the investigation energy harvesting applications. The introduction of DEHP improved the dielectric permittivity and moderately decreased the Young's modulus of the terpolymer, resulting an improved electromechanical performances.

The pseudo-piezoelectric effect of electrostrictive polymers was use to harvest electrical energy from mechanical vibration by applying a DC bias electric field on the electrostrictive polymers. Based on the constitutive equation of electrostrictive effect, an model of the current generated from mechanical vibration via electrostrictive polymers was established. On the basis of this model, the energy harvesting performances of pure and 2.5 wt.% DEHP modified terpolymer were investigated with different strain amplitude and frequency of mechanical vibration and different DC bias electric field. The experimental results demonstrates that these three parameter should be carefully chosen since the electrostrictive polymers are lossy material due to the viscoelasticity nature of polymers. DEHP modified terpolymer shows a higher short-circuit current of 3.635 μA than pure terpolymer at $E=$ 10 MV/m, 10 Hz and a strain of 5 %.

The maximum power occurs at a optimal load resistance. The corresponding optimal load resistance is 8 MΩ and 6 MΩ for pure and DEHP modified terpolymers, respectively. Due to the higher electrostrictive coefficient (M_{31}), modified terpolymer shows a higher power density as high as 607 μW/cm^3 than pure terpolymer. Based on the quadric relationship between the energy conversion efficiency and DC bias electric field, an estimated energy conversion efficiency as high as 34 % and a corresponding electrical power density of 4.31 mW/cm^3 can be achievable for modified terpolymer working at an DC bias electric field of 30 MV/m.

In summary, DEHP modified terpolymer exhibits improved energy harvesting performances in contrast with pure terpolymer. The high energy conversion efficiency and power density is very attractive for potential applications.

Chapter 5

Micropump Fabricated via DEHP Modified Terpolymer

Micropump is one of the most important components for the emerging microfluidic technology. Electrostrictive polymers with excellent electromechanical performances are promising as drivers of micropumps due to their good mechanical properties, lightweight, low cost and importantly, the ease of processability in contrast with their inorganic counterparts such as piezoelectric ceramics.

In this chapter, a valveless micropump in which 15 wt.% DEHP modified terpolymer with improved electromechanical properties was used as the actuation diaphragm was presented. The back pressure at zero flow rate and flow rate at zero back pressure were measured to investigate the pumping performances of the as-prepared micropump. At an applied electric field of 20 MV/m with a frequency of 1 Hz, a back pressure of 240 Pa and a flow rate of 10.1 μL/min were achieved. The modification of terpolymer with DEHP contributed to the good pumping performance at an electric field lower than 20 MV/m and the resulting micropump is promising for low-frequency pumping applications.

5.1 Introduction of microfluidic technology and micropump

Microfluidic devices, which exhibit the ability of manipulation of fluids in channels with dimensions of tens to hundreds of micrometers, has been a very attractive technology in the past 20 years due to their wide range of practical benefits in chemical, medical and biological fields. The field of microfluidics originated from the development of four fields: molecular analysis, biodefence, molecular biology and microelectronics [224]. The most essential advantage of microfluidic devices is the small volume of reagents used for laboratory operations such as analysis, reaction and therefore they are much cheaper, faster and more environmentally friendly than their macro-scale counterparts. As a result, they are also well-known as the lab-on-chip (LOC) devices, which can be used as a powerful tool for research activities. For example, chemist can use the micrometer-scale total analysis systems (μTAS) to synthesize and analyze new molecules and materials. Microfluidics integrated cells-on-chips [225] or organs-on-chips [226] microsystems can be employed to realize multiple functions including tissue culture, cell separation and biological analyses (as is shown in Fig. 5.1). Furthermore, they can be exploited as a chemical or biological detector for environment monitoring, to precisely control the drug delivery [227] as well as to be an integrated cooling system for microelectronic devices [228]. Microfluidic devices are generally fabrication on silicon, glass and emerging plastic materials such as poly(dimethylsiloxane) (PDMS) and polycarbonate (PC) via photolithography and related technologies which have been widely used in silicon microelectronics and micro-electromechanical systems (MEMS) [224].

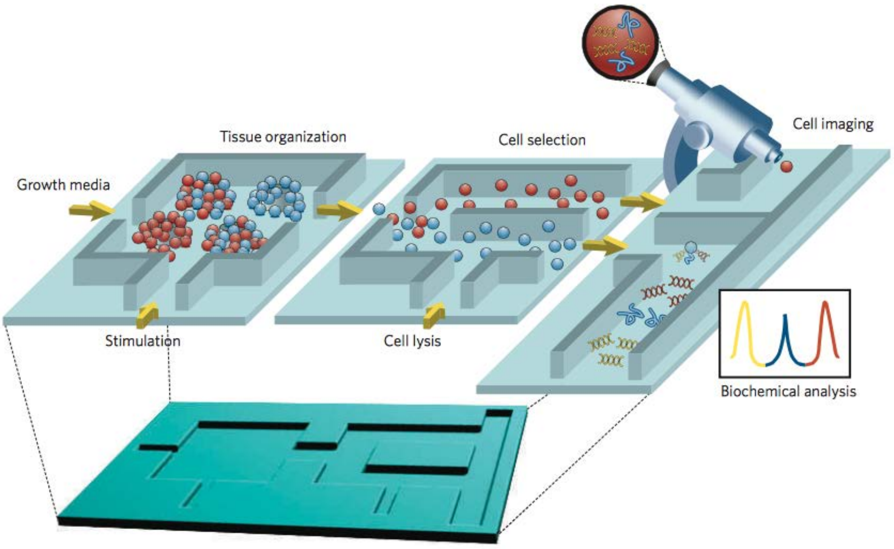

Figure 5.1: Microfluidics integrated cells-on-chips systems for tissue organization, cell culture and analysis [225].

Generally speaking, a multi-functional microfluidic device must have a series of delicated components which are used to introduce, move and mix the fluid as well as to detect and purify the products. One of the most important and fundamental components is the micropump which provides the drive force of the fluid transport within the microfluidic devices. Since the first report of piezoelectric MEMS based micropump in 1984 [229], extensive investigations on micropump have been conducted. The general conception and development of micropump can be referred to the several review papers [230–232]. A brief introduction of micropump is given here for a general understanding.

According to the pumping mechanism how the pressure is exerted on the working fluid, micropumps can be broadly divided into two main categories [230, 231]: (i) mechanical displacement micropumps, which exert oscillatory or rotational pressure forces on the working fluid through one or more moving boundaries (vibration diaphragm, rotary, pneumatic and phase change pumps *etc.*); and (ii) electro/magneto-dynamic micropumps, which provide a direct energy transfer to pumping power and generate constant/steady flows due to the continuous addition of energy (electro/magneto-hydrodynamic and electro-osmotic pumps, *etc.*). Displacement micropumps can be further classified into aperiodic and periodic micropumps. Aperiodic micropumps operate on the basis of aperiodic movement of the moving boundaries and only a limited volume of working fluid can be pumped. In contrast, the operation of periodic micropumps is in a periodic manner, including the reciprocating motion of a piston, or diaphragm and rotary elements (gears, vanes).

Among periodic micropumps, the reciprocating displacement micropumps, which produce pressure on working fluid via the periodic movement of the moving boundaries or surface, are the most widely reported micropumps. In most cases, the moving boundary or surface is a diaphragm, and therefore, these pumps are also called membrane or diaphragm micropumps. Fig. 5.2 presents the typically structure of a reciprocating displacement micropump and pumping mechanism. As is shown, a diaphragm micropump consists of three components: an actuator or driver which is bounded on diaphragm, a pump chamber with diaphragm on one side and two passive check valves (one at inlet and the other one at outlet). During operation, the volume of pump chamber is alternatively increased and

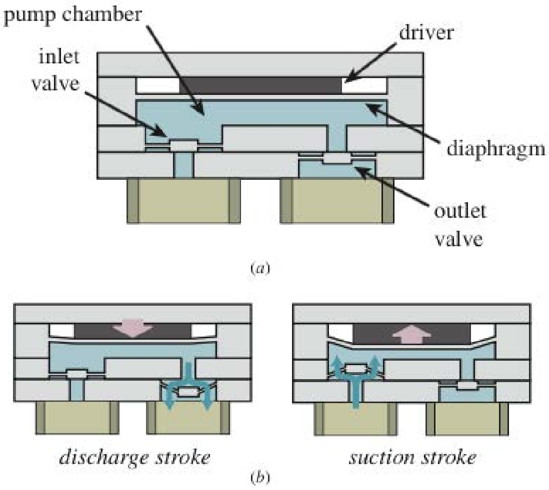

Figure 5.2: Schematic illustration of (a) structure and (b) operation of a typical reciprocating displacement micropump [230].

decreased by the movement of the diaphragm driven by the actuator, and the inlet valve and outlet valve are correspondingly opened and closed respectively, leading to the flow of working fluid from inlet to outlet. The choice of diaphragm material is very important, since it is the origin of the drive force of a micropump. The most common materials used for diaphragm are silicon, glass and plastics. For a micropump driven by low frequency or low force actuators, materials with low Young's modulus which can produce a large volume change will be preferable for diaphragm.

The actuation of diaphragm is often achieved by piezoelectric ceramics such as lead zirconate titanate (PZT) due to their high piezoelectric and electromechanical coupling coefficients. However, the fabrication process such as deposition of a thin film of piezoelectric ceramics onto the silicon is complicated and time-consuming which will increase the manufacturing cost. In addition, PZT materials are brittle and have a very high Young's modulus, low strain level of 0.1 % and energy density below 0.1 J/cm^3 [148]. Alternatively, electroactive polymer such as piezoelectric P(VDF-TrFE) and electrostrictive PVDF-based terpolymers are very promising for actuator applications due to their low cost, lightweight, flexibility, ease of processability, bio-compatibility and excellent electromechanical properties. In contrast with piezoelectric ceramics, the electric field induced strain for electrostrictive PVDF-based terpolymers can be as high as 7 % [161] and the elastic energy density can reach 1.1 J/cm^3 [156]. Xia *et al.* [164] reported the first electroactive polymer based micropump in which irradiated P(VDF-TrFE) polymer thin film with a thickness of 80 μm was used as the diaphragm actuator. A flow rate of 25 μL/min at 63 Hz with a back pressure of 350 Pa for methanol was achieved at an applied electric field of 90 MV/m. Very recently, piezoelectric P(VDF-TrFE) based micropump fabricated via inkjet printing was demonstrated by Pabst *et al.* [233]. The actuators are printed on a polyethylene terephthalate (PET) substrate and consist of a sandwich structure of P(VDF-TrFE) film and two printed silver electrodes. The resulting micropump exhibited a maximum flow rate of 130 μL/min at zero back pressure and a maximum back pressure of 56 Pa at zero flow rate at an applied electric field about 100 MV/m and 30 Hz.

As demonstrated in Chapter 3, modified terpolymers with 15 % DEHP loading exhibit improved electromechanical properties with about 7 times higher transverse strain and about 26 times higher elastic energy density than pure terpolymer at an electric field of 20 MV/m and 0.1 Hz. In this chapter, 15 % DEHP modified terpolymers were investigated for valveless micropump applications.

5.2 Materials used for micropump application

In this chapter, terpolymers P(VDF-TrFE-CFE) modified with 15 % DEHP with good electromechanical properties were used for micropump applications. The preparation and property investigation of modified terpolymer has been carried out and reported by Capsal *et al.* in our group [234]. DEHP modified terpolymer was prepared via solution-casting method. The casted film were placed in an oven at 60 °C for 12 h to totally remove the residual solvent and subsequently annealed at 103 °C for 1 h to improve the crystallinity of the samples. The comparison of materials properties and electromechanical performances of pure and 15 wt.% DEHP modified terpolymers is listed in Table 5.1.

Table 5.1: Comparison of material properties and electromechanical performances at 30 MV/m and 0.1 Hz for pure and 15 wt.% DEHP modified terpolymers.

DEHP Loading (wt.%)	ε_r 0.1 Hz	Y (MPa) 0.1 Hz	E_b (MV/m)	M_{31} (m^2/V^2)	S_{31} (%)	$YS_{31}^2/2$ (J/cm^3)
0	57	160	200	2.6×10^{-18}	0.234	3.38×10^{-4}
15	800	50	160	2.2×10^{-17}	2.0	1.0×10^{-2}

5.3 Work principles of valveless micropump

For conventional diaphragm micropumps, two movable check valves are used to stop reverse flow and to ensure the flow of working fluid in one direction. However, micropumps with passive check valves suffer from problems such as the relative large pressure drop at the valves and the sensitivity to bubbles and small particles which will result into blockage problems [235]. Furthermore, wear and fatigue of the movable parts can be a critical issue. These may lead to the reduced lifetime, reliability and declined performance of the micropump [236]. And, the complicated structure of check valves is not practical for pumps with very small size.

To overcome the aforementioned problems, valveless micropumps were developed and reported in a number of literatures. The conception of valveless pump was first proposed by Stemme *et al.* [237] in 1993. In such a pump, diffuser/nozzle elements are used to replace the two movable check valves to rectify the flow of working fluid. As is illustrated in Fig. 5.3, a diffuser is a duct or channel with a diverging/expanding cross section which will decrease the velocity of fluid by transforming the kinetic energy in the form of velocity into potential energy in the form of pressure, while a nozzle is a duct or channel with a converging cross section which will increase the velocity of fluid by transforming potential energy into kinetic energy. As a result, the pressure loss in diffuser direction is lower than that in nozzle direction for a given pressure drop, which meets the pump conditions [238]. Based on the different flow properties of diffuser and nozzles, valveless pumps work as follows: During supply mode, the chamber volume is increased, and the inlet element works as a diffuser and the outlet element works as a nozzle, resulting into larger transported volume fluid into the chamber through inlet than through outlet; Duding pumping mode, the chamber volume is decreased, and the outlet element works as a diffuser and the inlet element works as a nozzle, leading to larger transported volume fluid out of chamber through outlet than through inlet. And therefore, a net fluid flow from inlet side to outlet side is realized via valveless pumps. For valveless pump with diffuser/nozzle elements, the pumping performance has a very close relationship with the geometries and

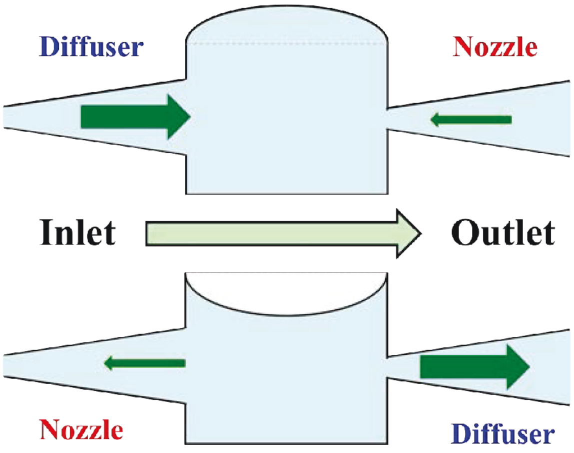

Figure 5.3: Pumping mechanism of a valveless pump: expansion of the chamber volume (upside) and contraction of chamber volume (downside); The arrow indicates direction of the fluid flow and the thicker, the higher volume flow of working fluid.

size of diffuser/nozzle elements. There are three main types of diffuser/nozzle geometries: conical, pyramidal and planar. The choice of diffuser shape is basically dependent on the fabrication process. Detailed investigations on the diffuser geometry ans size can be found in various literatures [238–240].

In contrast with micropumps with two movable check valves, the valveless micropump exhibit many advantages: Firstly, the diffuser/element can be easily and directly fabricated on the substrates via micro-machining, which will reduce the difficulty and cost of the manufacture of micropump and it can be more practical for pumps with small size; Secondly, no movable parts are included in diffuser/nozzle elements, leading to an elimination of mechanical fatigue problem, increased reliability and lifetime of the micropump. Furthermore, there is almost no limitation on the working frequency for valveless micropumps.

5.4 Design and fabrication of the valveless micropump

In our work, the valveless micropump design with diffuser/nozzle elements was used to investigate the performance of electrostrictive polymer driven micropump. There are two most common types of diffuser/nozzle elements: conical and planar (flat-walled). It has been demonstrated that, planar diffuser can make a more compact micropump than conical diffuser, since the length for conical diffuser achieving the best performance is 10 % - 80 % longer than that for planar diffuser [238]. Therefore, diffuser/nozzle elements with rectangular cross section, which has two diverging/converging side walls and two parallel walls (top and bottom), are adopted in our micropump.

Fig. 5.4a presents the top view of the structure of the designed micropump, including inlet/outlet chambers, two diffuser/nozzle elements with same size and a circular pump chamber. The diffuser efficiency is closely associated with the Reynolds number and

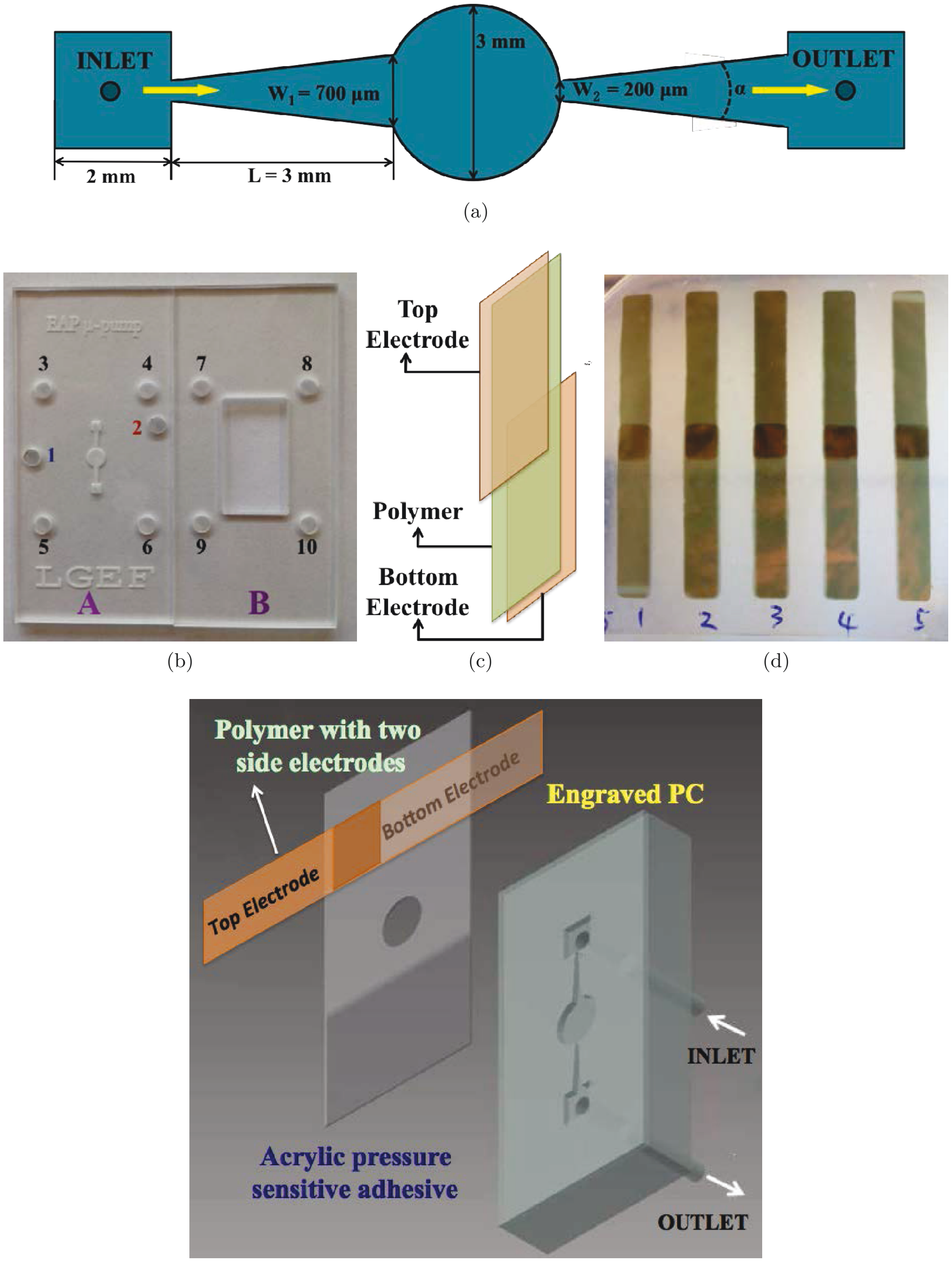

(a)

(b) (c) (d)

(e)

Figure 5.4: Design and fabrication of micropumps: (a) Top view of the structure of the micropump; (b) Photo of the engraved micropump on PC substrate; (c) Metalization of the polymer film; (d) Photo of polymer films with two side electrodes; (e) Schematic illustration of assembly process of the micropump system.

three dimensionless geometrical parameters: the area ratio between inlet/outlet A_i/A_o, the slenderness, which is the diffuser length divided by the neck width L/W_2, and the divergence angle α. As the goal of this work is to demonstrate the performance of the micropump driven by electrostrictive polymers, no delicated optimization of the fluidic design of the micropump was performed. The choice of the dimension parameters of the micropump was on the basis of the results reported by Olsson *et al.* [238], in which the pumping performances of planar diffuser/nozzle elements based micropumps with different dimensions in terms of diffuser angle, length, neck width was investigated. In our work, the diffuser length L is 3 mm, the neck width W_2 is 200 μm, and the divergence angle α is 9.5°. The diameter of the pump chamber is 3 mm and the side length of the square inlet/outlet chamber is 2 mm. Such a structure was engraved on a polycarbonate (PC) substrate by an automatic engraving machine Roland® EGX-350. The depth of the engraved micro-channel is 100 μm. Two through holes were drilled at the center of inlet/outlet chamber and polytetrafluoroethylene (PTFE) tubes with the inner diameter of 380 μm were glued to these two holes from backside. The as-prepared pump without driven membrane is illustrated in Fig. 5.4b (Plate A).

The as-prepared electrostrictive polymer films of terpolymer modified with 15 wt.% DEHP was metalized a 25-nm-thickness gold electrode on each side with a mask using a Cressington High Resolution Sputter Coater (208HR). As shown in Fig. 5.4c, the sizes of polymer films and gold electrode are 4.5 cm × 0.5 cm and 2.5 cm × 0.5 cm, respectively. The overlapping region of top and bottom electrodes with a size of 0.5 cm × 0.5 cm was used as the driving membrane for micropumps, which is clearly presented in Fig. 5.4d.

Fig. 5.4e illustrates the assembly process of the micropump system. The metalized electrostrictive film was bonded to the engraved plate A with the electrode overlapping region coinciding with the pumping chamber using acrylic pressure sensitive adhesive (3M ATG 969). The top electrode can be connected to the applied electric field through hole 2 and the bottom electrode can be connected to ground via hole 1 (as shown in Fig. 5.4b). Subsequently, plate A and plate B were clamped with screws through holes 3-10. As demonstrated, the electrostrictive polymer film in our work acts as both the driven actuator and the diaphragm of the micropump. In next section, the pumping performance of the as-prepared micropump will be investigated.

5.5 Investigation of performances of the micropump

5.5.1 Displacement of polymer diaphragm of micropump without liquid

The actuation performance of the as-prepared micropump was investigated by measuring the displacement of the center of the electrostrictive polymer diaphragm in air and the experimental setup is illustrated in Fig. 5.5. A square electric field with a frequency of 1 Hz produced by function generator and voltage amplifier was applied to the polymer diaphragm through top and bottom electrodes, and a laser vibrometer system (Polytech

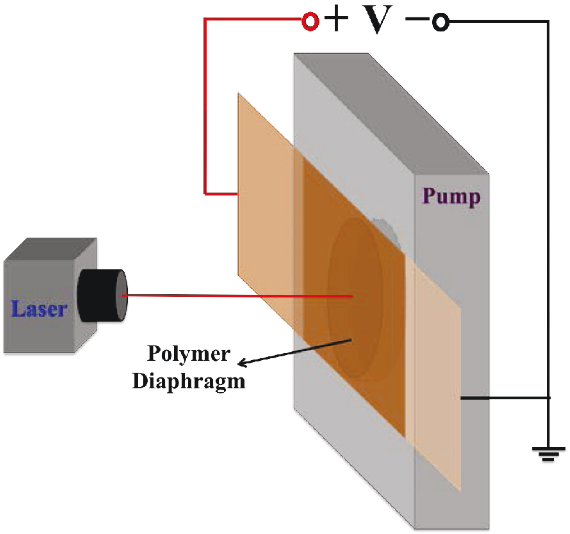

Figure 5.5: Schematic illustration of experimental setup for the displacement measurement of the electrostrictive polymer diaphragm.

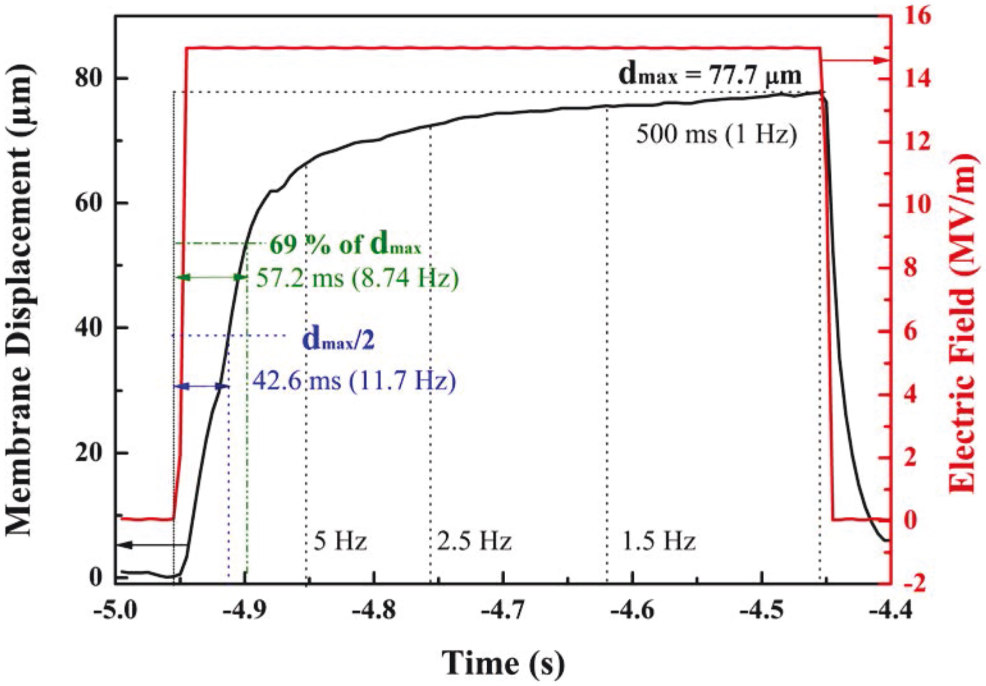

Figure 5.6: The real-time displacement of the center of the polymer diaphragm and applied electric field as a function of time in one cycle measured at 1 Hz. The value of time and frequency indicate the duration time of the applied electric field and the corresponding equivalent frequency of the applied electric field, respectively.

OFV-5000 vibrometer controller and OFV-505 sensor head) was used to measure the displacement of the center of the polymer diaphragm. The signal of applied electric field and displacement were recorded by an oscilloscope. The thickness of electrostrictive polymer film is about 65 μm.

Fig. 5.6 gives the real-time displacement of the center of the polymer diaphragm and applied electric field as a function of time in one cycle measured at 1 Hz. As the electric field changed from 0 MV/m to 15 MV/m, the displacement was significantly increased in a very shot time and afterwards reach a maximum value of 77.7 μm at the end of the cycle with a slow increasing rate. The hysteresis between the applied electric field and the induced displacement is associated with the viscoelastic nature of polymer materials. From the results presented in this figure, the frequency dependence of actuation performance of micropump can be derived. For instance, at a time duration of 57.2 ms of the application of electric field, the displacement of polymer diaphragm reaches a value of 69 % of the maximum displacement. That is to say, a maximum displacement of 53.6 μm will be achieved when an electric field of 15 MV/m with a frequency of 8.74 Hz is applied on the polymer diaphragm. Hence, we can conclude that the displacement will dramatically decreased at a work frequency larger than 5 Hz. As a result, the work frequency for electrostrictive polymer based micro-actuator should be carefully chosen.

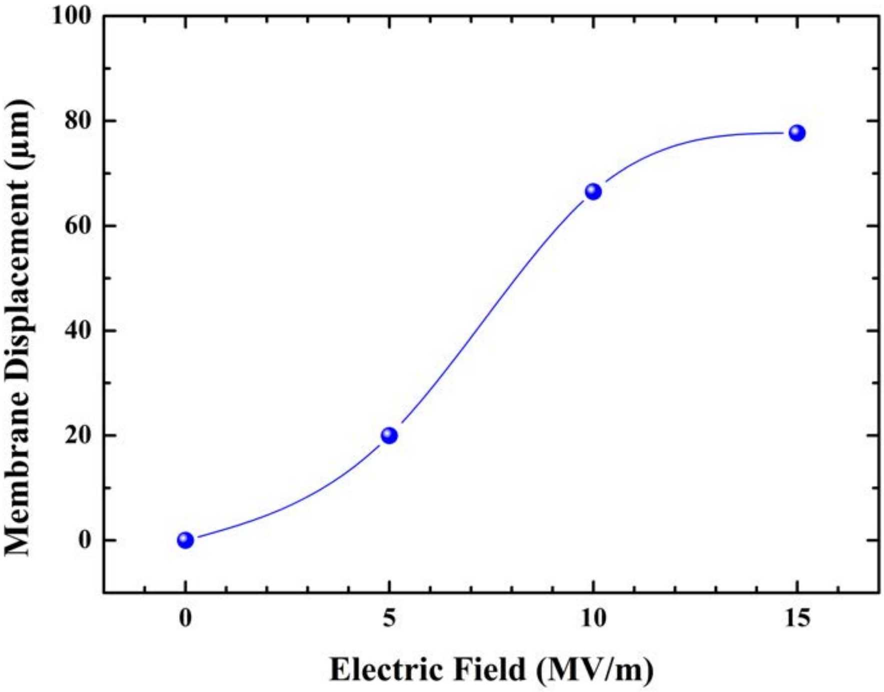

Figure 5.7: The displacement of the center of the polymer diaphragm as a function of applied electric field measured at 1 Hz (lines as guide for eyes).

The displacement of the center of the polymer diaphragm as a function of applied electric field measured at 1 Hz is presented in Fig. 5.7. It is demonstrated that the quadric relationship between field induced displacement and applied electric field is only available at low electric field. At high electric field, a saturation of displacement occurs due to the decrease of dielectric permittivity arising from the dielectric saturation of the dielectrics at high electric field. As reported in previous investigation [183, 234], the saturation electric field for pure terpolymer is larger than 50 MV/m, while for 15 wt% DEHP modified terpolymer, the saturation electric field is only about 6.7 MV/m. The results shows a maximum displacement of 77.7 μm at an electric field of 15 MV/m. The electric field required for previous reported irradiated P(VDF-TrFE) based micropump to reach the same level of displacement as our micropump is about 6 times higher [164]. It indicates that the modification of terpolymer with DEHP clearly improved the actuation performance, especially the decreased electric field.

5.5.2 Back pressure and flow rate

A. Measurement procedure

To generally investigate the pumping performance of the as-prepared micropump, two key parameters including the back pressure and the flow rate were measured at different applied electric field and frequency. The experimental setup and measuring process are schematically illustrated in Fig. 5.8. In order to reduce the risk of air bubble trapping in micropump channels, the water used for pump test was vacuumed to remove the micro air bubbles and the micropump system was pre-filled with ethanol since it has a lower surface tension than water. Subsequently, water with desired volume was injected into the micropump system using a syringe from inlet tube, and kept for a while until the fluid within the micropump reaching a stable state, as is shown in Fig. 5.8a. For the initial state of the micropump system, a fluid height difference (h_0) between the inlet and outlet tubes, which may be associated with losses due to the interaction between the micro-channel and the used fluid such as surface tension, was observed and this height difference was found to be a constant for a given micropump system. To make sure the reliability of the experimental data, the horizontal part AB of inlet tube acts as a liquid reservoir and the fluid height in inlet tube is kept a constant with a value equal to the length of vertical part BC of inlet tube during the whole measurement process.

Back pressure refers to the pressure imposed to the desired fluid flow in a confined space such as a tube or a duct by the pump. The measurement of maximum back pressure (at zero flow rate) is shown in Fig. 5.8b. In the following context, the group back pressure is refereed to maximum back pressure at zero flow rate for convenience. When the micropump is activated by the applied electric field, water will flow from inlet side to outlet side until that a new stable state is established. The back pressure is determined by the fluid height changes (Δh) in the outlet tubes compared to its initial fluid height.

Flow rate is the flow volume of liquid which passes per unit time. The maximum

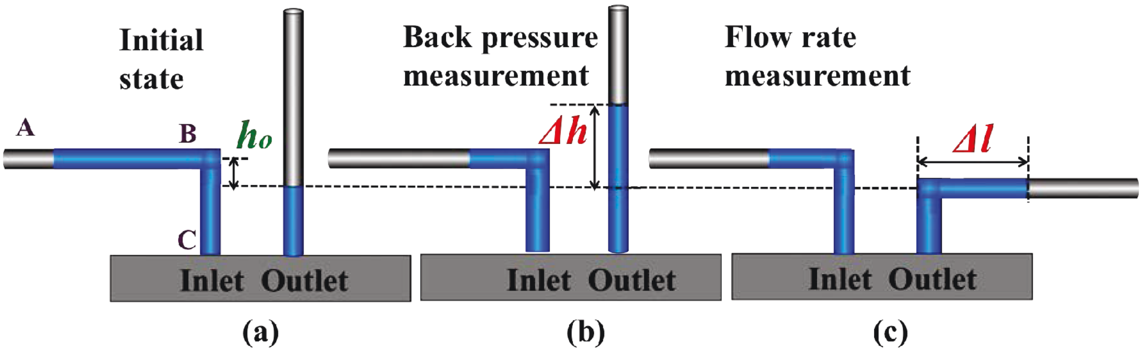

Figure 5.8: Schematic illustration of experimental setup for the pumping performance characterization of the micropump: (a) Initial state of the micropump; (b) Back pressure measurement; (c) Flow rate measurement.

flow rate at zero back pressure was measured by the procedure shown in Fig. 5.8c. In the following context, the group flow rate is refereed to maximum flow rate at zero back pressure for convenience. In order to keep a zero back pressure condition, the horizontal part of outlet tube is kept at the same height level as the initial fluid height in outlet tubes. As the micropump is activated by the applied electric field, a water flow from inlet side to outlet side is observed. The displacement ($\varDelta l$) in certain time of the water flow in the horizontal part of outlet tubes is measured. And the flow rate can be calculated from displacement ($\varDelta l$), time and the cross-section area of the tube.

B. Results and discussion

According to the model developed by Olsson *et al.* [241], for a given valveless micropumps with diffuser/nozzle elements, the generated back pressure (p) acting on the diaphragm has a linear relationship with the displacement of the diaphragm,

$$p = K_p d, \tag{5.1}$$

where K_p is a constant which is related with the properties of the pump and used liquid, and d is the displacement of the center of the polymer diaphragm. And the volume flow rate Q can be given by,

$$Q = 2\varDelta V f \left(\frac{\eta^{1/2} - 1}{\eta^{1/2} + 1} \right) = 2\varDelta V f C, \tag{5.2a}$$

$$\eta = \frac{\xi_n}{\xi_d}, \tag{5.2b}$$

where $\varDelta V$ is the volume change of the pump chamber per stroke, f is the work frequency of the pump, η is the diffuser efficiency of a diffuser/nozzle element, and ξ_n and ξ_d are the pressure loss efficiencies for nozzle and diffuser, respectively. $\eta > 1$ will contribute a fluid flow in diffuser direction, while $\eta < 1$ will contribute a fluid flow in nozzle direction [240]. The pressure loss efficiencies ξ is related with the cross-section area of the narrowest and widest part of the diffuser/nozzle elements, and therefore, the parameter C is a constant associated with the structure of the diffuser/nozzle.

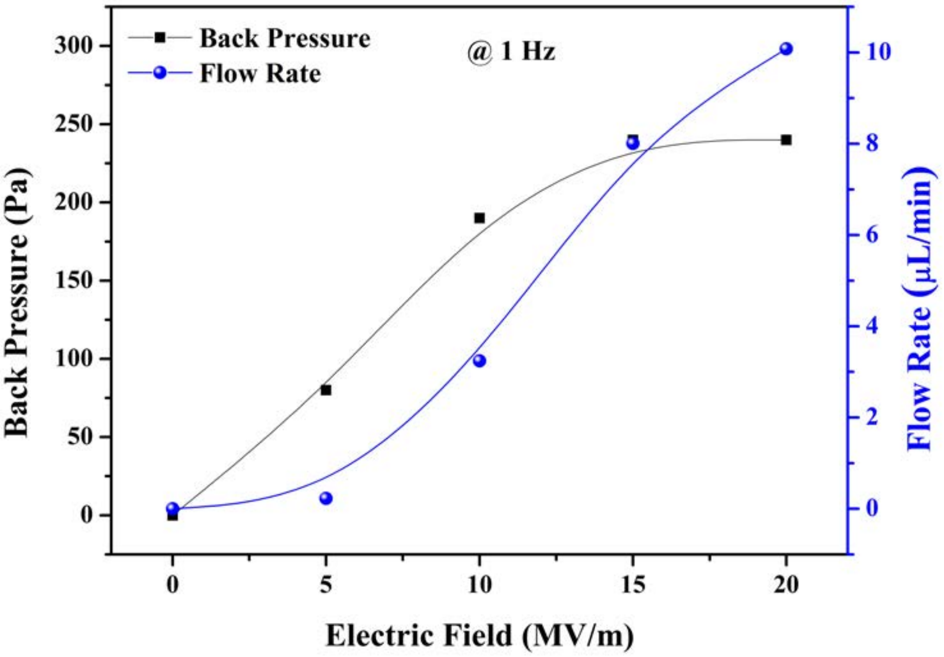

Figure 5.9: The back pressure and flow rate of the micropump as a function of electric field measured at 1 Hz (lines as guide for eyes).

Fig. 5.9 presents the back pressure and flow rate as a function of applied electric field at 1 Hz. As is depicted, both back pressure and flow rate increase with increased electric field and a saturation appears at high electric field. A back pressure of 240 Pa and a flow rate of 10.1 μL/min were observed at an applied electric field of 20 MV/m at 1 Hz. The back pressure and flow rate of the micropump as a function of frequency measured at 20 MV/m are illustrated in Fig. 5.10. A decrease of back pressure with frequency was observed, while for the flow rate, it undergoes firstly an increase and subsequently a decrease with increased frequency, and a peak value of 10.5 μL/min was achieved at 2 Hz.

The observed experimental results are in good agreement with the aforementioned model developed by Olsson *et al.*, which indicates the pumping performances of a given diffuser/nozzle elements based valveless micropump are closely dependent on the actuation performances of the polymer diaphragm. As is demonstrated in Eq. 5.1, the back pressure has a linear relationship with the displacement of the polymer diaphragm. And as a result, an increase of back pressure with electric field and a decrease of back pressure with frequency were observed due to the increase of displacement with electric field and the decrease of displacement with frequency, respectively (see Section 5.5.1). While for

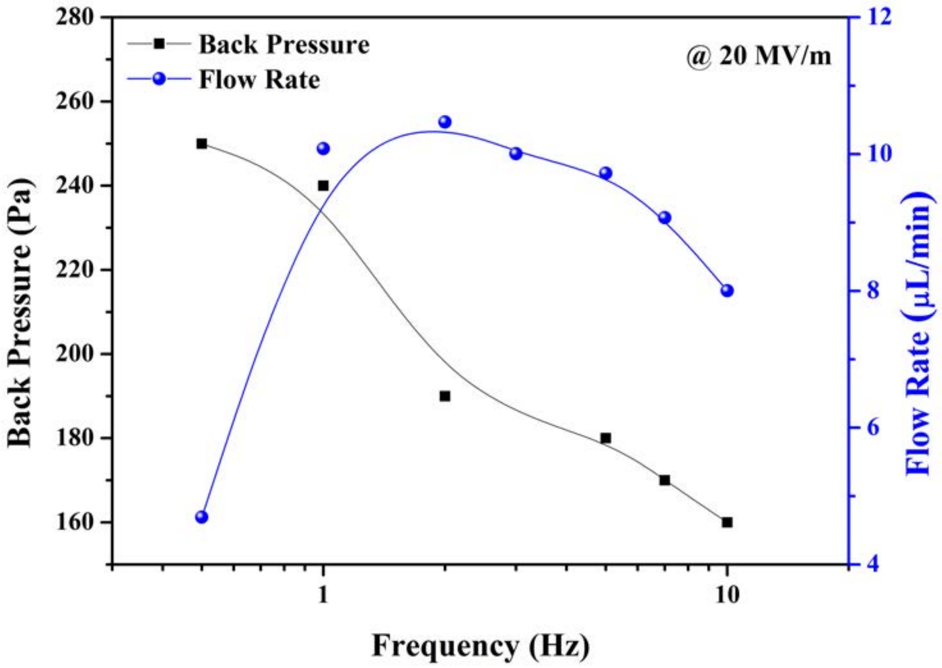

Figure 5.10: The back pressure and flow rate of the micropump as a function of frequency measured at 20 MV/m (lines as guide for eyes).

flow rate, it can be found from Eq. 5.2 that the flow rate is determined by work frequency (f) and the volume change of pump chamber ($\mathit{\Delta V}$) per stroke which is positively correlative with displacement (d). Therefore, flow rate increases with increasing electric field at a constant frequency due to the increased displacement. However, when micropump performs at different frequency and a constant electric field, the increase of the frequency results decreased displacement, especially at a frequency above 5 Hz (as shown in Fig. 5.6), and consequently decreased $\mathit{\Delta V}$. Therefore, a peak value of $\mathit{\Delta V} \times f$ will be achieved with increased frequency, which is responsible for the observed frequency dependency of flow rate. Furthermore, the saturation of displacement of polymer diaphragm caused by the dielectric saturation of DEHP modified electrostrictive polymer at high electric field can be responsible for the saturation of back pressure and flow rate at high electric field.

Table 5.2: Estimation of the constant parameter (C) and diffuser efficiency (η) of diffuser/nozzle elements.

f (Hz)	E (MV/m)	d (μm)	$\mathit{\Delta V}$ (mm^3)	Q (μL/min)	C (%)	η
1	15	77.7	0.27	8	24.3	2.69

Based on the measured flow rate and displacement of the polymer diaphragm, the constant parameter (C) and diffuser efficiency (η) of diffuser/nozzle elements were estimated and the results are given in Table 5.2. The change of the pump chamber volume per stroke was estimated as a part of sphere by

$$\varDelta V = \pi d \cdot \frac{3r^2 + d^2}{6}, \tag{5.3}$$

where d is the displacement of the polymer diaphragm, r is the diameter of the circular pump chamber with a value of 1.5 mm. For the investigated micropump, the measured η is 2.69, and rectifying factor C is 24.3 % (the idea η and corresponding C are 3.6 and 31 %, respectively). Both of these two value is higher than the previous reported micropump by Xia *et al.* [164]. The value of the parameter C, which can be used to characterizing the pumping efficiency, indicates that 24.3 % of the volume change of the pump chamber caused by the actuation of polymer diaphragm contributes to the net fluid flow.

5.6 Conclusion

In this chapter, a valveless micropump in which 15 wt.% DEHP modified terpolymer with improved electromechanical properties was used as the actuation diaphragm was presented. The back pressure at zero flow rate and flow rate at zero back pressure was measured for the investigation of the pumping performances of the as-prepared micropump.

It is demonstrated that, the improvement of pumping performance with elevated applied electric field was limit at high electric field due to the dielectric saturation of modified terpolymers. A decrease of back pressure and a flow rate peak were observed as the frequency increased. The observed pumping performance of the micropump can be contributed to the actuation performance of the polymer diaphragm at different electric field and frequency. At an applied electric field of 20 MV/m, a back pressure of 240 Pa and a flow rate of 10.1 μL/min at 1 Hz were achieved. The modification of terpolymer with DEHP contributed to the good pumping performance at an electric field lower than 20 MV/m and the resulting micropump is promising for low-frequency pumping applications.

Chapter 6

Conclusions and Future Work

6.1 Conclusions

Electroactive polymers (EAPs), which can perform conversion between mechanical energy and electrical energy, are very attractive smart materials due to their wide range of applications such as sensors, actuators, generators, artificial muscles and robots and so on. Among EAPs, PVDF-based electrostrictive terpolymers have been extensively investigated because of their excellent electromechanical performances (a field induced longitudinal strain of 7 % and an elastic energy density of 1.1 J/cm^3) and importantly, the bio-compatibility. However, PVDF-based electrostrictive terpolymers suffer a very high actuation electric field, which is not safe and convenient for practical applications.

In order to improve the electromechanical performances of PVDF-based electrostrictive terpolymers at low electric field, two different approaches of modification of terpolymers were carried out in this work. Since the electromechanical properties of electrostrictive polymer are determined by dielectric permittivity (ε_r), dielectric breakdown strength (DBS) and Young's modulus (Y), the influences of modification on these field properties and the final electromechanical properties of terpolymers were carefully characterized. And two applications based on modified terpolymer with improved electromechanical properties were investigated. Main conclusions of this work are summarized as follows:

1. In chapter 2, an organic/inorganic nanocomposite was prepared by introducing conductive carbon black (CB) nano-particles into terpolymer matrix on the basis of percolation theory. A percolation threshold of 4.68 wt.% was observed and nanocomposite with a CB loading of 4.5 wt.% exhibits an elevated dielectric of 140, which is

2.8 times higher than that of pure terpolymer, and low dielectric loss of 0.05, which is comparable to polymer matrix, at 100 Hz. Compared with ceramic or metal particle filled composites in which a high dielectric permittivity was achieved at expense of flexibility due to high loading of inorganic fillers, the as-prepared nanocomposites exhibit an enhanced dielectric permittivity and almost the same flexibility as pure terpolymer. The low Young's modulus, improved dielectric permittivity and low dielectric loss of nanocomposite enable it very attractive in actuator applications.

However, the thin insulating layer between CB fillers which contributes the great enhancement of dielectric permittivity also leads to enhanced local electric field and finally results in dramatically decreased dielectric breakdown strength (DBS) which limits its practical applications as an electrostrictive material. Therefore, the introduction of conductive carbon black brought about an enhanced dielectric permittivity, but more importantly, a significantly reduced DBS, leading to a declined electrostrictive performance of terpolymer.

2. In chapter 3, an all-organic composite was prepared by introducing small molecular plasticizer bis(2-ethylhexyl) phalate (DEHP) into electrostrictive terpolymer matrix based on the heterogeneous nature of semi-crystalline terpolymer and the important role that interface polarization plays for dielectric and electromechanical response. The experimental results indicate that, the introduced plasticizer DEHP expands the free volume of the terpolymer and increased the mobility of polymer chains. Hence, more charge carriers are trapped in the expanded interface region between amorphous and crystalline region, leading to a dramatically increased dielectric permittivity at low frequency due to the enforced interfacial polarization and moderately decreased dielectric breakdown strength. In addition, terpolymer becomes softer (lower Young's modulus) with increased DEHP loading than pure terpolymer.

   As expected, terpolymers modified with plasticizer DEHP exhibit improve electromechanical properties. Terpolymer with 10 wt.% DEHP loading has a field induced transverse strain of 1 % and elastic energy density of 4.81×10^{-3} J/cm^3 at an electric field of 30 MV/m and 0.1 Hz, which are about 5 times and 20 times higher than those of pure terpolymer, respectively. It is very interesting to find that, terpolymers with 10 wt.% DEHP loading shows better electrostrictive performance than terpolymers with 15 wt.% DEHP loading at higher electric field. It can be explained by the earlier appearance of dielectric saturation at a lower electric field for terpolymers with higher loading of DEHP due to the plasticizing effect of DEHP, which will contribute to decrease of electromechanical coefficient (M_{31}). In summary, in contrast with inorganic/organic composite, the modification of electrostrictive terpolymer with plasticizer DEHP provides a promising way to achieve an all-organic electroactive polymer with improved electromechanical properties.

3. In chapter 4, energy harvesting based on DEHP modified terpolymer was investigated. Terpolymer modified with 2.5 wt.% DEHP with smaller dielectric loss than terpolymers modified with higher content DEHP loading was used for energy harvesting via a pseudo-piezoelectric cycle in which a DC bias electric field was applied on electrostrictive polymers.

   Due to the improved electromechanical properties by DEHP, modified terpolymer exhibit an enhanced energy harvesting performance in contrast of pure terpolymer. The generated maximum short-circuit current and power density is 3.635 μA and 607 μW/cm^3 for modified terpolymer, respectively. Based on the quadric relationship between the energy conversion efficiency and DC bias electric field, an estimated energy conversion efficiency as high as 34 % and a corresponding electrical power density of 4.31 mW/cm^3 can be achievable for modified terpolymer working at an DC bias electric field of 30 MV/m.

4. In chapter 5, a valveless micropump in which 15 wt.% DEHP modified terpolymer with improved electromechanical properties was used as the actuation diaphragm was presented. The back pressure at zero flow rate and flow rate at zero back pressure were measured to investigate the pumping performances of the as-prepared micropump.

   The pumping performances have a close relationship with the frequency and amplitude of the applied electric field. At an applied electric field of 20 MV/m with a frequency of 1 Hz, a back pressure of 240 Pa and a flow rate of 10.1 μL/min were achieved. The modification of terpolymer with DEHP contributed to the good pumping performance at an electric field lower than 20 MV/m and the resulting micropump is promising for low-frequency pumping applications.

6.2 Future work and perspectives

To realize improved electromechanical performances of electrostrictive polymers at low electric field, a high dielectric permittivity and moderated reduced Young's modulus is required. Introducing conductive fillers into polymer is an very efficient way to realize high dielectric permittivity. However, it will also bring about the increase of Young's modulus and decease of dielectric breakdown strength, which is not favorable for high electromechanical performances. To solve these problems, field strategies can be applied: (i) The choice of conductive fillers with high aspect ratio will contribute a low loading of fillers and not too much increased Young's modulus; (ii) The surface modification of fillers with organic groups will increase the compatibility of inorganic fillers and polymer matrix, leading to a better dispersion and more uniform electric field distribution within the composites and therefore a high electric field; (iii) Introduction of more than one fillers into polymer matrix may be an interesting method for the improvement of the electromechanical performance of electrostrictive polymer.

Modification of electrostrictive polymer via plasticizer presented in this work provides a promising and effective approach to improve the electromechanical performances of electrostrictive polymer. To further develop this kind of all-organic electrostrictive polymer with high electromechanical performances, several topics remain worthy to be investigated:

1. Since the improved electromechanical performances of DEHP modified electrostrictive polymer arises from the enhanced interfacial polarization of the trapped charge carriers in the interface region between crystalline and amorphous regions, the investigation on the crystallinity of modified polymer with different processing method and quantitative characterization of the charge carriers by thermally stimulated current spectroscopy will be helpful to understand the interaction between the plasticizer and polymer, and the improvement mechanism of plasticizer on the electromechanical performances electrostrictive polymer.

2. Based on the well understand improvement mechanism, proper plasticizer can be employed to prepared novel all-organic polymers with excellent electromechanical performances.

3. From a point view of practical application, the toxicity and reliability of introduced plasticizer should be carefully investigated.

4. Micro sensors or actuators based on modified terpolymers can be developed by new fabrication technologies such as inkjet printing or 3D printing.

List of Figures

List of Tables

Bibliography

[1] Yoseph Bar-Cohen, editor. *Electroactive Polymer (EAP) as Actuators and Devices: Reality, Potential and Challenges*. SPIE PRESS, 2nd edition, 2004.

[2] Martin Zirkl, Anurak Sawatdee, Uta Helbig, Markus Krause, Gregor Scheipl, Elke Kraker, Peter Andersson Ersman, David Nilsson, Duncan Platt, Peter Bodö, Siegfried Bauer, Gerhard Domann, and Barbara Stadlober. An all-printed ferroelectric active matrix sensor network based on only five functional materials forming a touchless control interface. *Advanced Materials*, 23(18):2069–2074, 2011.

[3] Chengliang Sun, Jian Shi, Dylan J. Bayerl, and Xudong Wang. PVDF microbelts for harvesting energy from respiration. *Energy & Environmental Science*, 4:4508–4512, 2011.

[4] Yongbo Yuan, Timothy J. Reece, Pankaj Sharma, Shashi Poddar, Stephen Ducharme, Alexei Gruverman, Yang Yang, and Jinsong Huang. Efficiency enhancement in organic solar cells with ferroelectric polymers. *Nature Materials*, 10(4):296–302, 2011.

[5] Y. Yang and A. J. Heeger. Polyaniline as a transparent electrode for polymer light-emitting diodes: Lower operating voltage and higher efficiency. *Applied Physics Letters*, 64(10):1245–1247, 1994.

[6] Ashutosh K. Tripathi, Albert J. J. M. van Breemen, Jie Shen, Qi Gao, Marius G. Ivan, Klaus Reimann, Erwin R. Meinders, and Gerwin H. Gelinck. Multilevel information storage in ferroelectric polymer memories. *Advanced Materials*, 23(36):4146–4151, 2011.

[7] Matthias O. Franz and Hanspeter A. Mallot. Biomimetic robot navigation. *Robotics and Autonomous Systems*, 30(1):133–153, 2000.

[8] Deepak Trivedi, Christopher D. Rahn, William M. Kier, and Ian D. Walker. Soft robotics: Biological inspiration, state of the art, and future research. *Applied Bionics and Biomechanics*, 5(3):99–117, 2008.

[9] Won-Shik Chu, Kyung-Tae Lee, Sung-Hyuk Song, Min-Woo Han, Jang-Yeob Lee, Hyung-Soo Kim, Min-Soo Kim, Yong-Jai Park, Kyu-Jin Cho, and Sung-Hoon Ahn.

Review of biomimetic underwater robots using smart actuators. *International Journal of Precision Engineering and Manufacturing*, 13(7):1281–1292, 2012.

[10] John M. Hollerbach, Ian W. Hunter, and John Ballantyne. A comparative analysis of actuator technologies for robotics. *The Robotics Review*, 2:299–342, 1992.

[11] J. D. W. Madden, N. A. Vandesteeg, P. A. Anquetil, P. G. A. Madden, A. Takshi, R. Z. Pytel, S. R. Lafontaine, P. A. Wieringa, and I. W. Hunter. Artificial muscle technology: physical principles and naval prospects. *IEEE Journal of Oceanic Engineering*, 29(3):706–728, July 2004.

[12] I. W. Hunter and S. Lafontaine. A comparison of muscle with artificial actuators. In *Solid-State Sensor and Actuator Workshop, 1992. 5th Technical Digest., IEEE*, pages 178–185, June 1992.

[13] W. C. Roentgen. About the changes in shape and volume of dielectrics caused by electricity. *Section III in G. Wiedemann (Ed.), Annual Physics and Chemistry Series*, 11:771–786, 1880.

[14] M. P. Sacerdote. Strains in polymers due to electricity. *J. Phys. Ser.*, 3(8):282, 1899.

[15] Mototaro Eguchi. On the permanent electret. *Philosophical Magazine*, 49:178, 1925.

[16] P. R. Scheeper, A. G. H. van der Donk, W. Olthuis, and P. Bergveld. A review of silicon microphones. *Sensors and Actuators A: Physical*, 44(1):1–11, 1994.

[17] Heiji Kawai. The piezoelectricity of poly(vinylidene fluoride). *Japanese Journal of Applied Physics*, 8(7):975–976, 1969.

[18] J. G. Bergman. Pyroelectricity and optical second harmonic generation in polyvinylidene fluoride films. *Applied Physics Letters*, 18(5):203, 1971.

[19] Masahiko Tamura, Kiyohide Ogasawara, Nobuyuki Ono, and Sumio Hagiwara. Piezoelectricity in uniaxially stretched poly(vinylidene fluoride). *Journal of Applied Physics*, 45(9):3768–3771, 1974.

[20] T. Furukawa, J. Aiba, and E. Fukada. Piezoelectric relaxation in polyvinylidene fluoride. *Journal of Applied Physics*, 50(5):3615–3621, 1979.

[21] J. G. Bergman Jr, J. H. McFee, and G. R. Crane. Pyroelectricity and optical second harmonic generation in polyvinylidene fluoride films. *Applied Physics Letters*, 18(5):203–205, 1971.

[22] A. M. Glass, J. H. McFee, and J. G. Bergman Jr. Pyroelectric properties of polyvinylidene flouride and its use for infrared detection. *Journal of Applied Physics*, 42(13):5219–5222, 1971.

[23] J. H. McFee, J. G. Bergman Jr, and G. R. Crane. Pyroelectric and nonlinear optical properties of poled polyvinylidene fluoride films. *Ferroelectrics*, 3(1):305–313, 1972.

[24] G. Pfister, M. Abkowitz, and R. G. Crystal. Pyroelectricity in polyvinylidene fluoride. *Journal of Applied Physics*, 44(5):2064–2071, 1973.

[25] Takeshi Yamada, Toshinobu Ueda, and Toyoki Kitayama. Ferroelectric-to-paraelectric phase transition of vinylidene fluoride-trifluoroethylene copolymer. *Journal of Applied Physics*, 52(2):948–952, 1981.

[26] Hiroji Ohigashi and Keiko Koga. Ferroelectric copolymers of vinylidenefluoride and trifluoroethylene with a large electromechanical coupling factor. *Japanese Journal of Applied Physics*, 21(8A):L455, 1982.

[27] Ken'ichi Nakamura and Yasaku Wada. Piezoelectricity, pyroelectricity, and the electrostriction constant of poly(vinylidene fluoride). *Journal of Polymer Science Part A-2: Polymer Physics*, 9(1):161–173, January 1971.

[28] Hiroji Ohigashi. Electromechanical properties of polarized polyvinylidene fluoride films as studied by the piezoelectric resonance method. *Journal of Applied Physics*, 47(3):949–955, 1976.

[29] Mitsumasa Oshiki and Eiichi Fukada. Inverse piezoelectric effect and electrostrictive effect in polarized poly(vinylidene fluoride) films. *Journal of Materials Science*, 10(1):1–6, 1975.

[30] P. Herchenröder, Y. Segui, D. Horne, and D. Y. Yoon. Ferroelectricity of poly(vinylidene fluoride): Transition temperature. *Physical Review Letters*, 45:2135–2137, Dec 1980.

[31] T. Furukawa, G. E. Johnson, H. E. Bair, Y. Tajitsu, A. Chiba, and E. Fukada. Ferroelectric phase transition in a copolymer of vinylidene fluoride and trifluoroethylene. *Ferroelectrics*, 32(1):61–67, 1981.

[32] Qiming Zhang, Vivek Bharti, and X. Zhao. Giant Electrostriction and Relaxor Ferroelectric Behavior in Electron-Irradiated Poly(vinylidene fluoride-trifluoroethylene) Copolymer. *Science*, 280(5372):2101–2104, June 1998.

[33] W. Lehmann, H. Skupin, C. Tolksdorf, E. Gebhard, R. Zentel, P. Kruger, M. Losche, and F. Kremer. Giant lateral electrostriction in ferroelectric liquid-crystalline elastomers. *Nature*, 410(6827):447–450, 03 2001.

[34] Ron Pelrine, Roy Kornbluh, Qibing Pei, and Jose Joseph. High-speed electrically actuated elastomers with strain greater than 100 %. *Science*, 287(5454):836–839, 2000.

[35] Paul Brochu and Qibing Pei. Advances in dielectric elastomers for actuators and artificial muscles. *Macromolecular Rapid Communications*, 31(1):10–36, 2010.

[36] A. R. Hubert, D. S. Brodie, I. A. McAllister, and J. N. Gleason. Artificial muscle camera lens actuator, June 19 2014. US Patent App. 13/971,077.

[37] Tissaphern Mirfakhrai, John D.W. Madden, and Ray H. Baughman. Polymer artificial muscles. *Materials Today*, 10(4):30–38, 2007.

[38] Ravi Shankar, Tushar K. Ghosh, and Richard J. Spontak. Dielectric elastomers as next-generation polymeric actuators. *Soft Matter*, 3:1116–1129, 2007.

[39] Yoseph Bar-Cohen and Qiming Zhang. Electroactive polymer actuators and sensors. *MRS Bulletin*, 33:173–181, 3 2008.

[40] James Biggs, Karsten Danielmeier, Julia Hitzbleck, Jens Krause, Tom Kridl, Stephan Nowak, Enrico Orselli, Xina Quan, Dirk Schapeler, Will Sutherland, and Joachim Wagner. Electroactive polymers: Developments of and perspectives for dielectric elastomers. *Angewandte Chemie International Edition*, 52(36):9409–9421, 2013.

[41] Hideki Shirakawa, Edwin J. Louis, Alan G. MacDiarmid, Chwan K. Chiang, and Alan J. Heeger. Synthesis of electrically conducting organic polymers: halogen derivatives of polyacetylene, (ch). *J. Chem. Soc., Chem. Commun.*, pages 578–580, 1977.

[42] R. H. Baughman, L. W. Shacklette, R. L. Elsenbaumer, E. Plichta, and C. Becht. Conducting polymer electromechanical actuators. In J.L. Brédas and R.R. Chance, editors, *Conjugated Polymeric Materials: Opportunities in Electronics, Optoelectronics, and Molecular Electronics*, volume 182 of *NATO ASI Series*, pages 559–582. Springer Netherlands, 1990.

[43] R. H. Baughman. Conducting polymers in redox devices and intelligent materials systems. *Makromolekulare Chemie. Macromolecular Symposia*, 51(1):193–215, 1991.

[44] Qibing Pei and Olle Inganäs. Conjugated polymers and the bending cantilever method: Electrical muscles and smart devices. *Advanced Materials*, 4(4):277–278, 1992.

[45] Qibing Pei and Olle Inganäs. Electrochemical applications of the bending beam method. 1. mass transport and volume changes in polypyrrole during redox. *The Journal of Physical Chemistry*, 96(25):10507–10514, 1992.

[46] Elisabeth Smela, Olle Inganäs, and Ingemar Lundström. Controlled folding of micrometer-size structures. *Science*, 268(5218):1735–1738, 1995.

[47] Wen Lu, Andrei G. Fadeev, Baohua Qi, Elisabeth Smela, Benjamin R. Mattes, Jie Ding, Geoffrey M. Spinks, Jakub Mazurkiewicz, Dezhi Zhou, Gordon G. Wallace, Douglas R. MacFarlane, Stewart A. Forsyth, and Maria Forsyth. Use of ionic liquids for π -conjugated polymer electrochemical devices. *Science*, 297(5583):983–987, 2002.

[48] Edwin W. H. Jager, Elisabeth Smela, and Olle Inganäs. Microfabricating conjugated polymer actuators. *Science*, 290(5496):1540–1545, 2000.

[49] Susumu Hara, Tetsuji Zama, Wataru Takashima, and Keiichi Kaneto. Tris(trifluoromethylsulfonyl)methide-doped polypyrrole as a conducting polymer actuator with large electrochemical strain. *Synthetic Metals*, 156(2–4):351–355, 2006.

[50] R. H. Baughman. Conducting polymer artificial muscles. *Synthetic Metals*, 78(3):339 – 353, 1996.

[51] G. M. Spinks, V. Mottaghitalab, M. Bahrami-Samani, P. G. Whitten, and G. G. Wallace. Carbon-nanotube-reinforced polyaniline fibers for high-strength artificial muscles. *Advanced Materials*, 18(5):637–640, 2006.

[52] John D. Madden, Peter G. Madden, and Ian W. Hunter. Conducting polymer actuators as engineering materials. *Proc. SPIE*, 4695:176–190, 2002.

[53] J. M. Sansinena, V. Olazabal, T. F. Otero, J. M. Sansinena, C. N. Polo da Fonseca, and Marco-A. De Paoli. A solid state artificial muscle based on polypyrrole and a solid polymeric electrolyte working in air. *Chem. Commun.*, pages 2217–2218, 1997.

[54] John D. Madden, Ryan A. Cush, Tanya S. Kanigan, Colin J. Brenan, and Ian W. Hunter. Encapsulated polypyrrole actuators. *Synthetic Metals*, 105(1):61–64, 1999.

[55] E. Smela. Conjugated polymer actuators for biomedical applications. *Advanced Materials*, 15(6):481–494, 2003.

[56] T. F. Otero, J. G. Martinez, and J. Arias-Pardilla. Biomimetic electrochemistry from conducting polymers. a review: Artificial muscles, smart membranes, smart drug delivery and computer/neuron interfaces. *Electrochimica Acta*, 84:112–128, 2012.

[57] Sumio Iijima. Helical microtubules of graphitic carbon. *Nature*, 354(6348):56–58, 1991.

[58] Sumio Iijima and Toshinari Ichihashi. Single-shell carbon nanotubes of 1-nm diameter. *Nature*, 363(6430):603–605, 06 1993.

[59] D. S. Bethune, C. H. Klang, M. S. de Vries, G. Gorman, R. Savoy, J. Vazquez, and R. Beyers. Cobalt-catalysed growth of carbon nanotubes with single-atomic-layer walls. *Nature*, 363(6430):605–607, 06 1993.

[60] Guanghua Gao, Tahir Çagin, and William A. Goddard III. Energetics, structure, mechanical and vibrational properties of single-walled carbon nanotubes. *Nanotechnology*, 9(3):184, 1998.

[61] Ray H. Baughman, Anvar A. Zakhidov, and Walt A. de Heer. Carbon nanotubes–the route toward applications. *Science*, 297(5582):787–792, 2002.

[62] Ray H. Baughman, Changxing Cui, Anvar A. Zakhidov, Zafar Iqbal, Joseph N. Barisci, Geoff M. Spinks, Gordon G. Wallace, Alberto Mazzoldi, Danilo De Rossi, Andrew G. Rinzler, Oliver Jaschinski, Siegmar Roth, and Miklos Kertesz. Carbon nanotube actuators. *Science*, 284(5418):1340–1344, 1999.

[63] U. Vohrer, I. Kolaric, M. H. Haque, S. Roth, and U. Detlaff-Weglikowska. Carbon nanotube sheets for the use as artificial muscles. *Carbon*, 42(5–6):1159–1164, 2004. European Materials Research Society 2003, Symposium B: Advanced Multifunctional Nanocarbon Materials and Nanosystems.

[64] Tissaphern Mirfakhrai, Jiyoung Oh, Mikhail Kozlov, Eddie Chi Wah Fok, Mei Zhang, Shaoli Fang, Ray H. Baughman, and John D. W. Madden. Electrochemical actuation of carbon nanotube yarns. *Smart Materials and Structures*, 16(2):S243, 2007.

[65] Mark Hughes and Geoffrey M. Spinks. Multiwalled carbon nanotube actuators. *Advanced Materials*, 17(4):443–446, 2005.

[66] Dongbo Li, Walter F. Paxton, Ray H. Baughman, Tony Jun Huang, J. Fraser Stoddart, and Paul S. Weiss. Molecular, supramolecular, and macromolecular motors and artificial muscles. *MRS Bulletin*, 34:671–681, 9 2009.

[67] Mei Zhang, Ken R. Atkinson, and Ray H. Baughman. Multifunctional carbon nanotube yarns by downsizing an ancient technology. *Science*, 306(5700):1358–1361, 2004.

[68] Mei Zhang, Shaoli Fang, Anvar A. Zakhidov, Sergey B. Lee, Ali E. Aliev, Christopher D. Williams, Ken R. Atkinson, and Ray H. Baughman. Strong, transparent, multifunctional, carbon nanotube sheets. *Science*, 309(5738):1215–1219, 2005.

[69] A. M. Fennimore, T. D. Yuzvinsky, Wei-Qiang Han, M. S. Fuhrer, J. Cumings, and A. Zettl. Rotational actuators based on carbon nanotubes. *Nature*, 424(6947):408–410, 2003.

[70] Javad Foroughi, Geoffrey M. Spinks, Gordon G. Wallace, Jiyoung Oh, Mikhail E. Kozlov, Shaoli Fang, Tissaphern Mirfakhrai, John D. W. Madden, Min Kyoon Shin, Seon Jeong Kim, and Ray H. Baughman. Torsional carbon nanotube artificial muscles. *Science*, 334(6055):494–497, 2011.

[71] Márcio D. Lima, Na Li, Mônica Jung de Andrade, Shaoli Fang, Jiyoung Oh, Geoffrey M. Spinks, Mikhail E. Kozlov, Carter S. Haines, Dongseok Suh, Javad Foroughi, Seon Jeong Kim, Yongsheng Chen, Taylor Ware, Min Kyoon Shin, Leonardo D. Machado, Alexandre F. Fonseca, John D. W. Madden, Walter E. Voit, Douglas S. Galvão, and Ray H. Baughman. Electrically, chemically, and photonically powered torsional and tensile actuation of hybrid carbon nanotube yarn muscles. *Science*, 338(6109):928–932, 2012.

[72] Jae Ah Lee, Youn Tae Kim, Geoffrey M. Spinks, Dongseok Suh, Xavier Lepró, Mácio D. Lima, Ray H. Baughman, and Seon Jeong Kim. All-solid-state carbon nanotube torsional and tensile artificial muscles. *Nano Letters*, 14(5):2664–2669, 2014. PMID: 24742031.

[73] J. D. W. Madden, J. N. Barisci, P. A. Anquetil, G. M. Spinks, G. G. Wallace, R. H. Baughman, and I. W. Hunter. Fast carbon nanotube charging and actuation. *Advanced Materials*, 18(7):870–873, 2006.

[74] M. Shahinpoor, Y. Bar-Cohen, J. O. Simpson, and J. Smith. Ionic polymer-metal composites (IPMCs) as biomimetic sensors, actuators and artificial muscles - a review. *Smart Materials and Structures*, 7(6):R15, 1998.

[75] Mohsen Shahinpoor and Kwang J. Kim. Ionic polymer-metal composites: I. Fundamentals. *Smart Materials and Structures*, 10(4):819, 2001.

[76] Kwang J. Kim and Mohsen Shahinpoor. Ionic polymer–metal composites: II. Manufacturing techniques. *Smart Materials and Structures*, 12(1):65, 2003.

[77] Mohsen Shahinpoor and Kwang J. Kim. Ionic polymer–metal composites: III. Modeling and simulation as biomimetic sensors, actuators, transducers, and artificial muscles. *Smart Materials and Structures*, 13(6):1362, 2004.

[78] Mohsen Shahinpoor and Kwang J. Kim. Ionic polymer–metal composites: IV. Industrial and medical applications. *Smart Materials and Structures*, 14(1):197, 2005.

[79] Klaus Schmidt-Rohr and Qiang Chen. Parallel cylindrical water nanochannels in nafion fuel-cell membranes. *Nature Materials*, 7(1):75–83, 01 2008.

[80] Olivier Diat and Gerard Gebel. Fuel cells: Proton channels. *Nature Materials*, 7(1):13–14, 01 2008.

[81] Yoshitsugu Sone, Per Ekdunge, and Daniel Simonsson. Proton conductivity of nafion 117 as measured by a four-electrode AC impedance method. *Journal of The Electrochemical Society*, 143(4):1254–1259, 1996.

[82] S. Slade, S. A. Campbell, T. R. Ralph, and F. C. Walsh. Ionic conductivity of an extruded nafion 1100 EW series of membranes. *Journal of The Electrochemical Society*, 149(12):A1556–A1564, 2002.

[83] H. Takenaka, E. Torikai, Y. Kawami, and N. Wakabayashi. Solid polymer electrolyte water electrolysis. *International Journal of Hydrogen Energy*, 7(5):397–403, 1982.

[84] P. Millet, M. Pineri, and R. Durand. New solid polymer electrolyte composites for water electrolysis. *Journal of Applied Electrochemistry*, 19(2):162–166, 1989.

[85] Sia Nemat-Nasser and Jiang Yu Li. Electromechanical response of ionic polymer-metal composites. *Journal of Applied Physics*, 87(7):3321–3331, 2000.

[86] Sia Nemat-Nasser. Micromechanics of actuation of ionic polymer-metal composites. *Journal of Applied Physics*, 92(5):2899–2915, 2002.

[87] Choonghee Jo, David Pugal, Il-Kwon Oh, Kwang J. Kim, and Kinji Asaka. Recent advances in ionic polymer metal composite actuators and their modeling and applications. *Progress in Polymer Science*, 38(7):1037–1066, 2013.

[88] Yongjun Tang, Zhigang Xue, Xingping Zhou, Xiaolin Xie, and Chak-Yin Tang. Novel sulfonated polysulfone ion exchange membranes for ionic polymer-metal composite actuators. *Sensors and Actuators B: Chemical*, 202(0):1164–1174, 2014.

[89] Yongjun Tang, Chao Chen, Yun Sheng Ye, Zhigang Xue, Xingping Zhou, and Xiaolin Xie. The enhanced actuation response of an ionic polymer-metal composite actuator based on sulfonated polyphenylsulfone. *Polym. Chem.*, 5:6097–6107, 2014.

[90] Jianmei Lu, Feng Yan, and John Texter. Advanced applications of ionic liquids in polymer science. *Progress in Polymer Science*, 34(5):431–448, 2009.

[91] Jean Le Bideau, Lydie Viau, and Andre Vioux. Ionogels, ionic liquid based hybrid materials. *Chem. Soc. Rev.*, 40:907–925, 2011.

[92] Takanori Fukushima and Takuzo Aida. Ionic liquids for soft functional materials with carbon nanotubes. *Chemistry – A European Journal*, 13(18):5048–5058, 2007.

[93] Lirong Kong and Wei Chen. Carbon nanotube and graphene-based bioinspired electrochemical actuators. *Advanced Materials*, 26(7):1025–1043, 2014.

[94] Takanori Fukushima, Kinji Asaka, Atsuko Kosaka, and Takuzo Aida. Fully plastic actuator through layer-by-layer casting with ionic-liquid-based bucky gel. *Angewandte Chemie International Edition*, 44(16):2410–2413, 2005.

[95] Ken Mukai, Kinji Asaka, Kenji Kiyohara, Takushi Sugino, Ichiro Takeuchi, Takanori Fukushima, and Takuzo Aida. High performance fully plastic actuator based on ionic-liquid-based bucky gel. *Electrochimica Acta*, 53(17):5555–5562, 2008.

[96] Ichiroh Takeuchi, Kinji Asaka, Kenji Kiyohara, Takushi Sugino, Naohiro Terasawa, Ken Mukai, Takanori Fukushima, and Takuzo Aida. Electromechanical behavior of fully plastic actuators based on bucky gel containing various internal ionic liquids. *Electrochimica Acta*, 54(6):1762–1768, 2009.

[97] Ken Mukai, Kinji Asaka, Takushi Sugino, Kenji Kiyohara, Ichiroh Takeuchi, Naohiro Terasawa, Don N. Futaba, Kenji Hata, Takanori Fukushima, and Takuzo Aida. Highly conductive sheets from millimeter-long single-walled carbon nanotubes and ionic liquids: Application to fast-moving, low-voltage electromechanical actuators operable in air. *Advanced Materials*, 21(16):1582–1585, 2009.

[98] Jinzhu Li, Wenjun Ma, Li Song, Zhiqiang Niu, Le Cai, Qingsheng Zeng, Xiaoxian Zhang, Haibo Dong, Duan Zhao, Weiya Zhou, and Sishen Xie. Superfast-response and ultrahigh-power-density electromechanical actuators based on hierarchal carbon nanotube electrodes and chitosan. *Nano Letters*, 11(11):4636–4641, 2011. PMID: 21972899.

[99] Sheng Liu, Yang Liu, Hülya Cebeci, Roberto Guzmán de Villoria, Jun-Hong Lin, Brian L. Wardle, and Q. M. Zhang. High electromechanical response of ionic polymer actuators with controlled-morphology aligned carbon nanotube/nafion nanocomposite electrodes. *Advanced Functional Materials*, 20(19):3266–3271, 2010.

[100] G. Wu, G. H. Li, T. Lan, Y. Hu, Q. W. Li, T. Zhang, and W. Chen. An interface nanostructured array guided high performance electrochemical actuator. *J. Mater. Chem. A*, 2:16836–16841, 2014.

[101] Sung-Weon Yeom and Il-Kwon Oh. A biomimetic jellyfish robot based on ionic polymer metal composite actuators. *Smart Materials and Structures*, 18(8):085002, 2009.

[102] Zheng Chen, S. Shatara, and Xiaobo Tan. Modeling of biomimetic robotic fish propelled by an ionic polymer-metal composite caudal fin. *IEEE/ASME Transactions on Mechatronics*, 15(3):448–459, June 2010.

[103] Ma Zhenyi, Jerry I. Scheinbeim, Jar Wha Lee, and Brian A. Newman. High field electrostrictive response of polymers. *Journal of Polymer Science Part B: Polymer Physics*, 32(16):2721–2731, 1994.

[104] Ronald E. Pelrine, Roy D. Kornbluh, and Jose P. Joseph. Electrostriction of polymer dielectrics with compliant electrodes as a means of actuation. *Sensors and Actuators A: Physical*, 64(1):77–85, 1 1998.

[105] Jean-Sébastien Plante and Steven Dubowsky. Large-scale failure modes of dielectric elastomer actuators. *International Journal of Solids and Structures*, 43(25-26):7727–7751, 2006.

[106] Jinsong Leng, Liwu Liu, Yanju Liu, Kai Yu, and Shouhua Sun. Electromechanical stability of dielectric elastomer. *Applied Physics Letters*, 94(21):211901, 2009.

[107] Roy D. Kornbluh, Ron Pelrine, Qibing Pei, Richard Heydt, Scott Stanford, Seajin Oh, and Joseph Eckerle. Electroelastomers: Applications of dielectric elastomer

transducers for actuation, generation, and smart structures. *Proc. SPIE*, 4698:254–270, 2002.

[108] Qibing Pei, Ronald E. Pelrine, and Roy D. Kornbluh. Electroactive polymers, November 2 2004. US Patent 6,812,624.

[109] Qibing Pei, Ron Pelrine, Marcus A. Rosenthal, Scott Stanford, Harsha Prahlad, and Roy D. Kornbluh. Recent progress on electroelastomer artificial muscles and their application for biomimetic robots. *Proc. SPIE*, 5385:41–50, 2004.

[110] Paul Brochu, Xiaofan Niu, and Qibing Pei. Acrylic interpenetrating polymer network dielectric elastomers for energy harvesting. In Yoseph Bar-Cohen and Federico Carpi, editors, *Electroactive Polymer Actuators and Devices (EAPAD)*, volume 7976, pages 797606–797606. International Society for Optics and Photonics, 2011.

[111] S. M. Ha, W. Yuan, Q. Pei, R. Pelrine, and S. Stanford. Interpenetrating polymer networks for high-performance electroelastomer artificial muscles. *Advanced Materials*, 18(7):887–891, 2006.

[112] Soon Mok Ha, Il Seok Park, Michael Wissler, Ron Pelrine, Scott Stanford, Kwang J. Kim, Gabor Kovacs, and Qibing Pei. High electromechanical performance of electroelastomers based on interpenetrating polymer networks. *Proc. SPIE*, 6927:69272C–69272C–9, 2008.

[113] Cheng Huang, Q. M. Zhang, Gal deBotton, and Kaushik Bhattacharya. All-organic dielectric-percolative three-component composite materials with high electromechanical response. *Applied Physics Letters*, 84(22):4391–4393, 2004.

[114] F. Carpi, G. Gallone, F. Galantini, and D. De Rossi. Silicone-poly(hexylthiophene) blends as elastomers with enhanced electromechanical transduction properties. *Advanced Functional Materials*, 18(2):235–241, 2008.

[115] F. Carpi and D. D. Rossi. Improvement of electromechanical actuating performances of a silicone dielectric elastomer by dispersion of titanium dioxide powder. *IEEE Transactions on Dielectrics and Electrical Insulation*, 12(4):835–843, Aug 2005.

[116] Giuseppe Gallone, Federico Carpi, Danilo De Rossi, Giovanni Levita, and Augusto Marchetti. Dielectric constant enhancement in a silicone elastomer filled with lead magnesium niobate-lead titanate. *Materials Science and Engineering: C*, 27(1):110 – 116, 2007.

[117] Martin Molberg, Daniel Crespy, Patrick Rupper, Frank Nüesch, Jan-Anders E. Månson, Christiane Löwe, and Dorina M. Opris. High breakdown field dielectric elastomer actuators using encapsulated polyaniline as high dielectric constant filler. *Advanced Functional Materials*, 20(19):3280–3291, 2010.

[118] Björn Kussmaul, Sebastian Risse, Guggi Kofod, Rémi Waché, Michael Wegener, Denis N. McCarthy, Hartmut Krüger, and Reimund Gerhard. Enhancement of dielectric permittivity and electromechanical response in silicone elastomers: Molecular grafting of organic dipoles to the macromolecular network. *Advanced Functional Materials*, 21(23):4589–4594, 2011.

[119] Samuel Rosset and Herbert R. Shea. Flexible and stretchable electrodes for dielectric elastomer actuators. *Applied Physics A*, 110(2):281–307, 2013.

[120] Rik Verplancke, Frederick Bossuyt, Dieter Cuypers, and Jan Vanfleteren. Thin-film stretchable electronics technology based on meandering interconnections: fabrication and mechanical performance. *Journal of Micromechanics and Microengineering*, 22(1):015002, 2012.

[121] Ned Bowden, Scott Brittain, Anthony G. Evans, John W. Hutchinson, and George M. Whitesides. Spontaneous formation of ordered structures in thin films of metals supported on an elastomeric polymer. *Nature*, 393(6681):146–149, 05 1998.

[122] Mohammed Benslimane, Peter Gravesen, and Peter Sommer-Larsen. Mechanical properties of dielectric elastomer actuators with smart metallic compliant electrodes. *Proc. SPIE*, 4695:150–157, 2002.

[123] Samuel Rosset, Muhamed Niklaus, Philippe Dubois, and Herbert R. Shea. Metal ion implantation for the fabrication of stretchable electrodes on elastomers. *Advanced Functional Materials*, 19(3):470–478, 2009.

[124] Wei Yuan, Tuling Lam, James Biggs, Liangbing Hu, Zhibin Yu, Soonmok Ha, Dongjuan Xi, Matthew K. Senesky, George Grüner, and Qibing Pei. New electrode materials for dielectric elastomer actuators. *Proc. SPIE*, 6524:65240N–65240N–12, 2007.

[125] Tuling Lam, Henry Tran, Wei Yuan, Zhibin Yu, SoonMok Ha, Richard Kaner, and Qibing Pei. Polyaniline nanofibers as a novel electrode material for fault-tolerant dielectric elastomer actuators. *Proc. SPIE*, 6927:69270O–69270O–10, 2008.

[126] Wei Yuan, Liangbing Hu, Zhibin Yu, Tuling Lam, James Biggs, Soon M. Ha, Dongjuan Xi, Bin Chen, Matthew K. Senesky, George Grüner, and Qibing Pei. Fault-tolerant dielectric elastomer actuators using single-walled carbon nanotube electrodes. *Advanced Materials*, 20(3):621–625, 2008.

[127] Wei Yuan, Paul Brochu, Han Zhang, Antony Jan, and Qibing Pei. Long lifetime dielectric elastomer actuators under continuous high strain actuation. *Proc. SPIE*, 7287:72870O–72870O–8, 2009.

[128] Qibing Pei, Marcus Rosenthal, Scott Stanford, Harsha Prahlad, and Ron Pelrine. Multiple-degrees-of-freedom electroelastomer roll actuators. *Smart Materials and Structures*, 13(5):N86, 2004.

[129] Federico Carpi, Antonio Migliore, Giorgio Serra, and Danilo De Rossi. Helical dielectric elastomer actuators. *Smart Materials and Structures*, 14(6):1210, 2005.

[130] P. G. de Gennes and T. C. Chung. Réflexions sur un type de polymères nématiques. *Seances Acad. Sci. Ser. B*, 281:101, 1975.

[131] Christian Ohm, Martin Brehmer, and Rudolf Zentel. Liquid crystalline elastomers as actuators and sensors. *Advanced Materials*, 22(31):3366–3387, 2010.

[132] Donald L. Thomsen, Patrick Keller, Jawad Naciri, Roger Pink, Hong Jeon, Devanand Shenoy, and Banahalli R. Ratna. Liquid crystal elastomers with mechanical properties of a muscle. *Macromolecules*, 34(17):5868–5875, 2001.

[133] Jawad Naciri, Amritha Srinivasan, Hong Jeon, Nikolay Nikolov, Patrick Keller, and Banahalli R. Ratna. Nematic elastomer fiber actuator. *Macromolecules*, 36(22):8499–8505, 2003.

[134] Yanlei Yu, Makoto Nakano, Atsushi Shishido, Takeshi Shiono, and Tomiki Ikeda. Effect of cross-linking density on photoinduced bending behavior of oriented liquid-crystalline network films containing azobenzene. *Chemistry of Materials*, 16(9):1637–1643, 2004.

[135] Mizuho Kondo, Yanlei Yu, and Tomiki Ikeda. How does the initial alignment of mesogens affect the photoinduced bending behavior of liquid-crystalline elastomers? *Angewandte Chemie*, 118(9):1406–1410, 2006.

[136] Yanlei Yu and Tomiki Ikeda. Soft actuators based on liquid-crystalline elastomers. *Angewandte Chemie International Edition*, 45(33):5416–5418, 2006.

[137] H. Finkelmann and H. Wermter. Liquid crystalline elastomers as artificial muscles. In *ABSTRACTS OF PAPERS OF THE AMERICAN CHEMICAL SOCIETY*, volume 219, pages U493–U493. AMER CHEMICAL SOC 1155 16TH ST, NW, WASHINGTON, DC 20036 USA, 2000.

[138] Martin Chambers, Heino Finkelmann, Maja Remskar, Antoni Sanchez-Ferrer, Bostjan Zalar, and Slobodan Zumer. Liquid crystal elastomer-nanoparticle systems for actuation. *J. Mater. Chem.*, 19:1524–1531, 2009.

[139] C. Huang, Q. M. Zhang, and A. Jákli. Nematic anisotropic liquid-crystal gels—self-assembled nanocomposites with high electromechanical response. *Advanced Functional Materials*, 13(7):525–529, 2003.

[140] Rudolf Zentel. Liquid crystalline elastomers. *Advanced Materials*, 1(10):321–329, 1989.

[141] Hong Yang, Axel Buguin, Jean-Marie Taulemesse, Kosuke Kaneko, Stéphane Méry, Anne Bergeret, and Patrick Keller. Micron-sized main-chain liquid crystalline elastomer actuators with ultralarge amplitude contractions. *Journal of the American Chemical Society*, 131(41):15000–15004, 2009. PMID: 19778041.

[142] Andrew J. Lovinger. Ferroelectric polymers. *Science*, 220(4602):1115–1121, 1983.

[143] Toshiharu Yagi, Masayoshi Tatemoto, and Jun-ichi Sako. Transition behavior and dielectric properties in trifluoroethylene and vinylidene fluoride copolymers. *Polym. J.*, 12(4):209–223, 04 1980.

[144] Andrew J. Lovinger, T. Furukawa, G. T. Davis, and M. G. Broadhurst. Curie transitions in copolymers of vinylidene fluoride. *Ferroelectrics*, 50(1):227–236, 1983.

[145] K. Tashiro, K. Takano, M. Kobayashi, Y. Chatani, and H. Tadokoro. Structural study on ferroelectric phase transition of vinylidene fluoride-trifluoroethylene copolymers (iii) dependence of transitional behavior on vdf molar content. *Ferroelectrics*, 57(1):297–326, 1984.

[146] Andrew J. Lovinger, D. D. Davis, R. E. Cais, and J. M. Kometani. The role of molecular defects on the structure and phase transitions of poly(vinylidene fluoride). *Polymer*, 28(4):617–626, 1987.

[147] Takeo Furukawa. Ferroelectric properties of vinylidene fluoride copolymers. *Phase Transitions: A Multinational Journal*, 18(3-4):143–211, 1989.

[148] Q. M. Zhang, Vivek Bharti, and X. Zhao. Giant electrostriction and relaxor ferroelectric behavior in electron-irradiated poly(vinylidene fluoride-trifluoroethylene) copolymer. *Science*, 280(5372):2101–2104, 1998.

[149] Xing-Zhong Zhao, Vivek Bharti, Q. M. Zhang, T. Romotowski, F. Tito, and R. Ting. Electromechanical properties of electrostrictive poly(vinylidene fluoride–trifluoroethylene) copolymer. *Applied Physics Letters*, 73(14):2054–2056, 1998.

[150] Zhong-Yang Cheng, Vivek Bharti, Tian Mai, Tian-Bing Xu, Q. M. Zhang, T. Ramotowski, Kenneth A. Wright, and Robert Ting. Effect of high energy electron irradiation on the electromechanical properties of poly(vinylidene fluoride-trifluorethylene) 50/50 and 65/35 copolymers. *IEEE Transactions on Ultrasonics, Ferroelectrics, and Frequency Control*, 47(6):1296–1307, Nov 2000.

[151] Z.-Y. Cheng, V. Bharti, T.-B. Xu, Haisheng Xu, T. Mai, and Q. M. Zhang. Electrostrictive poly(vinylidene fluoride-trifluoroethylene) copolymers. *Sensors and Actuators A: Physical*, 90(1-2):138–147, 2001.

[152] F. Bauer, E. Fousson, Q. M. Zhang, and L. M. Lee. Ferroelectric copolymers and terpolymers for electrostrictors: synthesis and properties. In *Electrets, 2002. ISE 11. Proceedings. 11th International Symposium on*, pages 355–358, 2002.

[153] F. Bauer, E. Fousson, Q. M. Zhang, and L. M. Lee. Ferroelectric copolymers and terpolymers for electrostrictors: synthesis and properties. *IEEE Transactions on Dielectrics and Electrical Insulation*, 11(2):293–298, Apr 2004.

[154] F. Bauer. Relaxor fluorinated polymers: novel applications and recent developments. *IEEE Transactions on Dielectrics and Electrical Insulation*, 17(4):1106–1112, August 2010.

[155] Haisheng Xu, Z.-Y. Cheng, Dana Olson, T. Mai, Q. M. Zhang, and G. Kavarnos. Ferroelectric and electromechanical properties of poly(vinylidene-fluoride–trifluoroethylene–chlorotrifluoroethylene) terpolymer. *Applied Physics Letters*, 78(16):2360–2362, 2001.

[156] F. Xia, Z.-Y. Cheng, H. S. Xu, H. F. Li, Q. M. Zhang, G. J. Kavarnos, R. Y. Ting, G. Abdul-Sadek, and K. D. Belfield. High electromechanical responses in a poly(vinylidene fluoride–trifluoroethylene–chlorofluoroethylene) terpolymer. *Advanced Materials*, 14(21):1574–1577, 2002.

[157] T. C. Chung and A. Petchsuk. Synthesis and properties of ferroelectric fluoroterpolymers with curie transition at ambient temperature. *Macromolecules*, 35(20):7678–7684, 2002.

[158] Q. M. Zhang, Hengfeng Li, Martin Poh, Feng Xia, Z. Y. Cheng, Haisheng Xu, and Cheng Huang. An all-organic composite actuator material with a high dielectric constant. *Nature*, 419(6904):284–287, 09 2002.

[159] C. Huang and Q. Zhang. Enhanced dielectric and electromechanical responses in high dielectric constant all-polymer percolative composites. *Advanced Functional Materials*, 14(5):501–506, 2004.

[160] S. Zhang, N. Zhang, C. Huang, K. Ren, and Q. M. Zhang. Microstructure and electromechanical properties of carbon nanotube/poly(vinylidene fluoride-trifluoroethylene-chlorofluoroethylene) composites. *Advanced Materials*, 17(15):1897–1901, 2005.

[161] F. Bauer, E. Fousson, and Q. M. Zhang. Recent advances in highly electrostrictive P(VDF-TrFE-CFE) terpolymers. *IEEE Transactions on Dielectrics and Electrical Insulation*, 13(5):1149–1154, 2006.

[162] Shihai Zhang, Ziqi Liang, Qing Wang, and Q. M. Zhang. Ink-jet printing of ferroelectric poly(vinylidene fluoride-trifluoroethylene) copolymers. In *MRS Proceedings*, volume 889, pages 0889–W05. Cambridge Univ Press, 2005.

[163] Seung Tae Choi, Jeong Yub Lee, Jong Oh Kwon, Seungwan Lee, and Woonbae Kim. Liquid-filled varifocal lens on a chip. *Proc. SPIE*, 7208:72080P–72080P–9, 2009.

[164] Feng Xia, Srinivas Tadigadapa, and Q. M. Zhang. Electroactive polymer based microfluidic pump. *Sensors and Actuators A: Physical*, 125(2):346–352, 2006.

[165] Shihai Zhang, Bret Neese, Kailiang Ren, Baojin Chu, and Q. M. Zhang. Microstructure and electromechanical responses in semicrystalline ferroelectric relaxor polymer blends. *Journal of Applied Physics*, 100(4):044113–044113, 2006.

[166] IEEE Standard on Piezoelectricity. *ANSI/IEEE Std. 176-1987*, 1988.

[167] I. Krakovskỳ, T. Romijn, and A. Posthuma de Boer. A few remarks on the electrostriction of elastomers. *Journal of Applied Physics*, 85(1):628–629, 1999.

[168] C.-W. Nan, Y. Shen, and Jing Ma. Physical properties of composites near percolation. *Annual Review of Materials Research*, 40:131–151, 2010.

[169] Z.-M. Dang, Y.-H. Lin, and C.-W. Nan. Novel ferroelectric polymer composites with high dielectric constants. *Advanced Materials*, 15(19):1625–1629, 2003.

[170] Lan Wang and Zhi-Min Dang. Carbon nanotube composites with high dielectric constant at low percolation threshold. *Applied Physics Letters*, 87(4):042903, 2005.

[171] Cheng Huang, R. Klein, Feng Xia, Hengfeng Li, Q. M. Zhang, Francois Bauer, and Z. Y. Cheng. Poly (vinylidene fluoride-trifluoroethylene) based high performance electroactive polymers. *IEEE Transactions on Dielectrics and Electrical Insulation*, 11(2):299–311, 2004.

[172] Avrom I. Medalia. Electrical conduction in carbon black composites. *Rubber Chemistry and Technology*, 59(3):432–454, 1986.

[173] Séverine Humbert, Olivier Lame, Roland Séguéla, and Gérard Vigier. A re-examination of the elastic modulus dependence on crystallinity in semi-crystalline polymers. *Polymer*, 52(21):4899–4909, 2011.

[174] C. Chiteme and D. S. Mclachlan. Measurements of universal and non-universal percolation exponents in macroscopically similar systems. *Physica B: Condensed Matter*, 279(1):69–71, 2000.

[175] Kaleem Ahmad, Wei Pan, and Sui-Lin Shi. Electrical conductivity and dielectric properties of multiwalled carbon nanotube and alumina composites. *Applied Physics Letters*, 89(13):133122–133122, 2006.

[176] C. Pecharromán and J. S. Moya. Experimental evidence of a giant capacitance in insulator–conductor composites at the percolation threshold. *Advanced Materials*, 12(4):294–297, 2000.

[177] Z.-M. Dang, Lan Wang, YI Yin, Qing Zhang, and Q.-Q. Lei. Giant dielectric permittivities in functionalized carbon-nanotube/electroactive-polymer nanocomposites. *Advanced Materials*, 19(6):852–857, 2007.

[178] Hui-Min Bao, Jiao-Fan Song, Juan Zhang, Qun-Dong Shen, Chang-Zheng Yang, and Q. M. Zhang. Phase transitions and ferroelectric relaxor behavior in P(VDF-TrFE-CFE) terpolymers. *Macromolecules*, 40(7):2371–2379, 2007.

[179] S. Pelissou, P. Benca, and L. H. Gross. Electrical properties of metallocene polyethylene. In *IEEE International Conference on Solid Dielectrics*, 2004.

[180] Xin Zhou, Xuanhe Zhao, Zhigang Suo, Chen Zou, James Runt, Sheng Liu, Shihai Zhang, and Q. M. Zhang. Electrical breakdown and ultrahigh electrical energy density in poly (vinylidene fluoride-hexafluoropropylene) copolymer. *Applied Physics Letters*, 94(16):162901–162901, 2009.

[181] Z. Rubin, S. A. Sunshine, M. B. Heaney, I. Bloom, and I. Balberg. Critical behavior of the electrical transport properties in a tunneling-percolation system. *Physical Review B*, 59(19):12196, 1999.

[182] Ping Sheng, E. K. Sichel, and J. I. Gittleman. Fluctuation-induced tunneling conduction in carbon-polyvinylchloride composites. *Physical Review Letters*, 40(18):1197, 1978.

[183] Jean-Fabien Capsal, Mickaël Lallart, Jeremy Galineau, Pierre-Jean Cottinet, Gaël Sebald, and Daniel Guyomar. Evaluation of macroscopic polarization and actuation abilities of electrostrictive dipolar polymers using the microscopic Debye/Langevin formalism. *Journal of Physics D: Applied Physics*, 45(20):205401, 2012.

[184] Zhi-Min Dang, Jin-Kai Yuan, Sheng-Hong Yao, and Rui-Jin Liao. Flexible nanodielectric materials with high permittivity for power energy storage. *Advanced Materials*, 25(44):6334–6365, 2013.

[185] Sasidhar Siddabattuni, Thomas P. Schuman, and Fatih Dogan. Dielectric properties of polymer–particle nanocomposites influenced by electronic nature of filler surfaces. *ACS Applied Materials & Interfaces*, 5(6):1917–1927, 2013.

[186] Yoseph Bar-Cohen. *Biomimetics: Biologically Inspired Technologies*. CRC Press, 2005.

[187] Mickaël Lallart, Jean-Fabien Capsal, Abdoul Kader Mossi Idrissa, Jérémy Galineau, Masae Kanda, and Daniel Guyomar. Actuation abilities of multiphasic electroactive polymeric systems. *Journal of Applied Physics*, 112(9):094108, 2012.

[188] T. J. Lewis. Interfaces: nanometric dielectrics. *Journal of Physics D: Applied Physics*, 38(2):202, 2005.

[189] Friedrich Kremer and Andreas Schonhals, editors. *Broadband Dielectric Spectroscopy.* Springer Science & Business Media, 2003.

[190] J. M. Davies, R. F. Miller, and W. F. Busse. Dielectric properties of plasticized polyvinyl chloride. *Journal of the American Chemical Society*, 63(2):361–369, 1941.

[191] George Wypych, editor. *Handbook of Plasticizers*, chapter 10, Effect of Plasticizers on Properties Plasticizered Materials. William Andrew Publishing, 2nd edition, 2012.

[192] Pei Xu and Xingyuan Zhang. Investigation of MWS polarization and dc conductivity in polyamide 610 using dielectric relaxation spectroscopy. *European Polymer Journal*, 47(5):1031–1038, 2011.

[193] J. Su, Q. M. Zhang, and R. Y. Ting. Space-charge-enhanced electromechanical response in thin-film polyurethane elastomers. *Applied Physics Letters*, 71(3):386–388, 1997.

[194] Sujesha Sudevalayam and Purushottam Kulkarni. Energy harvesting sensor nodes: Survey and Implications. *Communications Surveys & Tutorials, IEEE*, 13(3):443–461, 2011.

[195] J. A. Paradiso and T. Starner. Energy scavenging for mobile and wireless electronics. *Pervasive Computing, IEEE*, 4(1):18–27, Jan 2005.

[196] N. G. Stephen. On energy harvesting from ambient vibration. *Journal of Sound and Vibration*, 293:409–425, 2006.

[197] R. J. M. Vullers, R. van Schaijk, I. Doms, C. Van Hoof, and R. Mertens. Micropower energy harvesting. *Solid-State Electronics*, 53(7):684–693, 2009.

[198] Adnan Harb. Energy harvesting: State-of-the-art. *Renewable Energy*, 36(10):2641 2654, 2011.

[199] Triet Le, Karti Mayaram, and Terri Fiez. Efficient far-field radio frequency energy harvesting for passively powered sensor networks. *IEEE Journal of Solid-State Circuits*, 43(5):1287–1302, 2008.

[200] Duncan Graham-Rowe. Wireless power harvesting for cell phones. *www.technologyreview.com*, June 2009.

[201] Bryce Kellogg, Aaron Parks, Shyamnath Gollakota, Joshua R Smith, and David Wetherall. Wi-fi backscatter: Internet connectivity for RF-powered devices. In *Proceedings of the 2014 ACM conference on SIGCOMM*, pages 607–618. ACM, 2014.

[202] Shad Roundy, Eli S. Leland, Jessy Baker, Eric Carleton, Elizabeth Reilly, Elaine Lai, Brian Otis, Jan M. Rabaey, Paul K. Wright, and V. Sundararajan. Improving power output for vibration-based energy scavengers. *Pervasive Computing, IEEE*, 4(1):28–36, 2005.

[203] Terry M. Tritt and M. A. Subramanian. Thermoelectric materials, phenomena, and applications: a bird's eye view. *MRS Bulletin*, 31(03):188–198, 2006.

[204] Gael Sebald, Daniel Guyomar, and Amen Agbossou. On thermoelectric and pyroelectric energy harvesting. *Smart Materials and Structures*, 18(12):125006, 2009.

[205] A. Cuadras, M. Gasulla, and Vittorio Ferrari. Thermal energy harvesting through pyroelectricity. *Sensors and Actuators A: Physical*, 158(1):132–139, 2010.

[206] Shashank Priya. Advances in energy harvesting using low profile piezoelectric transducers. *Journal of Electroceramics*, 19(1):167–184, 2007.

[207] K. A. Cook-Chennault, N. Thambi, and A. M. Sastry. Powering MEMS portable devices – a review of non-regenerative and regenerative power supply systems with special emphasis on piezoelectric energy harvesting systems. *Smart Materials and Structures*, 17(4):043001, 2008.

[208] S. P. Beeby, M. J. Tudor, and N. M. White. Energy harvesting vibration sources for microsystems applications. *Measurement Science and Technology*, 17(12):R175, 2006.

[209] P. D. Mitcheson, E. M. Yeatman, G. K. Rao, A. S. Holmes, and T. C. Green. Energy harvesting from human and machine motion for wireless electronic devices. *Proceedings of the IEEE*, 96(9):1457–1486, Sept 2008.

[210] Steven R. Anton and Henry A. Sodano. A review of power harvesting using piezoelectric materials (2003–2006). *Smart Materials and Structures*, 16(3):R1, 2007.

[211] Clive A. Randall, Namchul Kim, John-Paul Kucera, Wenwu Cao, and Thomas R. Shrout. Intrinsic and extrinsic size effects in fine-grained morphotropic-phase-boundary lead zirconate titanate ceramics. *Journal of the American Ceramic Society*, 81(3):677–688, 1998.

[212] Thomas R. Shrout and Shujun J. Zhang. Lead-free piezoelectric ceramics: Alternatives for PZT? *Journal of Electroceramics*, 19(1):113–126, 2007.

[213] Jian Fang, Haitao Niu, Hongxia Wang, Xungai Wang, and Tong Lin. Enhanced mechanical energy harvesting using needleless electrospun poly(vinylidene fluoride) nanofibre webs. *Energy & Environmental Science*, 6(7):2196–2202, 2013.

[214] Luana Persano, Canan Dagdeviren, Yewang Su, Yihui Zhang, Salvatore Girardo, Dario Pisignano, Yonggang Huang, and John A Rogers. High performance piezoelectric devices based on aligned arrays of nanofibers of poly(vinylidenefluoride-co-trifluoroethylene). *Nature Communications*, 4:1633, 2013.

[215] Yiming Liu, Kailiang Ren, Heath F. Hofmann, and Qiming Zhang. Electrostrictive polymers for mechanical energy harvesting. In *Smart Structures and Materials*, pages 17–28. International Society for Optics and Photonics, 2004.

[216] Yiming Liu, Kai Liang Ren, Heath F. Hofmann, and Qiming Zhang. Investigation of electrostrictive polymers for energy harvesting. *IEEE Transactions on Ultrasonics, Ferroelectrics, and Frequency Control*, 52(12):2411–2417, 2005.

[217] Kailiang Ren, Yiming Liu, H. Hofmann, Q. M. Zhang, and John Blottman. An active energy harvesting scheme with an electroactive polymer. *Applied Physics Letters*, 91(13):132910, 2007.

[218] P.-J. Cottinet, Daniel Guyomar, Mickael Lallart, Benoit Guiffard, and Laurent Lebrun. Investigation of electrostrictive polymer efficiency for mechanical energy harvesting. *IEEE Transactions on Ultrasonics, Ferroelectrics, and Frequency Control*, 58(9):1842–1851, 2011.

[219] P.-J. Cottinet, Mickael Lallart, Daniel Guyomar, Benoit Guiffard, Laurent Lebrun, Gael Sebald, and Chatchai Putson. Analysis of AC-DC conversion for energy harvesting using an electrostrictive polymer P(VDF-TrFE-CFE). *IEEE Transactions on Ultrasonics, Ferroelectrics, and Frequency Control*, 58(1):30–42, 2011.

[220] Daniel Guyomar, Mickaël Lallart, and Pierre-Jean Cottinet. Electrostrictive conversion enhancement of polymer composites using a nonlinear approach. *Physics Letters A*, 375(3):260–264, 2011.

[221] Pierre-Jean Cottinet, Daniel Guyomar, and Mickaël Lallart. Electrostrictive polymer harvesting using a nonlinear approach. *Sensors and Actuators A: Physical*, 172(2):497–503, 2011.

[222] E. Fukada. History and recent progress in piezoelectric polymers. *IEEE Transactions on Ultrasonics, Ferroelectrics, and Frequency Control*, 47(6):1277–1290, Nov 2000.

[223] Chieh Chang, Van H. Tran, Junbo Wang, Yiin-Kuen Fuh, and Liwei Lin. Direct-write piezoelectric polymeric nanogenerator with high energy conversion efficiency. *Nano Letters*, 10(2):726–731, 2010.

[224] George M. Whitesides. The origins and the future of microfluidics. *Nature*, 442(7101):368–373, 2006.

[225] Jamil El-Ali, Peter K. Sorger, and Klavs F. Jensen. Cells on chips. *Nature*, 442(7101):403–411, 2006.

[226] Sangeeta N. Bhatia and Donald E. Ingber. Microfluidic organs-on-chips. *Nature Biotechnology*, 32(8):760–772, 08 2014.

[227] S. Zafar Razzacki, Prasanna K. Thwar, Ming Yang, Victor M. Ugaz, and Mark A. Burns. Integrated microsystems for controlled drug delivery. *Advanced Drug Delivery Reviews*, 56(2):185–198, 2004.

[228] Vamsee K. Pamula and Krishnendu Chakrabarty. Cooling of integrated circuits using droplet-based microfluidics. In *Proceedings of the 13th ACM Great Lakes Symposium on VLSI*, pages 84–87. ACM, 2003.

[229] J. G. Smits and N. V. Vitafin. Piezo-electrical micropump. *European Patent EP0134614, Netherlands*, 1984.

[230] D. J. Laser and J. G. Santiago. A review of micropumps. *Journal of Micromechanics and Microengineering*, 14(6):R35, 2004.

[231] Brian D. Iverson and Suresh V. Garimella. Recent advances in microscale pumping technologies: A review and evaluation. *Microfluidics and Nanofluidics*, 5(2):145–174, 2008.

[232] Farid Amirouche, Yu Zhou, and Tom Johnson. Current micropump technologies and their biomedical applications. *Microsystem Technologies*, 15(5):647–666, 2009.

[233] Oliver Pabst, Stefan Hölzer, Erik Beckert, Jolke Perelaer, Ulrich S. Schubert, Ramona Eberhardt, and Andreas Tünnermann. Inkjet printed micropump actuator based on piezoelectric polymers: Device performance and morphology studies. *Organic Electronics*, 15(11):3306–3315, 2014.

[234] Jean-Fabien Capsal, Jérémy Galineau, Mickaël Lallart, Pierre-Jean Cottinet, and Daniel Guyomar. Plasticized relaxor ferroelectric terpolymer: Toward giant electrostriction, high mechanical energy and low electric field actuators. *Sensors and Actuators A: Physical*, 207:25–31, 2014.

[235] Jae Sung Yoon, Jong Won Choi, Il Hwan Lee, and Min Soo Kim. A valveless micropump for bidirectional applications. *Sensors and Actuators A: Physical*, 135(2):833–838, 2007.

[236] Peter Woias. Micropumps - past, progress and future prospects. *Sensors and Actuators B: Chemical*, 105(1):28–38, 2005.

[237] Erik Stemme and Goran Stemme. A valveless diffuser/nozzle-based fluid pump. *Sensors and Actuators A: Physical*, 39(2):159–167, 1993.

[238] Anders Olsson, Peter Enoksson, Goran Stemme, and Erik Stemme. Micromachined flat-walled valveless diffuser pumps. *Journal of Microelectromechanical Systems*, 6(2):161–166, 1997.

[239] X. N. Jiang, Z. Y. Zhou, X. Y. Huang, Y. Li, Y. Yang, and C. Y. Liu. Micronozzle/diffuser flow and its application in micro valveless pumps. *Sensors and Actuators A: Physical*, 70(1):81–87, 1998.

[240] Vishal Singhal, Suresh V. Garimella, and Jayathi Y. Murthy. Low reynolds number flow through nozzle-diffuser elements in valveless micropumps. *Sensors and Actuators A: Physical*, 113(2):226–235, 2004.

[241] Anders Olsson, Goran Stemme, and Erik Stemme. A valve-less planar fluid pump with two pump chambers. *Sensors and Actuators A: Physical*, 47(1):549–556, 1995.

INSA
INSTITUT NATIONAL
DES SCIENCES
APPLIQUÉES
LYON

FOLIO ADMINISTRATIF

THÈSE SOUTENUE DEVANT L'INSTITUT NATIONAL DES SCIENCES APPLIQUÉES DE LYON

NOM : **YIN** DATE de SOUTENANCE : **07 Mai 2015**
(avec précision du nom de jeune fille, le cas échéant)

Prénom : **Xunqian**

TITRE : **MODIFICATION OF ELECTROSTRICTIVE POLYMERS AND THEIR ELECTROMECHANICAL APPLICATIONS**

NATURE : **Doctorat** Numéro d'ordre : **2015ISAL0041**

Ecole doctorale : **Electronique, Electrotechnique, Automatique (EEA)**

Spécialité : **Génie Électrique**

RESUME :

Electroactive polymers (EAPs), which can realize the conversion between electrical and mechanical energy, have been emerging as one of the most interesting smart materials in the past two decades due to their low density, excellent mechanical properties, ease of processing, low price and potential applications in the fields of sensors, actuators, generators, biomimetic robots and so on. Among all of EAPs, ferroelectric poly(vinylidene fluoride) [PVDF] based electrostrictive terpolymers have been greatly investigated due to their high electromechanical response. A longitudinal strain of 7 % and an elastic energy density as high as 1.1 J/cm^3 have been observed for PVDF based terpolymers. One major concern for PVDF based electrostrictive polymers is the requirement of high driven electric field, which is not convenient and safe for practical applications. In addition, the electromechanical performances of electrostrictive polymers are closely related to the material properties such as dielectric properties, mechanical properties and the dielectric breakdown strength. The object of this work is to modify electrostrictive terpolymers with different approaches to improve the electromechanical performances and to develop some applications based on modified terpolymers.

Firstly, an organic/inorganic (terpolymer/carbon black) nanocomposite was prepared to improve the dielectric permittivity based on the percolation theory. The dielectric properties, dielectric breakdown strength and the mechanical properties were carefully investigated for electrostrictive applications. Results indicate that the introduction of conductive carbon black brought about an enhanced dielectric permittivity, but more significantly reduced the dielectric breakdown strength, leading to a declined electrostrictive performance of terpolymer.

Secondly, based on the heterogeneous nature of semi-crystalline terpolymer and the important role that interface polarization plays for dielectric and electromechanical response, small molecular plasticizer bis(2-ethylhexyl) phalate (DEHP) was introduced into electrostrictive terpolymer to form an all-organic polymer composite with improved electromechanical performances. As expected, the introduction of DEHP contributes to greatly increased dielectric permittivity at low frequency, decreased Young's modulus and moderately reduced dielectric breakdown strength of terpolymers, which are closely related with the increased mobility of polymer chains caused by DEHP. As a result, DEHP modified terpolymers exhibit well improved electromechanical performances in contrast with pure terpolymer.

Finally, two applications including mechanical energy harvesting and microfluidic pump based on DEHP modified terpolymers were investigated.

MOTS-CLÉS : Electrostrictive polymers; Carbon black; Plasticizer DEHP; Composite; Energy harvesting; Microfluidic pump

Laboratoire de recherche : **Laboratoire de Génie Électrique et Ferroélectricité (LGEF) de l'INSA de Lyon**

Directeur de thèse : **Pr. Daniel GUYOMAR**
Co-directeur de thèse : **Dr. Jean-Fabien CAPSAL**

Président de jury : **Dr. Gisèle BOITEUX**, Directrice de Recherche CNRS

Composition du jury :	Présidente & Examinatrice :	**Dr. Gisèle BOITEUX**	Directrice de Recherche CNRS
	Rapporteur :	**Pr. Benoît GUIFFARD**	Professeur à l'Université de Nantes
	Rapporteur :	**Dr. Eric DANTRAS**	Maître de Conférences HDR à l'Université de Toulouse
	Examinatrice :	**Pr. Colette LACABANNE**	Professeur à l'Université de Toulouse
	Examinateur :	**Pr. Denis REMIENS**	Professeur à l'Université de Valenciennes
	Directeur de Thèse	**Pr. Daniel GUYOMAR**	Professeur à L'INSA de Lyon
	Co-Directeur de Thèse :	**Dr. Jean-Fabien CAPSAL**	Maître de Conférences à L'INSA de Lyon